Colloidal Interaction of Cellulose with Solid-acid Catalyst and Its Implications for Hydrolysis

by

Ziyang Zhang

A Dissertation

Submitted to the Faculty of

Worcester Polytechnic Institute

In partial fulfillment of the requirements for the

Degree of Doctor of Philosophy

In

Chemical Engineering

December 2021

Dr. Michael Timko, Academic Advisor Chemical Engineering Department, WPI	Dr. Aaron Deskins, Committee Member Chemical Engineering Department, WPI
Dr. Andrew Teixeira, Committee Member Chemical Engineering Department, WPI	Dr. Christopher Lambert, Committee Member Chemical Engineering Department, WPI

Dr. Susan Roberts, Head of Chemical Engineering Department, WPI

Acknowledgements

Completing this dissertation is by far one of the greatest achievements in my life. I could never find another four years during which scientific research is my only pursuit. My past four years was also characterized as selfish because of limited time I spent with family and friends who support me in the course of Ph.D. My words can only express how much I appreciate their patience, love and resources that my beloved family and friends gave me.

I am very fortunate to have Prof. Michael Timko as my doctoral advisor. He is the most resourceful, rigorous and enthusiastic individual I have ever met in my life. The most enjoyable time that I had during Ph.D. is discussing science with him in hallway, classroom, office and laboratory. His clear thoughts and critical thinking really motivate me to become a careful engineer or scientist and yet maintain endless imaginations and curiosity. At human level, Prof. Timko fills in the feeling of missing my family when I was away from home. He also makes tendinous science full of fun and never gets bored. He influences me to be a positive person with great respect to science and people influenced by science.

I also would like to thank my committee members. Prof. Lambert has lent his lab (I called it an island) to me during pandemic. He constantly provides advice in all levels including technical details, critical thinking and writing. I will never finish this dissertation without his support. Prof. Teixeira has been an enthusiastic and resourceful professor. His class on kinetics and reactor design is one of my favorite classes and I will keep digging into it even after I graduate. Prof. Teixeira has been a great professor in teaching as he constantly came up with creative ways for me to learn. Prof. Deskins is a great professor who always makes class fun and inspiring. His teaching in experimental design helps me perform well in job interview. I appreciate all committee members' instructive comments and suggestions that improve my Ph.D. work significantly.

I would like to acknowledge our collaborators' resource and help for completing this dissertation. First, I would like thank Prof. Ping He from Lamar University. Prof. He has provided insightful and constructive suggestion for surface wetting study. I would like to thank Prof. Granados-Focil from Clark University for his discussion and comments for improving my Ph.D. work. Prof. Albrecht in Biomedical Engineering of Worcester Polytechnic Institute has fabricated patterned silicon wafer for studying surface wetting. Prof. Schmidt-Rohr at Brandeis University has provided solid state NMR for cellulose crystalinity characterization. Prof. Rahbar and his Ph.D. student, Mobin have assisted with molecular dynamics simulations.

I am fortunate to have joined a supportive and fun research team who create a wonderful environment for me to grow and do science. Prof. Geoffrey Tompsett has been a great professor and "manager" and takes numerous actions to fix instrument and ensure lab safety; Tom Partington fixed every piece of lab to make sure we were safe and ran experiments without delay; Doug White provided high-quality work on maintaining instruments such as XRD and SEM; Dr. Alex Maag has helped me with scientific writing and trained me to be a successful teaching assistant with safety awareness; Dr. Maksim Tyufekchiev is the cellulose "leader" who influences my research direction and thinking on cellulose decomposition; Dr. Avery Brown taught me how to perform deconvolution on XRD spectrum; Dr. Azadeh Zaker helped me with various things such as Matlab coding, Igor plotting and covered me up in teaching assistant duties; Dr. Feng Cheng provided me with advices on cellulose decomposition and HPLC trouble shooting; Joe Heng, a current PhD student in University of Massachusetts, spent tremendous time fixing HPLC and "washing" sample vials; Tongjie Zhang, a current Ph.D. student in Drexel University, was an interesting additive to our lab and made it fun.

I also want to thank undergraduates for their support on my projects. I specifically want to express my gratitude to Wenli Wang, Alexander N. Korpacz, Claudia R. Dufour and Zachary J. Weiland for their initiative work on mixture contact angles measurements; Katie Ralph came in during pandemic but helped complete salt-cellulose interaction study in tough times; I would like to acknowledge Emily Proctor's lead on cellobiose solubility work which has resulted in a publication; Katerine Gomez spent two summers functionalizing solid catalyst with sulfonic acid.

Lastly, I want to express my gratitude for my family. My wife, Yuxin Li, endless supports me and it is of great comfort with her; my father and mother are the primary reasons for me to pursue Ph.D. study; my older brother, Yuchen Zhang has been a great pleasant and listener in y bad times; my young brother, Ke Zhang, always motivates and encourages me to do great research.

Table of Contents

Acknowledgements 1

Contents 5

Lists of Figures 15

Lists of Tables 23

Abstract 25

Chapter 1 28

Introduction 28

1.1 Biomass as Renewable Energy Sources 28

1.2 Surface Energy Determination Using Liquid Mixtures 30

1.2.1 Liquid Mixtures Method Accommodating Owens, Wendt, Rabel and Kaelble (OWRK) Model 32

1.2.2 Liquid Mixtures Method Accommodating van Oss model 32

1.2.3 Liquid Mixture Approach for Determining Biomass Particles Surface Energies 33

1.2.4 A Generalized Theory for Quantifying Liquid Mixtures Surface Tension Parameters 34

1.3 Colloid Particles Surface Charge and Models 34

1.3.1 Colloidal Interaction of Cellulose with Solid Acid Catalysts and its Implications 34

1.4 Polyelectrolyte Promoted Cellulose 36

1.5 Hofmeister Series Salts Promoted Cellulose Hydrolysis Reaction 36

Reference 38

Chapter 2 49

Objective and Approach 49

2.1 Objectives 49

2.2 Method and Approach 50

Chapter 3 52

Binary Liquid Mixture Contact-Angle Measurements for Precise Estimation of Surface Free Energy 52

3.1 Abstract 52

3.2 Introduction 53

3.3 Experimental 55

3.3.1 Polydimethylsiloxane Preparation 55

3.3.2 Functionalized Glass Substrates 56

3.3.3 Mixture Preparations 56

3.4 Theory 57

3.5 Results and Discussions 62

3.5.1 Liquid Selection and Binary Mixture Surface Tensions 62

3.5.2 Determination of PDMS Surface Energy 66

3.5.3 Surface Energy of Functionalized Silicon Dioxide Surface 72

3.5.4 Uncertainty analysis 76

3.6 Conclusions 78

3.7 References 79

Chapter 4 85

Accurate Measurement of Acid and Base Surface Energy of Polymer Materials Using Aqueous Mixtures and van Oss-Chaudhury-Good (*v*OCG) Model 85

4.1 Abstract 85

4.2 Introduction 85

4.3 Experimental 90

4.3.1 Polydimethylsiloxane (PDMS) Cast 90

4.3.2 Mixture Preparations 90

4.3.3 Contact Angle Measurement 91

4. 5 Theory 91

4.5.1 Chemically Resolved Surface Tension and Surface Energy Models 93

4.5.2 Mixing Rules to Capture the Effects of Solvent-Solvent Interactions on Surface Tension 95

4.5.3 Using Contact Angle Measurements Obtained from Binary Liquid Mixtures to Determine Solid Surface Energy 98

4.6 Results and Discussions 99

4.6.1 Composition-Dependent Surface Tension 99

4.6.2 Liquid Selection and Mixtures' Contact Angles on PDMS, PVC and PMMA 103

4.6.3 Liquid Surface Tension Components 106

4.6.4 Effect of Water Surface Energy Components Variation on Surface Mixture Tension Fitting 109
4.6.5 Polymers Surface Energy Determination 112
4.6.6 Contact Angle Prediction Using Determined Surface Energy Components 115
4.7 Conclusions 116
4.8 ACKNOWLEDGEMENT 117
4.9 Reference 117
Chapter 5 125
Liquid Mixture Wetting on Patterned and Irregular PDMS Surfaces 125
5.1 Abstract 125
5.2 Introduction 126
5.3 Experimental 129
5.3.1 Materials and Chemicals 129
5.3.2 Fabrication of Patterned Silicon Wafer 129
5.3.3 Preparation of Smooth and Rough PDMS 130
5.3.4 Contact Angle Drop Solutions 130
5.3.5 Contact Angle Measurements 131
5.4 Results and Discussions 131
5.4.1 Wetting on Smooth PDMS 131
5.4.2 Wetting on Irregular Surfaces 133

5.4.3 Wetting on Patterned Surfaces-Cassie Baxter-Wenzel Transition 136
5.5 Conclusions 137
5.6 Reference 138
Chapter 6 140
Biomass Powder Surface Energy Determination Using Liquid Mixture with Washburn-Lucas Method 140
6.1 Abstract 140
6.2 Introduction 141
6.3 Experimental 143
6.4 Wicking method 143
6.5 Theory 144
6.6 Results and Discussions 146
6.6.1 Selected Liquid Properties 146
6.6.2 Liquid mixtures penetration in cellulose and chitin columns. 148
6.6.3 Liquid mixtures penetration in chitin columns 153
6.6.4 Cellulose and Chitin Surface Energy by OWRK model 155
6.7 Conclusions 157
6.8 Acknowledgement 158
6.9 Reference 158
Chapter 7 164

D.L.V.O. Analysis of Cellulose and Solid-Acid Catalyst Interaction for Hydrolysis Reaction. 164

7.1 Abstract 164

7.2 Introduction 165

7.3 Theory 168

7.3.1 D.L.V.O. Theory 168

7.3.2 PKa-PH-Surface Potential Model 172

7.4 Resultes and Discussions 176

7.4.1 Determination of Hamaker Constant and Surface Potential 176

7.4.2 Parametric Analysis 183

7.4.3 Particle Size Effect on Cellulose-Catalyst Adsorption 186

7.4.4 D.L.V.O. interaction for cellulose and literature reported catalysts. 188

7.4.5 Non-D.L.V.O. interaction for cellulose and catalysts 191

7.4.6 Hydration forces 192

7.4.7 Steric forces 193

7.4.8 Hydrophobic forces 194

7.5 Conclusion 194

7.6 References 196

Chapter 8 205

Revised Design Principals for Solid-acid Catalysts 205

8.1 Abstract 205

8.2 Revised Design Principals for Solid-acid Catalysts 205
8.3 Conclusions 216
8.4 Reference 216
Chapter 9 220
Polydiallyldimethylammonium chloride (PolyDDA) Enhanced Hydrolysis Reaction of Cellulose with Solid Acid 220
9.1 Abstract 220
9.2 Introduction 221
9.3 Experimental 223
9.3.1 Materials 223
9.3.2 Ball-milling 224
9.3.3 Zeta potential measurement 224
9.3.4 Cellulose Hydrolysis 224
9.3.5 Product Quantification: 226
9.4 Results and Discussions 226
9.4.1 Effects of polyDDA on Glucose Yield 226
9.4.2 Differentiating Homogeneous and Hetergeeneous Contributions 228
9.5 Conclusion 234
9.6 References 235
Chapter 10 240

Salt-Promoted Cellulose Hydrolysis: A Hofmeister Series Study 240
10.1 Abstract 240
10.2 Introduction 240
10.3 Experimental 243
10.3.1 Materials and Chemicals 243
10.3.2 Ball-Milling Pretreatment 243
10.3.3 Cellulose Hydrolysis 244
10.3.4 HPLC Analysis 245
10.3.5 X-Ray Diffraction (XRD) 245
10.3.6 Raman Microscopy 245
10.3.7 Solid State Nuclear Magnetic Resonance (ssNMR) 245
10.3.8 Molecular Dynamics (MD) Simulations 246
10.4 Results and Discussions 248
10.4.1 X-Ray Diffraction and Raman Analysis of Amorphous Cellulose Treated in Salts Solutions 248
10.4.2 Solid State NMR Analysis of Amorphous Cellulose Treated with Salt Solutions. 251
10.4.3 Inorganic salts Promoted Cellulose Hydrolysis 252
10.4.4 Guanidinium Chloride Promoted Cellulose Hydrolysis 253
10.4.5 Maximizing glucose yield in the presence of guanidinium chloride 256
10.4.6 Molecular Dynamic Simulations 257

10.4.7 Hofmeister Series for Salts Effect on Cellulose Hydrolysis and Crystallization suppression 260
10.5 Conclusions 261
10.6 Reference 261
Chapter 11 268
Conclusions and Recommendation 268
Chapter 12 274
Appendix A 274
Accurate Measurement of Acid and Base Surface Energy of Polymer Materials Using Aqueous Mixtures and van Oss-Chaudhury-Good (vOCG) Model 274
Matlab Code 274
Appendix B 280
D.L.V.O. Analysis of Cellulose and Solid-Acid Catalyst Interaction for Hydrolysis Reaction 280
List of Symbols 280
Number of articles published on cellulose hydrolysis using solid acid in 14 years 282
Shear Force Effect on Cellulose-Catalyst Aggregation 283
Temperature Effect on Cellulose-Solid-Acid Interactions 286
Solvent Effect on Cellulose-Solid-Acid Interaction 287
Reference 288
DLVO Matlab Code 288

Appendix C 292

Salt-Promoted Cellulose Hydrolysis: A Hofmeister Series Study 292

Lists of Figures

Figure 1.1 Schematics of typical scientific approach to tackle cellulose depolymerizations 30

Figure 1. 2 Schemitic of polycations induced colloidal particles aggregations 36

Figure 1. 3 Empirical Hofmeister series for protein solubility, salting-in salts increase protein solubility while salting-out salt precipitates protein 37

Figure 3. 1 Surface tension of water-DMSO, water-ethylene glycol, water-formamide and water-glycerol comparison between predicted using Equation (3.4) and literature data are not available for the water-formamide mixture. 64

Figure 3. 2 Dispersive and polar surface tension of water-dimethyl sulfoxide (DMSO), water-formamide, water-ethylene glycol and water-glycerol binary mixtures using Equation (3.4-3.9). 66

Figure 3. 3 (a) Contact angle of water-DMSO, water-formamide and water-ethylene glycol on flat PDMS; Owens-Wendt plots using contact angle of three liquid mixtures: **(b)** water-DMSO mixtures, **(c)** water-formamide mixtures and **(d)** water-ethylene glycol mixtures. 68

Figure 3. 4 Owens-Wendt plot for flat PDMS using multiple pure liquids, including DMSO, benzyl alcohol, formamide, ethylene glycol, glycerol and water. 71

Figure 3. 5 Owens-Wendt plot using three binary mixtures (water-formamide, water-ethylene glycol, water-dimethyl sulfoxide) on PDMS 72

Figure 3. 6 Contact angle of **(a)** water-formamide and **(b)** water-glycerol on functionalized glass. 73

Figure 3. 7 Owens-Wendt plot for ETS, HTS and OTS coated silicon dioxide (glass) using (**a)** water-glycerol mixtures and (**b**) water-formamide mixtures. 74

Figure 3. 8 Statistically analysis of surface energy determination of PDMS. **A-F**: surface energy determined using different number of contact angles data points; **G**: standard error decrease as number of data points used increases; **H**: Uncertainty drops as number of data points used for surface energy determination increases. 77

Figure 4. 1 Flowchart for using liquid mixtures to determine solid surface energy components using acid-base theory: (a) shows algorithm for estimating chemically and compositionally resolved surface tension parameters; (b) is procedure for determining surface energy using (a) as inputs. 92

Figure 4. 2 Comparisons of predicted values of the total liquid surface tension, $\gamma LG, mix$ with measured values for several binary mixtures as functions of the mole fraction of water (x_w) present in the mixture; (**A**) shows predictions based on the OWRK energy model and QMR mixing rule, (**B**) is for the *v*OCG surface energy model and QMR mixing rule, (**C**) is for OWRK surface energy model and MPK mixing rule, and (**D**) is for *v*OCG surface energy model and MPK mixing rule. 101

Figure 4. 3 Measured contact (θ) angles of water-DMSO, water-formamide and water-ethylene glycol mixtures on polydimethylsiloxane (*PDMS*), polyvinyl chloride (*PVC*) and poly(methyl methacrylate) (*PMMA*) as functions of water mole fraction, *Xw*. 105

Figure 4. 4 (Left) Polar ($\gamma LG, mixP$), and (Right) dispersive component ($\gamma LG, mixd$) components from OWRK model for water-DMSO; (b) water-formamide and (c) water-ethylene glycol..... 107

Figure 4. 5 Lewis van der Waals ($\gamma LG, mixLW$), acid ($\gamma LG, mix+$) and base ($\gamma LG, mix-$) components from vOCG model for (a) water-DMSO; (b) water-formamide and (c) water-ethylene glycol..... 109

Figure 4. 6 water-dimethyl sulfoxide mixture surface tension as a function of water mole fraction (x_w). The red line represents the theoretical surface tension predicted by modified acid-base theory with different water acid/base ratio..... 110

Figure 4. 7 water-formamide mixture surface tension as a function of water mole fraction (x_w). The red line represents the theoretical surface tension predicted by modified acid-base theory with different water acid/base ratio..... 111

Figure 4. 8 water-formamide mixture surface tension as a function of water mole fraction (x_w). The red line represents the theoretical surface tension predicted by modified acid-base theory with different water acid/base ratio..... 112

Figure 4. 9 Parity plot comparing predicted contact angle and measured contact angle..... 116

Figure 5. 1 Comparison between experimental contact angles and predicted contact angles using equation (4). And $r = f = 0$. Left is water-dimethyl sulfoxide mixtures on smooth PDMS, and right is water-ethylene glycol mixtures on smooth PDMS. 132

Figure 5. 2 Comparison between measured contact angles and predicted contact angles on silane derivatized surfaces: the red line represents phenyltrimethoxysilane coated surfaces and black line represents trimethoxy(octadecyl)silane coated glass slides..... 133

Figure 5. 3 Comparsion between measured contact angles and predicted contact angles on irregular PDMS surfaces: **A** is water-dimethyl sulfoxide mixtures on PDMS and **B** is water-ethylene glycol mixtures contact angles on PDMS. Wetting parameter (f) and roughness parameter (r) are fitting parameters. 134

Figure 5. 4 Liquid surface tension components effect on contact angles. γLd and γLp are determined by method specified in chapter 3. **A** and **C** are water-dimethyl sulfoxide, and **B** and **D** are water-ethylene glycol. All contact angles are measured on irregular PDMS surfaces. 135

Figure 5. 5 wetting transition of water-dimethyl sulfoxide on two different PDMS surfaces. The dimensions of A-surface are 25 × 10 × 25 and dimensions of surface B is 50 × 50 × 50 *um*. . 137

Figure 6. 1 Washburn-Lucas wicking instrumentation setup, the glass tube bottom is sealed by Watman filter paper and the top is open 144

Figure 6. 2 Molecular structures of selected liquids: formamide, dimethyl sulfoxide (top) and ethanol (not shown) and substrate materials: cellulose and chitin powder (bottom)..... 147

Figure 6. 3 Hexane uptake in cellulose and chitin. 149

Figure 6. 4 (a) Water-dimethyl sulfoxide,(b) water-formamide adsorption mass in microcrystalline cellulose column as functions of penetration time..... 150

Figure 6. 5 Determined penetration constant and contact angles of water-dimethyl sulfoxide (left) and water-formamide (right) in cellulose. 153

Figure 6. 6 (a) Water-dimethyl sulfoxide, **(b)** water-formamide adsorption mass in chitin column as functions of penetration time. 154

Figure 6. 7 Liquid mixtures penetration rate constant as functions of water mole fraction. The left is for water-dimethyl sulfoxide penetrating in chitin and right is water-formamide penetrating in chitin. 155

Figure 6. 8 OWRK model Surface energy of cellulose (left) and chitin as determined using liquid mixtures contact angle 156

Figure 7. 1 Schematic of D.L.V.O. interaction energy as a function of particles separation. The red dash line represents electrostatic repulsion and the green dash line is the vdw attraction. .. 172

Figure 7. 2 The surface potential of ZSM5 and activated carbon bearing different acid head group as a function of media pH. The pKa of acid head group is taken as 2.5, 1.0 and -2 from weak acid to strong acid. The substrate (ZSM5 and activated carbon) surface density is assumed as 1.0/nm^2, functionalized acid surface density is taken as 0.05/nm^2. Equilibrium constant for ZSM5 is assumed as 5 and particle size is assumed as 1 um..... 182

Figure 7. 3 D.L.V.O. interaction energy barrier as function of *pH* and Hamaker constant. The left is for pKa = 2.5 and the right is for pKa = -2. The pKa for substrate materials is assumed as 5 and has surface density of 1.5/nm^2. The surface acid density is assumed as 0.075/nm^2 and article size is taken as 1 um..... 186

Figure 7. 4 D.L.V.O. interaction energy as a function of separation for different functionalized activated carbon particle size. The *pKa* is 1.5, acid head group coverage of activated carbon is assumed as 1.5/nm^2, *pH* is assumed as 3.5 and cellulose particle size is taken as 2 um. 187

Figure 7. 5 D.L.V.O. interaction energy at different *pH* as a function of separation for (a) Nafion, (b) ZSM5, (c) carboxylic acid (*pKa* = 2.5) functionalized activated carbon and (d) sulfonated polystyrene (*pKa* = 1); cellulose particle radius is taken as 1 um while catalyst radius is assumed as 100 nm and ionic strength is taken as 0.1 mM..... 190

Figure 8. 1 Schematics of particle-particle interactional energy as functions of particle separation (yellow sphere represents cellulose and blue sphere represents solid-acid catalyst: (a) like-charge colloidal interactional energy as function of particle separation, (b) unlike-charge colloidal interaction as function of separation, (c) approximated single hydrogen bonding

interaction energy between cellulose chain and chlorobenzene. Note that the *x*-axis scale is 20 nm in Figure 8.1a and Figure 8.1b and 0.5 nm in Figure 8.1c..... 206

Figure 8. 2 DLVO interaction energy as a function of cellulose-catalyst separation for reported catalysts at *pH* = 5..... 209

Figure 8. 3 DLVO maximum energy barrier as a function of acid group *pKa* and solution *pH*, assuming acid head group density of 5 nm^{-2}, Hamaker constant of 2×10^{-20} J..... 210

Figure 8. 4 The DLVO energy barrier height as function of Hamaker constant for different values of the surface potential..... 211

Figure 8. 5 DLVO energy barrier as a function of temperature for cellulose interacting with polystyrene, zirconia, and carbon catalysts. The cellulose diameter is assumed as 5 μm. The surface potential for the catalyst is assumed to be −30 mV and catalysts surface potential are assumed to be – 50 mV..... 212

Figure 8. 6 Interaction energy of cellulose with bifunctional catalysts having different ratio of acid to base site density, assuming pK_a as 1 and pK_b as 5.75, total site density Γtot as 5 nm^{-2}.213

Figure 8. 7 Critical shear rate ($\gamma *$) as a function of catalyst surface potential, assuming catalyst Hamaker constant is 2×10^{-20} J; cellulose surface potential is -27 mV; cellulose diameter is 1 μm. 215

Figure 9. 1 Schematic of polyelectrolyte enhanced cellulose-solid acid coagulation. 223

Figure 9. 2 Glucose yield as functions of time for different solid acid catalysts: ZSM-22, ZSM-5, Amberlyst-15 and vinyl sulfonic acid. Reaction conditions: 0.2g ball milled cellulose (50 minutes), 0.1 g catalyst, 0.1mL polyDDA, 150 ^{o}C..... 227

Figure 9. 3 Glucose yield as functions of time for celluloas reacting with Amberlyst-15 and ZSM-22. Reaction conditions: 0.2g ball-milled cellulose (50 minutes), 0.1g solid catalyst, 0.1mL polyDDA, 150 ºC..... 228

Figure 9. 4 Measured glucose yield as function of pH after reaction for all tested solid acid catalysts: Amberlyst-15, ZSM-22, ZSM-5 and vinyl sulfonic acid. Circles represent catalysts categories. Data points include 2, 5 and 8 hours reaction..... 230

Figure 9. 5 Schematic showing tow possible explination for improved glucose yield promoted by polyDDA. Green circle represents solid-acid catalysts and gray circle represents cellulose. First pathway is proton attacking cellulose and second pathway is cellulose-solid-acid interaction. The red cross is undesired pathway while green check is desired pathway. 231

Figure 9. 6 Glucose yield for three conditions: Cellulose and Amberlyst-15, cellulose, Amberlyst-15 and polyDDA, cellulose and sulfuric acid (sulfuric acid has the same pH as supernatant). Reaction conditions: 1 hour at 150 ºC..... 232

Figure 9. 7 Ball-milled cellulose reacting with Amberlyst-15 and PolyDDA. PolyDDA concentration is varied as 1 wt%, 2wt%, 3 wt% and 4 wt%. Black line represents cellulose interacting with polyDDA, green data points repreesents cellulose reacting with Amberlyst-15 in the presence of polyDDA, and red data points represents cellulose reacting..... 234

Figure 12. 1 shows the number of annually published articles since 2006. The data was obtained from Web of Science with the search keywords “solid acid catalyst cellulose hydrolysis”..... 282

Figure 12. 2 Schematic of reaction system of lab-scale batch reactor for cellulose hydrolysis. Left is the side view of the glass tube reactor and right is top view for velocity profile..... 284

Figure 12. 3 Shear rate distribution within glass tube reactor. R_o is assumed as 2 cm and inner cylinder radius R_i is 0.5 cm. 285

Figure **12**. 4 ssNMR of Avicel and microcrystalline cellulose treated with guanidinium chloride and ammonium chloride 292

Lists of Tables

Table 3. 1 Physical Properties of Testing Liquids and Mixtures[18, 21-23] 63

Table 3. 2 Surface Energy and Components (mN/m) of PDMS determined by Probe Liquids .. 69

Table 3. 3 Surface Energy and Components (mN/m) of Silane Derivatized Glass 75

Table 4. 1 Resulting mathematical expressions for chemically resolved surface tension of OWRK and vOCG models under different mixing rules..... 98

Table 4. 2 Binary interaction parameters of water-DMSO, water-formamide and water-ethylene glycol using QMRs and MKP mixing rules..... 102

Table 4. 3 Surface tension parameters for selected probe liquids[40] 104

Table 4. 4 Summary of surface free energy (mN/m) determined by liquid mixtures contact angles 114

Table 6. 1 Testing liquid physical properties for determining cellulose surface energy 147

Table 6. 2 Water-dimethyl sulfoxide mixtures properties and penetration constant 150

Table 6. 3 Water-formamide mixtures properties and penetration constant 151

Table 7. 1 Calculated Hamaker constant ($\times 10 - 20$J) for different solid-acid catalysts interacting with cellulose in water using Lifshitz theory..... 178

Table 7. 2 Zeta potential (ζ, mV) of cellulose and selected catalysts from literatures and predicted surface potential ($\psi 02$, mV) 179

Table 8. 1 Hamaker constants and reported zeta potential for representative solid-acid catalysts interacting with cellulose 208

Abstract

Lignocellulose based biomass has become one of the most promising renewable energy sources for potentially replacing fossil fuel-based energy source such as coal and natural gas. Solid-acid catalysts, e.g. carbon, polystyrene or metal oxides are proposed to decompose cellulose into reduced sugares due to their advantages such as ease of separation, recyclability, reusability and cost-effectiveness. However, current design principals for solid-acid mostly focuses on molecular binding of functionalized solid with cellulose. In fact, both cellulose and solid acid catalysts are colloidal particles, meaning interfacial colloidal interaction between cellulose and solid acid catalysts are important rather than molecular interpretation. Unfortunately, interfacial surface interaction at colloidal level remains largely unknown.

The Derjaguin and Landau, Verwey and Overbeek model (D.L.V.O.) is widely used for analyzing colloid surface interactions and designing a colloid system either promoting colloid stability or instability. To apply DLVO analysis to cellulose-solid acid catalysts interaction, van der Waals attractions have to be analyzed beforehand. Surface energy has been used to indirectly determine the Hamaker constant, a constant that dictates strength of van der Waals attraction. However, a common approach that uses pure liquids contact angles has problems associated with surface compatibility, toxicity and evaporation. Here, we have developed a new method which uses contact angles of water-organic solvent (dimethyl sulfoxide, formamide and ethylene glycol) to precisely estimate polymer surface energies components using theories including Owens-Wendt and van Oss. New method has precisely and accurately measured surface energies for polymer surfaces such as PDMS, PMMA and PVC. The success of applying mixtures method on polymer surfaces has motivated us to extend it to biomass particles such as cellulose and chitin. Analysis

shows that mixture approach can result in similar surface energy components to values reported in literatures.

Using determined surface energies values, we calculate the Hamaker constant and apply DLVO theory to rationally design solid-acid catalysts with enhanced capacity for adsorbing cellulose. Results show that cellulose-solid acid particles interaction is favored for the cases where catalysts have a large Hamaker constant (or high surface energy) and low surface charges. A series of recommendations are made for enhancing cellulose-solid acid catalysts adsorption, including using weak acid e.g. pKa > 2-3), high temperature ($T > 150^oC$), bifunctional catalysts with roughly equal amount of acid/base site density and high shear rate (e.g. $> 10\ s^{-1}$). To overcome electrostatic repulsion and increase coagulation, we introduced a cationic polyelectrolyte, poly-diallyldimethyl-ammonium chloride to weaken solid acid surface negative charge (e.g. Amberlyst-15, ZSM-22). Our results show that addition of polyDDA increases product (glucose) yield by roughly 10%.

We then investigate interfacial surface interaction between cellulose with liquid of reaction medium, to enhance surface reactivity. Cellulose is typically mechanically pretreated to remove crystallites prior to acid hydrolysis. However, certain liquids, such as water, can trigger cellulose recrystallization and reduce reactivity. Hydrophobic effects at the water-cellulose interface has motivated us to engineer and control interfacial interactions by adding inorganic/organic salts. Our studies show that salts contribute differently to glucose yield: guanidinium chloride increases glucose yield by around 16% compared to reaction without salts added, while ammonium chloride, lithium chloride increase glucose yield slightly by less than 5%. Further cellulose structure characterization analysis such as X-Ray diffraction and Raman reveals that guanidinium chloride may be able to suppress crystal growth and reduces cellulose crystal size, increasing accessibility while other salts such as lithium chloride and ammonium chloride have little effect on cellulose

crystal size growth. Further, molecular dynamic (MD) simulation analysis shows that guanidinium chloride and HCl suppresses cellulose crystal growth the most while ammonium chloride has helped the growth of cellulose crystal the most. MD simulations have also shown that guanidinium chloride can influence glycosidic bonds angle distribution, revealing its interferes with cellulose chain structures.

Chapter 1

Introduction

1.1 Biomass as Renewable Energy Sources

World energy consumption is projected to increase by 30% by 2026.[1-5] Fossil fuels including petroleum, natural gas and coal are conventionally used for powering the economy. However, policy makers have slowly moved to renewable energy not only because of fear that fossil fuel would eventually be consumed completely, but also the promise to promoting sustainability and addressing climate change issues.[6-9] Among all forms of renewable energy resources, including hydropower, biofuel, wind energy and solar energy, biofuels produced from biomass have gained considerable interests and have been applied in fields such as industry and transporation worldwide.[10-12] Of various biomass sources, lignocellulose takes nearly half of all biomasses by weight. Therefore, decomposing cellulose into monomers becomes a key step in promoting sustainability and solve energy problem.[13, 14]

In effort of decomposing biomass, nationally supported projects, international collaboration are all getting involved in this hot field, attempting to develop economically beneficial catalysts and processes.[15-17] Representative processes include decarboxylation, hydrogenation and purification; and premier catalysts comprise liquid acids/bases, enzymes or solid-acid bearing functional groups.[18-21] Designing and implementing those technologies can be extremely difficult if fundamental knowledge in small-scale (e.g. molecular and colloidal) interactions, including biomass-catalysts, biomass solvent or biomass-biomass interactions are lacking.[22-24]

Fundamental understandingof interactions at biomass-catalysts and biomass-solvents interfaces are the cores for advanced technologies and process development.[25-27] Indeed, sizable companies invest vast amount of funding on research and development (R&D) prior to industrial implementation, and biomass degradation is no exception.[28] Figure 1.1 shows a typical approach for biofuel production starting from R&D and ending in industrial implement. The production of D-glucose from biomass-derived cellulose is an important industry for promoting sustainability.[29-31] Produced D-glucose can be transformed into value-added platform chemicals such as hydroxymethylfurfurals (HMFs) and ethanol.[29, 32] The annual production and assumption of ethanol from biomass increases from 5 billion gallons to 10 million gallons. Successful implementation of industrial process generally starts from pilot-scale R&D facility. When conducting lab-scale trial, it is crucially important to optimize process parameters, including reaction conditions, reactor types, product purifications.

Before pilot-scale production, catalysts are an important part that worth investigating.[33] Due to cellulose's insoluble nature in typical solvents,[34] regardless of catalysts being selected for cellulose decomposition, adsorption, reaction and subsequent desorption all happen at the cellulose-solvent interface.[35] Various catalysts can be selected, including liquid acids, solid acids and enzymes. Solid-acid catalysts have its own advantages over liquid acid and enzymes such as tunable surface groups, separable and recyclable.[30, 36] With cellulose and solid-acid both being colloid particles ranging from 10-100 micrometers, colloidal interactions must be considered when selecting or designing solid catalysts. Not only solid-solid particles interaction, but cellulose structure is also a crucial factor that could impact the process. Therefore, chemistry, or molecular interaction at water/organic solvents interfaces are extremely critical to examine.

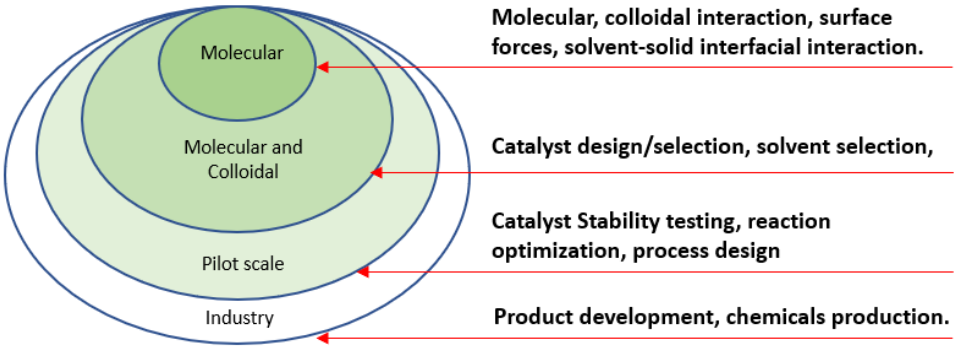

Figure 1.1 Schematics of typical scientific approach to tackle cellulose depolymerizations

In addition, chemistry at solid-solvent interfaces could impact cellulose-solid acid interactions.[37] Considering that cellulose and solid-acid catalysts are all colloid particles, forces such as electrostatic and van der Waals affect how particles interact with each other. Of these two interactions, van der Waals forces is mainly dictated by Hamaker constant, a parameter that is related to surface energy of solid materials.[38, 39] Surfaces with large surface energy, such as metal or metal oxides possess high affinity to attract liquids or other particles[40, 41]. Oppositely, polymer materials e.g. polystyrene or Nafion have small surface energy and thus a small Hamaker constant compared to metal/metal oxide or carbon catalyst.[42] Fundamental knowledge on cellulose and solid-acid surface properties are clearly important.

1.2 Surface Energy Determination Using Liquid Mixtures

Surface energy of biomass particles or other materials are important for cellulose-solvent and cellulose-solid acid interactions.[43, 44] The most striking applications is its use for characterizing interfacial interactions. According to molecular and interfacial theory, surface energy is correlated to the Hamaker constant (A) by an equation, e.g. $\gamma = -A/(24\pi D_o^2)$, where A is Hamaker constant and D_o is minimum separation surfaces are in contact.[45] Clearly, surfaces with large Hamaker

constant will have large interfacial surface energy and tendency to adsorb. Current techniques for measuring surface energies include atomic force microscopy, indention method or drop tower methods.[46, 47] Those methods require precise control and specially designed instrumentation. Contact angle method is most widely used due to its simplicity, and high reproducibility.

Correlating contact angles data with surface energy is a challenging work, especially when selected liquids have diverse molecular structures and physical properties.[48, 49] Therefore, even a small uncertainty goes into contact angle measurements would eventually propagate to a large uncertainty in surface energy determinations.[50] For example, current techniques use a variety of liquids with different physical and chemical properties.[51, 52] Those properties can impact contact angle measurements accuracy and precision. For instance, volatile liquids such as ethanol and methanol are usefor contact angle measurement, but evaloration of droplets during contact angle measurement significantly affect its accuracy.[53-55] Depending on substrate materials, some liquids may not be compatible with substrate materials, forming chemical reaction.

Liquid mixtures have several benefits over pure liquids. The first obvious benefits are that liquid mixtures composition can be adjusted, resulting in systematic variation of molecular interactions changes, and surface tension changes. Depending on individual liquid surface tension, liquid mixtures could have a wide span of surface tension ranges. Moreover, selecting liquids that are compatible with solid surfaces, non-volatile, nontoxic and chemically inert. The main challenge is that liquid surface tension parameters have to be characterized before using them for solid surface energy determination. Mixing rules have been developed starting from van der Waals. Depending on the surface wetting model used, we will characterize those liquids mixtures surface tension parameters using mixing rule.[56, 57]

1.2.1 Liquid Mixtures Method Accommodating Owens, Wendt, Rabel and Kaelble (OWRK) Model

Perhaps, the OWRK method is the most widely used approach to evaluate polymer and hydrocarbon surface energies.[58] Those polymer materials are mostly hydrophobic, meaning London dispersion is the main forces compared to polar interaction.[59, 60] Therefore, OWRK model, which divides surface energy into dispersion and polar, is mainly used for polymer surface energy determination for reasons mentioned before. For years, pure liquids, including water, ethanol and dimethyl sulfoxide are prepared for contact angle measurement. Water is a good choice because it is polar, forming larger contact angles compared to non-polar solvent. However, liquid such as ethanol are low surface tension organic solvent. It tends to form small angles on polymer surfaces, adding uncertainty in contact angle measurements.

Instead of using several (usually > 2) pure liquids, choosing two miscible liquids with varied composition will be beneficial for the reasons mentioned. Challenges is how to obtain mixtures surface tension parameters. Mixing rules such as cubic rules are good starting point as those mixing rules root in molecular interaction, which is origin of surface tension.

1.2.2 Liquid Mixtures Method Accommodating van Oss model

More advanced surface energy models are discussed in Fowkes's groundbreaking paper.[61] In Fowkes discussion, molecular interactions at interfaces include not only dispersion, but also polar interactions that consists of many types, including hydrogen bonding, acid-base interactions, induction. van Oss improved existing OWRK model by further explaining polar interactions. In van Oss discussions, polar interaction is fundamentally a proton donor-acceptor interaction. For example, water is both a proton donor and acceptor liquids; non-polar liquid such

as hexane is neither a strong proton donor nor a strong acceptor.[62] When applied to all organic solvents, proton donors and acceptors are classified as acid-base interaction.

In this sense, van Oss divides polar into acid and base components. But the challenge is that some surfaces are simply protons acceptors instead of protons donors, meaning acid term might be negligible. Therefore, in using pure liquids measuring contact angles and using those angles for acid term calculations, negative value is often obatined. This is not surprising because of its relatively small value compared to the base term. For a long time, researchers have questioned the van Oss model due to its inability to capture the acid term accurately. Improvements are suggested in studies, mainly focusing on credibility of pure liquids used for contact angle measurement. Liquids such as ethanol easily evaporate, casting question on its data quality.

Liquid mixtures approach provide an alternative for van Oss model. First of all, liquid mixture elimitates problems like evaporation and compatbility, improving crediability of data. Most importantly, adjusting composition would supply numerous data points, making data fitting more precise comparing to the case where 3-4 liquids are used.

1.2.3 Liquid Mixture Approach for Determining Biomass Particles Surface Energies

The core application of new surface energy determination technique in on biomass materials. Biomasses are usually in forms of powders. Measuring contact angles by applying droplet on powders would cause problems. For example, even high-pressurized pellet has porosity and roughness that affect integrity of contact angles measurement. Other methods add adhesion agent to force particles tightly bind, but it brings in other compounds which produce erroneous data because unwanted liquid-agents interaction affect surface energy determination. Instead, Washburn method remains the most popular methods for powder wetting characterization. Again, we introduce liquid mixtures method for contact angle measurements.

1.2.4 A Generalized Theory for Quantifying Liquid Mixtures Surface Tension Parameters

Liquid mixture surface tensions data are generated abundantly.[63] Common methods include tensiometer, Noüy ring method and wicking methods.[64-66] Despite those methods are well established for liquid surface tension measurement, surface tension parameters such as polar, dispersive or acid/base components are challenging to measure directly. Molecular dynamics is a powerful tool to extract molecular interaction, but only van der Waals force is defined in common force field such as CHARMM or Amber.[67-70]

Liquid mixtures surface tension parameters can be estimated by using an existing mixing rule. Depending on the number of liquids being mixed, this estimation should accommodate the number of freedoms. Of various mixing rules, Quadratic Mixing Rules (QMRs) and Mathias-Klotz-Prausnitz (MKP) Mixing Rules are two of mostly used rules.[56, 71] Considering that molecular interactions such as polar, dispersive or acid/base interactions are columbic forces fundamentally, applying geometric combing rule, or Berthelot's rule, is reasonable.[72]

1.3 Colloid Particles Surface Charge and Models.

Universally, almost all particles suspending in liquid media will be charged. Charge regulated colloidal interaction is more significant than we thought due to discussions below:

1.3.1 Colloidal Interaction of Cellulose with Solid Acid Catalysts and its Implications

Solid-acid catalysts have been proposed to depolymerize cellulose.[30, 33, 36, 73] The ideal of solid acid comes from enzymes such as exoglucanases, endoglucanases, and β-glucosidase.[74] Those three enzymes work synergistically to peel off cellulose fibers. When examining those enzymes, they have two characteristics. 1). Enzymes have a cellulose binding domain (CBD) that adsorb cellulose.[75, 76] This binding domain ensures cellulase attach to cellulose for subsequent glycosidic bond breaking. 2). Cellulase also a cellulose catalyzing domain (CCD) which performs

glycosidic bond breakage and produce D-glucose units. Based on this unique characteristic of cellulase enzymes, solid-acid catalysts were designed in a way like enzyme's working mechanism.

Typically, hydrogen bonding is used to mimic cellulase's binding domain. Of various hydrogen bonding, chloride (Cl) and hydroxyl group (-OH) are routinely selected for cellulose-solid acid catalysts binding.[73, 77] Meanwhile, sulfonic acid groups are used as catalyzing domains for breaking glycosidic bond. Therefore, various soldi particles, such as polystyrene, Nafion, activated carbon and iron oxides are reported. Functionalizing these particles with CBD and CCD reportedly significantly increases glucose yield.

However, reported by Tyufekchiev,[78] commonly used particles, such as chloromethyl polystyrene with sulfonic acid, are not hydrothermally stable during hydrolysis reaction. This results in leaching homogeneous acids, e.g. hydrochloride acid, which performs hydrolysis reaction and decomposes cellulose. Therefore, observed glucose yield from solid acid is actually an accumulative effect of both homogeneous and heterogeneous catalyzing results. This observation has forced the filed to re-examine design principals for solid acid catalysts.

Solid-acid and cellulose particles are both particles in reaction solvents (e.g. water). The questions come first is how particle-particle interact with each other in a way enzyme does with cellulose. Clearly, both cellulose and solid-acid catalysts are much larger than enzyme because enzymes are in nano-meter scale while cellulose and solid-acid catalysts are tens of micrometers scale. Those length scales follow into colloid domain. Therefore, colloidal interactions must consider for solid-acid catalysts design.

1.4 Polyelectrolyte Promoted Cellulose

Applications of polyelectrolyte for enhancing colloid aggregation has been widely used in industry, those polycations include Nucleic acids, Poly (L-lysine), Poly (L-glutamic acid) and Carrageenan. Mechanism of polycations-induced aggregation is described in Figure 1.2.[79, 80] Polycation chains could confine particles and form patch-like aggregates.[81] Those aggregates' mobility is significantly reduced therefore forms stable aggregations.[82] Polycations also could attract negatively charged particles, bridging particle together and forms particle strands. Those strands can entangle with each other and crosslink, forming coagulation.

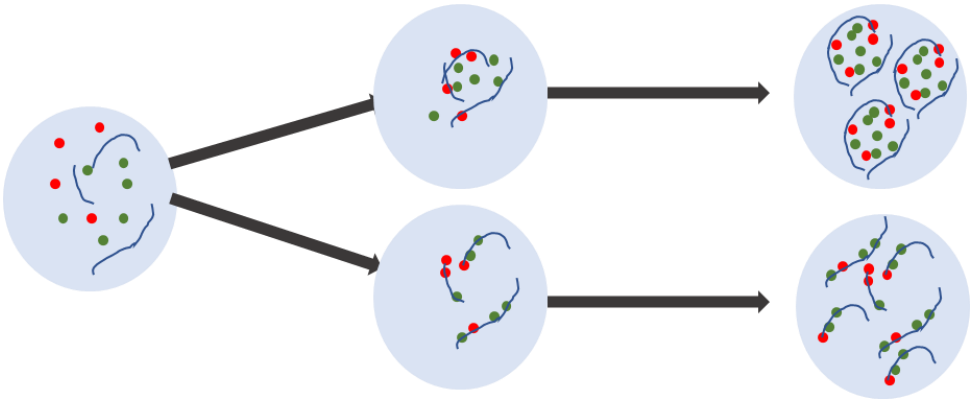

Figure 1. 2 Schemitic of polycations induced colloidal particles aggregations

The observations that cellulose and solid acid disperse and suspend in water have implications that adding polyelectrolyte can break "colloidal stability", promoting cellulose-solid-acid specific aggregation. Although the technique is widely used in pulp industry or composite materials fabrication, researchers in heterogeneous catalysis have not thought in this way.

1.5 Hofmeister Series Salts Promoted Cellulose Hydrolysis Reaction

Solvent-cellulose interactions is crucial for decomposing cellulose because solvent affect cellulose structures and reactivity. Solvents have several properties that affect there interactions with

cellulose, including polarity, swelling ability, dissolving ability and its effect on proton activity. Of those properties, swelling and dissolving capacity of solvents are particularly important. In general sense, solvents that dissolve cellulose would keep fiber chains open for catalysts attack.[34, 83, 84] Water is the typical solvent chosen for cellulose hydrolysis. However, previous study has shown that hydrophobic interaction between water and cellulose can increase cellulose crystalinity and hence reduce reactivity.

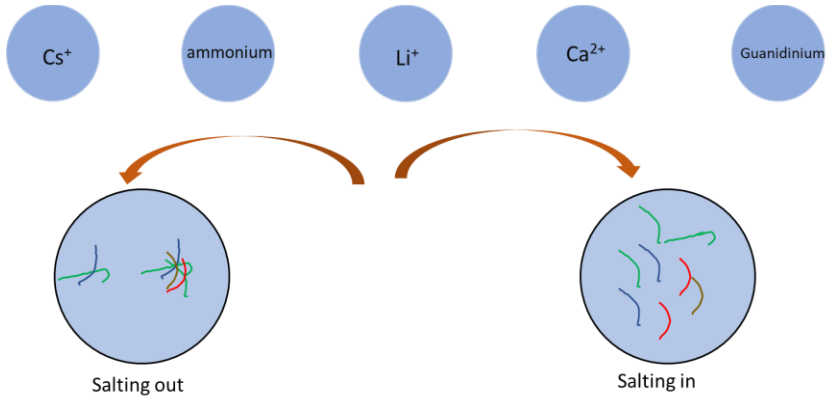

Figure 1. 3 Empirical Hofmeister series for protein solubility, salting-in salts increase protein solubility while salting-out salt precipitates protein

Suppressing cellulose recrystallization becomes one of the keys for pushing glucose yield from cellulose hydrolysis. Organic/inorganic salts are widely studied for their ability to salting-in/salting out proteins.[85-88] Some salts, termed chaotropic salts, can dissolve proteins (Figure 1.3) This behavior is beneficial for keeping amorphous cellulose. Although salts are reported in literatures for promoting cellulose hydrolysis, the mechanism of salt-assist cellulose hydrolysis remains unknown.[89-92]

Reference

1. Criqui, P. and N. Kouvaritakis, *World energy projections to 2030.* International journal of global energy issues, 2000. **14**(1-4): p. 116-136.
2. Aydin, G., *The modeling and projection of primary energy consumption by the sources.* Energy Sources, Part B: Economics, Planning, and Policy, 2015. **10**(1): p. 67-74.
3. Cabeza, L.F., et al., *Comparison of past projections of global and regional primary and final energy consumption with historical data.* Renewable and Sustainable Energy Reviews, 2018. **82**: p. 681-688.
4. Beretta, G.P., *World energy consumption and resources: an outlook for the rest of the century.* International journal of environmental technology and management, 2007. **7**(1-2): p. 99-112.
5. Pérez-Lombard, L., J. Ortiz, and C. Pout, *A review on buildings energy consumption information.* Energy and buildings, 2008. **40**(3): p. 394-398.
6. Oliveira, A.C., *The energy shift: towards a renewable future.* International Journal of Low-Carbon Technologies, 2007. **2**(3): p. 289-299.
7. Sims, R.E., *Renewable energy: a response to climate change.* Solar energy, 2004. **76**(1-3): p. 9-17.
8. Quaschning, V.V., *Renewable energy and climate change*. 2019: John Wiley & Sons.
9. Edenhofer, O., et al., *Renewable energy sources and climate change mitigation: Special report of the intergovernmental panel on climate change*. 2011: Cambridge University Press.
10. Singhvi, M.S., S. Chaudhari, and D.V. Gokhale, *Lignocellulose processing: a current challenge.* Rsc Advances, 2014. **4**(16): p. 8271-8277.

11. Hill, J., *Environmental costs and benefits of transportation biofuel production from food- and lignocellulose-based energy crops: a review.* Sustainable agriculture, 2009: p. 125-139.

12. Blanch, H., *Addressing the need for alternative transportation fuels: the Joint BioEnergy Institute.* 2008.

13. Banerjee, G., J.S. Scott-Craig, and J.D. Walton, *Improving enzymes for biomass conversion: a basic research perspective.* Bioenergy research, 2010. **3**(1): p. 82-92.

14. Saini, J.K., R. Saini, and L. Tewari, *Lignocellulosic agriculture wastes as biomass feedstocks for second-generation bioethanol production: concepts and recent developments.* 3 Biotech, 2015. **5**(4): p. 337-353.

15. Shen, D. and S. Gu, *The mechanism for thermal decomposition of cellulose and its main products.* Bioresource technology, 2009. **100**(24): p. 6496-6504.

16. Girisuta, B., L. Janssen, and H. Heeres, *Kinetic study on the acid-catalyzed hydrolysis of cellulose to levulinic acid.* Industrial & engineering chemistry research, 2007. **46**(6): p. 1696-1708.

17. Wang, K., K.H. Kim, and R.C. Brown, *Catalytic pyrolysis of individual components of lignocellulosic biomass.* Green Chemistry, 2014. **16**(2): p. 727-735.

18. Theander, O., *Chemical analysis of lignocellulose materials.* Animal Feed Science and Technology, 1991. **32**(1-3): p. 35-44.

19. Dedsuksophon, W., et al., *Hydrolysis/dehydration/aldol-condensation/hydrogenation of lignocellulosic biomass and biomass-derived carbohydrates in the presence of Pd/WO3–ZrO2 in a single reactor.* Bioresource technology, 2011. **102**(2): p. 2040-2046.

20. Mansfield, S.D., C. Mooney, and J.N. Saddler, *Substrate and enzyme characteristics that limit cellulose hydrolysis.* Biotechnology progress, 1999. **15**(5): p. 804-816.

21. Tomme, P., R. Warren, and N. Gilkes, *Cellulose hydrolysis by bacteria and fungi.* Advances in microbial physiology, 1995. **37**: p. 1-81.

22. Cho, H.M., A.S. Gross, and J.-W. Chu, *Dissecting force interactions in cellulose deconstruction reveals the required solvent versatility for overcoming biomass recalcitrance.* Journal of the American Chemical Society, 2011. **133**(35): p. 14033-14041.

23. Rodriguez Quiroz, N., et al., *Understanding Acidity of Molten Salt Hydrate Media for Cellulose Hydrolysis by Combining Kinetic Studies, Electrolyte Solution Modeling, Molecular Dynamics Simulations, and 13C NMR Experiments.* ACS Catalysis, 2019. **9**(11): p. 10551-10561.

24. Loerbroks, C., E. Boulanger, and W. Thiel, *Solvent Influence on Cellulose 1, 4-β-Glycosidic Bond Cleavage: A Molecular Dynamics and Metadynamics Study.* Chemistry–A European Journal, 2015. **21**(14): p. 5477-5487.

25. Medronho, B. and B. Lindman, *Competing forces during cellulose dissolution: From solvents to mechanisms.* Current Opinion in Colloid & Interface Science, 2014. **19**(1): p. 32-40.

26. Tarabanko, N., et al., *Electrical Double Layer as a Model of Interaction between Cellulose and Solid Acid Catalysts of Hydrolysis.* ChemPhysChem, 2019. **20**(5): p. 706-718.

27. Zhang, Z., et al., *Rational design of solid-acid catalysts for cellulose hydrolysis using colloidal theory.* Physical Chemistry Chemical Physics, 2021. **23**(17): p. 10236-10243.

28. Ahmad, J., et al., *Techno economic analysis of a wind-photovoltaic-biomass hybrid renewable energy system for rural electrification: A case study of Kallar Kahar.* Energy, 2018. **148**: p. 208-234.

29. Wang, Y., C.A. Brown, and R. Chen, *Industrial production, application, microbial biosynthesis and degradation of furanic compound, hydroxymethylfurfural (HMF).* AIMS microbiology, 2018. **4**(2): p. 261.

30. Onda, A., T. Ochi, and K. Yanagisawa, *Selective hydrolysis of cellulose into glucose over solid acid catalysts.* Green Chemistry, 2008. **10**(10): p. 1033-1037.

31. Fan, L.-t., M.M. Gharpuray, and Y.-H. Lee, *Cellulose hydrolysis*. Vol. 3. 2012: Springer Science & Business Media.

32. Li, M., et al., *High conversion of glucose to 5-hydroxymethylfurfural using hydrochloric acid as a catalyst and sodium chloride as a promoter in a water/γ-valerolactone system.* RSC advances, 2017. **7**(24): p. 14330-14336.

33. Huang, Y.-B. and Y. Fu, *Hydrolysis of cellulose to glucose by solid acid catalysts.* Green chemistry, 2013. **15**(5): p. 1095-1111.

34. Liebert, T., *Cellulose solvents–remarkable history, bright future*, in *Cellulose solvents: for analysis, shaping and chemical modification*. 2010, ACS Publications. p. 3-54.

35. Inglezakis, V. and S. Poulopoulos, *Adsorption, ion exchange and catalysis*. Vol. 3. 2006: Elsevier.

36. Lai, D.m., et al., *Hydrolysis of cellulose into glucose by magnetic solid acid.* ChemSusChem, 2011. **4**(1): p. 55-58.

37. Medronho, B. and B. Lindman, *Brief overview on cellulose dissolution/regeneration interactions and mechanisms.* Advances in colloid and interface science, 2015. **222**: p. 502-508.

38. Bergström, L., et al., *Spectroscopic ellipsometry characterisation and estimation of the Hamaker constant of cellulose.* Cellulose, 1999. **6**(1): p. 1-13.

39. Notley, S.M., B. Pettersson, and L. Wågberg, *Direct measurement of attractive van der Waals' forces between regenerated cellulose surfaces in an aqueous environment.* Journal of the American Chemical Society, 2004. **126**(43): p. 13930-13931.

40. Kuang, Q., et al., *High-energy-surface engineered metal oxide micro-and nanocrystallites and their applications.* Accounts of chemical research, 2014. **47**(2): p. 308-318.

41. Zhou, Z.-Y., et al., *Nanomaterials of high surface energy with exceptional properties in catalysis and energy storage.* Chemical Society Reviews, 2011. **40**(7): p. 4167-4185.

42. Paul, D.K., et al., *Characteristics of self-assembled ultrathin Nafion films.* Macromolecules, 2013. **46**(9): p. 3461-3475.

43. Samyn, P., *Wetting and hydrophobic modification of cellulose surfaces for paper applications.* Journal of Materials Science, 2013. **48**(19): p. 6455-6498.

44. Whang, H.S. and B.S. Gupta, *Surface wetting characteristics of cellulosic fibers.* Textile Research Journal, 2000. **70**(4): p. 351-358.

45. Israelachvili, J.N., *Intermolecular and surface forces*. 2015: Academic press.

46. Calvimontes, A., *The measurement of the surface energy of solids using a laboratory drop tower*. npj Microgravity, 2017. **3**(1): p. 1-14.

47. Zubar, T., et al., *Method of surface energy investigation by lateral AFM: application to control growth mechanism of nanostructured NiFe films.* Scientific reports, 2020. **10**(1): p. 1-10.

48. Zhang, Z., et al., *Binary liquid mixture contact-angle measurements for precise estimation of surface free energy.* Langmuir, 2019. **35**(38): p. 12317-12325.

49. Rudawska, A. and E. Jacniacka, *Evaluating uncertainty of surface free energy measurement by the van Oss-Chaudhury-Good method.* International Journal of Adhesion and Adhesives, 2018. **82**: p. 139-145.

50. Vuckovac, M., et al., *Uncertainties in contact angle goniometry.* Soft Matter, 2019. **15**(35): p. 7089-7096.

51. Chibowski, E. and M. Jurak, *Comparison of contact angle hysteresis of different probe liquids on the same solid surface.* Colloid and polymer science, 2013. **291**(2): p. 391-399.

52. Taherian, F., et al., *What is the contact angle of water on graphene?* Langmuir, 2013. **29**(5): p. 1457-1465.

53. Fan, L.T., et al., *Contact angle of ethanol and n-propanol aqueous solutions on metal surfaces.* Chemical engineering & technology, 2011. **34**(9): p. 1535-1542.

54. Sefiane, K., L. Tadrist, and M. Douglas, *Experimental study of evaporating water–ethanol mixture sessile drop: influence of concentration.* International journal of heat and mass transfer, 2003. **46**(23): p. 4527-4534.

55. Wang, Z., et al., *Evaporation of ethanol-water mixture drop on horizontal substrate.* Drying Technology, 2008. **26**(6): p. 806-810.

56. Zabaloy, M.S., *Cubic mixing rules.* Industrial & engineering chemistry research, 2008. **47**(15): p. 5063-5079.

57. Kwak, T. and G. Mansoori, *Van der Waals mixing rules for cubic equations of state. Applications for supercritical fluid extraction modelling.* Chemical engineering science, 1986. **41**(5): p. 1303-1309.

58. Owens, D.K. and R. Wendt, *Estimation of the surface free energy of polymers.* Journal of applied polymer science, 1969. **13**(8): p. 1741-1747.

59. Bucko, T., et al., *Improved density dependent correction for the description of London dispersion forces.* Journal of chemical theory and computation, 2013. **9**(10): p. 4293-4299.

60. Ángyán, J., et al., *London dispersion forces in molecules, solids and nano-structures: an introduction to physical models and computational methods*. 2020: Royal Society of Chemistry.

61. Fowkes, F.M., *Dispersion force contributions to surface and interfacial tensions, contact angles, and heats of immersion.* 1964, ACS Publications.

62. Della Volpe, C. and S. Siboni, *Acid–base surface free energies of solids and the definition of scales in the Good–van Oss–Chaudhury theory.* Journal of Adhesion Science and Technology, 2000. **14**(2): p. 235-272.

63. Christmann, K., *Introduction to surface physical chemistry*. Vol. 1. 2013: Springer Science & Business Media.

64. Hartland, S., *Surface and interfacial tension: measurement, theory, and applications*. 2004: CRC Press.

65. YIN, D.-x., P.-s. MA, and S.-q. XIA, *Progress on methods for measuring surface tension of liquids.* Bulletin of Science and Technology, 2007. **3**(23): p. 424-33.

66. Tian, Y., R.G. Holt, and R.E. Apfel, *A new method for measuring liquid surface tension with acoustic levitation.* Review of scientific instruments, 1995. **66**(5): p. 3349-3354.

67. Robustelli, P., S. Piana, and D.E. Shaw, *Developing a molecular dynamics force field for both folded and disordered protein states.* Proceedings of the National Academy of Sciences, 2018. **115**(21): p. E4758-E4766.

68. Vanommeslaeghe, K., et al., *CHARMM general force field: A force field for drug‐like molecules compatible with the CHARMM all‐atom additive biological force fields.* Journal of computational chemistry, 2010. **31**(4): p. 671-690.

69. Caleman, C., et al., *Force field benchmark of organic liquids: density, enthalpy of vaporization, heat capacities, surface tension, isothermal compressibility, volumetric expansion coefficient, and dielectric constant.* Journal of chemical theory and computation, 2012. **8**(1): p. 61-74.

70. Terzis, A., et al., *Characterisation of acid–base surface free energy components of urea–water solutions.* Colloids and Surfaces A: Physicochemical and Engineering Aspects, 2018. **538**: p. 774-780.

71. Valderrama, J.O., *The state of the cubic equations of state.* Industrial & engineering chemistry research, 2003. **42**(8): p. 1603-1618.

72. Forsman, J. and C.E. Woodward, *Limitations of the Derjaguin approximation and the Lorentz− Berthelot mixing rule.* Langmuir, 2010. **26**(7): p. 4555-4558.

73. Shuai, L. and X. Pan, *Hydrolysis of cellulose by cellulase-mimetic solid catalyst.* Energy & Environmental Science, 2012. **5**(5): p. 6889-6894.

74. Jayasekara, S. and R. Ratnayake, *Microbial cellulases: an overview and applications.* Cellulose, 2019. **22**.

75. Tormo, J., et al., *Crystal structure of a bacterial family-III cellulose-binding domain: a general mechanism for attachment to cellulose.* The EMBO journal, 1996. **15**(21): p. 5739-5751.

76. Ciolacu, D., J. Kovac, and V. Kokol, *The effect of the cellulose-binding domain from Clostridium cellulovorans on the supramolecular structure of cellulose fibers.* Carbohydrate research, 2010. **345**(5): p. 621-630.

77. Zeng, M. and X. Pan, *Insights into solid acid catalysts for efficient cellulose hydrolysis to glucose: progress, challenges, and future opportunities.* Catalysis Reviews, 2020: p. 1-46.

78. Tyufekchiev, M., et al., *Cellulase-inspired solid acids for cellulose hydrolysis: structural explanations for high catalytic activity.* Acs Catalysis, 2018. **8**(2): p. 1464-1468.

79. Bayraktutan, T., Y. Onganer, and K. Meral, *Polyelectrolyte-induced H-aggregation of Merocyanine 540 and its application in metal ions detection as a colorimetric sensor*. Sensors and Actuators B: Chemical, 2016. **226**: p. 52-61.

80. Alfano, J.C., et al., *Polyelectrolyte-induced aggregation of microcrystalline cellulose: reversibility and shear effects.* Journal of colloid and interface science, 2000. **223**(2): p. 244-254.

81. Breen, C., *The characterisation and use of polycation-exchanged bentonites.* Applied Clay Science, 1999. **15**(1-2): p. 187-219.

82. Vogt, C.d., et al., *Mobility of proteins in highly hydrated polyelectrolyte multilayer films.* The Journal of Physical Chemistry B, 2012. **116**(17): p. 5269-5278.

83. Sathitsuksanoh, N., A. George, and Y.H.P. Zhang, *New lignocellulose pretreatments using cellulose solvents: a review.* Journal of Chemical Technology & Biotechnology, 2013. **88**(2): p. 169-180.

84. Liu, L. and H. Chen, *Enzymatic hydrolysis of cellulose materials treated with ionic liquid [BMIM] Cl.* Chinese Science Bulletin, 2006. **51**(20): p. 2432-2436.

85. Okur, H.I., et al., *Beyond the Hofmeister series: Ion-specific effects on proteins and their biological functions.* The Journal of Physical Chemistry B, 2017. **121**(9): p. 1997-2014.

86. Piazza, R. and M. Pierno, *Protein interactions near crystallization: a microscopic approach to the Hofmeister series.* Journal of Physics: Condensed Matter, 2000. **12**(8A): p. A443.

87. Hyde, A.M., et al., *General principles and strategies for salting-out informed by the Hofmeister series.* Organic Process Research & Development, 2017. **21**(9): p. 1355-1370.

88. Leberman, R., *The Hofmeister series and ionic strength.* FEBS letters, 1991. **284**(2): p. 293-294.

89. Jiang, Z., et al., *Mechanistic understanding of salt-assisted autocatalytic hydrolysis of cellulose.* Sustainable Energy & Fuels, 2018. **2**(5): p. 936-940.

90. Liu, L., et al., *Corn stover pretreatment by inorganic salts and its effects on hemicellulose and cellulose degradation.* Bioresource technology, 2009. **100**(23): p. 5865-5871.

91. Salajková, M., L.A. Berglund, and Q. Zhou, *Hydrophobic cellulose nanocrystals modified with quaternary ammonium salts.* Journal of Materials Chemistry, 2012. **22**(37): p. 19798-19805.

92. vom Stein, T., et al., *Salt-assisted organic-acid-catalyzed depolymerization of cellulose.* Green Chemistry, 2010. **12**(10): p. 1844-1849.

Chapter 2

Objective and Approach

2.1 Objectives

This work is motivated by promoting lignocellulose-based renewable energy production to replace fossil fuel energy at least partially. This will allow us to create a sustainable environment where net carbon release is neutralized. This thesis seeks to rationalize emerging new catalysts-solid acid design. Currently strategies focus on molecular interactions but lacking colloid and interfacial interaction interpretation. To better understand colloid interaction of cellulose particles with solid-acid such as zeolite or functionalized polystyrene, cellulose surface properties such as surface energy is directly related to Hamaker constant, a constant used for analyzing colloidal interaction. Hamaker constant is related to solid surface free energy, e.g. Hamaker constant of solid-liquid interaction is related to liquid-solid interfacial surface energy while solid-solid interaction relates to solid surface energy. Building on DLVO analysis, we further investigate how polycations affect cellulose-solid acid catalysts. The last part of the objective is focused on cellulose-solvent (with salt added) interaction. Therefore, specific objectives are:

1) The first objective is to develop a new method to estimate surface energy using contact angle measurements. New method relies on using water-organic solvent (formamide, dimethyl sulfoxide and ethylene glycol) for contact angles measurement. Those angles will be combined with wetting theory for obtaining surface energy components.
2) Second objective focuses on using estimated surface energy and surface potential to model colloidal interaction between cellulose and solid acid catalysts. Recommendations are suggested for designing solid acid catalysts capable of attracting cellulose.

3) The third objective is to tune particles surface charges with polycations for promoting particle-particle coagulation. Adding polyelectrolyte would change solid acid catalysts surface change density. Identifying a proper polycation dosage which neutralizes surface charge will enhance particle coagulations. Therefore, further systematic surface potential/zeta potential of particles with various polycations dosage is recommended.
4) Not only particle-particle interaction is important, but studies also show that solvent-cellulose interaction will have great impact on cellulose reactivity. Previous studies have found that cellulose instantly re-crystallizes in hydrolysis reaction, decreasing reactivity and limits maximum glucose yield. First goal is to change water environment by adding salts and evaluate its performance on cellulose degradation.
5) Based on cellulose hydrolysis performance, the next objective is to gain cellulose structure analysis under salts treatment and interpret/relate structure changes to glucose yield.

2.2 Method and Approach

To achieve above objectives, the following experiments were carried out:

1) Measuring contact angles of water-dimethyl sulfoxide, water-formamide and water-ethylene glycol on smooth PDMS. Using those data along with Owens-Wendt wetting model, surface energy will be obtained and validated by comparing with pure liquid method.
2) To extend binary mixture method, a generalized mixing rule is to create to extract more detailed surface tension parameters with complicated molecular interaction such as polar, dispersive, acid and base. To validate method further, polymer surfaces with various hydrophobicity (PDMS, PVC, PMMA) are tested. Surface energies components will be compared against literature values.

3) After validating binary mixture method, it is extended to biomass particles. Capillary penetration of liquid mixture (with varied composition) in column packed with cellulose and chitin will be collected and used later on for surface energy analysis.
4) To model DLVO interaction between cellulose and solid acid, besides surface energy and Hamaker constant, solid acid surface potential was modeled and used for calculations. DLVO energy barrier (electrostatic repulsion) will be computed under different conditions such as particle size, ionic strength, *pH*, acid *pKa* and acid/base site density). Each condition will be discussed in detail and desired conditions will be specified.
5) Polycations will be added to solid acid-cellulose system. Glucose yield under different polycation dosage will be analyzed. Zeta potential of solid acid in the presence of polycation is to be measured.
6) Salts are selected based on Hofmeister series. Salts are added into reaction system to evaluate their ability for promoting glucose yield. Then cellulose structure changes will be evaluated using XRD, Raman and solid-state NMR. Best performed and worst performed salts will be further analyzed using molecular dynamics.

Chapter 3

Binary Liquid Mixture Contact-Angle Measurements for Precise Estimation of Surface Free Energy

3.1 Abstract

Surface free energy remains a fundamental material property to characterize the interfacial interactions between liquid and solid. Here, we developed a precise approach to determine surface energy by using contact angles of binary mixtures of water-dimethyl sulfoxide, water-formamide, water-ethylene glycol and water-glycerol and analyzed using the Owens-Wendt method. A mixing equation was developed to estimate liquid dispersive surface tension ($\gamma^{d}_{L,mix}$) and polar surface tension ($\gamma^{p}_{L,mix}$) parameters for binary mixtures. To test the approach, two hydrophobic surfaces, flat PDMS and silane-derivatized glass were prepared and the contact angle of mixtures on the surfaces were obtained. Surface energy of PDMS determined by three binary mixtures agrees with that from pure solvents, but the uncertainty decreases to less than 13%; remarkably, the uncertainty drops to around 5% once we combined measured contact angles from all the mixtures, namely, water-dimethyl sulfoxide, water-formamide and water-ethylene glycol. Surface energies of silane-derivatized glass bearing ethyl (C_2), hexyl (C_6) and octadecyl (C_{18}) alkyl chains were determined with water-formamide and water-glycerol mixtures. Measured contact angles fit the Owens-Wendt model, and surface energy value determined from different binary mixtures agree with each other within error. Contact angle measurements of liquid mixtures is a simple method for determination of surface energy that improves the precision of surface energy determined be measurements of multiple pure solvents.

3.2 Introduction

Surface free energy (SFE) is an important parameter for applications that relate to adhesion,[1] binding affinity,[2] adsorption,[3] and interfacial intermolecular forces.[4] Measurement of surface energy is non-trivial, and the field has attracted intense interest for many years.[5] Several studies[6, 7] describe the use of atomic force microscopy (AFM) to measure force-distance curves of liquid-solid interfaces and subsequent determination of surface energy by analysis of these data. Similarly, Xu *et al.*[8] described an indentation technique in which a solid film is indented by a rigid sphere and its deflection is measured by optical interferometry. Analysis of the indentation data using nonlinear von Karman plate theory provides an estimate of surface energy. However, use of these methods remains limited due to their difficulty and requirement of specialized instrumentation.

To date, the most widely used method of determining surface energy is based on measurement of the liquid-solid contact angle.[9, 10] When measured for a single liquid (typically water), contact angle provides a measure of the relative hydrophobicity or hydrophilicity of a surface. Sometimes, this is sufficient, but in many others quantitative knowledge of the surface energy is required. Typically, surface energy is calculated by combining contact angles of multiple liquids measured on a single surface with theoretical models such as the Owens-Wendt model,[11] Zisman method,[12] or Neumann method.[13] The main advantages of the contact angle measurement method include speed, convenience, and the low cost of the necessary instrumentation.

The precision of surface energy determined using the multiple liquid approach depends on the number of liquids that can be tested, and the range of appropriate liquids is limited by several considerations. First, the method requires detailed liquid surface tension data, which are available

only for select liquids; likewise, uncertainty in these values contributes to uncertainty in the determination of surface energy.[14] Additionally, the liquids should be non-volatile, as rapid evaporation introduces uncertainty into the contact angle measurement.[15] Lastly, test liquids should be non-toxic and not interact chemically with the surface under investigation.[16] Only a handful of liquids satisfy these requirements for any given surface, thereby placing a practical limit on the precision of surface energy determinations made using the multiple liquid contact angle approach.[10, 14]

Several researchers have suggested the use of liquid mixtures to effectively expand the amount of data that can be obtained using the multiple liquid approach, thereby potentially improving the precision of surface energy measurements.[17, 18] The advantage of using mixtures is that surface tension properties of the test liquid mixture can be adjusted over a continuous range by systematic variation of mixture composition.[17] For binary mixtures, two pure liquids, each of which is inert, nontoxic, and nonvolatile, can be selected and tested across the entire composition range to provide sufficient data points to increase the precision of the surface energy measurement. Although the feasibility of using liquids mixtures has been discussed in the literature, the approach has not been pursued due to concerns over potential preferential adsorption between individuals liquid to the solid surface.[9, 13]

The purpose of the present study is to examine whether contact angle measurements of binary mixtures consisting of water and an organic liquid can be used to determine surface free energy. Four different binary mixtures, water-dimethyl sulfoxide, water-formamide, water-glycerol, and water-ethylene glycol were prepared over a range of compositions. Composition-dependent surface tensions of the various binary mixtures were calculated by a newly defined mixing equation.[19] Static contact angles were measured on two model surfaces: flat

polydimethylsiloxane (PDMS) and silane-functionalized glass slides. The contact angle data were then interpreted to determine surface energies using a form of the Owens-Wendt model[10] modified to accommodate liquid mixtures. The results of this study can be used as the basis for a new, precise method to estimate surface energy that uses the simple contact angle measurement technique.

3.3 Experimental

Materials: Glycerol (99.5 %), ethylene glycol (99.8%) and benzyl alcohol (analytical standard) were purchased from Sigma-Aldrich Corporation (Natick, MA), dimethyl sulfoxide (DMSO) was purchased from AMRESCO, Inc. (Solon, OH), and formamide (99.5%) was purchased from Alfa Aesar (Ward Hill, MA). Water was de-ionized prior to use on a Millipore Synergy UV water purification system (Billerica, MA) to a minimum resistivity of 17.9 MΩ•cm. The Sylgard 184 silicone elastomer kit consisting of polydimethylsiloxane (PDMS) elastomer and hardener was purchased from Dow Corning (Midland, MI) was used to prepare PDMS surfaces. Alkyl silanes were obtained from Gelest (Morrisville, PA). Glass slides (22 × 40 mm) were purchased from Globe Scientific Inc. (Mahwah, NJ). Silicon wafer was purchased from Virginia Semiconductor (Fredericksburg, VA).

3.3.1 Polydimethylsiloxane Preparation

The PDMS pre-polymer mixture was prepared by mixing the elastomer and hardener in a 10:1 ratio. To form the surface, polymer was cast on a flat 76.3 mm diameter silicon wafer. The wafer was cleaned in piranha solution, consisting of sulfuric acid and hydrogen peroxide in a 3:1 ratio, for 1.0 hour *(Safety note: piranha solution reacts violently with organic compounds and should not be stored in closed containers.)* The cleaned silicon wafer was thoroughly rinsed with DI water and ethanol, dried under a stream of nitrogen, and immediately placed at the bottom of a

polystyrene Petri dish (Corning Inc., Corning, NY). The PDMS mixture was cast onto the wafer, degassed in a vacuum oven at 25 mmHg of pressure for two hours and finally baked for five hours at 70 °C. After cooling, the PDMS was removed from the polymer cast, resulting in a PDMS surface that replicated the flat wafer surface.

3.3.2 Functionalized Glass Substrates

Glass slides were to provide a flat, nonporous ~~glass~~ surface for functionalization. Before functionalization, the slides were cleaned by a piranha solution (3:7, H_2O_2: H_2SO_4) and rinsed with water and methanol. The derivatization solution consisted of 5 mM toluene solutions of the alkyltrichlorosilane (either OTS, HTS, and ETS). The cleaned glass slides were immersed in the silane solution and gently stirred for 24 h to derivatize the surface. The coated slide was rinsed with toluene and dried at 100 °C overnight.

3.3.3 Mixture Preparations

Glycerol, DMSO, ethylene glycol and formamide were chosen as the liquids to prepare the aqueous liquid mixtures. Binary liquid mixtures were made consisting of water and one of the organics in varying proportions. A total of 6 compositions were prepared for each mixture, ranging from pure water to pure organic, with increments of 0.2 mole fraction units. Mixtures were magnetically stirred thoroughly prior to contact angle measurement.

3.3.4 Contact Angle Measurement

Contact angle measurements were performed using a Ramé-Hart Automated Dispensing System (Netcong, NJ; Model No. 100-00) with Rame-Hart Drop Image Standard v.2.0.10 software for analysis. Droplet volumes were consistently 5 µL regardless of the mixture or surface. Care was taken to ensure the precision of the measurement, including conducting the measurement within

minutes of removing the PDMS from the mold (and using the freshly exposed side), gently placing the test droplet on the surface, and visually inspecting the PDMS surface for contaminants after each measurement. Contact angle measurements were performed three times for each solution on different locations of each surface. Liquids were evaluated in random sequence to avoid introduction of sampling artifacts.

3.4 Theory

Several methods[10] have previously been used to determine the surface free energy (SFE) of a solid. The basis of most of these methods is Young's equation,[20] a thermodynamic approach that minimizes the total interfacial energy between the solid (S), liquid (L), and gas (G) phases:

$$\gamma_{SG} = \gamma_{SL} + \gamma_{LG}\cos(\theta) \qquad [3.1]$$

where γ_{SG}, γ_{SL} and γ_{LG} represent the interfacial surface tension of solid-gas, solid-liquid, and liquid-gas interfaces, respectively. Young's equation is inherently a mechanical expression which does not take into account chemical aspects of the liquid-solid interaction. Fundamentally, wetting is a chemo-mechanical phenomenon, and models which account for chemical interactions have greater explanatory power and have the potential to be more predictive than purely mechanical theories. Accordingly, several models use Equation (3.1) as the starting point to capture the chemical aspects of solid-liquid and liquid-gas interactions that give rise to the macroscopic contact angle behavior.[10] One of the most common chemical models is the Owens-Wendt method.[11] The Owens-Wendt method divides the surface energy into contributions from dispersive and polar interactions (e.g. $\gamma_S = \gamma_S^d + \gamma_S^p$) to obtain the following geometric-mean relationship for solid-liquid interfacial surface tension (γ_{SL}):

$$\gamma_{SL} = \gamma_S + \gamma_L - 2\sqrt{\gamma_S^d \gamma_L^d} - 2\sqrt{\gamma_S^p \gamma_L^p} \qquad [3.2]$$

Substituting Equation (3.2) into Young's equation results in the Owens-Wendt contact angle model:

$$\frac{\gamma_L(1+\cos\theta)}{2\sqrt{\gamma_L^p}} = \sqrt{\frac{\gamma_L^d}{\gamma_L^p}}\sqrt{\gamma_S^d} + \sqrt{\gamma_S^p} \qquad [3.3]$$

Equation (3.3) can be recast as a linear expression for direct evaluation of surface energy with $\frac{\gamma_L(1+\cos\theta)}{2\sqrt{\gamma_L^p}}$ as the dependent variable and $\sqrt{\frac{\gamma_L^d}{\gamma_L^p}}$ is the independent variable. Accordingly, the square of the slope of the linearized Owens-Wendt plot is γ_S^d and the square of the intercept is equal to γ_S^p.

Using the Owens-Wendt's approach requires contact angle data from at least two liquids with known γ_L^d and γ_L^p to determine values for the two unknowns, γ_S^d and γ_S^p. Ideally, data from many more than two liquids can be used to improve the precision of the estimates of γ_S^d and γ_S^p by fitting the data to the linearized form of the Owens-Wendt equation. When using a small number of liquids, uncertainty arises both from random errors but – more importantly – from systematic errors associated with attempting to model the complex chemical phenomenon of surface wetting using just two parameters. Unfortunately, limitations on liquid selection – i.e., they should be nontoxic, readily available, non-volatile, non-reactive, non-surface swelling, sufficiently studied – present a challenge, as the number of pure liquids that meet these criteria is necessarily finite. In practice, only a handful of liquids are used in most studies, including water, diiodomethane, bromobenzene, nitromethane, bromonaphthalene, formamide, DMSO, glycerol and ethylene glycol, toluene, *n*-hexane, etc.[10, 12, 21-23] Of these, diiodomethane, bromobenzene, nitromethane and bromonaphthalene are toxic, meaning that their use should be minimized when possible. Non-polar liquids such as toluene and *n*-hexane are volatile and swell common polymer

test surfaces such as PDMS.[24] Because of these restrictions, only a limited range of liquids are available for contact angle measurement, including water, DMSO, formamide, glycerol and ethylene glycol.

Modifying the Owens-Wendt method to permit its use for binary liquid mixtures, the focus of this work, can be of great practical use to the field. Unlike using pure liquids – which can provide only a handful of discrete points, [10, 14, 21] using binary liquids can allow acquisition of many data points simply by changing the composition of the mixture for determining best-fit parameters in the Owens-Wendt model. Moreover, studying wetting for binary mixtures permits acquisition of multiple data points without introduction of multiple types of liquid-surface interactions, as would be the case if multiple pure liquids were used. Since liquid-surface interactions are more complex than can be fully captured in a two-parameter model such as the one proposed by Owens-Wendt, the simplification of binary mixtures may reasonably be expected to improve precision – provided that suitable models can be developed to describe the surface energy of the liquid mixture itself.

In the liquid mixture approach, the forms of Equations (3.2) and (3.3) remain unchanged, with the only modification being that effective mixture gas-liquid surface tensions are used in place of their pure component values. Accordingly, the approach requires 1) pure component surface tension data, including γ_L^d and γ_L^p, for the liquids to be used 2) composition-dependent gas-liquid surface tension values appropriate for the mixture(s) in question and 3) a method to convert pure component surface tension parameters to describe the polar and dispersive components of the mixture surface tension, which we term $\gamma_{L,mix}^d$ and $\gamma_{L,mix}^p$. Since γ_L^d and γ_L^p are available for several pure liquids,[24] the focus falls on availability of composition-dependent surface tension data γ_L and decomposing these data into dispersive and polar contributions.

The correlation method reported by Connors and Wright[18] has been widely used to estimate composition dependent values of γ_L. In their approach, Connors and Wright[19] assumed that (i) gas-liquid interactions can be described by assuming that the organic component can exist in either free or adsorbed states and (ii) both states contribute equally to the surface tension so that the number of binding sites is proportional to the number of water molecules. The resulting equation to determine the mixture surface tension, $\gamma_{L,mix}$, of a binary mixture (consisting of components "1" and "2") is:

$$\gamma_{L,mix} = \gamma_L^1 - \left(1 + \frac{bx_1}{1 - ax_1}\right)(x_2)(\gamma_L^1 - \gamma_L^2) \quad [3.4]$$

where x_i is the molar fraction of each liquid component, γ_L^2 is the pure liquid surface tension of component *i, a* and *b* are combined partition coefficient parameters reported by Connors and Wright[18] for many relevant liquids.

Using Equation (3.3) requires decomposition of γ_L into its dispersive and polar components. The γ_L^d and γ_L^p parameters are not generally available for mixtures, which means that a method is required to convert pure-component values into mixture values. Fowkes[25] proposed that the dispersion interactions between dissimilar liquids is the geometric mean of their individual dispersive surface tensions, as shown by Equation (3.5):

$$\gamma_{L,mix}^d = (\gamma_L^{d,1} \cdot \gamma_L^{d,2})^{1/2} \quad [3.5]$$

where $\gamma_L^{d,1}$ and $\gamma_L^{d,2}$ are the dispersive surface tension of pure liquid 1 and 2, respectively; $\gamma_{L,mix}^d$ is the dispersive component to the surface tension of the resulting mixture. Equation (3.5) establishes a theoretical basis for estimating $\gamma_{L,mix}^d$ from pure component values as the geometric mean of the pure-component values, yet it does not consider the effect of mixture composition. Mixing rules

used for many years for pressure-volume-temperature predictions of non-ideal gas behavior provide inspiration.[26] To extend the van der Waals equation of state to mixtures, Berthelot[27] suggested use of mixture "*a*" and "*b*" parameters based on pure component values. To estimate the value of the attractive van der Waals *a* mixture term, Berthelot[27] suggested using the geometric mean of the pure component attractive *a* parameter, an approach which is analogous to the recommendation by Fowkes[25] that has been found accurate for dissimilar molecules which interact with one another primarily by dispersive interactions. The Berthelot[28] mixing rule takes the form:

$$a_{mix} = \sum_{i}^{n} \sum_{j}^{n} x_i x_j \, a_{ij} \qquad [3.6]$$

where a_{mix} is the attractive term appropriate for the mixture, x_i and x_j are the mole fractions of component *i* and *j*, and a_{ij} is given as:

$$a_{ij} = \left(1 - \delta_{ij}\right)\sqrt{a_i a_j} \qquad [3.7]$$

where a_i and a_j are the van der Waals parameters of the pure fluids and δ_{ij} is an empirical fitting parameter, sometimes termed the binary interaction parameter. By equating the van der Waals *a* terms with the dispersive component of the surface tension (i.e., $a_i = \gamma_L^{d,i}$), the form of the Berthelot mixing rule can be adopted for modeling dispersive component of the surface tension $\gamma_{L,mix}^{d}$:

$$\gamma_{L,mix}^{d} = x_1^2 \gamma_L^{d,1} + 2x_1 x_2 (1 - \delta_{12}) \left(\gamma_L^{d,1} \gamma_L^{d,2}\right)^{1/2} + x_2^2 \gamma_L^{d,2} \qquad [3.8]$$

The polar component of the mixture surface tension $\gamma_{L,mix}^{p}$, can then be calculated by difference:

$$\gamma_{L,mix}^{p} = \gamma_{L,mix} - \gamma_{L,mix}^{d} \qquad [3.9]$$

recalling that the sum of the polar and dispersive components must equal to $\gamma_{L,mix}$.

Equations (3.8) and (3.9) allow convenient calculation of $\gamma_{L,mix}^{d}$ and $\gamma_{L,mix}^{p}$ for any binary mixture given $\gamma_{L,mix}$ and pure component values of γ_{L}^{d} and γ_{L}^{p}. In principle, $\gamma_{L,mix}$ can be based on experimental measurements or predicted using Equation (3.4). Furthermore, combined use of Equations (3.3), (3.8), and (3.9) allows estimation of solid surface energy parameters, i.e., γ_{S}^{d} and γ_{S}^{p}, based on a set of contact angles measured for binary mixtures with varying compositions.

As is common practice for pressure-volume-temperature equations of state, the value of δ_{12} that appears in Equation (3.8) can be adjusted to fit available data. Fitting δ_{12} in Equation (3.8) requires measurements of $\gamma_{L,mix}^{d}$; however, these data are not typically available and an alternative approach is to use measured contact angle data, measured or estimated values of $\gamma_{L,mix}$, and Equations (3.3), (3.8), and (3.9) to fit δ_{12}, which is the approach that we have adopted in this work and similar to the approach of Stammitti-Scarpone and Acosta.[29] A sample calculation for fitting δ_{12} is provided in the Supporting Information. Alternatively, δ_{12} can be set to zero. In practice, we find that the error introduced by setting δ_{12} equal to zero is less than 2%, providing confidence in the fitting approach.

3.5 Results and Discussions

3.5.1 Liquid Selection and Binary Mixture Surface Tensions

Glycerol, DMSO, formamide, glycerol, and ethylene glycol were selected as organic liquids for contact angle measurements as binary mixtures with water. Water was chosen as it is by far the most commonly used liquid for contact angle measurements. The other liquids are selected as they are non-volatile (Table 3.1), highly miscible with water,[30-32] generally safe to handle, and neither swell nor react with test substrates such as PDMS.[33] As suggested previously, liquids

should be selected for contact angle measurements which span as wide of a range as possible in terms of chemical interactions, as quantified by their values of γ_L^d/γ_L^p. The γ_L^d/γ_L^p ratio of the selected liquids ranges from 0.44 to 4.50 with water (0.44) being the most polar and DMSO (4.5) as the least polar, as shown in Table 3.1. To maximize the range of γ_L^d/γ_L^p for any given liquid pair, water was always one of the mixture components. In addition to surface energy data, Table 3.1 also provides other relevant physical property data including normal boiling point temperatures (T_B), and values of the "*a*" and "*b*" parameters used in Equation (3.4) for estimation of $\gamma_{L,mix}$. T_B data in Table 3.1 shows that water is the most volatile liquid used in this study.

Table 3. 1 Physical Properties of Testing Liquids and Mixtures[18, 21-23]

Liquid	γ_L	γ_L^p	γ_L^d	γ_L^d/γ_L^p	T_B (°C)	a^a	b^a	$\delta_{12}{}^b$
Water	72.8	51	21.8	0.44	100	-	-	-
Dimethyl sulfoxide	44	8	36	4.50	189	0.869	0.603	0.31
Formamide	58	19	39	2.05	210	0.698	0.780	0.41
Glycerol	64	30	34	1.13	290	0.958	0.448	0.21
Ethylene glycol	48	19	29	1.53	196	0.793	0.825	0.45

[a] Combined partition coefficient of surface tension of binary mixtures; [b] Best-fit binary interaction parameters obtained using equation (3,4,8 and 9) and experimental data.

The data in **Table 3.1** can be used along with equations (3.4), (3.8) and (3.9) to estimate the overall ($\gamma_{L,mix}$), polar ($\gamma_{L,mix}^p$) and dispersive ($\gamma_{L,mix}^d$) surface tension parameters of the water-liquid mixtures used in this work. **Figure 3.1** compares the predicted surface tension of the water-liquid mixtures $\gamma_{L,mix}$ as calculated by Equation (3.4) to measured values available in the literature.[34-36] Estimates for the water-DMSO mixtures agree with values reported by Markarian and Terzyan[34] to within an average of 4% at 22 °C. Mulqueen and Blankschtein[37]

reported surface tension data for water-glycerol mixtures that agree to within 1.2% of the values estimated using Equation (3.4). Similarly, the predicted water-glycerol mixture surface tension are consistent with reported literature values, as shown in **Figure 3.1**. No literature data of surface tension are available for the water-formamide system. The accuracy of the surface energy predictions for DMSO-water, ethylene glycol water and glycerol-water mixtures build confidence in the method and suggests the use of water-formamide system, considering that formamide satisfies all other stated criteria.

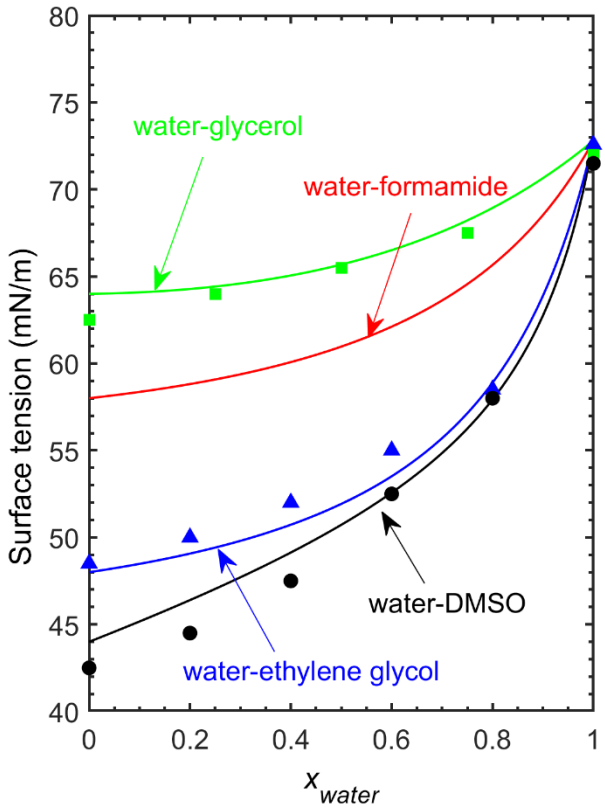

Figure 3. 1 Surface tension of water-DMSO, water-ethylene glycol, water-formamide and water-glycerol comparison between predicted using Equation (3.4) and literature data are not available for the water-formamide mixture.

The next step was to decompose the overall mixture surface energy, $\gamma_{L,mix}$, into its polar and dispersive components, using the approach outlined in the Theory section. An important question that must be addressed at this point is the ability of the simple estimation approach to account for potential differences in surface aggregation between polar and nonpolar liquid components, a concern raised previously by Kwok, *et al*.[13] Capturing surface aggregation behavior at the vapor-liquid interface of binary liquid mixtures is a necessary requirement for successful modeling of the liquid-solid interface, making this part of the analysis critical. Unfortunately, no $\gamma^{p}_{L,mix}$ and $\gamma^{d}_{L,mix}$ data are available for mixtures, meaning that we must use the reasonableness of the trends obtained to judge the method.

Figure 3.2 plots estimated mixture values of $\gamma^{p}_{L,mix}$ and $\gamma^{d}_{L,mix}$ as functions of the mole fraction of water in the mixture (x_w), which shows that the polar component of surface tension increases as the water content increases. In parallel, the value of the corresponding dispersive component smoothly decreases. Given that water is more polar than all of the liquids selected for this study, both of these trends are expected. Interestingly, both $\gamma^{d}_{L,mix}$ and $\gamma^{p}_{L,mix}$ vary nonlinearly with composition for all 4 mixtures, especially for $x_w > 0.8$. The nonlinearity of $\gamma^{d}_{L,mix}$ and $\gamma^{p}_{L,mix}$ with composition is consistent with aggregation of the nonpolar component near the surface, as is required to prevent disruption of water-water hydrogen bonds.[38] Accordingly, Figure 3.2 suggests that the mixing rule approach of decomposing γ_L into γ^{p}_{L} and γ^{d}_{L} properly captures part of the preferential surface aggregation expected for the nonpolar component of the nonpolar-polar liquid pairs, building confidence in the approach. Lastly, Table 3.1 provides best-fit values of δ_{12}, which fall in the range from 0.2 to 0.5, similar to the values that the binary interaction parameter takes in pressure-volume-temperature equations of state.

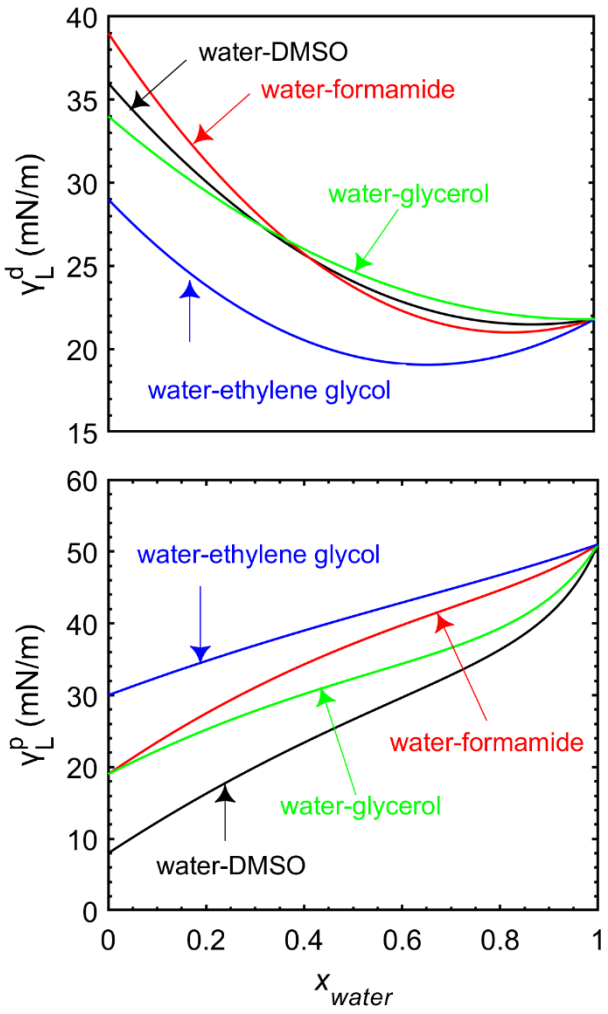

Figure 3. 2 Dispersive and polar surface tension of water-dimethyl sulfoxide (DMSO), water-formamide, water-ethylene glycol and water-glycerol binary mixtures using Equation (3.4-3.9).

3.5.2 Determination of PDMS Surface Energy

The next step was to generate contact angle data. To this end, static contact angles were measured for water-DMSO, water-formamide and water-ethylene glycol on a flat PDMS surface. Composition was varied in 0.2 mole fraction increments, including the pure component end points. Each data point is the average of three measurements taken from different positions on the same PDMS surface and error bars are the standard deviations of these measurements. Contact angles measured for the pure liquids agreed with literature values to the limits of experimental

uncertainty.[31, 32] As expected for the hydrophobic PDMS surface, measured organic liquid-water contact angles increase monotonically with increasing water concentration. The relationship between contact angle and water content is nearly linear, indicating preferential adsorption of either liquid component is insignificant and contrasting with skepticism previously expressed in the literature.[12]

The Owens-Wendt or OWRK model has been widely used to extract surface energy components from contact angle data, especially for low surface energy materials such as polyethylene, paraffin, and similar. The original OWRK method was developed for pure liquids, and the Theory section describes an approach to extend the OWRK method to binary mixture. As in the original OWRK method, the modified OWRK method can be linearized in the form of Equation (3). Figure 3.3b, 3.3c and 3.3d are the resulting modified-OWRK plot, constructed using the PDMS contact angle data from Figure 3.3a. Each data point in Figure 3.3 represents a specific composition and six different compositions were made in total. Three measurements taken from different locations of the same PDMS pieces were made at each composition and the error bars are calculated based on the uncertainties in the contact angle measurements using standard error propagation methods. The supporting information includes a sample calculation for uncertainty in Owens-Wendt's plot.

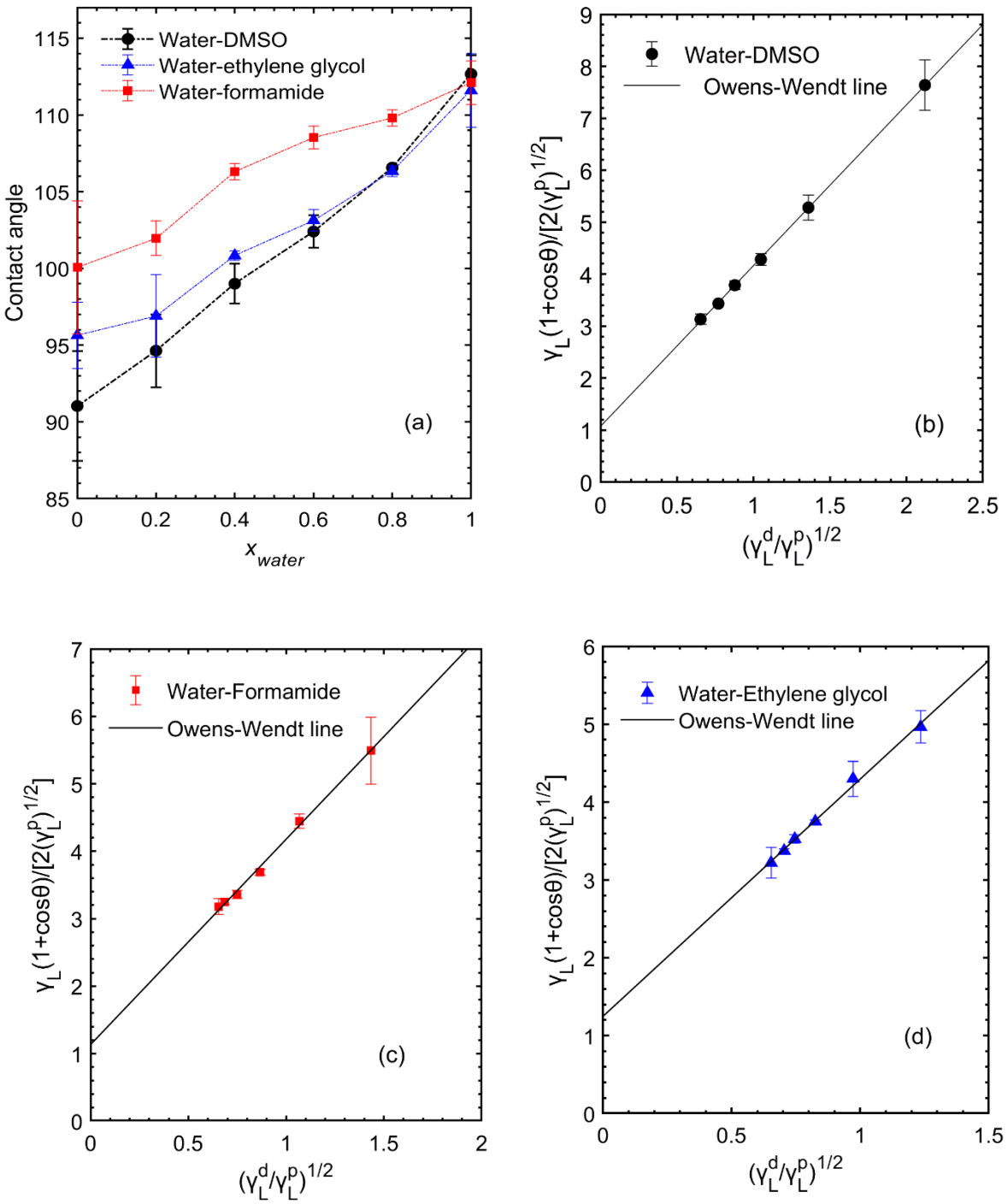

Figure 3. 3 (a) Contact angle of water-DMSO, water-formamide and water-ethylene glycol on flat PDMS; Owens-Wendt plots using contact angle of three liquid mixtures: **(b)** water-DMSO mixtures, **(c)** water-formamide mixtures and **(d)** water-ethylene glycol mixtures.

Table 3.2 provides values of γ_S, γ_S^d, and γ_S^p determined from contact angle measurements using the new analysis method. The values of γ_S, γ_S^d, and γ_S^p obtained using the three different liquid pairs agree with one another to within the limits of experimental uncertainty. Surface energy values are consistent even in the case of water-formamide, for which predicted values of $\gamma_{L,mix}$ were based entirely on experimental data for the pure substances. The test case of water-formamide demonstrates the robustness of the method in the absence of mixture data.

Table 3. 2 Surface Energy and Components (mN/m) of PDMS determined by Probe Liquids

Surface Energy	water-DMSO	water-formamide	water-ethylene glycol	Pure liquids	All available data
γ_S	10.7 ± 0.7	10.6 ± 1.1	10.8 ± 1.1	10.4 ± 1.4	10.6 ± 0.4
γ_S^d	9.6 ± 0.6	9.3 ± 1.0	9.3 ± 1.0	9.4 ± 1.3	9.2 ± 0.4
γ_S^p	1.1 ± 0.3	1.3 ± 0.4	1.5 ± 0.4	1.0 ± 0.4	1.4 ± 0.2

Surface energy values estimated using the binary mixture method are in reasonable agreement with values reported previously.[27, 39-41] For example, Lee *et al*.[39] reported 12.54, 11.05, and 1.49 mN/m for γ_s, γ_s^d, and γ_s^p, respectively. These values are comparable to those estimated here.

A major question in this work is if liquid mixtures can improve the precision of surface energy estimates. Burdzik *et al*.[14] reported that the uncertainty of dispersive surface energy estimated using the multiple liquid method and the OWRK model can be as great as –50% to 43%, depending on the accuracy of the liquid surface tension parameters. Even more remarkably, the uncertainty of literature estimates of γ_S^p can be as great as 100%,[14] especially for hydrophobic

polymer surfaces for which the value is typically less than 2 mN/m, as it is here. In comparison, Table 3.2 shows that the liquid mixture method provides relative uncertainties of γ_S ranging from 6 to 15%, a clear improvement in precision.

As further comparison, we performed a separate OWRK analysis using the pure liquid data shown in Figure 3.3 (e.g., water, DMSO, formamide, and ethylene glycol) as well as benzyl alcohol and glycerol. Just as the mixture method used 6 discrete contact angle measurements representing different compositions, the pure liquid analysis also included 6 discrete contact angle measurements. Figure 3.4 contains the OWRK plot for the pure liquid contact angle data, showing a straight line could be obtained. Likewise, Table 3.2 shows that the surface energy values obtained using the pure liquids agree with those obtained using mixtures; however, the uncertainties of the surface energy values obtained using the mixed liquid method are typically much less than those estimated using pure liquids. This is likely a consequence of the large uncertainty in the contact angle measurements obtained for formamide, pointing to the fact that the pure liquid approach is vulnerable to uncertainty by inclusion of a poorly behaved liquid.

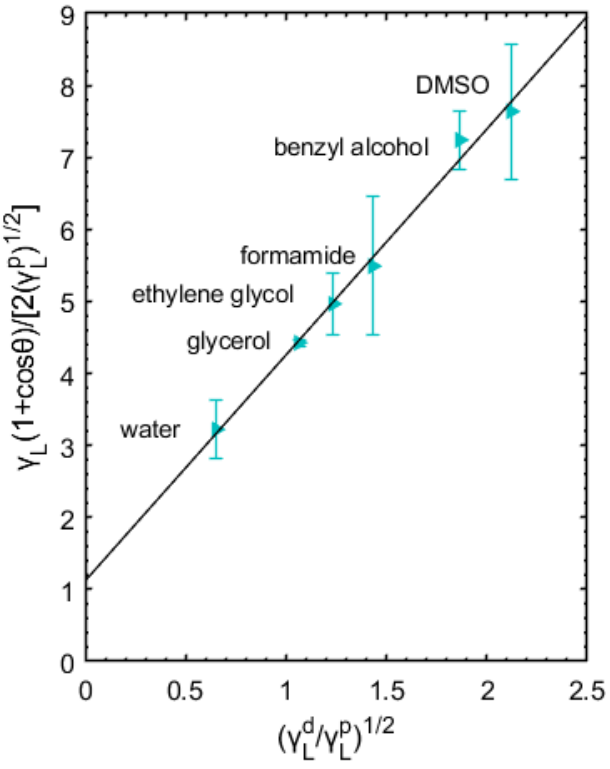

Figure 3. 4 Owens-Wendt plot for flat PDMS using multiple pure liquids, including DMSO, benzyl alcohol, formamide, ethylene glycol, glycerol and water.

Encouraged by the consistent results obtained using three different binary mixtures, we combined all available data mixtures and compiled it as an Owens-Wendt plot, as shown in **Figure 3.5a**. Plotting all eighteen contact angle data points (six data points for each of the three binary mixtures, 54 measurements) again yields a straight Owens-Wendt trend line. The estimated values of the γ_s, γ_s^d, and γ_s^p terms agree with those obtained using pure liquids, as shown by the values provided in Table 3.2. Moreover, including all available data in the analysis reduces the standard deviation of γ_s^d to 5%, 14% for γ_s^p, and 4% for γ_s.

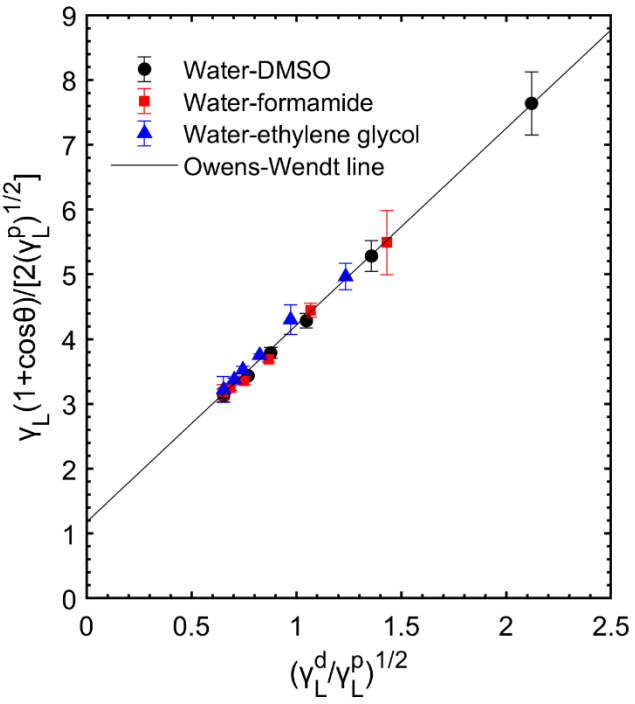

Figure 3. 5 Owens-Wendt plot using three binary mixtures (water-formamide, water-ethylene glycol, water-dimethyl sulfoxide) on PDMS

3.5.3 Surface Energy of Functionalized Silicon Dioxide Surface

Having established the utility of the Owens-Wendt analysis method of liquid mixture contact angle data for a PDMS surface, we evaluated its use for discriminating differences in the surface energy of engineered surfaces, using silicon dioxide (glass) surfaces derivatized with ETS, HTS, and OTS for testing. Accordingly, we measured static contact angles for water-formamide and water-glycerol mixtures on the silanized glass surface, and the results are shown in Figure 3.6a and 3.6b. As with the PDMS surface, most of the measured contact angles increase almost linearly with increasing water content. Contact angles measured for glycerol-rich water mixtures on HTS-coated glass are the exception to the linear trend, potentially a consequence of experimental uncertainty. As expected,[42, 43] contact angle measurements followed the trend in hydrophobicity consistent with silane carbon chain length, i.e., the hydrophobicity trend was OTS (C_{18}) > HTS (C_6) > ETS

(C_2). Contact angles measured using pure liquids for the OTS functionalized surface agree with values reported previously by Tillman *et al.[44]* and Maboudian *et al.*[45]

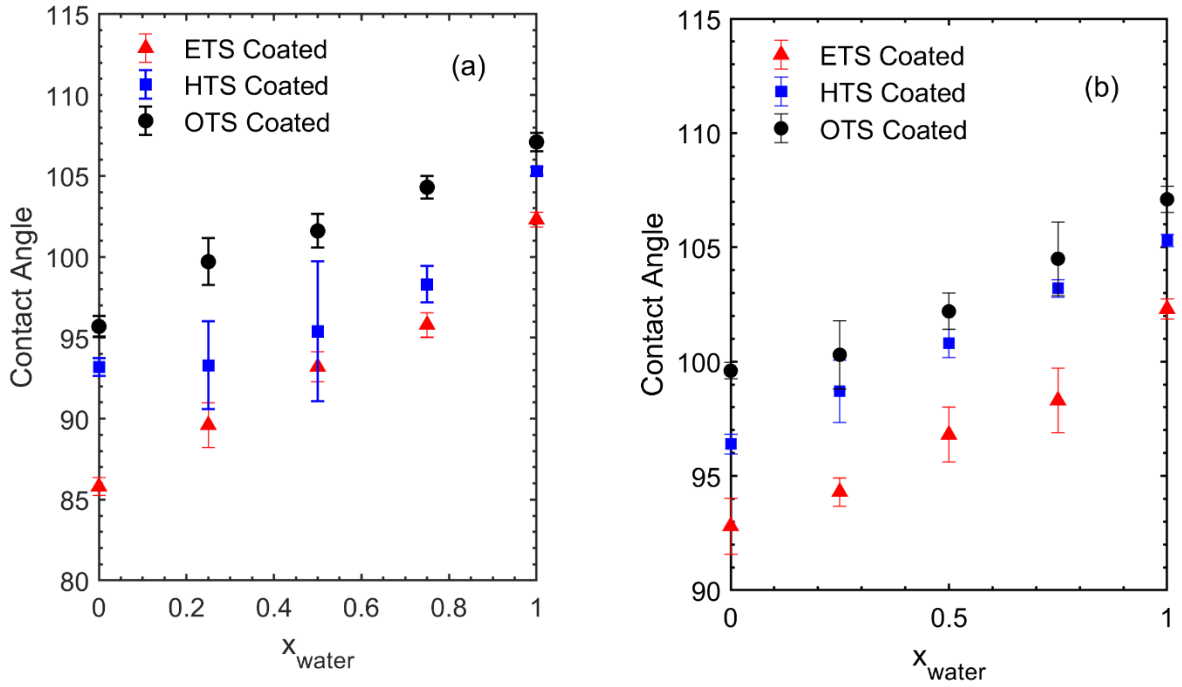

Figure 3. 6 Contact angle of **(a)** water-formamide and **(b)** water-glycerol on functionalized glass.

The next step was to apply the modified OWRK analysis to extract γ_S^d and γ_S^p from the contact angle data measured on the silanized surfaces. Figure 3.7 provides the details of the OWRK analysis. As in previous example, the OWRK plots of the functionalized glass surfaces result in straight-lines, and Table 3.3 provides the surface energy parameters estimated from the best-fit slopes and intercepts. As expected, surface energy decreases with increasing alkyl chain length from ETS (C_2) to OTS (C_{18}). Regardless of the alkyl tail group, the polar surface energy remains approximately 2 mN/m, consistent with the fact that OTS, HTS and ETS all are hydrocarbons. The

net result of constant γ_S^p and decreasing overall surface energy is that γ_S^d decreases with increasing alkyl group chain length, seemingly a consequence of reduced interactions between the liquid and the underlying glass surface. Quantitatively, **Table 3.3** shows that surface energy estimated from water-formamide and water-glycerol are self-consistent, with differences on the order of 10%. In summary, therefore, Figures 3.6 and 3.7 and Table 3.3 establish that the multiple liquid approach can be used to differentiate surface energy of engineered surfaces.

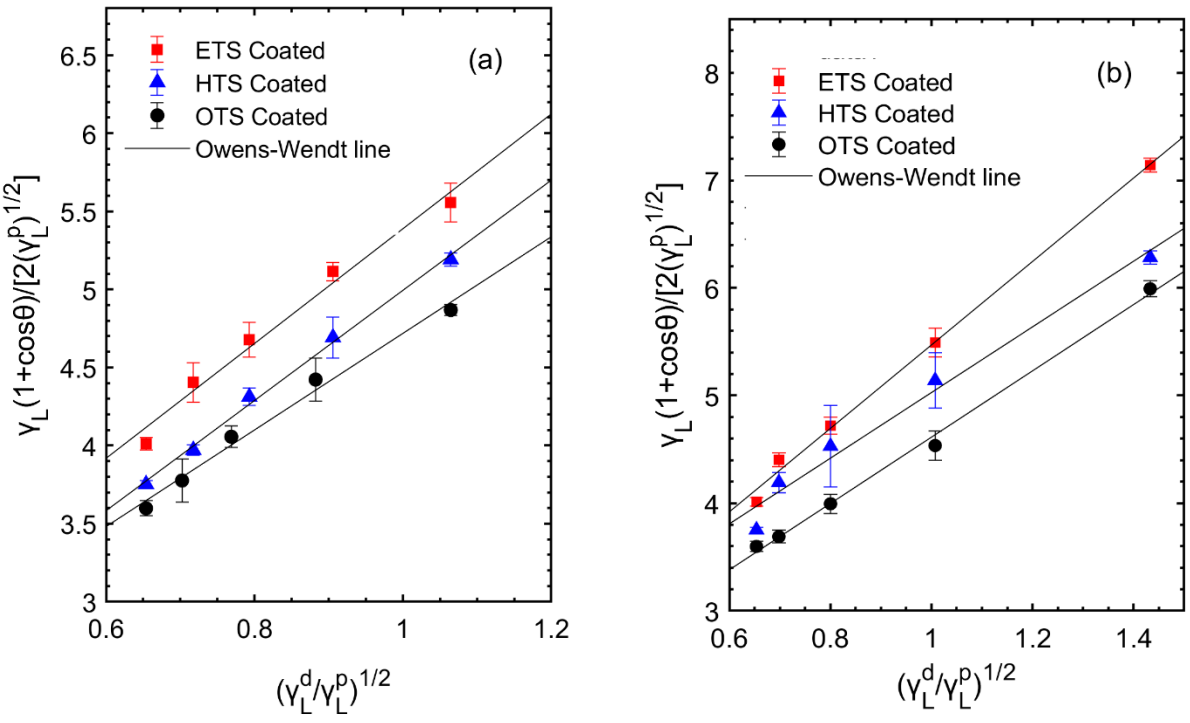

Figure 3. 7 Owens-Wendt plot for ETS, HTS and OTS coated silicon dioxide (glass) using **(a)** water-glycerol mixtures and (**b**) water-formamide mixtures.

Table 3. 3 Surface Energy and Components (mN/m) of Silane Derivatized Glass

Derivatization Agent	water- formamide			water- glycerol		
	γ_S	γ_S^d	γ_S^p	γ_S	γ_S^d	γ_S^p
OTS	11.8 ± 0.6	9.5 ± 0.5	2.3 ± 0.3	12.2 ± 1.2	9.6 ± 1.1	2.6 ± 0.5
HTS	13.2 ± 1.5	9.3 ± 1.3	3.9 ± 0.8	14.6 ± 0.9	12.5 ± 0.8	2.1 ± 0.3
ETS	17.5 ± 0.7	15.0 ± 0.7	2.5 ± 0.3	16.3 ± 1.4	13.5 ± 1.3	2.8 ± 0.5

The data and analysis shown here indicate that the liquid mixture approach can be used for precise determination of surface energy parameters. We have used two hydrophobic surfaces – PDMS and silane-derivatized glass – for development of this new method. Applying the method to hydrophilic surfaces should be possible. For hydrophilic surfaces, we suggest selection of nonpolar-midpolar solvent pairs as the water-midpolar liquid mixtures used in this work will tend to spread on hydrophilic surfaces, reducing the precision of the contact angle measurement. The midpolar liquids used here – e.g., DMSO, glycerol, ethylene glycol, and formamide – are all candidates for mixtures with a nonpolar solvent for study of hydrophilic surfaces. The nonpolar solvent should meet the criteria outlined previously in the text in terms of surface compatibility, availability of data, volatility, toxicity, and safety – and be miscible with the selected midpolar solvent(s). In fact, any liquid that has met these criteria has yielded reliable data when used for surface energy determination in this work. A further area of future work is incorporation of theories other than the Owens-Wendt surface energy theory. Several alternative theories have been proposed,[11, 12, 19] and the current method might feasibly be modified to accommodate surface energy theories other than Owens-Wendt.

Lastly, we are careful to note that the liquid mixture approach remains prone to systematic errors, such as the presence of impurities in one or both of the liquids used for contact angle

measurements. Hence, although the liquid mixture approach can guarantee precision, it does not necessarily improve accuracy. The usual admonishments on careful surface measurements apply, chiefly use of high purity liquids, study of clean (or representative surfaces), and consistent methodology. In particular, solvent impurities can influence the actual mixture liquid tension, hence propagating into errors in the extracted values of the relevant surface energy parameters. For this reason, we suggest study of at least two liquid pairs to help identify instances in which one of the liquids contains an impurity at concentrations great enough to bias the experimental data.

Future work can compare surface energy determined using the mixture approach to that measured using AFM[6, 7] or predicted by theory. The uncertainty of surface energy determined using the multiple solvent approach has typically been so great that such comparisons were not especially useful.[14]

3.5.4 Uncertainty analysis

Statistically, when performing linear regression, more data points will increase precision. Therefore, we analyze the effect of data points on surface energy distributions. To test this, we calculated the uncertainty in the surface energy based on all possible combinations of two data points (N=2), three data points (N=3), and so forth. Figure 3.8A-F show that measurement uncertainty decreases with $N^{1/2}$, which is what randomized error would predict. Therefore, Figure 3.8 suggests that the multiple liquid and mixture approaches can be used to increase precision to levels even greater than demonstrated here.

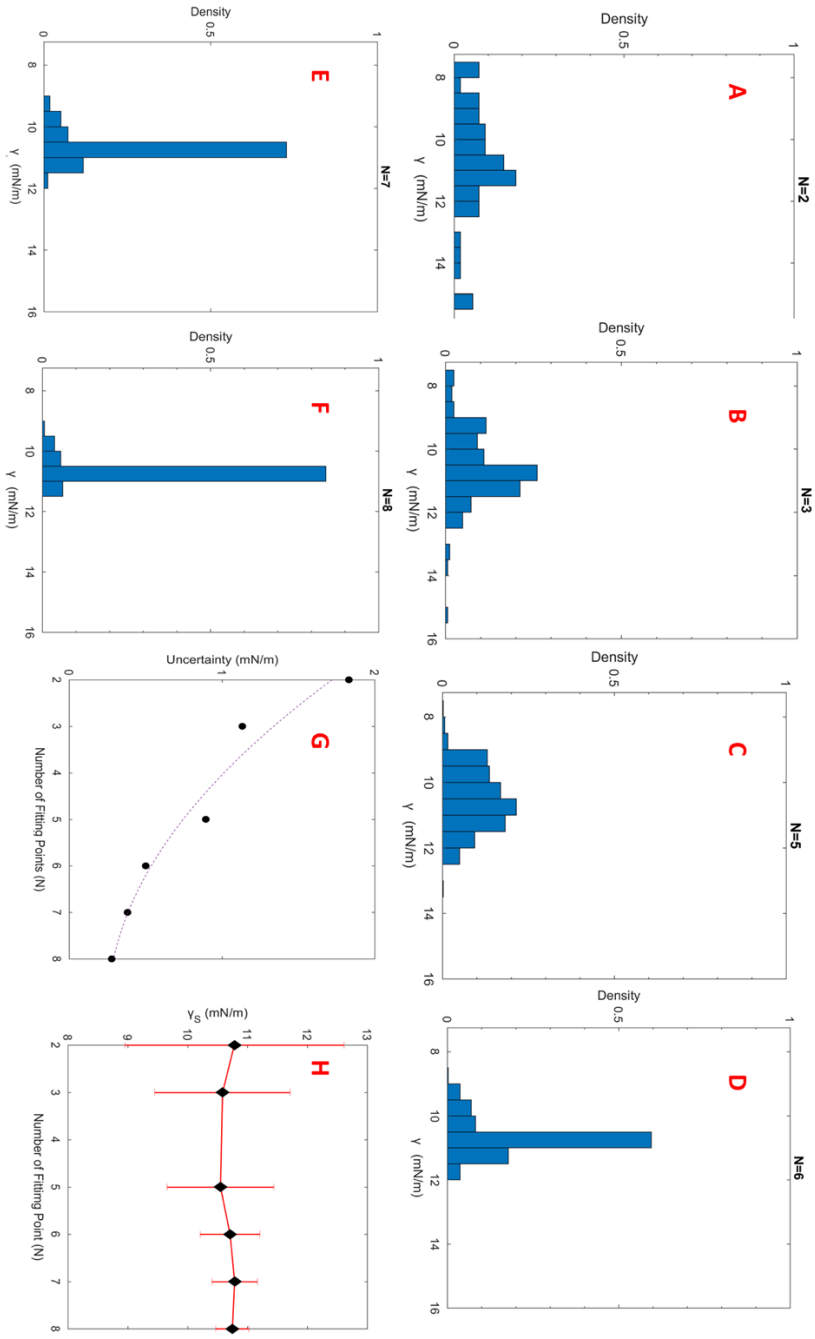

Figure 3. 8 Statistically analysis of surface energy determination of PDMS. **A-F**: surface energy determined using different number of contact angles data points; **G**: standard error decrease as number of data points used increases; **H**: Uncertainty drops as number of data points used for surface energy determination increases.

3.6 Conclusions

Surface energy is an important parameter in many applications involving surface wetting and adhesion. The most common surface energy determination method is based on contact angle measurements. Unfortunately, contact angle measurement of a single liquid (usually water) provides only information on surface hydrophobicity or hydrophilicity. Measurements obtained for a series of liquids can be used for determination of the surface energy and – by use of an appropriate theory – deconstruction of the overall surface energy into components arising from different chemical interactions. The precision of surface energy parameters that can be determined using the multiple liquid approach is limited by the number of liquids that can be studied. However, the range of liquids suitable for the multiple liquid approach is limited by many factors, including safety, availability of data, and volatility.

Here, we developed a simple and precise technique that uses static contact angle data obtained for binary liquid mixtures to determine surface free energy using the Owens-Wendt model. Unlike the multiple liquid approach, the mixture approach can be used to determine an arbitrarily large number of independent measurements since each mixture – in effect – is its own liquid. A new method was developed to separate liquid mixture surface energy into its polar ($\gamma_{L,mix}^{p}$) and dispersive ($\gamma_{L,mix}^{d}$) components suitable for use in a modified version of the Owens-Wendt model. To test the method, contact angle data were obtained on two chemically distinct hydrophobic surfaces, PDMS and silane-derivatized glass. Water was used in all mixtures, and the other liquids were glycerol, ethylene glycol, formamide, and DMSO. Subsequent analysis indicated that the multiple liquid approach yielded estimates of surface energy parameters, γ_S^p, γ_S^d, and γ_s, that agreed with values obtained using multiple liquids and with literature values (where available). Uncertainty decreased with the number of independent data points, and the current

analysis indicated that the multiple liquid method could yield surface energy parameters with less than 13% and sometimes less than 5% uncertainty. Likewise, tests with silane-derivatized glass indicated that the method could be used to differentiate surface energy of engineered surfaces. This work provides a valuable approach for straight-forward and simple estimation of surface energy parameters.

3.7 References

1. Hallab, N.J., et al., *Evaluation of metallic and polymeric biomaterial surface energy and surface roughness characteristics for directed cell adhesion.* Tissue engineering, 2001. **7**(1): p. 55-71.
2. Yang, J., J. Bei, and S. Wang, *Enhanced cell affinity of poly (D, L-lactide) by combining plasma treatment with collagen anchorage.* Biomaterials, 2002. **23**(12): p. 2607-2614.
3. Baszkin, A. and D.J. Lyman, *The interaction of plasma proteins with polymers. I. Relationship between polymer surface energy and protein adsorption/desorption.* Journal of biomedical materials research, 1980. **14**(4): p. 393-403.
4. Good, R.J., *Surface free energy of solids and liquids: thermodynamics, molecular forces, and structure.* Journal of colloid and interface science, 1977. **59**(3): p. 398-419.
5. Kumikov, V. and K.B. Khokonov, *On the measurement of surface free energy and surface tension of solid metals.* Journal of Applied Physics, 1983. **54**(3): p. 1346-1350.
6. Butt, H.-J., B. Cappella, and M. Kappl, *Force measurements with the atomic force microscope: Technique, interpretation and applications.* Surface science reports, 2005. **59**(1-6): p. 1-152.
7. Relini, A., et al., *Measurement of the surface free energy of streptavidin crystals by atomic force microscopy.* Langmuir, 2003. **19**(7): p. 2908-2912.

8. Xu, X., et al., *Surface tension measurement from the indentation of clamped thin films.* Soft matter, 2016. **12**(23): p. 5121-5126.
9. Good, R.J., *Contact angle, wetting, and adhesion: a critical review.* Journal of adhesion science and technology, 1992. **6**(12): p. 1269-1302.
10. Żenkiewicz, M., *Methods for the calculation of surface free energy of solids.* Journal of Achievements in Materials and Manufacturing Engineering, 2007. **24**(1): p. 137-145.
11. Owens, D.K. and R. Wendt, *Estimation of the surface free energy of polymers.* Journal of applied polymer science, 1969. **13**(8): p. 1741-1747.
12. Johnson, R.E., *Contact angle, wettability, and adhesion.* Advances in chemistry series, 1964. **43**: p. 112.
13. Kwok, D.Y. and A.W. Neumann, *Contact angle measurement and contact angle interpretation.* Advances in colloid and interface science, 1999. **81**(3): p. 167-249.
14. Burdzik, A., et al., *Impact of reference values used for surface free energy determination: An uncertainty analysis.* International Journal of Adhesion and Adhesives, 2018. **82**: p. 1-7.
15. Bourges-Monnier, C. and M. Shanahan, *Influence of evaporation on contact angle.* Langmuir, 1995. **11**(7): p. 2820-2829.
16. Rudawska, A. and E. Jacniacka, *Analysis for determining surface free energy uncertainty by the Owen–Wendt method.* International Journal of Adhesion and Adhesives, 2009. **29**(4): p. 451-457.
17. Rulison, C., *So you want to measure surface energy.* Charlotte NC (cf. p. 99), 1999.

18. Chaudhury, M.K. and G.M. Whitesides, *Direct measurement of interfacial interactions between semispherical lenses and flat sheets of poly (dimethylsiloxane) and their chemical derivatives.* Langmuir, 1991. **7**(5): p. 1013-1025.

19. Connors, K.A. and J.L. Wright, *Dependence of surface tension on composition of binary aqueous-organic solutions.* Analytical Chemistry, 1989. **61**(3): p. 194-198.

20. Young, T., *III. An essay on the cohesion of fluids.* Philosophical transactions of the royal society of London, 1805(95): p. 65-87.

21. Annamalai, M., et al., *Surface energy and wettability of van der Waals structures.* Nanoscale, 2016. **8**(10): p. 5764-5770.

22. Petke, F.D. and B.R. Ray, *Temperature dependence of contact angles of liquids on polymeric solids.* Journal of colloid and interface science, 1969. **31**(2): p. 216-227.

23. Lee, S., J.-S. Park, and T.R. Lee, *The wettability of fluoropolymer surfaces: Influence of surface dipoles.* Langmuir, 2008. **24**(9): p. 4817-4826.

24. Jańczuk, B. and T. Białłopiotrowicz, *Surface free-energy components of liquids and low energy solids and contact angles.* Journal of Colloid and Interface Science, 1989. **127**(1): p. 189-204.

25. Fowkes, F.M., *Additivity of intermolecular forces at interfaces. i. determination of the contribution to surface and interfacial tensions of dispersion forces in various liquids1.* The Journal of Physical Chemistry, 1963. **67**(12): p. 2538-2541.

26. Kwak, T. and G. Mansoori, *Van der Waals mixing rules for cubic equations of state. Applications for supercritical fluid extraction modelling.* Chemical engineering science, 1986. **41**(5): p. 1303-1309.

27. Kim, Y.G., et al., *Study on the surface energy characteristics of polydimethylsiloxane (PDMS) films modified by C4F8/O2/Ar plasma treatment.* Applied Surface Science, 2019. **477**: p. 198-203.

28. DE S, C., *ACADÉMIE DES SCIENCES.* 1882.

29. Stammitti-Scarpone, A. and E. Acosta, *Solid-liquid-liquid wettability and its prediction with surface free energy models.* Advances in colloid and interface science, 2019. **264**: p. 28-46.

30. Costanzo, G., et al., *Formamide as the main building block in the origin of nucleic acids.* BMC Evolutionary Biology, 2007. **7**(2): p. 1-8.

31. Alexandridis, P. and L. Yang, *SANS investigation of polyether block copolymer micelle structure in mixed solvents of water and formamide, ethanol, or glycerol.* Macromolecules, 2000. **33**(15): p. 5574-5587.

32. Kirchner, B. and M. Reiher, *The Secret of Dimethyl Sulfoxide− Water Mixtures. A Quantum Chemical Study of 1DMSO− n Water Clusters.* Journal of the American Chemical Society, 2002. **124**(21): p. 6206-6215.

33. Sia, S.K. and G.M. Whitesides, *Microfluidic devices fabricated in poly (dimethylsiloxane) for biological studies.* Electrophoresis, 2003. **24**(21): p. 3563-3576.

34. Markarian, S.A. and A.M. Terzyan, *Surface tension and refractive index of dialkylsulfoxide+ water mixtures at several temperatures.* Journal of Chemical & Engineering Data, 2007. **52**(5): p. 1704-1709.

35. Tsierkezos, N.G. and I.E. Molinou, *Thermodynamic properties of water+ ethylene glycol at 283.15, 293.15, 303.15, and 313.15 K.* Journal of Chemical & Engineering Data, 1998. **43**(6): p. 989-993.

36. Mallinson, S., G. McBain, and G. Horrocks. *Viscosity and surface tension of aqueous mixtures*. in *20th Australasian Fluid Mechanics Conference Perth, Australia. Australasian Fluid Mechanics Society*. 2016.

37. Mulqueen, M. and D. Blankschtein, *Prediction of equilibrium surface tension and surface adsorption of aqueous surfactant mixtures containing ionic surfactants.* Langmuir, 1999. **15**(26): p. 8832-8848.

38. Jiang, L., et al., *Real-time monitoring of hydrophobic aggregation reveals a critical role of cooperativity in hydrophobic effect.* Nature communications, 2017. **8**(1): p. 1-8.

39. Lee, S.A., S.H. Oh, and W. Lee, *The effect of direct fluorination of polydimethylsiloxane films on their surface properties.* Journal of colloid and interface science, 2009. **332**(2): p. 461-466.

40. Stanton, M.M., et al., *Super-hydrophobic, highly adhesive, polydimethylsiloxane (PDMS) surfaces.* Journal of colloid and interface science, 2012. **367**(1): p. 502-508.

41. Fox, H., P. Taylor, and W. Zisman, *Polyorganosiloxanes... surface active properties.* Industrial & Engineering Chemistry, 1947. **39**(11): p. 1401-1409.

42. Kulkarni, S.A., S.B. Ogale, and K.P. Vijayamohanan, *Tuning the hydrophobic properties of silica particles by surface silanization using mixed self-assembled monolayers.* Journal of Colloid and Interface Science, 2008. **318**(2): p. 372-379.

43. Han, X., et al., *Tuning the hydrophobicity of ZSM-5 zeolites by surface silanization using alkyltrichlorosilane.* Applied surface science, 2011. **257**(22): p. 9525-9531.

44. Tillman, N., et al., *Incorporation of phenoxy groups in self-assembled monolayers of trichlorosilane derivatives. Effects on film thickness, wettability, and molecular orientation.* Journal of the American Chemical Society, 1988. **110**(18): p. 6136-6144.

45. Maboudian, R., W.R. Ashurst, and C. Carraro, *Self-assembled monolayers as anti-stiction coatings for MEMS: characteristics and recent developments.* Sensors and Actuators A: Physical, 2000. **82**(1-3): p. 219-223.

Chapter 4

Accurate Measurement of Acid and Base Surface Energy of Polymer Materials Using Aqueous Mixtures and van Oss-Chaudhury-Good (*v*OCG) Model

4.1 Abstract

Polymer surface free energy is an important property for applications including surface coating, adhesion and self-cleaning. In those applications, understanding molecular interactions, such as dispersive, acid and base interaction is necessary. For a long time, van Oss-Chaudhury-Good (vOCG) method is used to estimate surface free energy components using contact angles of pure liquids. However, vOCG method suffers from problem associated with negative surface energy components such as acid term (γ_S^+), casting doubts on its accuracy and precision. Negative surface energy components are attributed to lack of enough contact angles data of pure liquids because selected liquids must satisfy requirements such as surface compatibility and known surface tension parameters. Here, we used liquid mixtures, including water-formamide, water-dimethyl sulfoxide and water-ethylene glycol, for contact angle measurements. By varying water mole fraction, we obtained abundant data points for contact angle measurements, we extended mixing theory to extract dispersive, acid and base components of mixtures. By using abundant data points, we have precisely and accurately measured surface energies of commonly used polymers such as PVC, PMMA and PDMS. This also solve negative surface energy components problem that is introduced by using pure liquids.

4.2 Introduction

Surface energy is an important physical property, and its manipulation is crucial for applications including cell adhesion, biomedical devices, thin films, ink printing, and many others.[1-10] Manipulation of surface energy is indicative for designing superhydrophobic polymer-based

surfaces for applications ranging from self-cleaning, antifouling to drag and friction reduction.[11-14] For example, Fluorinated Polyhedral Oligomeric SilSesquioxanes (*FluoroPOSS*) have been used for controlling liquid wetting for manufacturing printed circuit boards.[13, 15] Similarly, lubricant-infused nano-structures utilizing trimethylchlorosilane surface modification are reported for directing flow during water harvesting from humid air.[16]

Controlling surface energy requires its accurate and precise measurement.[17-19] By far the most common method of estimating surface energy involves contact angle measurement.[20] However, the accuracy and precision of this technique have been questioned.[21] Alternative approaches include atomic force microscopy (AFM), indentation measurement,[22, 23] and drop tower measurement for microgravity environments.[24] While these sophisticated approaches can directly measure surface energy, they typically require commensurately complex instrumentation and methods – and the expertise to use them. Contact angles can be measured rapidly using inexpensive equipment and contact angle measurement remains the most widely used technique for surface characterization and subsequent surface energy estimation.

Contact angle measurement is a direct way of characterizing surface wetting rather than capturing surface energy. One popular way to capture the chemical information pertaining to surface energy is to divide it into chemically resolved surface energy.[25, 26] The resulting empirical models are qualitatively similar to theories that have been used to model solubility, inasmuch as liquids tend to spread on surfaces with similar properties and are repelled from surfaces with differing properties.[27]

Several different models have been developed over the past century to resolve interfacial surface energy into different types and numbers of molecular interactions.[28] The Owens-Wendt (OWRK) model divides surface energy into polar and dispersive components and has been used

for many different polymer surfaces with low surface energy.[29] Unfortunately, the OWRK model always predicts net attraction between adjacent solute molecules and cannot explain the high water affinity of polymers such as polyethylene oxide, an important polymer used to make surfaces hydrophilic.[30] In response to this shortcoming, van Oss, Chaudhury, and Good (*v*OCG) retained the dispersive term from the OWRK model and replaced the polar component with two terms that capture acid-base interactions. The *v*OCG treatment of the polar term leads to successful prediction of the water solubility of polyethylene oxide.[30, 31] The OWRK and *v*OCG models remain popular.

Values of the parameters appearing in the OWRK and *v*OCG models can be estimated using contact angle measurements of several different liquids – at least two for the dispersion and polar terms appearing in the OWRK model and three if the acid/base term appearing in the *v*OCG model is resolved. While the multi-solvent approach is generally accepted and widely utilized,[32] the method presents several problems. The most challenging of these problems from a theoretical perspective is that the multi-solvent approach often yields negative values for the acid term appearing in the *v*OCG model, which is clearly not physical and hinders rational surface design.[33-35] Although mathematically three liquids should be sufficient for determining three unknowns, Volpe and Siboni [36] pointed out that values of the *v*OCG surface energy terms rely on the accuracy of the parameters of the individual liquids and the precision of measured contact angles. Uncertainties in either of these are exacerbated by nonlinearity of the governing equation,[37, 38] resulting in instances where negative values become statistically possible even when they are physically unrealistic.

Avoiding negative surface energy terms therefore requires reducing the uncertainty of probe inputs, which can be accomplished in various ways, for example by making multiple

measurements of the contact angle to reduce uncertainty in this value. Unfortunately, uncertainty in contact angle measurement is not the main contributing factor to imprecise or negative values of surface energy terms. Alternatively, obtaining measurements for more liquids than required mathematically (i.e., >2 for OWRK or >3 for *v*OCG) can reduce uncertainty by constraining the non-linear fitting equations.[39] Unfortunately, only a handful of liquids are suitable for precision measurement of contact angles, as they must satisfy criteria that include compatibility with the surface in question, availability of surface tension data, low volatility, and ideally low toxicity.[40] Restrictions on solvent selection places a limit on the number of liquid that can be used for contact angle measurement.

In a previous study, the authors presented a new approach for resolving chemical contributions to surface energy using contact angle measurements made for a series of binary liquid mixtures.[40] The two liquids present in the binary mixture must be mutually miscible in all proportions and should be selected so that the surface tensions of their mixtures spans as wide of a range as possible. Contact angles measured for mixtures with five or more distinct compositions reduced the uncertainties of OWRK surface energy parameters estimated for polydimethylsiloxane (PDMS) surface and silane-coated glass slides by an order of magnitude relative to the multi-solvent approach.[40] The binary liquid approach therefore has promise for solving the problem with negative values of parameters appearing in the *v*OCG.

Successful reduction of surface energy estimations uncertainties using binary liquid mixtures motivates further development [35]. Unfortunately, the previous work on the use of binary liquid mixtures for evaluating surface energy was limited to models consisting of at most two terms, such as the OWRK model,[40] which has severe limitations as previously described.[40] Similarly, the previous work used the simplest possible model for capturing surface tension of

mixtures. Adoption of more sophisticated models has potential to afford better fits to experimental data. Extending the binary liquid mixture approach to more sophisticated surface energy models with more than two parameters, such as the *v*OCG model, could therefore be useful for rational surface design, especially for surfaces with minor – yet non-negligible – acidity, especially polymers.[41-43] Removing the co-dependency of surface tension fitting parameters on contact angles would make identifying sources of uncertainty easier and reduce interdependence of surface tension and surface energy parameter values.

The objective of the current study is development of a new mixing model to generalize the earlier binary liquid measurement method to extend the method to models with more than two terms (e.g., *v*OCG). Surface tension of the binary mixture is described using a mixing model requiring one or more parameters that are fit to experimental datal; the fitting parameter plays a role similar to that played by the binary interaction parameter that is well-known in pressure-volume-temperature equations of state.[44] Several different mixing rules were evaluated for their effects on parameter estimates and uncertainties. The surface tension model was then combined with the OWRK and *v*OCG wetting models, and their corresponding surface energy parameters were estimated by regression using contact angle measurements obtained for binary liquid mixtures of varying compositions. A series of common polymers with differing hydrophobicity and acid/base properties, including polydimethylsiloxane (*PDMS*), polyvinyl chloride (*PVC*) and poly (methyl methacrylate) (*PMMA*), were used as model surfaces to evaluate the precision of the new method. The result is a generalized method that permits robust and precise resolution of the chemical contributions to surface energy.

4.3 Experimental

Materials: Ethylene glycol (99.8%) was obtained from Sigma-Aldrich Corporation (Natick, MA), dimethyl sulfoxide (DMSO) was purchased from AMRESCO, Inc. (Solon, OH), and formamide (99.5%) was purchased from Alfa Aesar (Ward Hill, MA). Water was de-ionized prior to use on a Millipore Synergy UV water purification system (Billerica, MA) to a minimum resistivity of 17.9 MΩ•cm prior to use. The Sylgard 184 silicone elastomer kit consisting of polydimethylsiloxane (PDMS) elastomer and hardener was purchased from Dow Corning (Midland, MI) was used to prepare PDMS surfaces. Silicon wafers were purchased from Virginia Semiconductor (Fredericksburg, VA). Polyvinyl chloride (PVC) and poly(methyl methacrylate) (PMMA) sheets (30.5 cm × 61 cm) were purchased from McMaster-Carr and used immediately after removing their protective covers.

4.3.1 Polydimethylsiloxane (PDMS) Cast

The PDMS pre-polymer mixture was prepared by mixing elastomer and hardener in a 10:1 mass ratio. The resulting polymer mixture was cast onto a flat 100 mm diameter silicon wafer. The wafer was cleaned in piranha solution, consisting of sulfuric acid and hydrogen peroxide in a 3:1 ratio (mol/mol), for 1.0 h. The cleaned silicon wafer was thoroughly rinsed with D.I. water and 70% ethanol, dried using nitrogen, and immediately placed at the bottom of a polystyrene Petri dish (Corning Inc., Corning, NY). The PDMS mixture was then cast onto the wafer, degassed in a vacuum oven at 25 mmHg of pressure for 2 h and finally baked for 5 h at 70 °C. After cooling, the PDMS was removed from the polymer cast and used immediately for testing.

4.3.2 Mixture Preparations

DMSO, ethylene glycol and formamide were chosen as the constituents of the binary mixtures used for contact angle measurements. The corresponding binary liquid mixtures consisted of water

and one of the organics in varying proportions. A total of 6 compositions were prepared for each mixture, ranging from pure water to the pure organic, with increments of 0.2 mole fraction units.

4.3.3 Contact Angle Measurement

Contact angle measurements were performed using a Ramé-Hart Automated Dispensing System (Netcong, NJ; Model No. 100-00) with Rame-Hart Drop Image Standard v.2.0.10 software for analysis. A consistent droplet volume of 5 μL was used for all tests. Contact angle measurements were performed three times for each solution on different locations of each surface. Average values are reported here.

4. 5 Theory

The new procedure for estimating surface energy and decomposing it into individual molecular interactions consists of two steps, shown schematically in Figure 4.1. The first of these steps, shown in Figure 4.1a, requires as input chemically resolved liquid-gas surface tension parameters for two or more pure liquids; liquid-vapor surface tension values for binary mixture(s) of the same two liquids as a function of composition; and an appropriate mixing rule that can capture the dependence of liquid-gas surface tension on composition contact angle measurements for a binary mixture(s) as a function of composition. Following an iterative fitting procedure, shown in Figure 4.1a, the output of the first step is chemically and compositionally resolve surface tension of the binary mixture that is the input for the second step. The other input to the second step is contact angle data on a surface of interest for different compositions of the same binary liquid mixture.

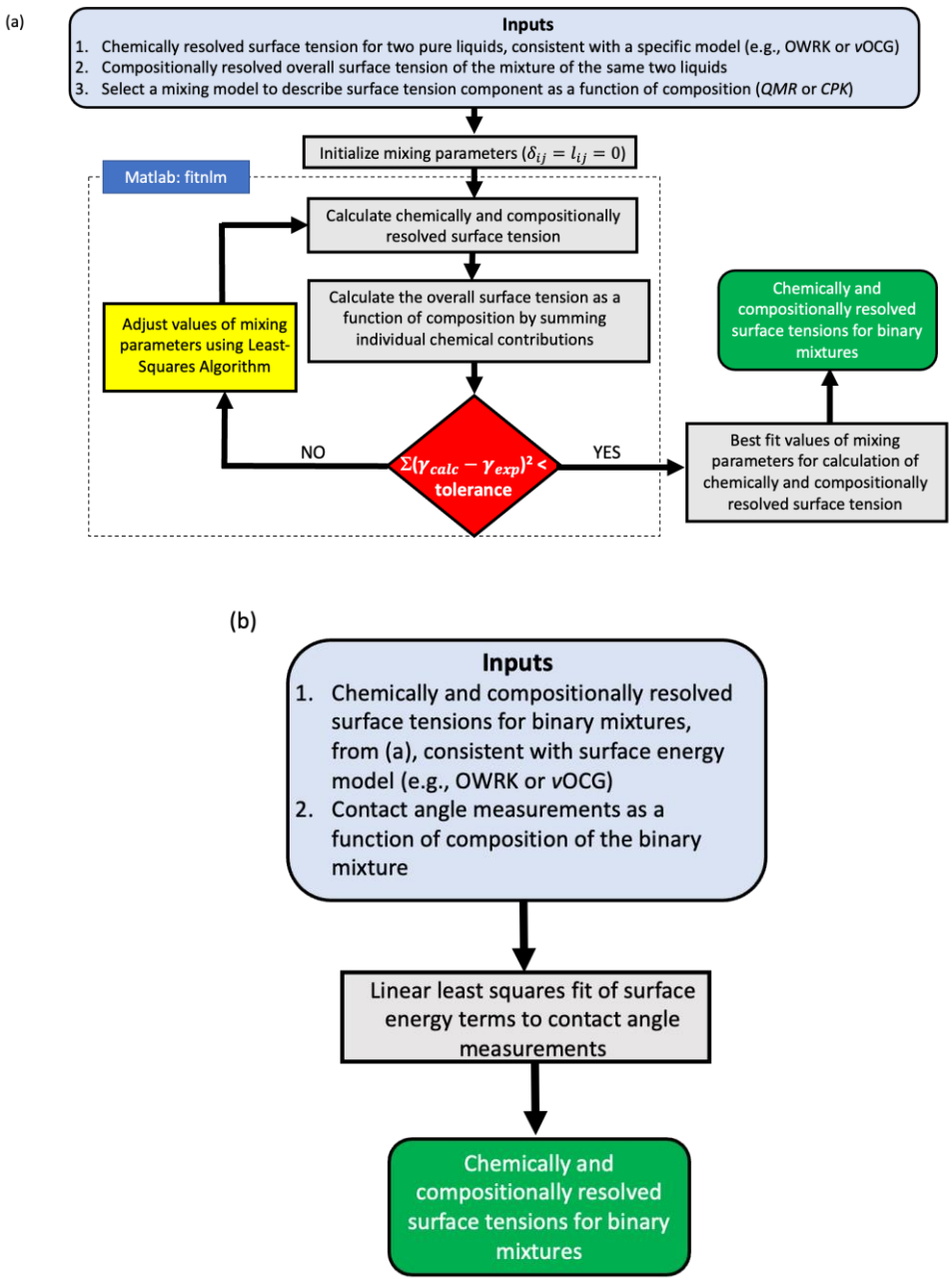

Figure 4. 1 Flowchart for using liquid mixtures to determine solid surface energy components using acid-base theory: (a) shows algorithm for estimating chemically and compositionally resolved surface tension parameters; (b) is procedure for determining surface energy using (a) as inputs.

In both cases, the chemical resolution of the surface tension and surface energy outputs depends on the terms appearing in the surface wetting model, and can include terms arising from dispersion forces, polar forces, and other interactions.[45] Selecting the form of the model allows the user to decide which terms to include. In this work, the popular OWRK and *v*OCG models are used to demonstrate the approach.

Figure 4.1 provides an overview of the approach used here. Key decisions include selecting the model used to capture chemical contributions to surface tension, and surface energy; and the model used to capture liquid-liquid mixing effects on surface properties. The rest of the Theory section discusses these two topics (in Sections 3.1 and 3.2)

4.5.1 Chemically Resolved Surface Tension and Surface Energy Models

Figure 4.1 shows that a critical step is selection of an appropriate model to capture chemical contributions to surface properties. Different types of models describe surface properties using different types of chemical interactions, affording some flexibility. Young's equation [46] describes wetting of a liquid droplet on a solid surface arising from mechanical equilibrium at the solid (*S*), liquid (*L*) and gas (*G*) interface:

$$\gamma_{SG} = \gamma_{LS} + \gamma_{LG}cos(\theta) \qquad [4.1]$$

where γ_{SG}, γ_{LS} and γ_{LG} are the surface energies at the solid-gas, solid-liquid, and liquid-gas interfaces, respectively; θ is the static contact angle. In most applications, γ_{SG}, termed the surface energy, is the parameter of interest. Determining γ_{SG} requires knowledge of the liquid-solid interfacial surface energy (γ_{LS}) to solve equation (4.1).

Many models have been proposed to capture the effects of molecular interactions on surface energy, including the OWRK and *v*OCG models mentioned in the Introduction. The well-

known OWRK model was developed by Owens-Wendt-Rabel-Kaelble to describe surface energy as two types of interactions, arising from dispersive and polar interactions.[29, 47, 48] The total solid surface energy becomes $\gamma_{SG} = \gamma_{SG}^{d} + \gamma_{SG}^{p}$, in which γ_{SG}^{d} and γ_{SG}^{p} respectively denote dispersive and polar surface energies at the solid-gas interface. Therefore, the corresponding expression for the liquid-solid interface (γ_{LS}) can be written as:

$$\gamma_{LS} = \gamma_{LG} + \gamma_{SG} - 2\left(\sqrt{\gamma_{LG}^{d}\gamma_{SG}^{d}} + \sqrt{\gamma_{LG}^{p}\gamma_{SG}^{p}}\right) \quad [4.2]$$

Substituting γ_{LS} from the OWRK model into Young's equation results in the following equation:

$$\gamma_{LG}(1 + cos\theta) = 2\left(\sqrt{\gamma_{LG}^{d}\gamma_{SG}^{d}} + \sqrt{\gamma_{LG}^{p}\gamma_{SG}^{p}}\right) \quad [4.3]$$

Solving equation (4.3) for γ_{SG}^{d} and γ_{SG}^{p} requires measuring contact angles of at least two well-characterized liquids on the surface in question. Data from more than two liquids – or liquid mixtures – can constrain the fit to improve precision.

A more chemically detailed theory than OWRK, proposed by van Oss–Chaudhury–Good (*v*OCG), describes surface wetting as a combination of van der Waals forces and acid-base interactions. Acid-base interactions occur between proton acceptors and proton donors – in Brønsted theory or between electron donors (acids) and electron acceptors (bases) in Lewis theory. The corresponding acid-base contribution to the surface energy is described as the geometric mean of acid and base components:

$$\gamma_{LS} = \gamma_{LG} + \gamma_{SG} - 2\left(\sqrt{\gamma_{LG}^{LW}\gamma_{SG}^{LW}} + \sqrt{\gamma_{LG}^{+}\gamma_{SG}^{+}} + \sqrt{\gamma_{LG}^{-}\gamma_{SG}^{-}}\right) \quad [4.4]$$

where γ_{LG}^{LW} and γ_{SG}^{LW} are Lewis-van der Waals or dispersion energy component at the liquid-gas and solid-gas interfaces, respectively. Similarly, γ_{LG}^{+} and γ_{SG}^{+} are the energy components arising from acid interactions at the liquid-gas and solid-gas interfaces; γ_{LG}^{-} and γ_{SG}^{-} are the corresponding terms arising from base interactions.

Similar to the OWRK model, substituting Equation (4.4) into Young's equation and re-arranging yields an expression for γ_{LG} in terms of the measured contact angle:

$$\gamma_{LG}(1 + cos\theta) = 2\left(\sqrt{\gamma_{LG}^{LW}\gamma_{SG}^{LW}} + \sqrt{\gamma_{LG}^{+}\gamma_{SG}^{+}} + \sqrt{\gamma_{LG}^{-}\gamma_{SG}^{-}}\right) \quad [4.5]$$

Equation (4.5) can be used for estimating solid surface energy components, e.g. γ_{SG}^{LW}, γ_{SG}^{-} and γ_{SG}^{+}, by fitting the model[35, 39] to contact angle measurements of liquids with known γ_{LG}^{LW}, γ_{LG}^{+} and γ_{LG}^{-} values[31, 49]. The value of the combined acid-base term can then be specified (e.g., $\gamma_{SG}^{AB} = \sqrt{\gamma_{SG}^{+}\gamma_{SG}^{-}}$), and the total surface energy is expressed as: $\gamma_{SG} = \gamma_{SG}^{LW} + \gamma_{SG}^{AB}$.

4.5.2 Mixing Rules to Capture the Effects of Solvent-Solvent Interactions on Surface Tension

Equation [4.3] or [4.5] for a binary mixture requires a model to capture the surface tension of the liquid-liquid mixture. In previous work, Zhang et al.[40] was inspired by mixing models originally developed for pressure-volume-temperature equations of state.[50, 51] These authors selected the relatively simple model developed by Berthelot and van der Waals [44, 52] to estimate γ_{mix} from the mixture composition, values of the pure liquids, and a single binary interaction parameter: [53, 54]

$$\gamma_{mix} = \sum_{i}^{n}\sum_{j}^{n} x_i x_j \gamma_{ij} \quad [4.6]$$

where

$$\gamma_{ij} = \left(1 - \delta_{ij}\right)\gamma_{ij}^{o} \quad [4.7]$$

$$\gamma_{ij}^{o} = \sqrt{\gamma_i \gamma_j} \quad [4.8]$$

where *n* is the number of liquids, γ_{mix} is the surface tension of liquid mixtures, x_i and x_j are mole fractions of liquid *i* and liquid *j*, γ_{ij} is either *i-j* unlike interaction energy (when $i \neq j$) or like-molecule interaction (when $i = j$), and δ_{ij} is the binary interaction parameter. The binary interaction parameter captures like interactions and becomes zero (i.e., $\delta_{11} = \delta_{22} = 0$) when $i = j$. When $i \neq j$, the value of the binary interaction parameter is regressed from data – typically between 0 and 1 – to capture interactions between the unlike liquids. Because of their form which gives rise to terms that are second order in mole fraction, Equations (6-8) are sometimes termed "quadratic mixing rules" (QMRs).[52]

The QMRs recommended by Berthelot and van der Waals [52, 55] can be considered the simplest mixing rule for capturing temperature-pressure-volume data using an equation of state. Many more sophisticated models have been proposed.[52] Among these, the Mathias-Klotz-Prausnitz (MKP) mixing rule is another well-adopted model that uses two parameters,δ_{ij} and l_{ji}, to capture molecular interactions:

$$\gamma_{mix} = \sum_{i}^{n}\sum_{j}^{n} x_i x_j \gamma_{ij} + \sum_{i}^{n} x_i \left(\sum_{j}^{n} x_j \left(\gamma_{ji}^{o}\right)^{\frac{1}{3}} \left(l_{ji}\right)^{\frac{1}{3}} \right)^{3} \quad [4.9]$$

where all terms have been defined previously. Again, in the case of *i-i* like-molecule interactions, $\delta_{11} = \delta_{22} = 0$ and $l_{11} = l_{22} = 0$. For unlike-molecule interactions, $\delta_{12} = \delta_{21}$ and $l_{12} = -l_{21}$. As explained for the QMRs, δ_{12} and l_{12} can take different values corresponding to dispersion and

polar interactions (OWRK) or dispersion, acid, and base interactions (*v*OCG). In practice, using single values for each of these parameters results in simpler models with fewer fit parameters.

Applying the mixing rules to the surface energy model results in a family of equations. Table 4.1 shows some four possible outcomes when either the QMR or MKP mixing rules are applied to either the OWRK or *v*OCG models. In Table 4.1, under QMRs subsection, equations (10-11) are expressions of binary mixtures' chemically resolved surface tensions, e.g., $\gamma_{LG,mix}^{P}$ and $\gamma_{LG,mix}^{d}$ for OWRK model, and equations (12-14) are expressions of $\gamma_{LG,mix}^{LW}$, $\gamma_{LG,mix}^{+}$ and $\gamma_{LG,mix}^{-}$ for *v*OCG model. Similarly, equations (15-16) are $\gamma_{LG,mix}^{P}$ and $\gamma_{LG,mix}^{d}$ of OWRK model derived from MKP mixing rule while equations (17-19) are $\gamma_{LG,mix}^{LW}$, $\gamma_{LG,mix}^{+}$ and $\gamma_{LG,mix}^{-}$ of *v*OCG model derived from MKP model. Within each models outcomes, they all contain a or a set of corresponding binary interaction parameters. For example, δ_{12}^{OQ} is the resulting binary interaction parameter of OWRK model under QMR mixing rule and δ_{12}^{vQ} is interaction parameter of vOCG model under MKP mixing rule. The same procedures also apply to MKP mixing rule. Since those binary interaction parameters are both liquid dependent (indicated by subscript "12") and models dependent (indicated by superscript "OQ, *v*Q, OM, *v*M"). A fitting procedure (will be discussed in following section) that takes a specific liquid pair's surface tension under specific models combination will be needed.

Table 4. 1 Resulting mathematical expressions for chemically resolved surface tension of OWRK and vOCG models under different mixing rules

Quadratic Mixing Rules (QMRs)	
Owens-Wendt-Rabel-Kaelble (OWRK)	*van Oss-Chaudhury-Good (vOCG)*
(10) $\gamma^{p}_{LG,mix} = x_1^2\gamma_{LG}^{p,1} + 2x_1x_2\left(1-\delta_{12}^{OQ}\right)\left(\gamma_{LG}^{p,1}\gamma_{LG}^{p,2}\right)^{1/2} + x_2^2\gamma_{LG}^{p,2}$	**(12)** $\gamma^{LW}_{LG,mix} = x_1^2\gamma_{LG}^{LW,1} + 2x_1x_2\left(1-\delta_{12}^{vQ}\right)\left(\gamma_{LG}^{LW,1}\gamma_{LG}^{LW,2}\right)^{1/2} + x_2^2\gamma_{LG}^{LW,2}$
(11) $\gamma^{d}_{LG,mix} = x_1^2\gamma_{LG}^{d,1} + 2x_1x_2\left(1-\delta_{12}^{OQ}\right)\left(\gamma_{LG}^{d,1}\gamma_{LG}^{d,2}\right)^{1/2} + x_2^2\gamma_{LG}^{d,2}$	**(13)** $\gamma^{+}_{LG,mix} = x_1^2\gamma_{LG}^{+,1} + 2x_1x_2\left(1-\delta_{12}^{vQ}\right)\left(\gamma_{LG}^{+,1}\gamma_{LG}^{+,2}\right)^{1/2} + x_2^2\gamma_{LG}^{+,2}$
	(14) $\gamma^{-}_{LG,mix} = x_1^2\gamma_{LG}^{-,1} + 2x_1x_2\left(1-\delta_{12}^{vQ}\right)\left(\gamma_{LG}^{-,1}\gamma_{LG}^{-,2}\right)^{1/2} + x_2^2\gamma_{LG}^{-,2}$
Mathias-Klotz-Prausnitz (MKP)	
Owens-Wendt-Rabel-Kaelble (OWRK)	*van Oss-Chaudhury-Good (vOCG)*
(15) $\gamma^{p}_{LG,mix} = x_1^2\gamma_{LG}^{p,1} + 2x_1x_2(1-\delta_{12}^{OM})\left(\gamma_{LG}^{p,1}\gamma_{LG}^{p,2}\right)^{1/2} + x_2^2\gamma_{LG}^{p,2} + x_1x_2(x_1^2 - x_2^2)l_{12}^{OM}\left(\gamma_{LG}^{p,1}\gamma_{LG}^{p,2}\right)^{1/2}$	**(17)** $\gamma^{LW}_{LG,mix} = x_1^2\gamma_{LG}^{LW,1} + 2x_1x_2(1-\delta_{12}^{vM})\left(\gamma_{LG}^{LW,1}\gamma_{LG}^{LW,2}\right)^{1/2} + x_2^2\gamma_{LG}^{LW,2} + x_1x_2(x_1^2 - x_2^2)l_{12}^{vM}\left(\gamma_{LG}^{LW,1}\gamma_{LG}^{LW,2}\right)^{1/2}$
(16) $\gamma^{d}_{LG,mix} = x_1^2\gamma_{LG}^{d,1} + 2x_1x_2(1-\delta_{12}^{OM})\left(\gamma_{LG}^{d,1}\gamma_{LG}^{d,2}\right)^{1/2} + x_2^2\gamma_{LG}^{d,2} + x_1x_2(x_1^2 - x_2^2)l_{12}^{OM}\left(\gamma_{LG}^{d,1}\gamma_{LG}^{d,2}\right)^{1/2}$	**(18)** $\gamma^{+}_{LG,mix} = x_1^2\gamma_{LG}^{+,1} + 2x_1x_2(1-\delta_{12}^{vM})\left(\gamma_{LG}^{+,1}\gamma_{LG}^{+,2}\right)^{1/2} + x_2^2\gamma_{LG}^{+,2} + x_1x_2(x_1^2 - x_2^2)l_{12}^{vM}\left(\gamma_{LG}^{+,1}\gamma_{LG}^{p,2}\right)^{1/2}$
	(19) $\gamma^{-}_{LG,mix} = x_1^2\gamma_{LG}^{-,1} + 2x_1x_2(1-\delta_{12}^{vM})\left(\gamma_{LG}^{-,1}\gamma_{LG}^{-,2}\right)^{1/2} + x_2^2\gamma_{LG}^{-,2} + x_1x_2(x_1^2 - x_2^2)l_{12}^{vM}\left(\gamma_{LG}^{-,1}\gamma_{LG}^{-,2}\right)^{1/2}$
Overall Surface Tension ($\gamma_{LG,mix}$)	
(20) $\gamma_{LG,mix} = \gamma^{p}_{LG,mix} + \gamma^{d}_{LG,mix}$	**(21)** $\gamma_{LG,mix} = \gamma^{LW}_{LG,mix} + 2\sqrt{\gamma^{+}_{LG,mix}\,\gamma^{-}_{LG,mix}}$
Binary Interaction Parameters	
δ_{12}^{OQ}, δ_{12}^{OM}, l_{12}^{OM}	δ_{12}^{vQ}, δ_{12}^{vM}, l_{12}^{vM}

4.5.3 Using Contact Angle Measurements Obtained from Binary Liquid Mixtures to Determine Solid Surface Energy

Mixture surface tension data, a surface tension model, chemically resolved surface tension data for two pure liquids, and a mixing model are fed to an optimization routine, as shown in Figure 4.1a. After optimization, the output are best-fit values of chemically resolved surface tension parameters appropriate for the binary mixture, e.g., $\gamma^{d}_{LG,mix}$ and $\gamma^{p}_{LG,mix}$ if the OWRK model is used or $\gamma^{LW}_{LG,mix}$, $\gamma^{+}_{LG,mix}$, and $\gamma^{-}_{LG,mix}$ for the *v*OCG model. The surface tension at a given composition can therefore be determined using the selected mixing model, for example the QMR or MKP mixing rules. Then, contact angle data are measured as a function of composition on a surface of interest. These contact angle data can be linearized, as is common practice, for linear least squares determination of surface energy terms, for example γ^{P}_{SG} and γ^{d}_{SG} for the OWRK model or γ^{LW}_{SG}, γ^{-}_{SG} and γ^{+}_{SG} for the *v*OCG model. The Results and Discussion section applies this

approach to several model surfaces, using contact angle data obtained from mixtures of water-miscible organic solvents and water.

4.6 Results and Discussions

This study has two objectives. The first objective is to generalize existing methods for characterizing chemically resolved surface tension of liquid mixtures, i.e., for using data for pure liquids and composition for compositionally resolved description of surface tension in terms of intermolecular interactions. To accomplish this objective, we adopted two widely used mixing rules that have been successfully applied to equation of state of mixtures, which are Quadratic Mixing Rules (QMRs) and Mathias-Klotz-Prausnitz (MKP).[56] For each mixing rule, we then used surface tension data for determination of surface tension parameters, e.g., those appearing in the OWRK or *v*OCG models.

The second objective is to evaluate selected polymer surface energies, including PVC, PDMS and PMMA using the surface tension models and new measurements of binary liquid mixture contact angles. The new approach was evaluated to determine if negative surface energy components could improve the precision of parameter estimates and if negative parameter values could be avoided.

4.6.1 Composition-Dependent Surface Tension

The new surface energy characterization method requires an expression to model composition-dependent surface tension. Surface tension data were obtained from the literature for the water-DMSO,[57] water-formamide,[40] and water-ethylene glycol[58] mixtures. These literature data were then modeled using different variations of the QMRs and MPK-based expressions shown in the Table 4.1 as Equations (10-11) for the OWRK model and (12-14) for the vOCG model, respectively.

Figure 4.2 shows the results of fitting surface tension data using the QMRs (*A* and *B*) and using the MKP mixing rule (*C* and *D*) and inset parity comparison. In all cases, a single value is used for each fitting parameter appearing in the mixing rule. In other words, the values of the fitting parameters appearing in the OWRK model are equal to one another for polar and dispersion interaction and likewise the dispersion, acid, and base terms appearing in the *v*OCG model are set equal to one another. Best-fit values of these parameters (δ_{12}^{OQ} and δ_{12}^{vQ} for QMRs or δ_{12}^{OM}, δ_{12}^{vM}, l_{12}^{OM} and l_{12}^{vM} for MKP) were obtained by comparing surface tension of liquid mixtures from equation (20) and (21) with experimental values, and their fitting uncertainties are provided in Table 4.2.

Figure 4.2 shows surface tension fitting plots for four mixing and wetting models combinations: OWRK+QMRs, *v*OCG+QMRs, *v*OCG+MPK and vOCG+MPK. Figure 4.2 shows that – in all cases – the mixing rule models capture all observed trends in the literature surface tension data. Overall, the quality of fit as quantified by the regression parameter r^2 depends mainly on the mixing model (QMRs vs. MKP) and less on the interaction model (OWRK vs. *v*OCG). In all cases, r^2 is greater than 0.90 and is greater than 0.95 for the MKP-based model. The mean absolute error (MAE) for wetting models accommodating QMRs mixing rule is slightly worse (e.g., 1.19 mN/m for OWRK and 1.08 mN/m for vOCG) than MKP mixing rule (e.g., 0.83 mN/m for OWRK and 0.87 mN/m for vOCG model).

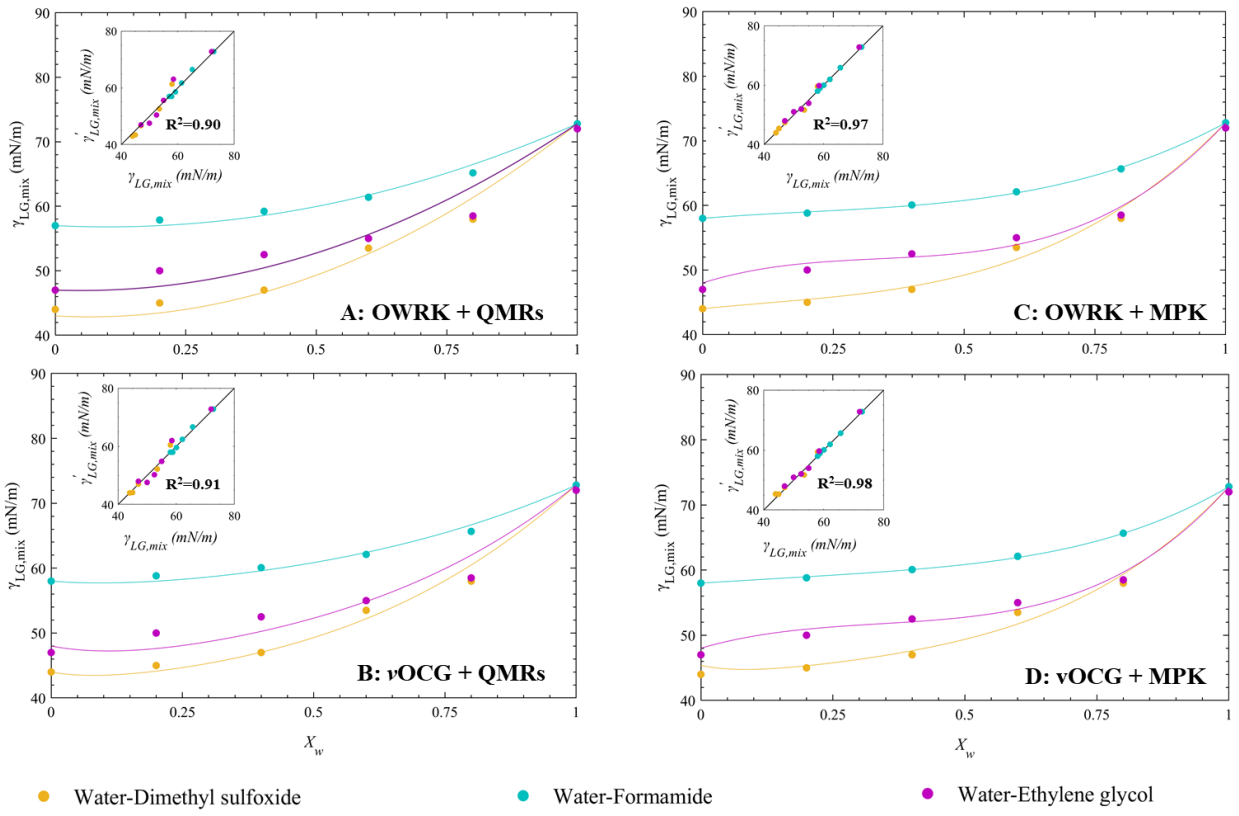

Figure 4. 2 Comparisons of predicted values of the total liquid surface tension, $\gamma_{LG,mix}$ with measured values for several binary mixtures as functions of the mole fraction of water (x_w) present in the mixture; (**A**) shows predictions based on the OWRK energy model and QMR mixing rule, (**B**) is for the *v*OCG surface energy model and QMR mixing rule, (**C**) is for OWRK surface energy model and MPK mixing rule, and (**D**) is for *v*OCG surface energy model and MPK mixing rule.

Having a r^2 close to unity does not necessarily justify the feasibility of mixing rules. This especially needs to be careful when dealing multiple variable regression analysis where overfitting may be a problem if degree of freedom is much greater than the number of constraints. When take a close look at figure 4.2C and 2D, although water-DMSO and water-formamide exbibits a singular trend, water-ethylene glycol has a few data points not following a singular trend,

Interestingly, the MKP-based model identifies an inflection point in the relationship between surface tension and composition for the water-ethylene glycol mixture that the QMRs-based model does not capture. This maybe relates to overfitting of equation (21) where it takes two adjustable parameters, and it is largely sensitive to experimental data quality.

Apparently, having multiple adjustable variables may lead to over fitting issue, departing developed models from "real model). However, having too few variables can lead to inaccuracy and underfitting of models. Akaike information criterion (A.I.C.) has been widely used to balance trade-off between these two situations: overfitting and underfitting. Therefore, we performed A.I.C. calculations for polynomials, e.g. $AIC(k) = -\frac{n}{2}log(L^o) + \frac{2}{n}(k+2)$ where n is sample size, L^o is maximum likelihood and k is number of variables. Calculated AIC values are listed in Table 4.2. Surprisingly, surface tension models using QMR mixing rule have the smallest values compared to models incorporated with MKP models, meaning QMR mixing rule can retain most of data information and predict well enough while MKP mixing rule tend to overfit existent data. Specifically, QMR mixing rule along with OWRK model gives the best performance while MKP mixing rule combining with OWRK has the worst balance between overfitting and underfitting. Thus, we will specifically focus on using QMR mixing models for subsequent surface energy analysis.

Table 4. 2 Binary interaction parameters of water-DMSO, water-formamide and water-ethylene glycol using QMRs and MKP mixing rules.

Model name	**Parameter**	**Water-DMSO**	**Water-formamide**	**Water-ethylene glycol**	**A. I. C.**
OWRK + QMR	δ_{12}^{OQ}	0.162 ± 0.046	0.069 ± 0.015	0.202 ± 0.052	-1.59

*v*OCG + QMR	δ_{12}^{vQ}	0.389 ± 0.038	0.202 ± 0.013	0.379 ± 0.045	0.96
OWRK + MKP	δ_{12}^{OM}	0.163 ± 0.042	0.069 ± 0.004	0.202 ± 0.024	11.53
	l_{12}^{OM}	0.316 ± 0.228	0.173 ± 0.019	0.563 ± 0.133	
*v*OCG + MKP	δ_{12}^{vM}	0.385 ± 0.038	0.200 ± 0.001	0.291 ± 0.022	11.48
	l_{12}^{vM}	0.210 ± 0.201	0.120 ± 0.009	0.530 ± 0.118	

Note: best-fit interaction parameters for different combinations of wetting model and mixing rule. Superscript of each parameters represents first letter of corresponding combinations, e.g., δ_{ij}^{OQ} represents interaction parameter for **O**WRK + **Q**MRs pair.

Lastly, Table 4.2 shows quantitative differences between each mixtures. For example, despite the similarity of r^2, values for δ_{ij} differentiates among liquid mixtures. For instance, in OWRK model, water-ethylene glycol has the greatest δ_{ij} (0.202) while water-formamide has the lowest value (0.069), which may suggest water-formamide interaction is stronger than water-ethylene glycol. For *v*OCG model, trend is similar but δ_{ij} are greater than those in OWRK models. For MPK mixing rule, Table 4.2 shows similar conclusion that water-ethylene glycol and water-DMSO have largest δ_{ij} and l_{ij} compared to water-formamide. Variation of δ_{ij} and l_{ij} may be an indicator for characterizing binary system molecular interaction. But in-depth knowledge should direct to using δ_{ij} and l_{ij} for calculating specific interaction type such as acid, base, or dispersion.

4.6.2 Liquid Selection and Mixtures' Contact Angles on PDMS, PVC and PMMA

Water and a series of organic liquids were selected for preparing binary mixtures for contact angle measurements. Water is an obvious choice for this purpose. Organic liquids included in this study were selected for their miscibility with water, lower volatility than water to minimize evaporation, chemical compatibility with substrates, availability of data, and safety. DMSO, formamide, and

ethylene glycol satisfy these criteria. Table 4.3 shows that the selected liquids all have normal boiling points greater than 100 ^{o}C, potentially mitigating evaporation issue during contact angle measurements.[59] Selected liquids are safe to handle as all liquids having lethal dose (LD_{50}) greater than 5000 mg/kg.[60] As for data requirements, Table4. 3 lists values of individual surface tension parameters appropriate for the OWRK and *v*OCG models. Finally, the selected liquids exhibit a wide range of polarity, which is required to ensure accurate fitting of corresponding contact angles to the surface wetting models.[40]

Table 4. 3 Surface tension parameters for selected probe liquids[40]

Liquid	**OWRK**			***v*OCG**				
	γ_{LG}	γ_{LG}^{d}	γ_{LG}^{p}	γ_{LG}^{LW}	γ_{LG}^{AB}	γ_{LG}^{+}	γ_{LG}^{-}	*B.P.*
Water	72.8	21.8	51	21.8	51	25.5	25.5	100
DMSO	44	36	8	36	8	0.5	32	189
Formamide	58	39	19	39	19	2.3	39.6	210
Ethylene glycol	48	29	19	29	19	3.0	30.1	196

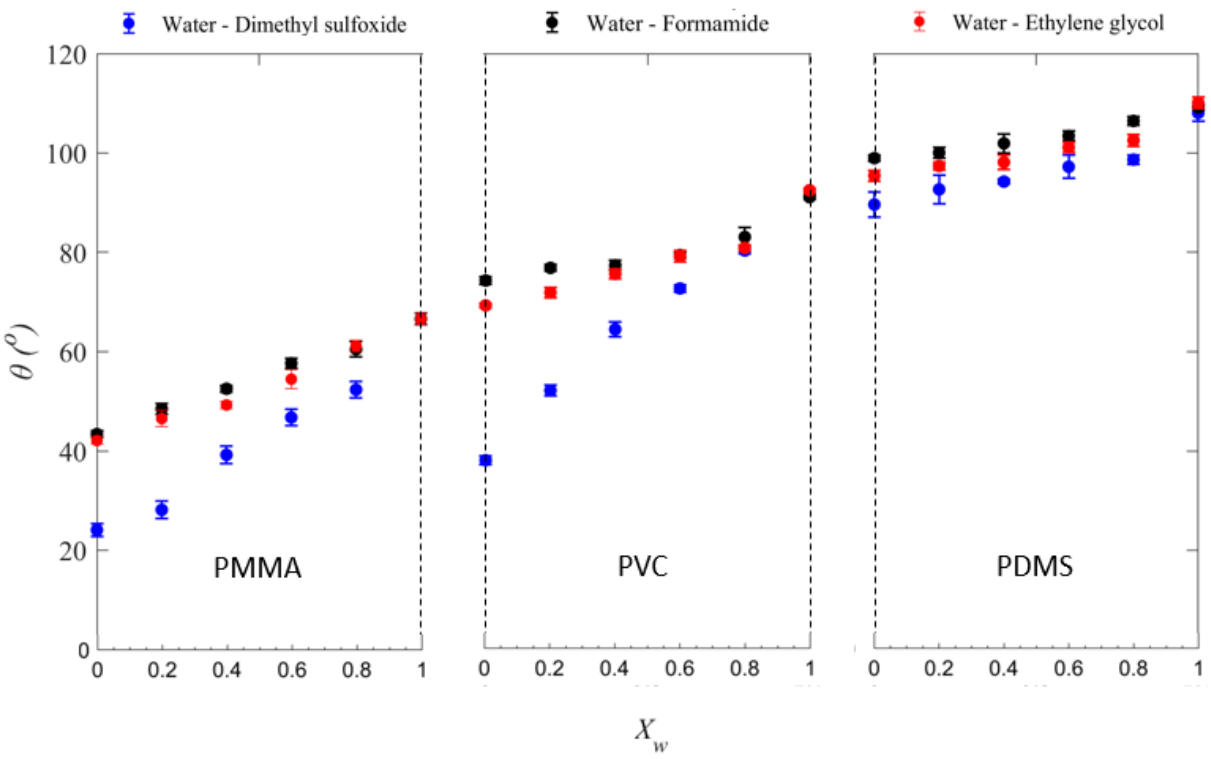

Figure 4. 3 Measured contact (θ) angles of water-DMSO, water-formamide and water-ethylene glycol mixtures on polydimethylsiloxane (*PDMS*), polyvinyl chloride (*PVC*) and poly(methyl methacrylate) (*PMMA*) as functions of water mole fraction, *Xw*.

The next step was measurement of contact angles for binary mixtures of water with DMSO, formamide, and ethylene glycol on PDMS, PVC, and PMMA surfaces, as shown in Figure 4.3. These three polymers were selected to represent a wide range of hydrophobicity, from mildly hydrophobic to highly hydrophobic [61-63]. Several consistency checks confirm the quality of the data presented in Figure 4.3. Error bars, which represent three measurements made at different locations on the samples, are less than 5°. For the pure liquids, which constitute the end points in Figure 4.3, contact angles measured in this study are in good agreement with previously reported measurements. For the liquid mixtures, measured contact angles increase with increasing water

content in the binary mixture – as expected for liquid interaction with hydrophobic surfaces. At a given composition, measured values of contact angle increase in the trend DMSO < formamide ~ ethylene glycol, which matches expectations based on their corresponding surface tensions (see Table 4.3).

4.6.3 Liquid Surface Tension Components

To this end, we have compared two mixing rules, QMRs and MKP. Apparently, QMRs mixing rule is simpler than MKP and easy to implement. Additionally, QMRs does not have over-fitting issues as compared to MKP whose two adjustable parameters exceed the need for this study. Therefore, we decided to use QMRs for the subsequent polymer surface energy determinations.

After obtaining best-fit binary interaction parameters, liquid surface tension components must be extracted for later polymer surface energy determination along with contact angles. Therefore, equation (10-11) is revisited for getting $\gamma^{p}_{LG,mix}$ and $\gamma^{d}_{LG,mix}$ of OWRK model. Figure 4.4 shows the results. In figure 4.4(left), since water is the most polar solvent, all mixtures $\gamma^{p}_{LG,mix}$ increases as water content increases; conversely, dispersion component ($\gamma^{d}_{LG,mix}$) drops as water increases, due to water's small size and dispersion force.

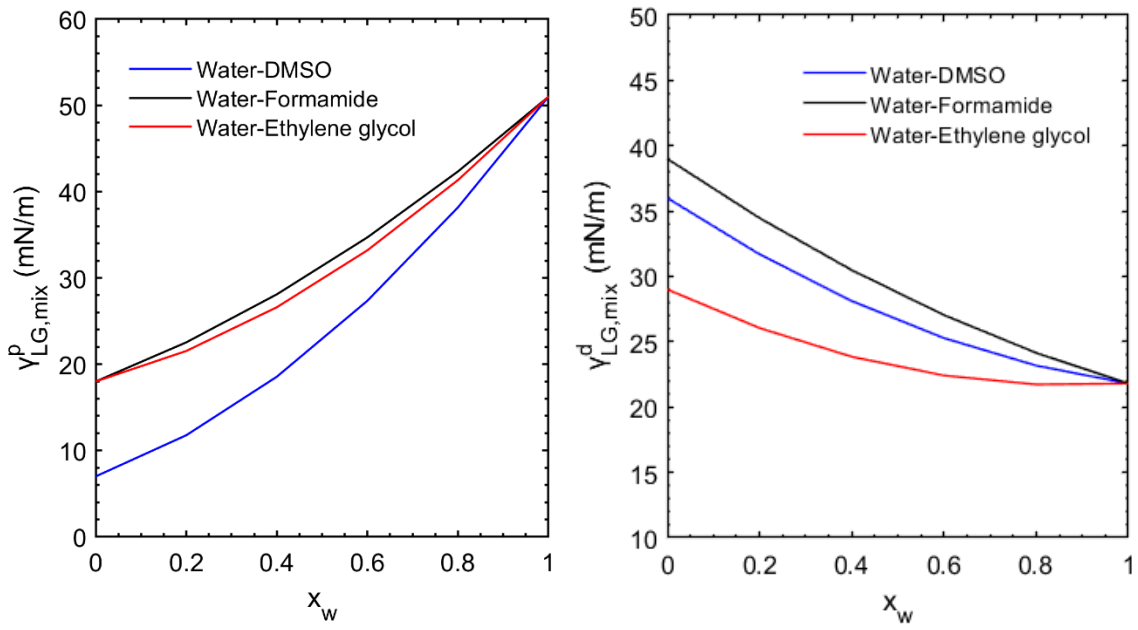

Figure 4. 4 (Left) Polar ($\gamma^{P}_{LG,mix}$), and (Right) dispersive component ($\gamma^{d}_{LG,mix}$) components from OWRK model for water-DMSO; (b) water-formamide and (c) water-ethylene glycol.

Similarly, equations (12-14) are revisited for determining $\gamma^{LW}_{LG,mix}$, $\gamma^{+}_{LG,mix}$ and $\gamma^{-}_{LG,mix}$ components and figure 4.4 is resulting plot. Figure 4.5 shows that calculated van der Waals, acid and base surface tension components for water-DMSO, water-formamide and water-ethylene glycol mixtures.in general, as water composition increases, van der Waals dispersion and basicity decreases while acidity increases. For van der Waals dispersion, formamide has the largest values while ethylene glycol has the smallest value. Formamide and DMSO are branched molecules while ethylene glycol is long chain molecules, which makes its interaction with other molecules spatially dependent. For pure solvents, the acidity components are all small due to their inability to accept electrons. The relatively small value for *pKa* also justify its small acidic components as DMSO has pKa around 35, formamide has *pKa* around 24 and ethylene glycol has *pKa* around 15. When water content increases, all solvent-water mixtures acid component increases because water is a

strong electron donor. For the basic term, the opposite trend was observed that all solvent-water mixtures base components drop as water content increases. Overall, the predicted acid/base/van der Waals components agree with the molecular aspect of interactions in aqueous solution.

Various experimental procedures are discussed for indirectly determine Lifshitz van der Waals/acid-base component of liquid mixtures. For example, Terzis *et al.* has developed a contact angle-based method to extract water-urea mixtures surface tension parameters. The problem with experimental approach is that correlating molecular knowledge of molecule interactions with macroscopic properties, such as static contact angle, can lead to significant uncertainty. The potential benefits of this method may be useful for validating experimentally determined surface tension components.

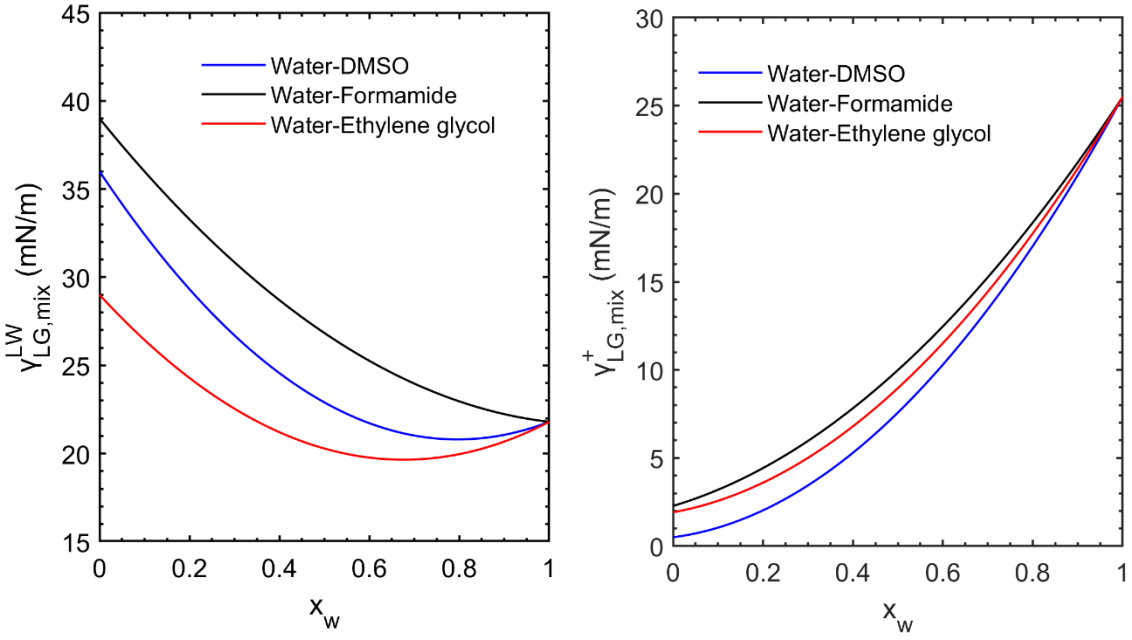

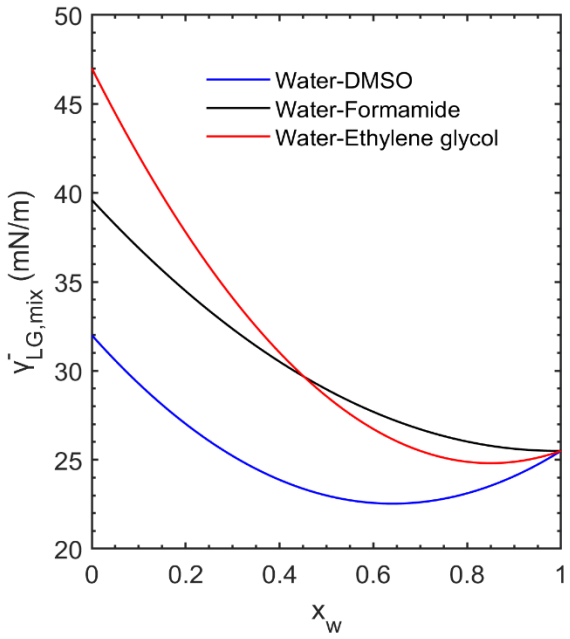

Figure 4. 5 Lewis van der Waals ($\gamma^{LW}_{LG,mix}$), acid ($\gamma^{+}_{LG,mix}$) and base ($\gamma^{-}_{LG,mix}$) components from vOCG model for (a) water-DMSO; (b) water-formamide and (c) water-ethylene glycol.

4.6.4 Effect of Water Surface Energy Components Variation on Surface Mixture Tension Fitting

Water surface tension parameters have been questioned in literatures. Main question is whether acid and base term of water have the same values. To evaluate how water's acid/base term ratio on our surface tension fitting, we varied water acid to base component ratio, e.g. $\delta_w = \gamma^{+}_{LG,w}/\gamma^{-}_{LG,w}$ as 0.5, 1.0, 1.5, 2.0, 2.5 and 3.0, under each δ_w value, the best fit binary interaction parameter (k_{ij}) is determined by Matlab non-linear regression. Figure 4.6, 4.7 and 4.8 show the results. The results show that δ_w has subtle influence on surface tension fitting. In fact, when we set δ_w=1, the fitting seems reasonably good.

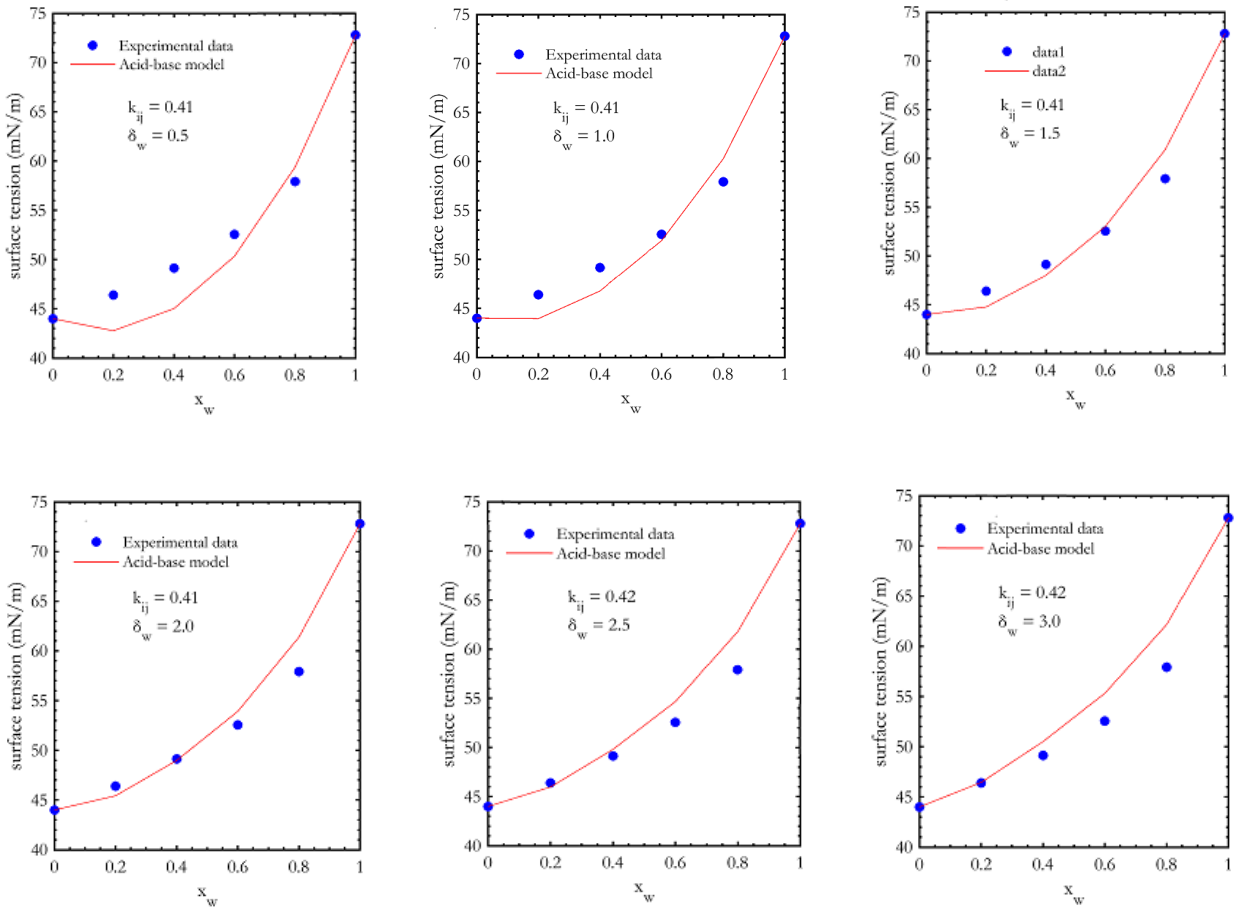

Figure 4. 6 water-dimethyl sulfoxide mixture surface tension as a function of water mole fraction (x_w). The red line represents the theoretical surface tension predicted by modified acid-base theory with different water acid/base ratio.

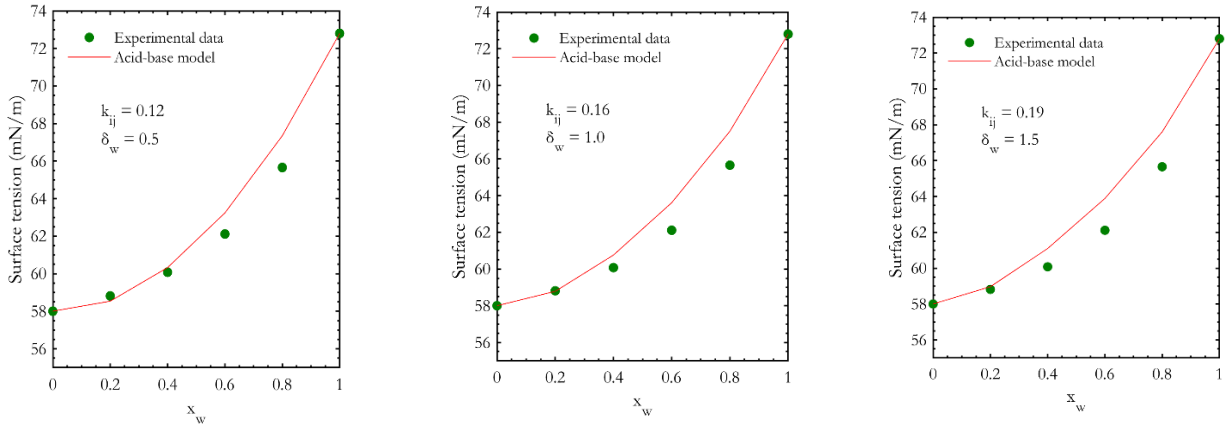

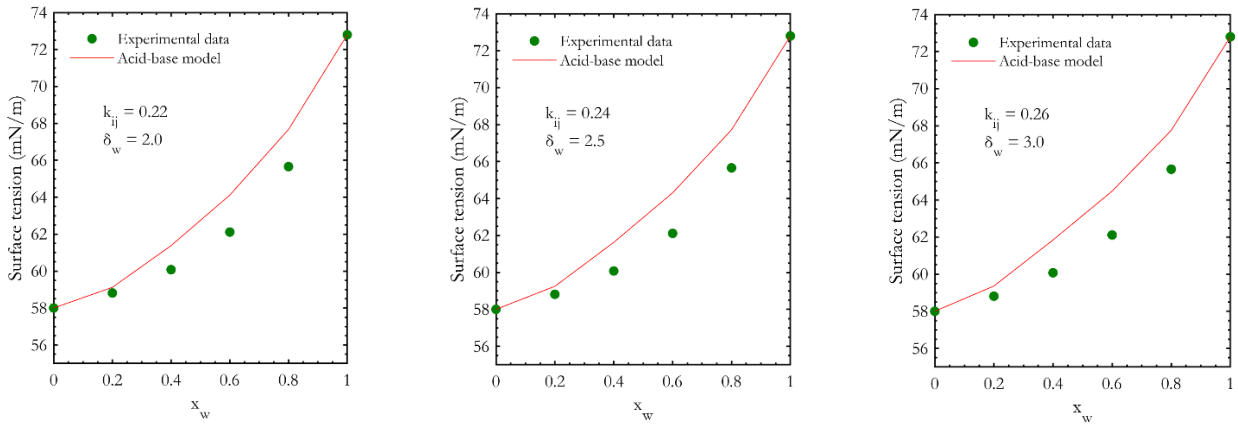

Figure 4. 7 water-formamide mixture surface tension as a function of water mole fraction (x_w). The red line represents the theoretical surface tension predicted by modified acid-base theory with different water acid/base ratio.

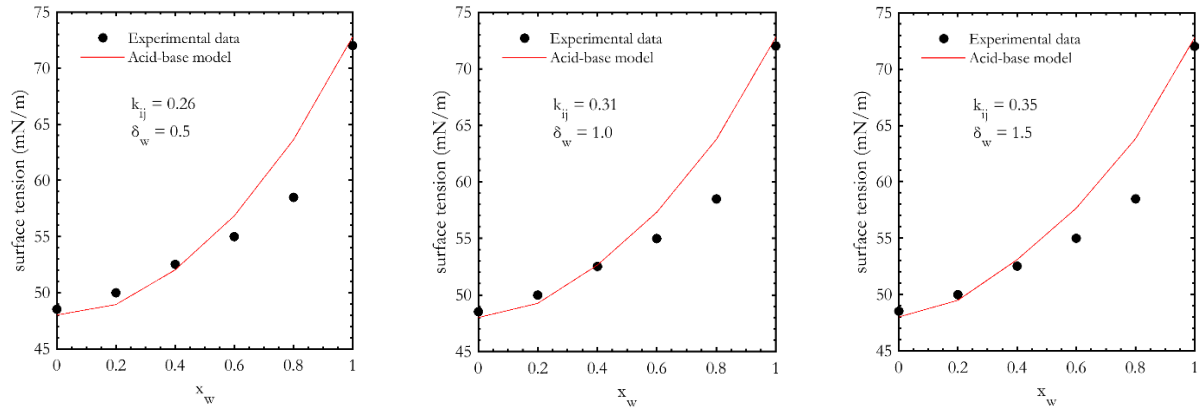

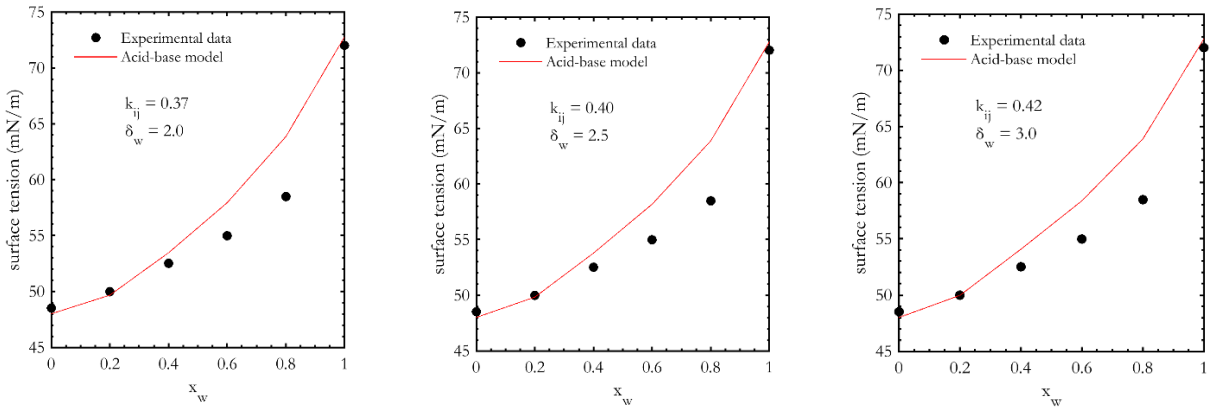

Figure 4. 8 water-formamide mixture surface tension as a function of water mole fraction (x_w). The red line represents the theoretical surface tension predicted by modified acid-base theory with different water acid/base ratio.

4.6.5 Polymers Surface Energy Determination

To this end, we have obtained all required data and models for obtaining polymer surface energy. specifically, we have developed theoretical basis for extracting water-organic mixtures surface tension components using equations (10-11 & 12-14). Composition-dependence of surface tension components, γ_{LG}^{d}, γ_{LG}^{p}, γ_{LG}^{LW}, γ_{LG}^{+} and γ_{LG}^{-} are analyzed in SI. Along with contact angles data, equations (3) and (5) are then used to extract γ_{SG}^{d}, γ_{SG}^{p}, γ_{SG}^{LW}, γ_{SG}^{+} and γ_{SG}^{-}. Table 4.4 provides surface energy components results for PDMS, PMMA and PVC, respectively.

Table 4.4 shows surface energy components of PDMS, PVC and PMMA for both OWRK and *v*OCG models. OWRK model consists of γ_{SG}^{d} and γ_{SG}^{d} components while *v*OCG model consists of γ_{SG}^{LW}, γ_{SG}^{+} and γ_{SG}^{-} components. For OWRK model, all mixtures give close value for total surface energy ranging from 10.25-11.13 mN/m, suggesting all liquid mixtures, water-DMSO, water-formamide and water-ethylene glycol, are suitable for PDMS surface energy determination. Determined total surface energy is also consistent with our previous results.[40] For specific

components, such as γ_{SG}^{d} and γ_{SG}^{p}, each mixtures has similar values as well. For more sophisticated *v*OCG model, again, all mixtures have similar total surface energy ranging from 11-12.33 mN/m. Despite that acid and base term vary, this is mainly because of relatively small values, especially acid term which is close to zero. A common problem with pure-liquid approach, as mentioned in introduction, is the negative acid term issue. However, in our mixture approach, all mixtures give positive acid terms, which recommend that using more data points would reduce the risk of using a few pure liquids in which some liquids may have large contact angles uncertainties.

Surface free energy of PVC is shown in Table 4.4 as well. For two components OWRK model, water-formamide and water-ethylene glycol mixtures estimate similar total surface energy (γ_{SG}) at around 23 mN/m, consistent with literature reported values. For example, Demirci et al. has shown that un-modified PVC has the surface energy of 28 mN/m, which is close to the value of 27.39 mN/m in Table 4.4. [64]. While water-DMSO estimates significantly large surface energy. This is due to DMSO is not compatible with PVC as DMSO is commonly used to swell/dissolve PVC.[65] Because of extra chemical interaction between DMSO and PVC, an exceed amount of interfacial energy will be released at liquid-solid interface, causing overestimation for surface energy. For *v*OCG model, the same observation is observed. Interestingly, the vOCG data indicates that the overestimation of PVC surface energy by water-DMSO mainly comes from γ_{SG}^{LW} component, but not γ_{SG}^{+} or γ_{SG}^{-}. Due to DMSO's incompatibility with PVC, later analysis will exclude DMSO from PVC.

For OWRK model, determined PMMA surface energy is between 37-41 mN/m, which is consistent with literature results. For example, Ozcan et al. [66] measured PMMA thin film surface energy using *v*OCG theory, and their determined total surface energy is within the range of 38-50 mN/m. water-DMSO and water-formamide have similar γ_{SG}^{d} and γ_{SG}^{p} terms, while water-ethylene

glycol seems overestimating γ_{SG}^{p} and underestimating γ_{SG}^{d}. This could be due to experimental uncertainty. For three components model, again, even for relatively small acid term (smaller than 1 mN/m), mixture approach does not result in negative acid term, further suggesting the observed negative acid term in literatures mainly comes from insufficient liquids for contact angles measurement. Uncertainties in pure liquid contact angles measurement will worsen the surface energy determination. Here, having six different compositions of mixtures (single mixtures) or eighteen data points (all available data column in table 4.4) improves the measurement and avoids negative acid term issue.

Table 4. 4 Summary of surface free energy (mN/m) determined by liquid mixtures contact angles

Polymer		Surface energy	Water-DMSO	Water-formamide	Water-ethylene glycol	All available data
PDMS	OWRK	γ_{SG}	11.13 ± 0.75	10.25 ± 0.43	10.35 ± 1.30	10.89 ± 0.49
		γ_{SG}^{d}	8.67 ± 0.61	7.95 ± 0.37	8.01 ± 1.16	8.85 ± 0.43
		γ_{SG}^{p}	2.46 ± 0.44	2.30 ± 0.21	2.34 ± 0.59	2.04 ± 0.24
	*v*OCG	γ_{SG}	10.96 ± 1.18	11.35 ± 0.74	12.33 ± 1.83	11.16 ± 1.88
		γ_{SG}^{LW}	9.26 ± 1.01	10.28 ± 0.64	11.18 ± 1.67	9.66 ± 1.85
		γ_{SG}^{+}	0.18 ± 0.35	0.12 ± 0.29	0.17 ± 0.60	0.20 ± 0.25
		γ_{SG}^{-}	4.02 ± 0.51	2.39 ± 0.22	1.93 ± 0.45	2.82 ± 0.26
PVC	OWRK	γ_{SG}	38.70 ± 3.01	23.15 ± 1.36	23.78 ± 2.57	20.42 ± 2.87
		γ_{SG}^{d}	38.36 ± 3.01	17.41 ± 1.17	19.63 ± 2.36	19.63 ± 2.83
		γ_{SG}^{p}	0.34 ± 0.11	5.74 ± 0.70	4.15 ± 1.02	0.79 ± 0.50
	*v*OCG	γ_{SG}	32.93 ± 1.49	24.98 ± 1.52	21.55 ± 1.82	25.72 ± 1.86
		γ_{SG}^{LW}	29.25 ± 1.26	21.0 ± 1.15	18.11 ± 1.52	21.03 ± 1.78

		γ_{SG}^{+}	0.94 ± 0.50	0.75 ± 0.44	0.57 ± 0.41	1.78 ± 0.25
		γ_{SG}^{-}	3.60 ± 0.62	5.27 ± 0.89	5.20 ± 0.91	3.09 ± 0.49
PMMA	**OWRK**	γ_{SG}	41.15 ± 2.26	41.78 ± 3.08	36.64 ± 4.19	40.79 ± 1.96
		γ_{SG}^{d}	30.63 ± 1.76	31.07 ± 2.63	23.53 ± 2.25	30.71 ± 1.64
		γ_{SG}^{p}	10.52 ± 1.42	10.71 ± 1.61	13.11 ± 3.54	10.08 ± 1.07
	***v*OCG**	γ_{SG}	43.45 ± 2.66	45.31 ± 1.60	43.49 ± 1.40	45.49 ± 2.11
		γ_{SG}^{LW}	42.60 ± 2.35	39.77 ± 1.55	40.1 ± 1.23	44.41 ± 2.01
		γ_{SG}^{+}	0.01 ± 0.02	0.64 ± 0.06	0.22 ± 0.05	0.02 ± 0.08
		γ_{SG}^{-}	18.05 ± 2.18	11.97 ± 0.38	13.03 ± 0.66	14.64 ± 0.65

4.6.6 Contact Angle Prediction Using Determined Surface Energy Components

Lastly, to further demonstrate accuracy of determined surface energy components of polymers, we have combined all the tested liquid mixtures on examined polymer surfaces on a combined parity plot. Noticing that contact angles range is from 0-120^{o}, suggesting that determined surface energy components have predicting ability. This predicting power is a combination of liquid surface tension properties, solid surface energy properties. Additionally, considering that those parameters, both for liquid and solid, captures the chemical aspects of molecular interaction such as acid-base interaction and van der waals interaction, the combined model is a chemo-mechanical approach for understanding the mechanical and chemical aspects of surface wetting.

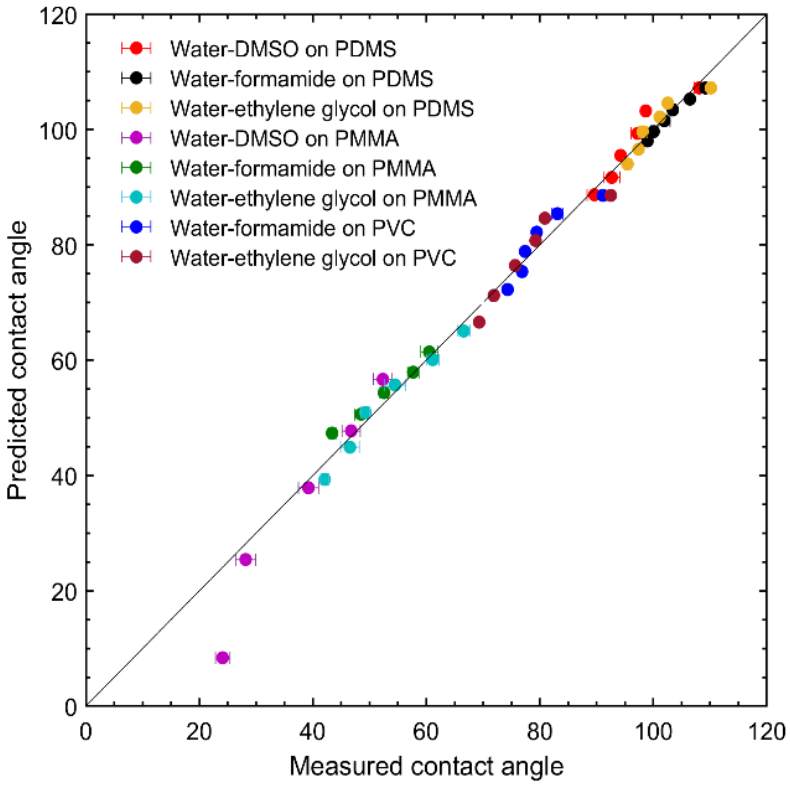

Figure 4. 9 Parity plot comparing predicted contact angle and measured contact angle

4.7 Conclusions

Quantifying solid surface acidity and basicity are important in a number of applications including cell adhesion and heterogeneous catalysis synthesis. vOCG model has long been developed to determine solid surface acid/base/van der waals surface energy components but suffers from problems associated with often negative acid components, consistency dependence on the liquids tested and accuracy problems. It also suffers from the problem of limited liquid available for contact angle measurements due to the parameters limitation for liquids.

Here, we developed a binary mixture approach for accurately and precisely determining polymer acid/base/van der waals surface energy components using vOCG model. We first developed a mixing theory to extract organic-water mixtures, including water-DMSO, water-formamide and water-ethylene glycol surface tension parameters ($\gamma_{L,mix}^{LW}$, $\gamma_{L,mix}^{+}$ and $\gamma_{L,mix}^{-}$). The

developed theory can predict surface tension for selected liquid mixtures well. To test our method, we selected commonly used polymer surfaces, including PDMS, PVC and PMMA, ranging from high energy surface to low energy surface. A series of contact angles of liquid mixtures on those surfaces were measured and then used to calculate acid/base/van der waals surface energy components. The results show that using mixtures can effectively eliminate negative acid-components problem, which is commonly encountered when using pure liquids. In contrast with pure-liquid approach in which the determined solid surface energy components rely largely on liquid combinations and its accuracy is greatly low, the liquid mixtures improve the accuracy and precision. Lastly, we used the determined surface energy parameters as a fixed physical property, evaluating its ability to predict contact angles of corresponding liquid mixtures on those polymer surfaces. The results show that all liquid mixtures and polymer surfaces (PVC, PMMA and PDMS) can be unified into a parity plot, suggesting the accuracy of the solid acid/base/van der waals parameters and its surface wetting predicting power.

4.8 ACKNOWLEDGEMENT

The work was funded by the U.S. National Science Foundation (Grant # CBET 1554283 to M.T.T.).

4.9 Reference

1. Mukherjee, A., N. Sekar, and S. Panda, *Influence of the Acid–Base Component of Surface Energy on Optical Properties of Immobilized Dyes.* Industrial & Engineering Chemistry Research, 2017. **56**(46): p. 13543-13551.
2. Gamelas, J., et al., *Unique combination of surface energy and Lewis acid–base characteristics of superhydrophobic cellulose fibers.* Langmuir, 2017. **33**(4): p. 927-935.

3. Park, S., et al., *The Lifshitz-van der Waals acid-base theory assisted fabrication of MFI-containing mixed matrix membranes for gas separations.* Microporous and Mesoporous Materials, 2018. **264**: p. 60-69.
4. Orndorf, N., S. Singla, and A. Dhinojwala, *Transition in the Acid-Base Component of Surface Free Energy of Ice upon the Premelting of its Second Molecular Bilayer.* arXiv preprint arXiv:2005.04475, 2020.
5. Nategh, M., et al., *Impact of Asphaltene Surface Energy on Stability of Asphaltene–Toluene System: A Parametric Study.* Langmuir, 2018. **34**(46): p. 13845-13854.
6. Han, B., et al., *Determination of surface energy parameters of hydrophilic porous membranes via a corrected contact angle approach.* Langmuir, 2019. **35**(47): p. 15009-15016.
7. Oh, I.-K., et al., *Surface Energy Change of Atomic-Scale Metal Oxide Thin Films by Phase Transformation.* ACS nano, 2020. **14**(1): p. 676-687.
8. Williams, D.R., *Particle engineering in pharmaceutical solids processing: surface energy considerations.* Current pharmaceutical design, 2015. **21**(19): p. 2677-2694.
9. Erickson, D., D. Sinton, and D. Psaltis, *Optofluidics for energy applications.* Nature Photonics, 2011. **5**(10): p. 583.
10. Hamza, A., et al., *Development of membranes with low surface energy to reduce the fouling in ultrafiltration applications.* Journal of Membrane Science, 1997. **131**(1-2): p. 217-227.
11. Sharifi-Aghili, A., et al., *When and How Self-cleaning of Superhydrophobic Surfaces Works.* Sci. Adv, 2020. **6**.

12. Blossey, R., *Self-cleaning surfaces—virtual realities.* Nature materials, 2003. **2**(5): p. 301-306.

13. Kota, A.K., G. Kwon, and A. Tuteja, *The design and applications of superomniphobic surfaces.* NPG Asia Materials, 2014. **6**(7): p. e109-e109.

14. Kuo, S.-W., et al., *Preparing low-surface-energy polymer materials by minimizing intermolecular hydrogen-bonding interactions.* The Journal of Physical Chemistry C, 2009. **113**(48): p. 20666-20673.

15. Wang, J., et al., *Fluorinated and thermo-cross-linked polyhedral oligomeric silsesquioxanes: New organic–inorganic hybrid materials for high-performance dielectric application.* ACS applied materials & interfaces, 2017. **9**(14): p. 12782-12790.

16. Dai, X., et al., *Hydrophilic directional slippery rough surfaces for water harvesting.* Science advances, 2018. **4**(3): p. eaaq0919.

17. Mi, H.-Y., et al., *Controlling superwettability by microstructure and surface energy manipulation on three-dimensional substrates for versatile gravity-driven oil/water separation.* ACS applied materials & interfaces, 2017. **9**(43): p. 37529-37535.

18. Chaudhury, M.K., *Interfacial interaction between low-energy surfaces.* Materials Science and Engineering: R: Reports, 1996. **16**(3): p. 97-159.

19. Huhtamäki, T., et al., *Surface-wetting characterization using contact-angle measurements.* Nature protocols, 2018. **13**(7): p. 1521-1538.

20. Subedi, D., *Contact angle measurement for the surface characterization of solids.* Himalayan Physics, 2011. **2**: p. 1-4.

21. Srinivasan, S., G.H. McKinley, and R.E. Cohen, *Assessing the accuracy of contact angle measurements for sessile drops on liquid-repellent surfaces.* Langmuir, 2011. **27**(22): p. 13582-13589.

22. Zubar, T., et al., *Method of surface energy investigation by lateral AFM: application to control growth mechanism of nanostructured NiFe films.* Scientific reports, 2020. **10**(1): p. 1-10.

23. Xu, X., et al., *Surface tension measurement from the indentation of clamped thin films.* Soft matter, 2016. **12**(23): p. 5121-5126.

24. Calvimontes, A., *The measurement of the surface energy of solids using a laboratory drop tower.* npj Microgravity, 2017. **3**(1): p. 1-14.

25. Shimizu, R.N. and N.R. Demarquette, *Evaluation of surface energy of solid polymers using different models.* Journal of Applied Polymer Science, 2000. **76**(12): p. 1831-1845.

26. Berro, H., N. Fillot, and P. Vergne, *Molecular dynamics simulation of surface energy and ZDDP effects on friction in nano-scale lubricated contacts.* Tribology international, 2010. **43**(10): p. 1811-1822.

27. Ata, S., et al., *Influence of matching solubility parameter of polymer matrix and CNT on electrical conductivity of CNT/rubber composite.* Scientific reports, 2014. **4**(1): p. 1-8.

28. Bradley, R.S., *LXXIX. The cohesive force between solid surfaces and the surface energy of solids.* The London, Edinburgh, and Dublin Philosophical Magazine and Journal of Science, 1932. **13**(86): p. 853-862.

29. Owens, D.K. and R. Wendt, *Estimation of the surface free energy of polymers.* Journal of applied polymer science, 1969. **13**(8): p. 1741-1747.

30. Van Oss, C. and R. Good, *Prediction of the solubility of polar polymers by means of interfacial tension combining rules.* Langmuir, 1992. **8**(12): p. 2877-2879.

31. Van Oss, C., *Acid—base interfacial interactions in aqueous media.* Colloids and Surfaces A: Physicochemical and Engineering Aspects, 1993. **78**: p. 1-49.

32. Janssen, D., et al., *Static solvent contact angle measurements, surface free energy and wettability determination of various self-assembled monolayers on silicon dioxide.* Thin Solid Films, 2006. **515**(4): p. 1433-1438.

33. Woodward, R.P., *Prediction of adhesion and wetting from Lewis acid base measurements.* TPOs in Automotive, 2000: p. 1-6.

34. Rudawska, A. and E. Jacniacka, *Evaluating uncertainty of surface free energy measurement by the van Oss-Chaudhury-Good method.* International Journal of Adhesion and Adhesives, 2018. **82**: p. 139-145.

35. Della Volpe, C. and S. Siboni, *Acid–base surface free energies of solids and the definition of scales in the Good–van Oss–Chaudhury theory.* Journal of Adhesion Science and Technology, 2000. **14**(2): p. 235-272.

36. Morra, M., *Some reflection on the evaluation of the Lewis acid–base properties of polymer surfaces by wetting measurements*. 1996, Elsevier.

37. Extrand, C., *Uncertainty in contact angle measurements from the tangent method.* Journal of adhesion science and Technology, 2016. **30**(15): p. 1597-1601.

38. Vuckovac, M., et al., *Uncertainties in contact angle goniometry.* Soft Matter, 2019. **15**(35): p. 7089-7096.

39. Della Volpe, C. and S. Siboni, *Some reflections on acid–base solid surface free energy theories.* Journal of Colloid and Interface Science, 1997. **195**(1): p. 121-136.

40. Zhang, Z., et al., *Binary liquid mixture contact-angle measurements for precise estimation of surface free energy.* Langmuir, 2019. **35**(38): p. 12317-12325.

41. Khoshkava, V. and M. Kamal, *Effect of surface energy on dispersion and mechanical properties of polymer/nanocrystalline cellulose nanocomposites.* Biomacromolecules, 2013. **14**(9): p. 3155-3163.

42. Wang, H., et al., *Wetting behavior and mechanism of wetting agents on low-energy surface.* Colloids and Surfaces A: Physicochemical and Engineering Aspects, 2013. **424**: p. 10-17.

43. Meuler, A.J., et al., *Examination of wettability and surface energy in fluorodecyl POSS/polymer blends.* Soft Matter, 2011. **7**(21): p. 10122-10134.

44. Kwak, T. and G. Mansoori, *Van der Waals mixing rules for cubic equations of state. Applications for supercritical fluid extraction modelling.* Chemical engineering science, 1986. **41**(5): p. 1303-1309.

45. Skriver, H.L. and N. Rosengaard, *Surface energy and work function of elemental metals.* Physical Review B, 1992. **46**(11): p. 7157.

46. Young, T., *III. An essay on the cohesion of fluids.* Philosophical transactions of the royal society of London, 1805(95): p. 65-87.

47. Kaelble, D., *Dispersion-polar surface tension properties of organic solids.* The Journal of Adhesion, 1970. **2**(2): p. 66-81.

48. Rabel, W., *Einige Aspekte der Benetzungstheorie und ihre Anwendung auf die Untersuchung und Veränderung der Oberflächeneigenschaften von Polymeren.* Farbe und Lack, 1971. **77**(10): p. 997-1005.

49. Gardner, D.J., *Application of the Lifshitz-van der Waals acid-base approach to determine wood surface tension components.* Wood and fiber science, 2007. **28**(4): p. 422-428.

50. Peng, D.-Y. and D.B. Robinson, *A new two-constant equation of state.* Industrial & Engineering Chemistry Fundamentals, 1976. **15**(1): p. 59-64.

51. Carnahan, N.F. and K.E. Starling, *Equation of state for nonattracting rigid spheres.* The Journal of chemical physics, 1969. **51**(2): p. 635-636.

52. Zabaloy, M.S., *Cubic Mixing Rules.* Industrial & Engineering Chemistry Research, 2008. **47**(15): p. 5063-5079.

53. Delhommelle, J. and P. Millié, *Inadequacy of the Lorentz-Berthelot combining rules for accurate predictions of equilibrium properties by molecular simulation.* Molecular Physics, 2001. **99**(8): p. 619-625.

54. Zhang, J. and D.Y. Kwok, *Calculation of Solid− Liquid Work of Adhesion Patterns from Combining Rules for Intermolecular Potentials.* The Journal of Physical Chemistry B, 2002. **106**(48): p. 12594-12599.

55. Nikitin, A., Y. Milchevskiy, and A. Lyubartsev, *AMBER-II: new combining rules and force field for perfluoroalkanes.* The Journal of Physical Chemistry B, 2015. **119**(46): p. 14563-14573.

56. Lazzaroni, M.J., et al., *High-pressure vapor− liquid equilbria of some carbon dioxide+ organic binary systems.* Journal of Chemical & Engineering Data, 2005. **50**(1): p. 60-65.

57. Markarian, S.A. and A.M. Terzyan, *Surface tension and refractive index of dialkylsulfoxide+ water mixtures at several temperatures.* Journal of Chemical & Engineering Data, 2007. **52**(5): p. 1704-1709.

58. Mallinson, S., G. McBain, and G. Horrocks. *Viscosity and surface tension of aqueous mixtures*. in *20th Australasian Fluid Mechanics Conference Perth, Australia. Australasian Fluid Mechanics Society*. 2016.

59. Bourges-Monnier, C. and M. Shanahan, *Influence of evaporation on contact angle.* Langmuir, 1995. **11**(7): p. 2820-2829.

60. Greene, S.A., *Sittig's handbook of pesticides and agricultural chemicals*. 2013: William Andrew.

61. Burton, Z. and B. Bhushan, *Hydrophobicity, adhesion, and friction properties of nanopatterned polymers and scale dependence for micro-and nanoelectromechanical systems.* Nano letters, 2005. **5**(8): p. 1607-1613.

62. Zhang, Y., et al., *Comparative studies on hydrophilic and hydrophobic segments grafted poly (vinyl chloride).* Chinese Journal of Polymer Science, 2018. **36**(5): p. 604-611.

63. Trantidou, T., et al., *Hydrophilic surface modification of PDMS for droplet microfluidics using a simple, quick, and robust method via PVA deposition.* Microsystems & nanoengineering, 2017. **3**(1): p. 1-9.

64. Demirci, N., M. Demirel, and N. Dilsiz, *Surface modification of PVC film with allylamine plasma polymers.* Advances in polymer technology, 2014. **33**(4).

65. Xie, W., et al., *Using the green solvent dimethyl sulfoxide to replace traditional solvents partly and fabricating PVC/PVC-g-PEGMA blended ultrafiltration membranes with high permeability and rejection.* Industrial & Engineering Chemistry Research, 2019. **58**(16): p. 6413-6423.

66. Ozcan, C. and N. Hasirci, *Evaluation of surface free energy for PMMA films.* Journal of applied polymer science, 2008. **108**(1): p. 438-446.

Chapter 5

Liquid Mixture Wetting on Patterned and Irregular PDMS Surfaces

5.1 Abstract

Surface wetting is one of the most important topic in surface science which is broadly applied in surface coating, self-cleaning, inkjet printing and adhesives. Fundamentally, both compositional and structural factors dictate solid-liquid interaction at interfaces. Theories on compositional effect typically includes molecular interaction including polar, dispersive acid-base interaction while structural effect includes topological considerations such as surface roughness and shapes Two branches both have a long history date back to over 100 years ago. However, these two branches exist separately mainly due to small overlaps between them in which mechanical/physical scientists interest in surface roughness while chemist/chemical engineers more or less focus on chemical aspect of surface wetting. Another challenge is lack of systematic contact angles data of liquids with continuous changes of molecular interactions on surfaces with systematically varied dimensions.

Here, we attempt to unify wetting theory by combining Owens-Wendt wetting model with Cassie-Baxter model to form a unified wetting model which includes both chemical and mechanical information. To test the model's ability in predicting static contact angles, we use water-organic liquid (dimethyl sulfoxide and ethylene glycol) mixtures with varied composition and surface tension; we tested mixture contact angles on three types of surfaces, including smooth PDMS, irregular PDMS and patterned PDMS. For smooth PDMS surface, Cassie-Baxter equation collapses into Wenzel model and unified model captures trend of measured contact angles. For irregular surface, we fit contact angles data into unified models and set roughness parameter (r) and wetting parameter (f) as fitting parameter. It turns out that all surfaces are in Wenzel model

with f close to 1. Unified model predicts contact angles reasonably well. Lastly, we fabricated patterned surfaces with varied pillar sizes. When measuring contact angles of liquid mixtures on patterned PDMS, it is observed that wetting transition from Wenzel to Cassie-Baxter state is possible as water content increases. This suggests that unified wetting model must be modified to introduce a critical surface tension that marks transition point. We recommend developing and modifying this unified model to include more complicated wetting phenomena.

5.2 Introduction

Surface wetting phenomena are of importance in a wide range of applications, ranging from biomedical device compatibility to energy technologies.[1] Two main approaches exist for engineering liquid-slide interactions, namely modifying the chemical composition of the surface and modifying its nano/microstructure.[2] In both cases, Young's equation is the original theoretical basis for understanding the effects of surface energy on contact angle (θ):[3]

$$\gamma_{SG} = \gamma_{SL} + \gamma_{LG}\cos(\theta) \qquad [5.1]$$

Where γ is the surface energy and *S*, *G*, and *L* refer to the solid, gas, and liquid phases. In the case of chemical composition modifications, a series of related theories attempt to parameterize various chemical interaction characteristics of the surface – for example, surface polarity, hydrogen bond capacity, and charge transfer tendencies.[4] Of these, the surface energy modeled recommended by Owens-Wendt-Rabel-Kaelble (OWRK) is one of the most common:[5]

$$0.5\gamma_L(1+\cos\theta) = \sqrt{\gamma_S^d\gamma_L^d} + \sqrt{\gamma_S^p\gamma_L^p} \qquad [5.2]$$

In Equation 2 the d and p superscripts denote dipole and polarizability forces, respectively. For modeling wetting behavior on patterned surfaces, on the other hand, the primary theory used to explain surface wetting is the Cassie-Baxter model, which relates the contact angle on the rough surface (θ^*) to its value on the smooth surface:[6]

$$\cos(\theta^*) = \mathrm{rf}\cos(\theta) + \mathrm{f} - 1 \qquad [5.3]$$

using the surface roughness factor, *r*, and surface wetted fraction, *f*.

Historically, the surface chemistry and surface patterning theories have existed separately, despite ample evidence that the two effects act synergistically in many important applications including to generate the well-known Lotus leaf effect,[7] A major challenge to unifying the two types of approaches has been a lack of reliable, quantitative measurements of contact angle, the primary metric used to understand surface energy. Typically, contact angle has been measured for a single solvent, generally water; this single data point is insufficient to determine independently all of the parameters required for a unified theory of wetting that combines surface composition and patterning effects. In some cases, contact angle is measured for a series of solvents – including water as well as organic solvents – and the entire data set is used to constrain the model. This is the typical case for determination of chemical parameters used in composition-based models. Still, the chemical properties of the different solvents vary widely and are not easily captured using simple parameters. Attempts to unify surface composition and surface patterning have either not been reported or at least not been generally accepted by the scientific community.

Here, we report a simple new method for measuring contact angle data sets involving binary solvent mixtures. The benefit of binary mixtures is that a wide range of properties can be accessed, and adjusting the composition provides access to any intermediate property in this range. As a result, contact angle can be measured over multiple points, without introducing new variables associated with use of many different solvents. In principle, many different solvent pairs can be used, making the technique easily generalizable. The main requirements are solvent miscibility and data availability. In practice, We have fully characterized mixtures of water with dimethyl sulfoxide, ethylene glycol, and dimethyl formamide.

We first applied this technique to model surface wetting on microscopically smooth surfaces – glass slides coated using alkyl silane, PDMS and binary mixtures of water and DMSO. Then, we used these data to determine composition parameters for the well-known OWRK model. As a comparison, we obtained OWRK parameters the usual way, by measuring contact angle for pure water, dimethyl sulfoxide and ethylene glycol.

Encouraged by the performance of the method for obtaining OWRK parameters describing the surface energy of the microscopically smooth surface, we tested the model for a regularly micropatterned surface. To model the surface energy of the patterned surface, we combined θ, as defined by the OWRK model (equation 1), with the form of the Cassie-Baxter model (equation 2) to derive a unified model of surface wetting:

$$\cos(\theta^*) = \mathrm{rf}\left[\left(\frac{2}{\gamma_L}\right)\left(\sqrt{\gamma_S^d\gamma_L^d} + \sqrt{\gamma_S^p\gamma_L^p}\right) - 1\right] + \mathrm{f} - 1 \qquad [5.4]$$

We then plotted measured contact angle data in the form suggested by equation (5.3). Figure 5.1 and 5.2 shows the results, indicating that the unified model captures the entire shape of the curve. Similar results were obtained for several solvent pairs, establishing the robustness of equation (5.3).

Lastly, we tested the unified theory for an irregularly micropatterned surface, taking as the test case a surface inspired by the moth eye.[8, 9] Again, we measured contact angles for binary mixtures of water and DMSO. Figure 5.2 shows the results of obtained when contact angle data are plotted as suggested by equation (5.3). Again, the fit to the data is excellent, once more establishing this general utility of equation (5.3) to use both chemical composition and surface microstructure data to model surface wetting.

In summary, we have developed a simple new technique to measure contact angles for a series of binary mixtures and used these data to establish a unified model of wetting that combines

surface composition and roughness effects. The new method was applied to model surface wetting on microscopically smooth surfaces, regularly micropatterned surfaces, and a biologically inspired micropatterned surface. In all cases, the unified model captured all observed trends. When the binary solvent mixture was applied to microscopically smooth surfaces, the precision of composition-dependent surface wetting parameters was improved by an order of magnitude. Because of the widespread importance of surface wetting phenomena and the simplicity of the unified model, we anticipate that it will be widely used in many fields which seek to tune surface wetting behavior using combined compositional and structural techniques.

5.3 Experimental

5.3.1 Materials and Chemicals

Glycerol (99.5+%) was purchased from Sigma-Aldrich Corporation (Natick, MA), dimethyl sulfoxide (DMSO) was purchased from AMRESCO, Inc. (Solon, OH), and formamide (99.5%) was purchased from Alfa Aesar (Ward Hill, MA). These solvents as well as deionized water from a Millipore (Billerica, MA) Synergy UV water purification system were used in the preparation of solutions to be used in the contact angle measurements. Polydimethylsiloxane (PDMS) elastomer and hardener from a Sylgard 184 Silicone Elastomer kit from Dow Corning (Midland, MI) were purchased. The ethanol from Pharma-AAPER (Brookfield, CT) were used in surface cleaning.

5.3.2 Fabrication of Patterned Silicon Wafer

Flat silicon wafer was pre-baked under 130 ^{o}C 10 minutes, and then it was cooled down to room temperature. 4.5 mL SU8 2035 was casted on baked silicon wafer and spin-coated at 1100 rpm for 30 minutes. After the spin-coating, the silicon wafer was heated at 65 ^{o}C for 2 minutes, 95 ^{o}C for 5 minutes and again 65 ^{o}C for 2 minutes. After the photoresist was coated on silicon wafer, the wafer was exposed to UV for 90 seconds using energy density of 160 J/cm^2 for 10 μm pillar height,

150 MJ/cm^2 and 20 seconds for 50 μm pillar height and 200 MJ/cm^2 and 20 seconds for 75 μm pillar height. Then the wafer was baked at 65 ^{o}C for 1 minute and 90 seconds at 96 ^{o}C. later, the wafer was immerged in developer solution for 3 minutes. Lastly, the silicon wafer was hard-baked at 150 ^{o}C for 60 minutes. The height of pillar was validated using profilometers and the variation is within 5%. Lastly, the silicon wafer surface was treated for preventing the bonding between the surface and PDMS casting.

5.3.3 Preparation of Smooth and Rough PDMS

The PDMS pre-polymer mixture was prepared by mixing the elastomer and hardener in a 10:1 mass ratio. To create the patterned surface polymer cast, the fabricated silicon wafer was placed at the bottom of a polystyrene dish (60 mm x 15 mm IVF Cell Culture Dish from Corning Incorporated, Corning, NY). The silicon wafer was washed with 40% ethanol-water mixtures and dried under nitrogen, then baked for 25 minutes at 50°C. The PDMS mixture was then added to the cast and degassed in the vacuum oven under 25 mmHg of pressure for three hours and then baked under vacuum for five hours at 70°C. After cooling, the PDMS was removed from the polymer cast resulting in a PDMS surface that replicated the patterned wafer surfaces. Smooth PDMS surfaces were cast directly onto the polystyrene with flat wafer attached to bottom and were prepared following the above method. The rough and smooth PDMS surfaces were again sonicated in ethanol for 10 minutes and dried using nitrogen and baking at 70°C for 25 minutes before being cut into 3 x 2 cm sections to be used in the contact angle measurements.

5.3.4 Contact Angle Drop Solutions

Water, glycerol, DMSO, and formamide were the liquids to be used in the sessile drop method. Binary solvents were made between water and one of the organics in varying molar ratios. To cover a large range of mixtures, 6 binary solvents were used ranging from pure water to pure

organic, increasing the mole fraction of water by 0.2. During the contact angle measurements, the binary solvents were used in a randomized sequence in order to reduce the effect of aging on the surface.

5.3.5 Contact Angle Measurements

Contact angle measurements were performed using a Ramé-Hart Automated Dispensing System (Netcong, NJ) Model No. 100-00. Ramé-Hart DROPimage software was used for the contact angle measurements. Using the dispensing system, 5 µL droplets of each binary solvent was placed on the PDMS surfaces. The DROPimage software measured the static contact angle. In addition to the static contact angle, the advancing and receding contact angles were measured by slowly lowering the dropper tip until it comes in contact with the static drop and adding 2 µL of solution to measure the advancing angle followed by removing 4 µL to measure the receding angle. Contact angle measurements were performed three times for each solution on the surfaces.

5.4 Results and Discussions

5.4.1 Wetting on Smooth PDMS

To test equation (4) applicability on smooth surfaces using Young contact angles, surface roughness parameter and wetting parameter should be equal to zero (e.g. $r = f = 0$). In equation (5.4), solid surface energy parameters, e.g. γ_S^d, γ_S^p) and liquid surface tension parameters (e.g. γ_L^d and γ_L^P) are required. Solid surface energy parameters are obtained using Owens-Wendt method described in Chapter 3. And Liquid surface tension parameters are calculated using method described in Chapter 3. We then used determined parameters and equation (5.4) to fit experimental contact angles into predicted contact angles. For water-dimethyl sulfoxide mixture, equation (5.4) captures the trend. For water-ethylene glycol mixture, overall, contact angles at small values ($<90^o$)

and large angles (>110^o) are predicted well except for the middle ranges contact angles. This could be experimental uncertainty or nonlinearity of mixtures contact angles.

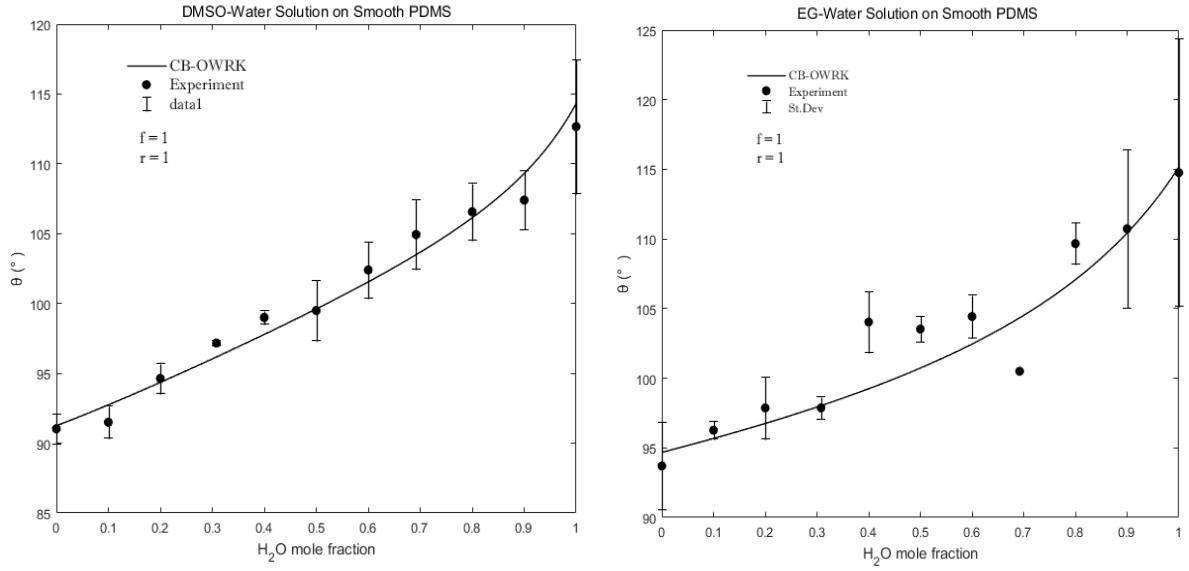

Figure 5. 1 Comparison between experimental contact angles and predicted contact angles using equation (4). And $r = f = 0$. Left is water-dimethyl sulfoxide mixtures on smooth PDMS, and right is water-ethylene glycol mixtures on smooth PDMS.

PDMS has small surface energy (< 15 mN/m), which is not representative surfaces because it cannot provide fitting validation for hydrophilic surfaces. Therefore, we used phenyltrimethoxysilane and phenyltrimethoxysilane to tune glass surface hydrophilicity. Figure 5.1 shows contact angles of water-dimethyl sulfoxide on both surfaces. Phenyltrimethoxysilane coated glass is much hydrophobic than phenyltrimethoxysilane coated glass. Contact angles differences of dimethyl sulfoxide between two surfaces has the largest values, which is around 25^o. The difference becomes smaller as water mole fraction increases. In both cases, equation (5.4) captures not only most of data points, but also the trend. Both figure 5.1 and 5.2 show equation's

predicting powder given accurate solid surface energy parameters and liquid surface tension parameters.

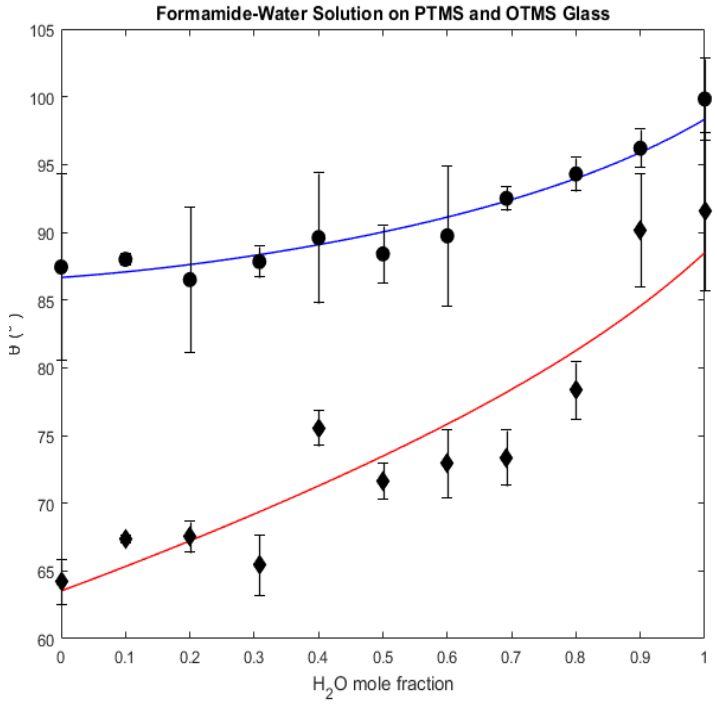

Figure 5. 2 Comparison between measured contact angles and predicted contact angles on silane derivatized surfaces: the red line represents phenyltrimethoxysilane coated surfaces and black line represents trimethoxy(octadecyl)silane coated glass slides.

5.4.2 Wetting on Irregular Surfaces

In reality, perfectly flat surfaces are nearly nonexistent. Therefore, surface roughness (r) in most cases, is greater than 1. However, wetting parameter, f, is an indication of either Wenzel state (fully wetted) or Cassie-Baxter state (non-wetted). To obtain these two crucial parameters, we performed data fitting using equation (4). Figure 5.3 shows the results. For water-dimethyl sulfoxide mixtures, regressed $r = 1.4$ and $f = 0.8$, which indicates that PDMS cast is slightly rough. Because of its small roughness, droplet tends to spread on surface and f is close to 1. For water-ethylene glycol mixtures,

fitted r = 1.1 and f = 0.9, which agrees with fact that water-ethylene glycol has lower surface tension compared to water-dimethyl sulfoxide. Therefore, wetting f gets closer to 1. Overall, fitting is promising, and equation (5.4) is adequate for predicting rough surface contact angles.

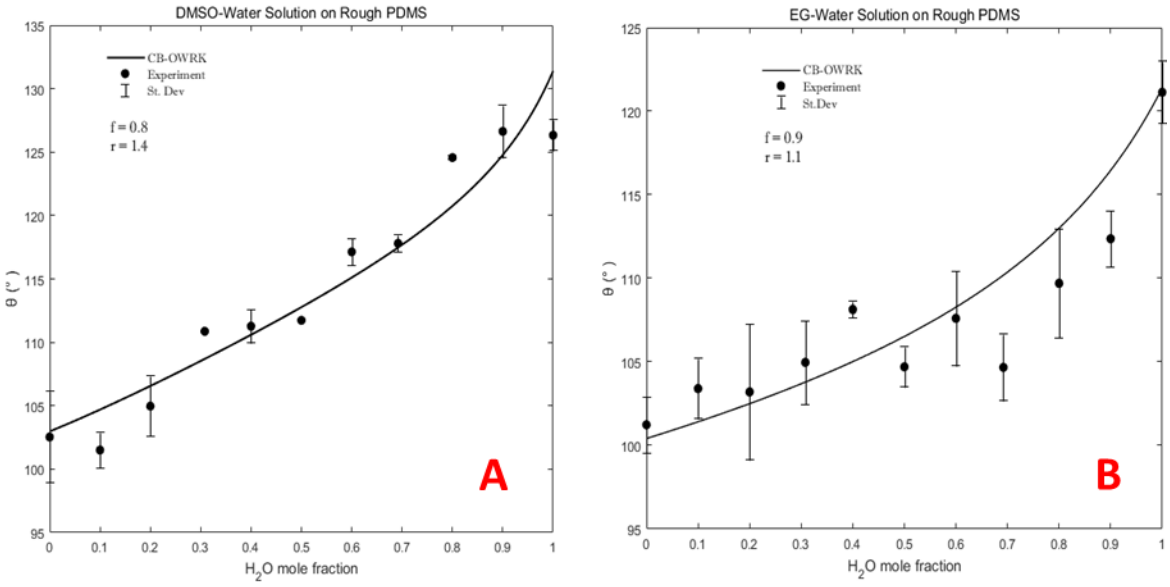

Figure 5. 3 Comparsion between measured contact angles and predicted contact angles on irregular PDMS surfaces: **A** is water-dimethyl sulfoxide mixtures on PDMS and **B** is water-ethylene glycol mixtures contact angles on PDMS. Wetting parameter (f) and roughness parameter (r) are fitting parameters.

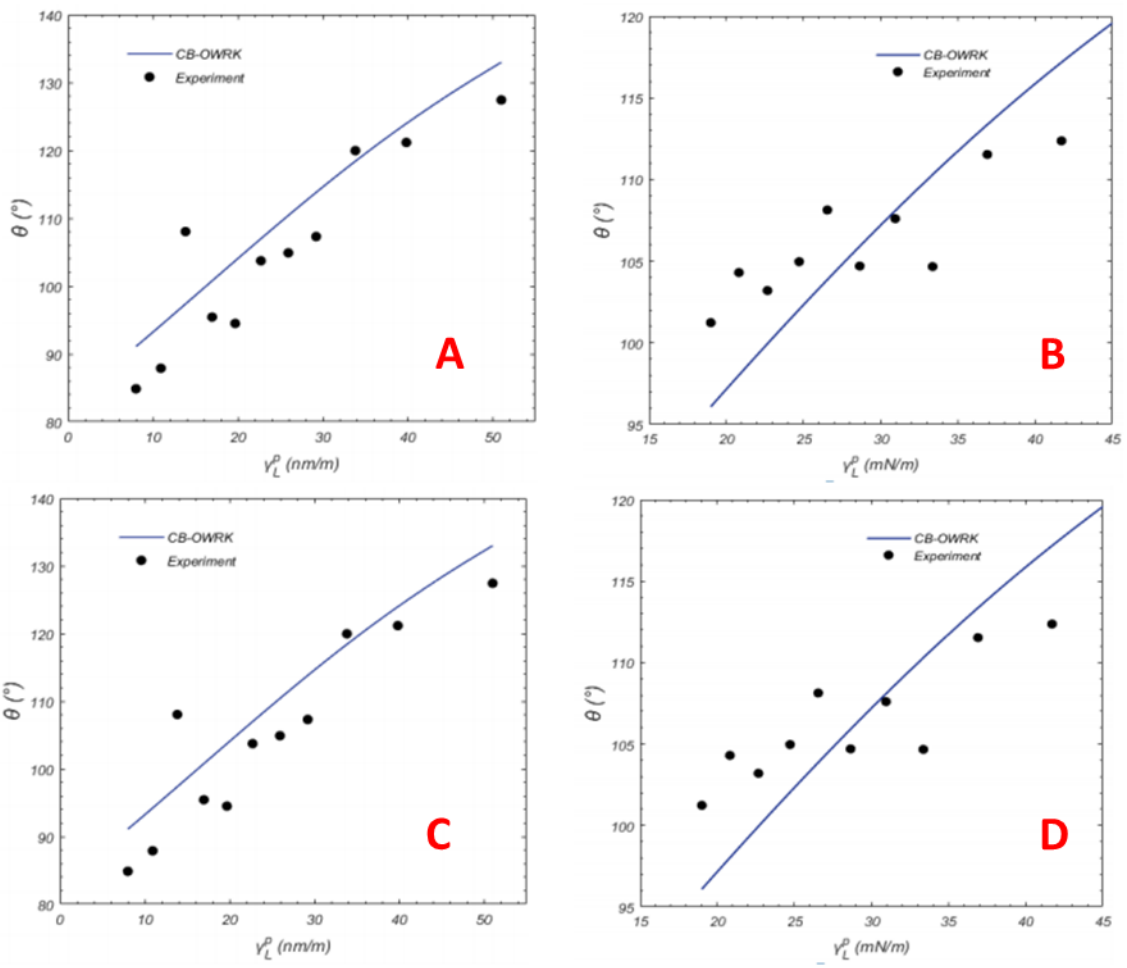

Figure 5. 4 Liquid surface tension components effect on contact angles. γ_L^d and γ_L^p are determined by method specified in chapter 3. **A** and **C** are water-dimethyl sulfoxide, and **B** and **D** are water-ethylene glycol. All contact angles are measured on irregular PDMS surfaces.

So far, all analysis is focused on evaluating equation (5.4) ability to unify wetting theory. However, those analysis will become impossible if liquid surface tension parameters are not calculated beforehand. Our mixing rules in chapter 4 bridges the gap and extends the use of liquid mixtures for contact angle measurement. Therefore, we use equation (5.4) and mixing rule to study γ_L^d and γ_L^P effect on contact angles. Figure 5.4 shows results.

5.4.3 Wetting on Patterned Surfaces-Cassie Baxter-Wenzel Transition

Equation (5.4) could also be used to investigate wetting transition. Wetting transition, also termed Cassie-Baxter-Wenzel transition, is a sudden contact angle change from large to small. This transition is important in many applications such as inkjet printing and surface coating. Traditionally, wetting transition is studied by ionic liquid due to its negligible vapor pressure and clear image under camera.[8-11] However, ionic liquids are expensive and nondegradable. Sometimes, identifying critical surface tension, γ_c at which transition happens is important. For precise control, surface tension of tested liquid must have small surface tension increments (e.g. 2-5 mN/m). Finding ionic liquid with systematic surface tension changes is challenging.

Here, we introduce use of liquid mixtures. We systematically varied liquid content from 0 to 100%. Then we measured contact angles on two PDMS surfaces with different feature. On both surfaces, wetting transition is observed. PDMS-A transition occurs at water mole fraction around 0.2 and sample B transition occurs at high water content (0.6), suggesting wetting transition depends on surface features.

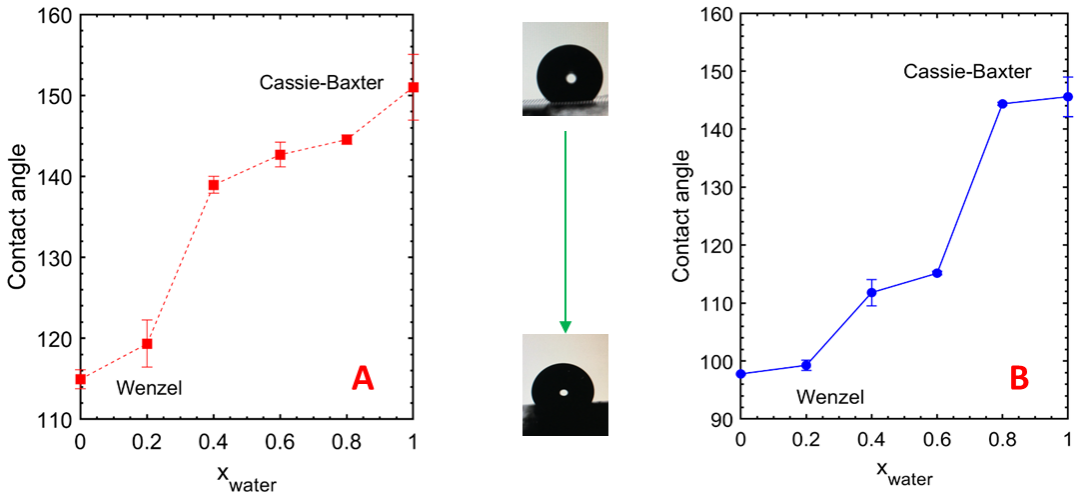

Figure 5. 5 wetting transition of water-dimethyl sulfoxide on two different PDMS surfaces. The dimensions of A-surface are 25 × 10 × 25 and dimensions of surface B is 50 × 50 × 50 *um*.

Equation (5.4) can be further modified to account for transition if critical surface tension is known. For example, if $\gamma_L<\gamma_c$, then equation (5.4) can be simplified as Cassie-Baxter form; if $\gamma_L>\gamma_c$, then Wenzel state will be reached, and equation (5.4) will simply become Wenzel wetting model.

5.5 Conclusions

In this chapter, we attempt to unify wetting theory by combining Cassie-Baxter state model with Wenzel state model. The combined equation has several powerful predicting abilities for PDMS contact angles. We first measured contact angles of water-dimethyl sulfoxide and water-ethylene glycol on both smooth PDMS and irregular PDMS. Using two surface energy parameters and two surface tension parameters along with Owens-Wendt model, unified model captures contact angles trend and exhibits good predicting accuracy. We then evaluate liquid surface tension components effect on contact angles predicting. Good correlation is found between γ_L^P, γ_L^d and contact angles, and model captures all data points.

We then use pattered surfaces and water-dimethyl sulfoxide mixtures to study wetting transition. As water content increases, a sudden contact angle increase is observed, which is believed as wetting transition. We recommend modifying unified model to account for critical surface tension above which Cassie-Baxter state will be obtained.

5.6 Reference

1. Xia, Y., D. Qin, and Y. Yin, *Surface patterning and its application in wetting/dewetting studies.* Current opinion in colloid & interface science, 2001. **6**(1): p. 54-64.
2. Roach, P., N.J. Shirtcliffe, and M.I. Newton, *Progess in superhydrophobic surface development.* Soft matter, 2008. **4**(2): p. 224-240.
3. Young, T., *III. An essay on the cohesion of fluids.* Philosophical transactions of the royal society of London, 1805(95): p. 65-87.
4. Fowkes, F.M., *Dispersion force contributions to surface and interfacial tensions, contact angles, and heats of immersion*. 1964, ACS Publications.
5. Owens, D.K. and R. Wendt, *Estimation of the surface free energy of polymers.* Journal of applied polymer science, 1969. **13**(8): p. 1741-1747.
6. Murakami, D., H. Jinnai, and A. Takahara, *Wetting transition from the Cassie–Baxter state to the Wenzel state on textured polymer surfaces.* Langmuir, 2014. **30**(8): p. 2061-2067.
7. Marmur, A., *The lotus effect: superhydrophobicity and metastability.* Langmuir, 2004. **20**(9): p. 3517-3519.
8. Tan, G., et al., *Broadband antireflection film with moth-eye-like structure for flexible display applications.* Optica, 2017. **4**(7): p. 678-683.

9. Nakata, K., et al., *Antireflection and self-cleaning properties of a moth-eye-like surface coated with TiO2 particles.* Langmuir, 2011. **27**(7): p. 3275-3278.

Chapter 6

Biomass Powder Surface Energy Determination Using Liquid Mixture with Washburn-Lucas Method

6.1 Abstract

Surface energy of cellulose and chitin is important for applications in membrane, superhydrophobic surface design and self-cleaning. Surface energy of cellulose and chitin has been previously determined by techniques such as inverse gas chromatography, wicking or sessile drop method. In all those methods, a wide range of liquids are selected. Liquids include hexane, octane, diiodomethane, water and ethylene glycol. Of those liquids, hexane and octane are volatile, degrading data quality. Diiodomethane can swell/bind with biopolymers such as proteins, further worsening accuracy and precision of determined surface energy.

We previously devised a liquid mixture approach method to mitigate problems associated with toxicity, compatibility and evaporation. Here, we extend the method to Washburn wicking method for both cellulose and chitin. Using water-dimethyl sulfoxide and water-formamide, we were able to analyze surface energy. Results show that water-dimethyl sulfoxide overestimates dispersion term of cellulose to 10-15%, possibly due to swelling issue. Water-formamide results in consistent surface energy values for both cellulose and chitin. We recommend careful operation and design of experiment by first selecting compatible liquids. This will avoid introducing new energy associated with chemical reaction or swelling/dissolution. We also recommend careful packed column preparation to ensure consistent packing and density. It is observed that local collapse of powder could affect stability of collected liquid mass penetration data. Overall, we strongly recommend the liquid mixture method because it not only provides information pertaining

to contact angles, but also interfacial interactions between biomass particles and organic liquid mixtures.

6.2 Introduction

Biomass derived materials are important in many applications such as oil-water separation,[1, 2] membrane filtration,[3, 4] and composite material development.[5, 6] In those applications, surface properties, such as surface energy and adhesion bonding with other composites are crucial for fabricating or modifying materials with desired chemical and mechanical properties. Tuning surface energy is fundamental for designing biomass-based materials with desired functionality. For example, cellulose has been modified to superhydrophobic for self-cleaning.[7] Chitin has been functionalized with methyltrichlorosilane for selective penetration of water-oil mixtures.[8]

When designing a cellulose or chitin-based composite, understanding or measuring surface energy is vital. Typically, biomass is often in the form of either cross-mixed fibers or powder,[9, 10] meaning that common approaches like sessile drop method for measuring contact angle cannot be easily done without proper sample preparation. Of all reported sample preparation methods, depositing powder onto a flat substrate (e.g. glass slide) to form a thin layer is the most developed technique. However, this method introduces complexity which would cause inaccuracy of contact angle measurement. First, spin-coated surfaces have roughness as large as 5 nm (R_q), making contact angle measurement inaccurate. Secondly, adhesive is often added to enhance powder bonding for pelletization. Added adhesive might affect accuracy of contact angle measurement because it interferes into prepared film matrix.[11, 12]

Other methods include Wilhelmy plate and column or thin-layer wicking methods. For Wilhelmy plate method, palletization, additive is often used to coat powders onto a substrate

material to prepare a tightly-bonded thin layer. However, introducing adhesive again may contaminate raw powder, leading questionable data. Wicking method is an alternative method. Benefits of wicking method is that it does not introduce any adhesive, accessible instrumentation and operating feasibility. Important considerations when preparing wicking column includes, but not limited to, consistent column packing (e.g. consistent porosity or packing density), narrow particle size distributions, and requires spherical particles shape. Another important factor is the liquid-powder compatibility. Selected liquids for penetration should not swell powder, as swelling may incur local powder collapse, producing concentrated pressure and prevent smooth penetration of liquid in porous structures. Selected liquids should also avoid chemical reaction as it will form/break bonds and produce extra energy.[12, 13] Reducing number of liquids used for penetration can be beneficial. However, reducing pure liquids may compromise accuracy and precision because the more liquids are tested, the more accurate surface energy will be.[14]

Liquid mixtures have been successfully used for characterizing surface energy by contact angle measurements.[14] Specifically, water-formamide, water-dimethyl sulfoxide and water-ethylene glycol are used for determining surface energy of polydimethylsiloxane (PDMS) and silane-derivatized silicon dioxide.[14] By adjusting liquid mixture compositions, we significantly improve surface energy determination. Expanding liquid mixtures approach to Washburn wicking method has not been done. As mentioned, using only two liquids would reduce solvent-induced complexity. By choosing two liquids that satisfy criteria, the method will yield abundant mixture contact angle data, which will improve accuracy of surface energy. Additionally, imbibition data of liquid mixtures is helpful for understanding liquid-biomass interactions.

In this study, we investigate the use of the Washburn method for determining surface energy of cellulose and chitin. Specifically, we choose water-formamide and water-dimethyl

sulfoxide as our testing liquids. By adjusting liquid mixture compositions, a series of mixtures with varied viscosity, surface tension and density are obtained. Subsequent penetration gives penetration constants that are used for extracting contact angles data. Lastly, we used contact angles along with Owens-Wendt model to characterize surface energy. we also comment on future work for improving the method.

6.3 Experimental

Materials: Ethylene glycol (99.8%) was purchased from Sigma-Aldrich Corporation (Natick, MA), dimethyl sulfoxide (DMSO) was purchased from AMRESCO, Inc. (Solon, OH), and formamide (99.5%) was purchased from Alfa Aesar (Ward Hill, MA). Water was de-ionized prior to use on a Millipore Synergy UV water purification system (Billerica, MA) to a minimum resistivity of 17.9 MΩ•cm. Microcrystalline cellulose (MCC) and chitin powders were obtained from Sigma Aldrich (Natick, MA). Cylindrical glass tube (I.D. 4 mm) was purchased from Fisher Scientific. Watham filter paper was purchased from Sigma Aldrich.

6.4 Wicking method

The Washburn method is used for obtaining contact angle of liquid mixture on biomass particles. A glass tube with 5 mm diameter and 15 cm length was used as packing column. Raw cellulose and chitin are packed into the glass column, and the column was shaked to ensure compact packing and consistent porosity and density. The height of the cellulose filled into column is consistently kept at 8 cm. The bottom of the column was supported by a Watman filter paper and glued to ensure the sealing. To obtain the contact angle for different composition of water-dimethyl sulfoxide and water-formamide, mixtures were prepared by mixing 0, 0.25, 0.5, 0.75 and 1 mole fraction of water into dimethyl sulfoxide. The mixture was then magnetically stirred at room temperature before the Washburn penetration. Then the testing liquid was placed into a wide-

opened beaker, the column was brought into contact with the surface of the liquid. The mass change of the testing liquid was recorded by WinCT-FR software connected to a balance.

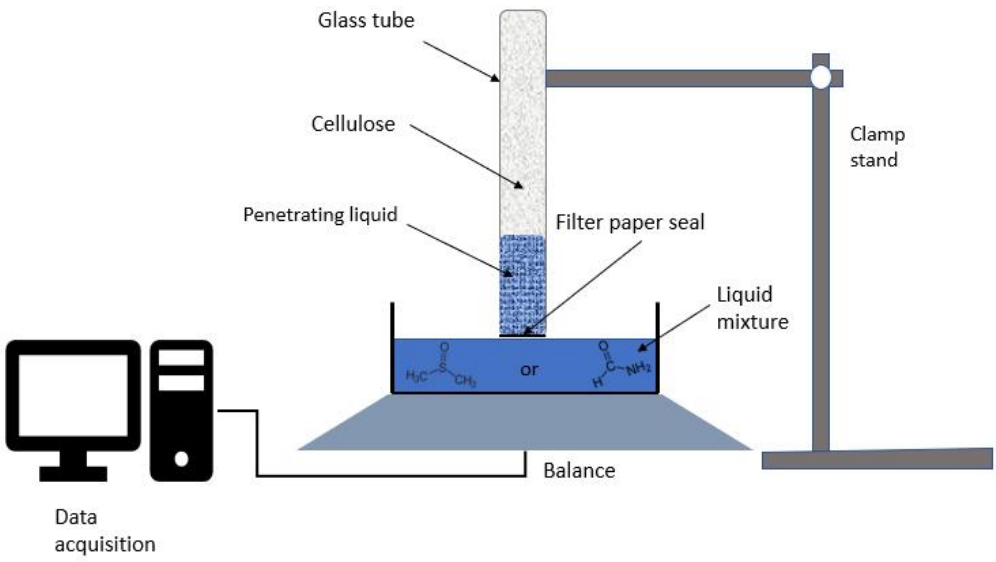

Figure 6. 1 Washburn-Lucas wicking instrumentation setup, the glass tube bottom is sealed by Watman filter paper and the top is open

6.5 Theory

Washburn-Lucas model: Washburn-Lucas equation (LW) describes the spontaneous penetration of liquid in porous tubes *via* capillary pressure. Back to early 20th century, Lucas and Washburn[15-17] have derived a theoretical model for describing liquid penetration:

$$\frac{dh}{dt} = \frac{(P_A + P_h + P_c)(r^2 + 4\varepsilon r)}{8\mu h} \tag{6.1}$$

where P_h is hydrostatic pressure, P_A is unbalanced atmospheric pressure, P_c is capillary pressure, h is liquid penetration height, μ is liquid viscosity, r is tube radius and ε is coefficient of slip. The capillary pressure is correlated with Young's contact angle (θ), liquid surface tension (γ) by:

$$p_c = \frac{2\gamma\cos\theta}{r} \tag{6.2}$$

Equation (6.1-6.2) combines all factors together and the resulting equations that captures liquid penetration rate within tube is:

$$h(t) = \sqrt{\frac{r\gamma\cos\theta}{2\mu}t} \tag{6.3}$$

In the case where liquid mass is more important than liquid penetration depth, equation (6.3) can be changed to the form:

$$m(t) = \pi r^2\rho(1-\varphi)\sqrt{\frac{r\gamma\cos\theta}{2\mu}t} = c\sqrt{\frac{r\gamma\rho\cos\theta}{\mu}t} \tag{6.4}$$

where $c = 0.71\ \pi r^2(1-\varphi)$. Rearranging equation (6.3) and obtain the following equation:

$$\frac{m(t)^2}{t} = c^2\frac{r\gamma\rho\cos\theta}{\mu} \tag{6.5}$$

Modified Washburn-Lucas model: Original Washburn-Lucas model often fails to predict the liquid penetration or uptake in porous structures.[18] Instead, a modified Washburn-Lucas model, which assumes homogeneous porous structures, is developed which significantly improves its predictive power.[19] In modified model, a pore shape factor has been introduced to correct original equation:

$$\delta = \frac{2\sqrt{\pi A}}{p^2} \tag{6.6}$$

where δ is correction factor, A and P represent cross sectional and perimeter of pore respectively. As a result, the modified Washburn-Lucas equation becomes:

$$m(t) = \varphi S \rho \sqrt{\frac{r \delta \sigma \cos\theta}{2\tau\mu} t} \quad (7)$$

In either equation (6.5) or equation (6.7), contact angles will be extracted for later surface energy calculations using OWRK models.[20]

6.6 Results and Discussions

The results and discussion divides into two sections. The first section is to evaluate the penetration of liquid mixtures in cellulose and chitin structures. The main task for this section is select proper mixing roles for surface tensions, viscosity and use those modeled parameters to evaluate the penetration speed of liquid mixtures in cellulose and chitin. In this section, we also used modified Lucas-Washburn equation to calculate contact angles. Comparing original Lucas-Washburn equation with modified equation will help us select a more precise model for surface energy measurement.

The second part of the discussion is using determined contact angles, coupled with wetting model, such as OWRK and vOCG models, to extract surface energies of chitin and cellulose biomass particles.

6.6.1 Selected Liquid Properties

The following liquids are selected for preparing mixtures for capillary penetration study, which are water, formamide and dimethyl sulfoxide and ethanol. Those liquids are selected for reasons described earlier.

In the selected solvents, none of them chemically reacts with cellulose and chitin. Lastly, the selected liquids must have known surface tension parameters, e.g. polar, dispersive surface

tensions. Solvents should also be miscible with water. The solubility of dimethyl sulfoxide, formamide and ethanol in water are .

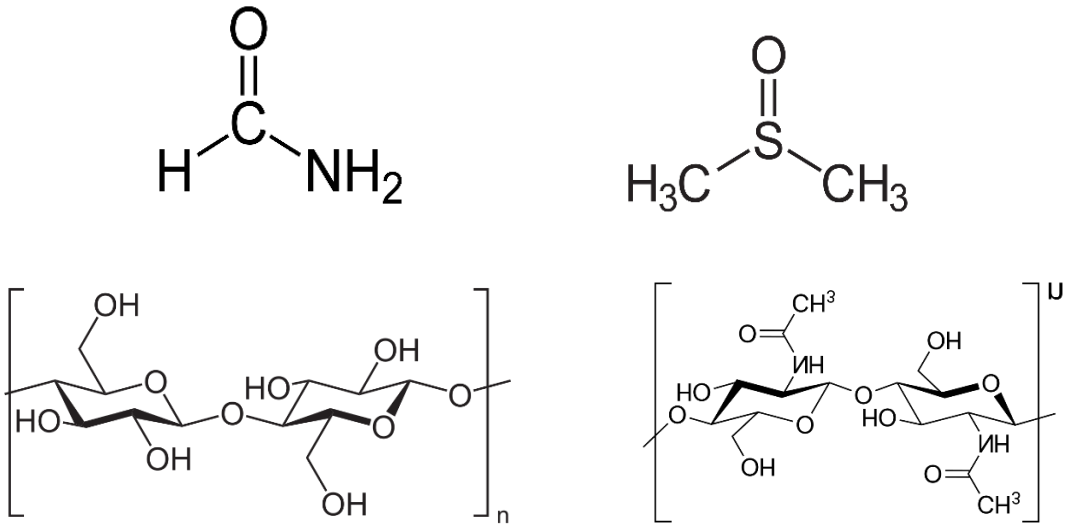

Figure 6. 2 Molecular structures of selected liquids: formamide, dimethyl sulfoxide (top) and ethanol (not shown) and substrate materials: cellulose and chitin powder (bottom).

Table 6. 1 Testing liquid physical properties for determining cellulose surface energy

Test liquid	Viscosity (Pa·s)	Surface tension (mN/m)	Density ($g \cdot cm^{-3}$)	a	b
Water	8.9×10^{-4}	72.8	0.97	-	-
DMSO	2.0×10^{-3}	44.0	1.10	0.869	0.603
Formamide	3.3×10^{-3}	58.0	1.13	0.698	0.780

Table 6.1 is viscosity, surface tension and density data for pure individual liquids. To expand Washburn-Lucas method for accommodating liquid mixtures, mixing models for those three parameters are needed. Binary mixture liquid viscosity was modeled by various theories,

including power series, equation of state (EOS) or transition state theory.[21] The most accepted approach is classic Grunberg-Nissan model.[22-25] For liquid binary mixture, viscosity of mixtures is:

$$\log(\mu_m) = x_1 \log(\mu_1) + x_2 \log(\mu_2) + x_1 x_2 G \qquad (6.6.6)$$

where μ_m is viscosity of liquid mixtures, x_1 and x_2 are mole fraction of liquid component "1" and "2", G is a adjustable parameter can be estimated by fitting experimental viscosity into eqn. (6). In this study, water-DMSO and water-formamide mixtures viscosity were obtained from literature and fitted into viscosity mixing model. Liquid mixtures surface tensions were also an important input for Washburn-model. We will previously reported theory in which $\gamma_{L,mix}$, of a binary mixture (consisting of components "1" and "2") is:

$$\gamma_{L,mix} = \gamma_L^1 - \left(1 + \frac{bx_1}{1 - ax_1}\right)(x_2)(\gamma_L^1 - \gamma_L^2) \qquad [6.7]$$

where x_i is the molar fraction of each liquid component, γ_L^2 is the pure liquid surface tension of component *i*, *a* and *b* are combined partition coefficient parameters reported by Connors and Wright[26] for many relevant liquids. Lastly, liquid mixtures density data will be modelled using existing theory.[27-29]

6.6.2 Liquid mixtures penetration in cellulose and chitin columns.

To use equation (6.5), capillary constant, *c*, must be determined beforehand. In this case, selecting a liquid with extremely low surface tension which makes it spread on cellulose or chitin, forming zero or near-zero contact angle. Typically *n*-hexane is used to determine constant *c*, due

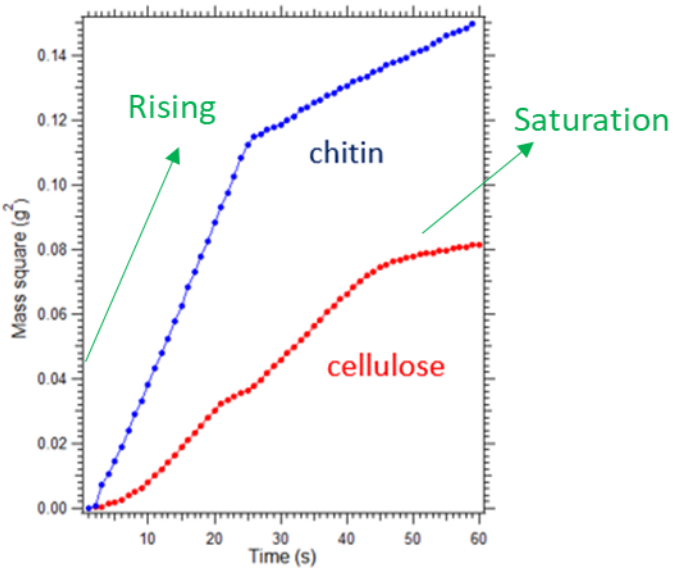

Figure 6. 3 Hexane uptake in cellulose and chitin.

to its low surface tension (18.43 mN/m).[30] Therefore, we use same approach and figure 6.3 shows the result. As we expected, hexane uptake speed, as measured by slope of figure 6.3, is much faster (around 3.5 times faster) in chitin than in cellulose. To use equation (6.5), surface tension (18.43 mN/m), viscosity (0.297 mPa s) [31] and density (0.655 g/cm^3)[32] are substituted into equation (6.5), resulting in determined penetration constant for chitin is 2.7×10^{13} and cellulose is 8.0×10^{14}.

Then, we conducted liquid mixtures uptake in both cellulose and figure 6.4 shows the results. Water-dimethyl sulfoxide and water-formamide compositions were systematically varied as 0, 10%, 25%, 50%, 75% and 100%. During liquid mixtures penetration, two stages were observed. In capillary uptake process, squared mass of liquid increases linearly with respect to time; once saturation was reached, liquid mixtures mass no longer changes. From Figure 6.4, water reaches saturation within 50 s while other liquid mixtures take longer time (more than 100 s) to be saturated.

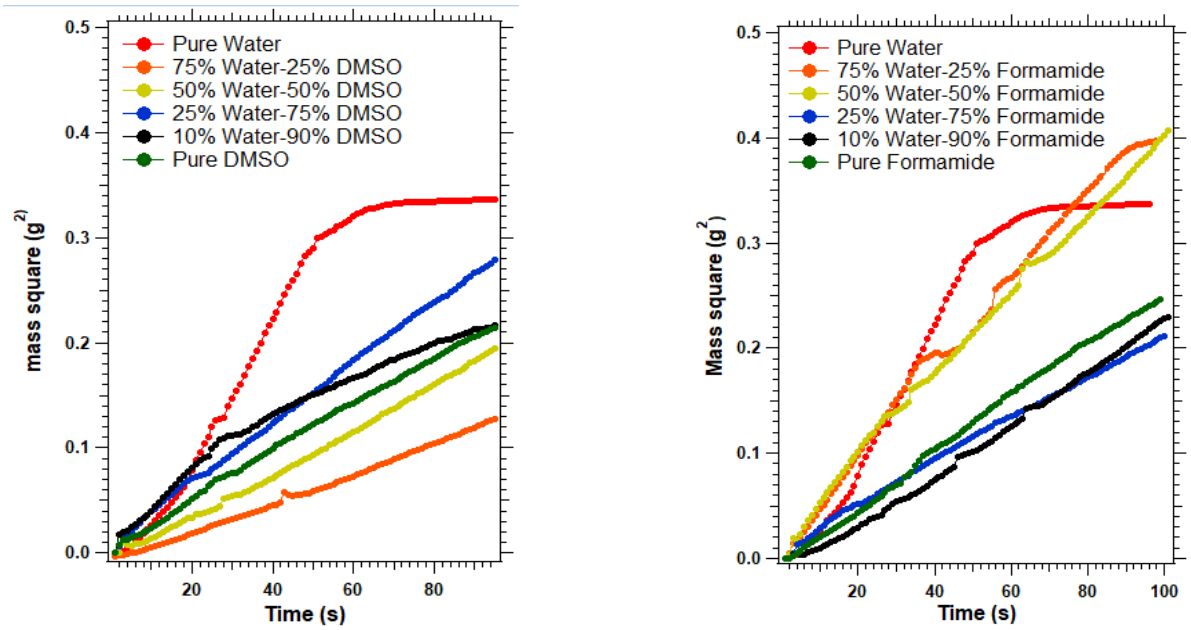

Figure 6. 4 (a) Water-dimethyl sulfoxide,(b) water-formamide adsorption mass in microcrystalline cellulose column as functions of penetration time.

Interestingly, as mixture concentration varies systematically, uptake rate does not follow the trend of organic solvent concentration changes. For example, in figure 6.4a, water without dimethyl sulfoxide has the fastest penetration speed in cellulose. This is because water not only has the highest surface tension, but also the lowest viscosity, which is shown in table 6.2. As water content decreases and dimethyl sulfoxide concentration increases, while liquid mixtures surface tension increases but the viscosity drops.[33] Therefore, the water-dimethyl sulfoxide uptake rate does not follow a trend as water concentration is varied systematically.

Table 6. 2 Water-dimethyl sulfoxide mixtures properties and penetration constant

Water fraction	Surface tension	viscosity	density	Penetration constant (c)
0	44.0	1.99	1.09	0.0026
0.1	45.2	2.16	1.09	0.0024
0.25	47.1	2.51	1.09	0.0021

0.5	50.7	3.45	1.09	0.0014
0.75	56.2	3.42	1.08	0.0013
1	72.8	0.89	0.99	0.0041

Similarly, water-formamide mixtures capillary speed is shown in figure 6.4b. Interestingly, penetration rate is divided visibly into two separated regions. Pure water, 75% water and 50% water mixtures stay close together while other liquid mixtures, formamide, 10%water-formamide and 25% water-formamide, whose slope are similar. It suggests that water again has the largest penetration rate due to its large surface tension and lowest viscosity. When water mole fraction becomes larger, mixtures surface tension drops steadily while viscosity stays relatively constant. Therefore, at high water content, slopes are close to each other. Data in figure 6.4 and table 6.3 are then plugged into equations to get contact angles of individual liquid mixtures. obtained contact angles are plotted in figure 6.5.

Table 6. 3 Water-formamide mixtures properties and penetration constant

Water fraction	Surface tension	viscosity	Density	Penetration constant
0	58.0	3.10	1.13	0.0023
0.1	58.4	3.04	1.11	0.0023
0.25	59.1	2.42	1.12	0.0026
0.5	61.0	1.64	1.09	0.0036
0.75	64.6	1.19	1.06	0.0040
1	72.8	0.89	0.99	0.0041

The liquid mixtures uptake slopes are plotted in figure 6.5 along with determined contact angles. For water-dimethyl sulfoxide in cellulose, the liquid uptake rate decreases first and then it increases. The trend agrees with water-dimethyl sulfoxide mixtures viscosity, indicating that viscosity is the main controlling factor that controls capillary action. Despite penetration constant

does not follow a increase trend, contact angles data almost linearly rise as water content increases. Determined contact angles for pure dimethyl sulfoxide is around 27^{o} while contact angle for pure water is about 64^{o}. Those data agree well with literature reported values.[34-37] contact angles of water-dimethyl sulfoxide mixtures are not typically reported in literature, but data in figure 6.5 might be useful for characterizing cellulose-liquid mixtures adsorption.[38] From figure 6.5, at low water content (<30%), contact angles increase slowly. At high water content (>50%), contact angles increase faster compared to low water content. This is because: at low water content where dimethyl sulfoxide is the main solvent, due to swelling or potential aggressive physiochemical interaction between cellulose and dimethyl sulfoxide, contact angles remain small, meaning cellulose-solvent mixtures interact strongly (high interfacial surface energy).[38-41] This extra interaction energy between cellulose and rich-dimethyl sulfoxide solvents may add exceed energy into discussion. Indeed, as water content increases, contact angle increases drastically. Because water interacts with cellulose through mostly van der Waals interaction, adding more water would enhance non-polar hydrophobic interaction and thus increases contact angle to as large as 63^{o}.

For water-formamide mixtures, trend looks completely different from water-dimethyl sulfoxide. Penetration speed increases as water concentration increases, which agrees with viscosity trend in table 6.3 where water has the smallest viscosity (0.89 mPa s) while formamide has the largest viscosity (3.10 mPa s). for contact angles, overall it follows the trend that contact angles increase from around 30^{o} to 63^{o}. Interestingly, contact angles increases for both water-dimethyl sulfoxide and water-formamide, no matter how penetrating speed changes. For water-dimethyl sulfoxide mixtures contact angles, water has contact angles around 62^{o}, which is close to reported angles of 69^{o}.[42] Dimethyl sulfoxide contact angles on cellulose is also comparable with literature reported values. For water-formamide mixtures, contact angles increase as water mole

fraction increases, agreeing with the fact that water is polar liquid while formamide is bipolar liquid.

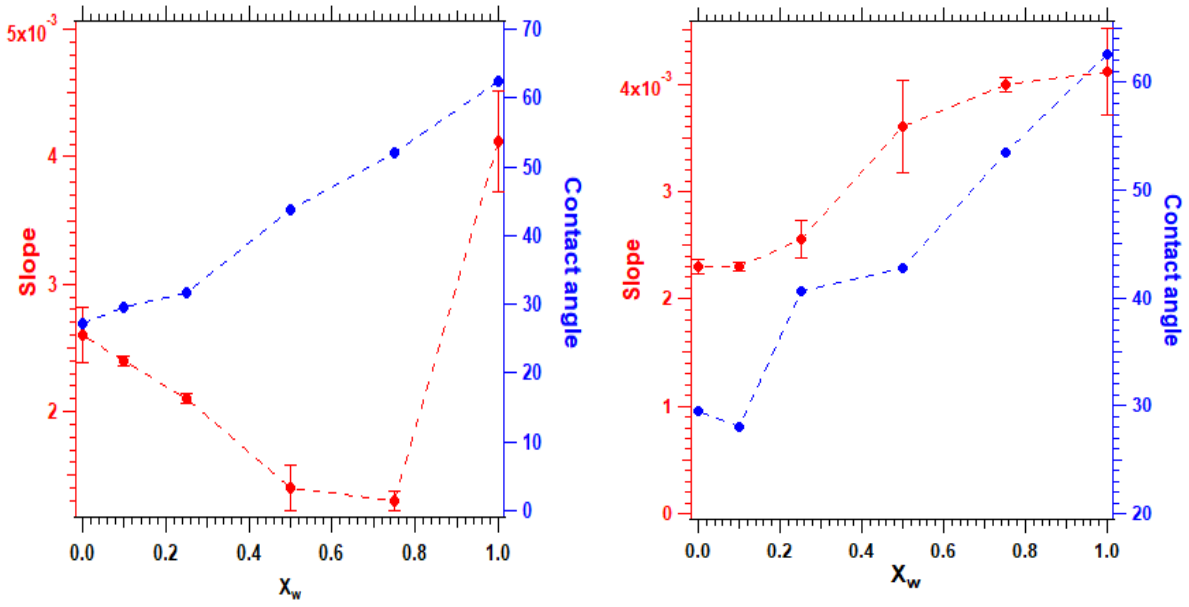

Figure 6. 5 Determined penetration constant and contact angles of water-dimethyl sulfoxide (left) and water-formamide (right) in cellulose.

6.6.3 Liquid mixtures penetration in chitin columns

To extend liquid mixture approach to biomass particles with different hydrophilicity and chemistry, we also applied the same procedure to chitin particles whose particles saize ranging from 10-50 um. Figure 6.6a and 6.6b show water-dimethyl sulfoxide and water-formamide penetration data within column packed with chitin powder. For water-dimethyl sulfoxide, pure water has again the highest penetration rate while 50% water mixture has the slowest penetration. In fact, mixtures other than pure water have small variation in penetration constant. This is because pure water has lowest viscosity, as explained in cellulose penetration. Similarly, for water-

formamide mixtures, again, water penetrates faster than any other mixtures, suggesting its preferential interactions with chitin.

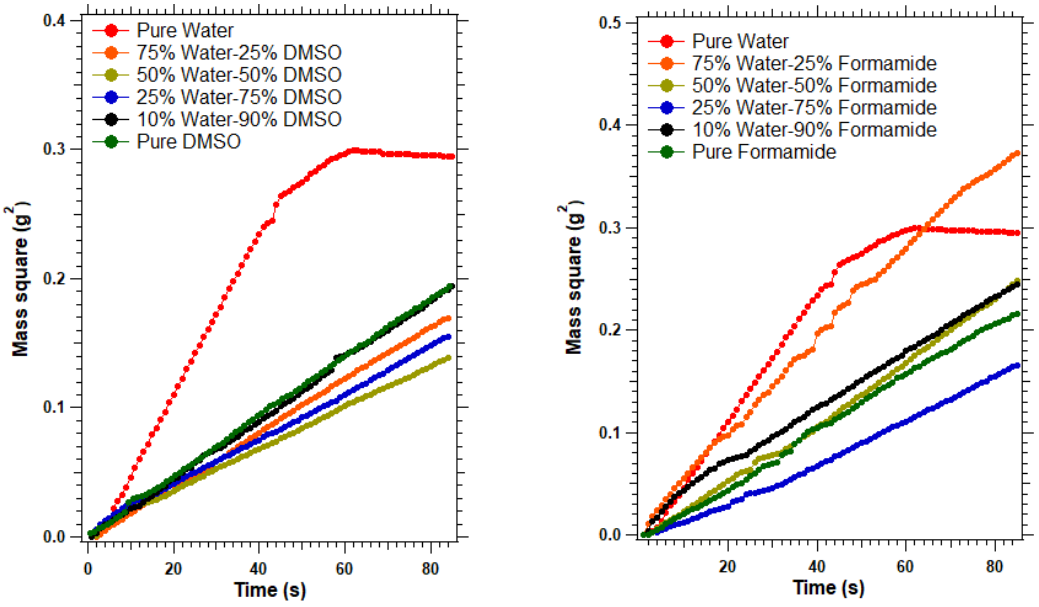

Figure 6. 6 (a) Water-dimethyl sulfoxide, **(b)** water-formamide adsorption mass in chitin column as functions of penetration time.

The slope from figure 6.6a and figure 6.6b are plotted in 7a and 7b along with determined contact angles using equation (6.5). Similar to cellulose case, penetration slope of water-dimethyl sulfoxide decreases first, reaching a global minima at water mole fraction 50%. This could be due to the relatively small viscosity compared to other liquid mixtures. Mixtures contact angles are also calculated and plotted in figure 6.7a and 6.7b. Water consistently has the greatest angles around 75^o while dimethyl sulfoxide has the angle at 65^o, formamide contact angle stays around 60^o. contact angles data is challenging to be compared to literatures valuse because of limited data availabe in literatures.

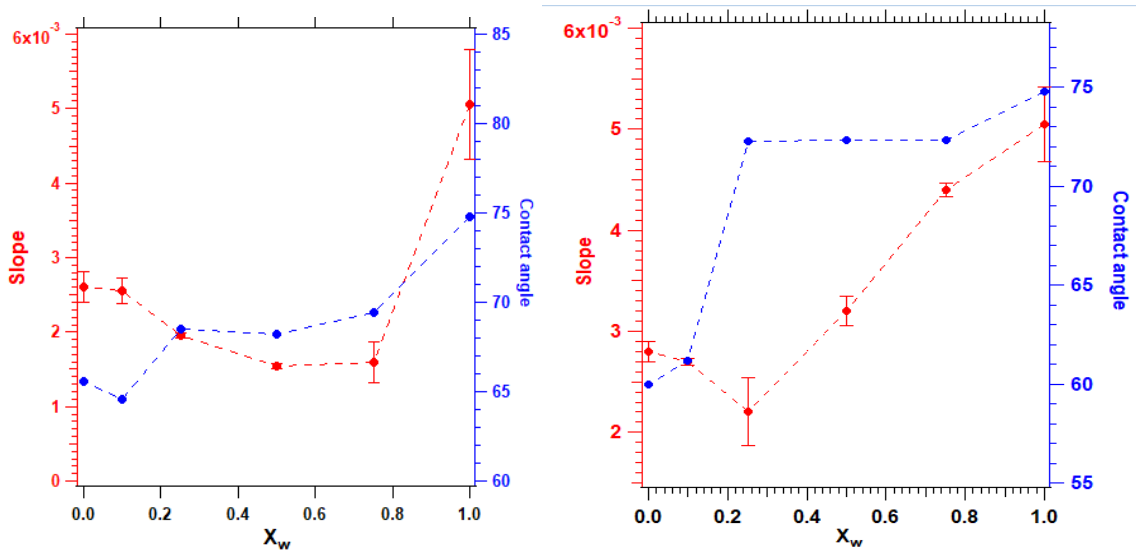

Figure 6. 7 Liquid mixtures penetration rate constant as functions of water mole fraction. The left is for water-dimethyl sulfoxide penetrating in chitin and right is water-formamide penetrating in chitin.

6.6.4 Cellulose and Chitin Surface Energy by OWRK model

OWRK model was used for determining cellulose and chitin surface energies. Figure 6.8 shows the linearized OWRK plots that is similar to Chapter 3 approach. From figure 6.8a, it presents two sets of analysis with the blue line being the best-fit line and the red line being the fixed intercept fitting. In either case, the regression coefficient (R^2) is similar, which is close to 0.93. However, determined surface energies are different under two analysis. If best-fit line is used, determined γ_{SG}^{d} is around 26.1 mN/m while γ_{SG}^{p} is around 16.8 mN/m. Those data deviates from literature values,[43, 44] although total surface energy agrees well with literature values. As mentioned, one of potential problem is that cellulose might preferentially interact with dimethyl sulfoxide, a welling agent for biomass pretreatment. Therefore, it is reasonable to lower polar term by fixing the intercept while finding best-fit slope. Here, we took average values of literature

reported as fixed polar term, and we regressed to best-fit slope. Surprisingly, the best-fit dispersive term (γ_{SG}^{d}) is 43.5 mN/m while fixing polar term as 4.1 mN/m, which completely agrees with reported values.

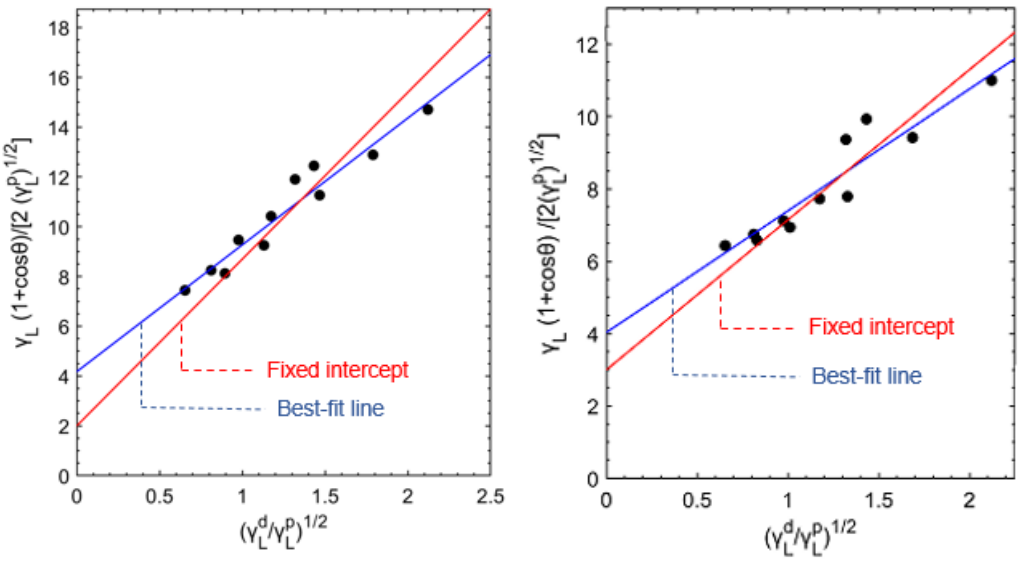

Figure 6. 8 OWRK model Surface energy of cellulose (left) and chitin as determined using liquid mixtures contact angle

For chitin, we performed identical analysis. When using best-fit regression line, we found γ_{SG}^{p} is about 16.8 mN/m and γ_{SG}^{d} is about 12.9 mN/m, summing up total surface energy is 29.7 mN/m. Compared to cellulose, chitin has less -OH group while has extra -NH_2 and -CH_3 group. Those groups make chitin less hydrophilic, or more hydrophobic. Therefore, chitin surface energy decreases compared to cellulose. For specific component, since -CH_3 is added in chitin, it would make chitin non-polar. Therefore, polar term should be similar to cellulose. However, we observed the opposite. Another analysis was performed similar to thecellulose analysis. We fixed the polar

term based on literature values and found the best-fit dispersive component. As shown in figure 6.8, after correction, γ_{SG}^{d} is 16.8 mN/m and γ_{SG}^{p} is 9.1 mN/m.

Overall, the method presented here needs improvement. Despite that direct comparison with literature values is impossible because of several reasons. First, methods that compress or spin-coat biomass powder into a thin film or pellet have flaws such as introducing surface roughness and liquid penetration, making contact angles measurement inaccurate. Second, not all used liquids for contact angles measurement are compatible with particles. For example, dimethyl sulfoxide data showed in this study can actually swell cellulose, overestimating surface energy.

To make approach robust and practical, a solvent that is not chemically reacting with selected biomass particles should be considered, e.g. ethanol. Another important liquid selection criteria is that preferential interaction between solvent and column should be avoided to decrease complexity. To obtain reproducible and consistent data, column packing should be validated before each run. Specifically, packing density should be consistent. The last opinion is that liquid should be selected in a wide range of chemical information. More data would provide more confidence for regression.

6.7 Conclusions

Powder surface energy is important for dispersion and surface interaction. However, conventional way that compresses powder into pellet or spin-coat powder into films have problems associated with porosity, roughness and liquid penetration into pellet. Washburn method remains the most widely used approach for estimating surface energy of powders.

In this study, binary mixture approach has been extended to Washburn for determining biomass particles surface energy. we tested two biomass particles with different hydrophobicity

and surface groups. To measuring contact angles of mixtures, two aqueous mixture systems were selected, water-dimethyl sulfoxide and water-formamide. The data shows that water-formamide and water-dimethyl sulfoxide overestimate cellulose polar component while underestimate dispersive component, as compared to literature reported values. Overall surface energy agrees well with literature values. For chitin, the same observation that polar term is overestimated while dispersive term is underestimated. This mainly is due to dimethyl sulfoxide's incompatibility with both cellulose and chitin because it swells those biomass particles.

6.8 Acknowledgement

I would like to thank Professor Lambert in Chemistry Department for generous lab access during pandemic time. I also would like to thank Professor Teixeira for interesting and inspiring discussions on particles packing.

6.9 Reference

1. Lu, Y. and W. Yuan, *Superhydrophobic/superoleophilic and reinforced ethyl cellulose sponges for oil/water separation: synergistic strategies of cross-linking, carbon nanotube composite, and nanosilica modification.* ACS applied materials & interfaces, 2017. **9**(34): p. 29167-29176.
2. Sai, H., et al., *Surface modification of bacterial cellulose aerogels' web-like skeleton for oil/water separation.* ACS applied materials & interfaces, 2015. **7**(13): p. 7373-7381.
3. Kaiser, A., W.J. Stark, and R.N. Grass, *Rapid production of a porous cellulose acetate membrane for water filtration using readily available chemicals.* Journal of chemical education, 2017. **94**(4): p. 483-487.

4. Ahn, E., et al., *A4 paper chemistry: synthesis of a versatile and chemically modifiable cellulose membrane.* ACS nano, 2020. **14**(5): p. 6173-6180.
5. Liu, A., L. Medina, and L.A. Berglund, *High-strength nanocomposite aerogels of ternary composition: poly (vinyl alcohol), clay, and cellulose nanofibrils.* ACS applied materials & interfaces, 2017. **9**(7): p. 6453-6461.
6. Fei, G., et al., *Fabrication of bacterial cellulose/polyaniline nanocomposite paper with excellent conductivity, strength, and flexibility.* ACS Sustainable Chemistry & Engineering, 2019. **7**(9): p. 8215-8225.
7. Wei, D.W., et al., *Superhydrophobic modification of cellulose and cotton textiles: Methodologies and applications.* Journal of Bioresources and Bioproducts, 2020. **5**(1): p. 1-15.
8. Duan, B., et al., *Hydrophobic modification on surface of chitin sponges for highly effective separation of oil.* ACS applied materials & interfaces, 2014. **6**(22): p. 19933-19942.
9. Gamble, J.F., W.-S. Chiu, and M. Tobyn, *Investigation into the impact of sub-populations of agglomerates on the particle size distribution and flow properties of conventional microcrystalline cellulose grades.* Pharmaceutical development and technology, 2011. **16**(5): p. 542-548.
10. Tobyn, M.J., et al., *Physicochemical comparison between microcrystalline cellulose and silicified microcrystalline cellulose.* International journal of pharmaceutics, 1998. **169**(2): p. 183-194.
11. Alghunaim, A., S. Kirdponpattara, and B.-m.Z. Newby, *Techniques for determining contact angle and wettability of powders.* Powder technology, 2016. **287**: p. 201-215.

12. Notley, S.M. and M. Norgren, *Surface energy and wettability of spin-coated thin films of lignin isolated from wood.* Langmuir, 2010. **26**(8): p. 5484-5490.
13. Hulikal Chakrapani, T. and W.K. den Otter, *Capillary imbibition of binary fluid mixtures in nanochannels.* Langmuir, 2020. **36**(42): p. 12712-12722.
14. Zhang, Z., et al., *Binary liquid mixture contact-angle measurements for precise estimation of surface free energy.* Langmuir, 2019. **35**(38): p. 12317-12325.
15. Lucas, R., *Ueber das Zeitgesetz des kapillaren Aufstiegs von Flüssigkeiten.* Kolloid-Zeitschrift, 1918. **23**(1): p. 15-22.
16. Cai, J., et al., *Lucas–washburn equation-based modeling of capillary-driven flow in porous systems.* Langmuir, 2021. **37**(5): p. 1623-1636.
17. Kennedy, S.B., et al., *Combinatorial screen of the effect of surface energy on fibronectin-mediated osteoblast adhesion, spreading and proliferation.* Biomaterials, 2006. **27**(20): p. 3817-3824.
18. Liu, Z., X. Yu, and L. Wan, *Capillary rise method for the measurement of the contact angle of soils.* Acta Geotechnica, 2016. **11**(1): p. 21-35.
19. Benavente, D., et al., *Predicting the capillary imbibition of porous rocks from microstructure.* Transport in porous media, 2002. **49**(1): p. 59-76.
20. Rudawska, A. and E. Jacniacka, *Analysis for determining surface free energy uncertainty by the Owen–Wendt method.* International Journal of Adhesion and Adhesives, 2009. **29**(4): p. 451-457.
21. Fillion, J.J., J.E. Bennett, and J.F. Brennecke, *The viscosity and density of ionic liquid+ tetraglyme mixtures and the effect of tetraglyme on CO2 Solubility.* Journal of Chemical & Engineering Data, 2017. **62**(2): p. 608-622.

22. Nhaesi, A.H. and A.-F.A. Asfour, *Densities and kinematic viscosities of ten ternary regular liquid systems at 293.15 and 298.15 K.* Journal of Chemical & Engineering Data, 2000. **45**(6): p. 991-995.

23. Carvalho, P.J., et al., *Effect of water on the viscosities and densities of 1-butyl-3-methylimidazolium dicyanamide and 1-butyl-3-methylimidazolium tricyanomethane at atmospheric pressure.* Journal of Chemical & Engineering Data, 2010. **55**(2): p. 645-652.

24. Sastry, N.V. and M.C. Patel, *Densities, excess molar volumes, viscosities, speeds of sound, excess isentropic compressibilities, and relative permittivities for alkyl (methyl, ethyl, butyl, and isoamyl) acetates+ glycols at different temperatures.* Journal of Chemical & Engineering Data, 2003. **48**(4): p. 1019-1027.

25. Wagh, P.S., A.N. Bhumkar, and M.V. Rathnam, *Excess Volume, Viscosity, and Isentropic Compressibility of Methyl Acrylate+ Alkane Binary Mixtures.* Journal of Chemical & Engineering Data, 2020. **65**(5): p. 2343-2350.

26. Connors, K.A. and J.L. Wright, *Dependence of surface tension on composition of binary aqueous-organic solutions.* Analytical Chemistry, 1989. **61**(3): p. 194-198.

27. Hankinson, R.W. and G.H. Thomson, *A new correlation for saturated densities of liquids and their mixtures.* AIChE Journal, 1979. **25**(4): p. 653-663.

28. Thomson, G., K. Brobst, and R. Hankinson, *An improved correlation for densities of compressed liquids and liquid mixtures.* AIChE journal, 1982. **28**(4): p. 671-676.

29. Shukla, R., et al., *Density, refractive index and molar refractivity of binary liquid mixture at 293.15, 298.15, 303.15, 308.15 and 313.15 K.* Arabian Journal of Chemistry, 2016. **9**: p. S1357-S1367.

30. Klein, T., et al., *Liquid viscosity and surface tension of n-hexane, n-octane, n-decane, and n-hexadecane up to 573 K by surface light scattering.* Journal of Chemical & Engineering Data, 2019. **64**(9): p. 4116-4131.

31. Aminabhavi, T., et al., *Density, viscosity, and refractive index of the binary mixtures of cyclohexane with hexane, heptane, octane, nonane, and decane at (298.15, 303.15, and 308.15) K.* Journal of Chemical & Engineering Data, 1996. **41**(3): p. 521-525.

32. Mopsik, F.I., *Dielectric constant of n-hexane as a function of temperature, pressure, and density.* Journal of research of the National Bureau of Standards. Section A, Physics and chemistry, 1967. **71**(4): p. 287.

33. Nieto-Draghi, C., J. Bonet Ávalos, and B. Rousseau, *Transport properties of dimethyl sulfoxide aqueous solutions.* The Journal of chemical physics, 2003. **119**(9): p. 4782-4789.

34. Gardner, D.J., et al., *Adhesion and surface issues in cellulose and nanocellulose.* Journal of adhesion science and technology, 2008. **22**(5-6): p. 545-567.

35. Dankovich, T.A. and D.G. Gray, *Contact angle measurements on smooth nanocrystalline cellulose (I) thin films.* Journal of adhesion science and technology, 2011. **25**(6-7): p. 699-708.

36. Peršin, Z., et al., *Determining the surface free energy of cellulose materials with the powder contact angle method.* Textile research journal, 2004. **74**(1): p. 55-62.

37. Hubbe, M.A., D.J. Gardner, and W. Shen, *Contact angles and wettability of cellulosic surfaces: A review of proposed mechanisms and test strategies.* BioResources, 2015. **10**(4): p. 8657-8749.

38. Zhang, X., et al., *Cellulose modification by recyclable swelling solvents.* Biotechnology for biofuels, 2018. **11**(1): p. 1-12.

39. Yoo, C.G., et al., *Elucidating structural characteristics of biomass using solution-state 2D NMR with a mixture of deuterated dimethylsulfoxide and hexamethylphosphoramide.* ChemSusChem, 2016. **9**(10): p. 1090-1095.

40. Zhang, X., et al., *Synergistic effect of pretreatment with dimethyl sulfoxide and an ionic liquid on enzymatic digestibility of white poplar and pine.* RSC advances, 2016. **6**(67): p. 62278-62285.

41. Wu, L., S.-H. Lee, and T. Endo, *Effect of dimethyl sulfoxide on ionic liquid 1-ethyl-3-methylimidazolium acetate pretreatment of eucalyptus wood for enzymatic hydrolysis.* Bioresource technology, 2013. **140**: p. 90-96.

42. Ma, B., et al., *Influence of cellulose/[Bmim] Cl solution on the properties of fabricated NIPS PVDF membranes.* Journal of Materials Science, 2017. **52**(16): p. 9946-9957.

43. Steele, D.F., et al., *Surface energy of microcrystalline cellulose determined by capillary intrusion and inverse gas chromatography.* The AAPS journal, 2008. **10**(3): p. 494-503.

44. Jacob, P.N. and J.C. Berg, *Acid-base surface energy characterization of microcrystalline cellulose and two wood pulp fiber types using inverse gas chromatography.* Langmuir, 1994. **10**(9): p. 3086-3093.

Chapter 7

D.L.V.O. Analysis of Cellulose and Solid-Acid Catalyst Interaction for Hydrolysis Reaction

7.1 Abstract

The physical interaction between cellulose and solid acid catalysts is believed an important step for heterogeneously converting cellulose to glucose in hydrolysis reaction. The classic D.L.V.O. theory was utilized to quantify the colloidal interaction between cellulose and selected wide range of solid acid catalysts, including ZSM5, zirconia, iron oxides, Nafion, polystyrene and activated carbon. To determine surface potential of selected catalysts bearing carboxylic acid and sulfonic acid group, a simple acid/base model was developed to quantify surface potential using measurable parameters including pKa, pH and acid density on surfaces. Using estimated surface potential and non-retarded Hamaker constant determined by Lifshitz theory, a parametric study was conducted to map out D.L.V.O. energy barrier with respect to pH, pKa and Hamaker constant. The result shows that all selected catalysts bearing carboxylic acid could adsorb cellulose due to the dominance of van der waals attraction over electrostatic repulsion. However, for catalysts bearing sulfonic acid, the cellulose-catalysts adsorption behave differently: Nafion, ZSM5 and polystyrene repels cellulose strongly, but zirconia, iron oxides and activated adsorb cellulose effectively. The analysis partially agreed with literature findings and could be used to screen catalysts substrates materials for effective solid acid catalysts design. Catalyst particle size has shown to have effect on cellulose-catalyst adsorption. A brief and qualitive discussion has been provided to reveal the non-D.L.V.O. forces effect and concludes that hydration is likely repulsive because of the affinity of cellulose and catalysts to adsorb water and surface roughness effect; steric repulsion is believed repulsive due to the localized chain extension and entropy reduction; hydrophobic interaction is believed having minimal effects on cellulose-catalyst adsorption due to their hydrophilicity. The

present study has provided theoretical insight into cellulose-catalysts adsorption with considerations involving Hamaker constant, pH, particle size, pKa and non-D.L.V.O. forces.

7.2 Introduction

Cellulose is the most abundant organic polymers on earth, and the effective depolymerization of cellulose into fermentable sugars is an important step for producing biomass-based chemicals and biofuel.[1-5] Despite its importance and promising future, cellulose degradation is difficult and challenging for many reasons.[6,7] Firstly, cellulose consists of thousands of β-1,4 linked glucose units that forms long linear fiber chains connecting each other with inter-/intra- hydrogen bonds. This molecular configuration leads to a crystalline and stiff structure that is mechanically strong and difficult to breakdown.[8-11] Secondly, cellulose dissolution in common industrial solvents such as water and ethanol is difficult, further reducing the reaction rate in hydrolysis reaction and placing a bottleneck.[12-15]

Many strategies have developed to chemically depolymerize cellulose using hydrolysis reaction, but they all have limitations in themselves.[16] For instance, liquid acid such as chloride acid (HCl) and sulfuric acid (H_2SO_4) have been utilized as homogeneous catalysts to hydrolyze and degrade cellulose.[17,18] Although those liquid acid catalysts are inexpensive and effective in depolymerizing cellulose, they suffer from pains associated with downstream separation cost, corrosion, which undermines its potential for commercialization.[19] Some study looked at biologically decomposing cellulose by incorporating enzymes that possess both binding domain and catalyzing domain into the reaction system as catalysts.[20-22] Despite enzyme systems such as *Pedobacter* and *Mucilaginibacter* can identify and cleave the C-O bonds effectively, it has some economical and technological roadblocks that prevent its commercialization. On the one hand, the design and synthesis of typical enzyme is expensive and time-consuming.[23] On the other hand,

because of the instability or even damages of enzyme at temperature greater than 50 °C, the enzymatic reaction is conducted at low temperature, which in turn lowering the production efficiency.[24]

Recently, catalysts design for catalytic hydrolyzing cellulose have shifted from homogeneous catalysts to heterogeneous catalysts.[25,16,90] Accordingly, many researches have used solid-acid catalyst instead to decompose cellulose.[27-29] Compared to mineral acid catalysts or enzymes, solid-acid catalysts have many advantages, including ease of separation, reusability, tunability of surface properties, reduced corrosion risk, and less harm to environment.[25] Three main categories of solid-acid catalysts are routinely reported in literatures, including metal oxide, polymer-based materials and sulfonated carbonaceous materials. For instance, Wattanapaphawong *et al*. examined the performance of a broad range of metal transition oxide in degrading cellulose and found zirconia (ZrO_2) has the highest lactic yield because of the synergetic effect of acid and base sites on zirconia surfaces.[30] Rinaldi *et al*. pioneered in using Amberlyst 15, a resin polymer bearing sulfonic acid group to depolymerize cellulose in 2008.[31] Yamaguchi and Hara have synthesized carbon materials bearing acid groups such as -COOH, -OH and -SO_3H and claimed that hydrogen bonds formed between phenolic glycosidic bonds is responsible for C-O cleavage.[32]

To date, solid-acid catalyst design has been guided by molecular-level intuition with little thought about physical interactions at the colloidal level. As a result, the strength of colloidal interactions between solid-acid catalysts and cellulose in the presence of water or other solvents remains largely unknown. In principal, the physical interaction between cellulose and solid-acid catalyst in aqueous solution is a solid-liquid-solid three-bodies interaction. This colloidal interaction not only includes molecular level dispersion or hydrogen bond if present, but also colloidal level interaction

such as vdw dispersion or electrostatic interactions. Tarabanko *et al*. has theoretically shown that electrostatic attraction between negatively charged catalysts and protonated cellulose is the main reason for cellulose-catalysts adsorption for further cellulose depolymerization.[33] However, this only applies to the case where the aqueous solution is highly acidic. And their theoretical study cannot be applied to a broad categories of catalysts with different surface acidity. Radtchenko *et al*. experimentally studied adsorption between cellulose and silica and found that possibly dispersion forces may be the causes for cellulose-silica adsorption.[34] Despite those evidences qualitatively demonstrate that colloidal interaction can dictate the adsorption between cellulose and catalysts, no comprehensive theoretical study is available to quantitatively demonstrate interaction magnitude between existing catalysts and cellulose. A better understanding of how catalysts properties and the aqueous solution properties can influence cellulose-catalysts adsorption is necessary for synthesizing desired catalysts and selecting proper reaction liquid media.

Herein, the objective of this manuscript is to examine colloidal interaction between cellulose and solid-acid catalyst. We first apply the Derjaguin-Landau-Verwey-Overbeek (DLVO) theory that takes account both van der Waals (vdw) attraction and electrostatic repulsion to cellulose-catalyst interaction. To perform the analysis, we select several commonly reported catalysts, including zirconia, ZSM-5, Nafion and carboxylic/sulfonic acid functionalized carbon materials to define the range of parameters such as Hamaker constant (A_{132}), *pKa*, surface potential (ψ_0) and *pH*. Based on those defined ranges, we then conduct parametric studies to quantitatively determine the sensitivity of D.L.V.O. interactive energy barrier with respect to A_{132} and *pH* for catalysts bearing sulfonic acid and carboxylic acid respectively, to establish what are the potential strategies can be implemented to enhance the cellulose-catalysts adsorption, in terms of properties such as surface

potential, *pH* and Hamaker constant. The effect of catalyst particles size on adsorption is also analyzed using D.L.V.O. framework. Then, we reduce the D.L.V.O. analysis to common literature reported catalysts including ZSM5, Nafion, carboxylic acid functionalized activated carbon and sulfated polystyrene to comment on the performance of current catalysts design from adsorption perspective. Lastly, we examine the non-D.L.V.O. interactions, including hydration forces, steric forces and hydrophobic forces and discuss how the catalysts might be engineered to enhance non-D.L.V.O. effect in cellulose-catalyst adsorption.

7.3 Theory

7.3.1 D.L.V.O. Theory

The implications of DLVO on particle-particle interactions during heterogeneously catalyzed cellulose hydrolysis were examined. A few simplifying were applied to reduce the scope of the problem without sacrificing accuracy or limiting the ramifications of the analysis: i) catalyst-cellulose interactions were modeled, without contributions from other biomass components and without consideration of catalyst-catalyst or cellulose-cellulose interactions; ii) all particles were assumed spherical and smooth; iii) the catalyst itself was is assumed to be chemically stable, meaning that surface properties such as charge density and dielectric constant remain fixed.

The general form of DVLO theory can be summarized as:

$$U = U_{vdw} + U_{edl} \tag{7.1}$$

where U is the total D.L.V.O. interaction energy, U_{vdw} is the interaction energy arising from vdw dispersion and U_{edl} represents the interaction energy of electrostatic double-layer forces. The vdw attraction (U_{vdw}) between two spherical particles follows a power law with respect to particle-particle separation (x), as derived by Hamaker:[37]

$$U_{vdw}(x) = -\frac{A_{132}}{6}\left[\frac{2R_1R_2}{d(2R_1+2R_2+x)} + \frac{2R_1R_2}{(2R_1+x)(2R_2+x)} + \ln\frac{(2R_1+2R_2+d)x}{(2R_1+x)(2R_2+x)}\right] \quad (7.2)$$

where R_1 and R_2 symbolize radius of cellulose and solid-acid catalyst particle, respectively. A_{132} is the combined nonretarded Hamaker constant between cellulose (denoted as "1") and solid-acid catalyst (denoted as "2") interacting across water (denoted as "3"). A_{132} can be measured directly or (more typically) can be used to estimated:[38]

$$A_{132} = -\left(\sqrt{A_{11}} - \sqrt{A_{33}}\right)\left(\sqrt{A_{22}} - \sqrt{A_{33}}\right) \quad (7.3)$$

where A_{11} is the Hamaker constant of cellulose-cellulose interacting across vacuum. Similarly, A_{22} denotes Hamaker constant between catalysts across vacuum and A_{33} is Hamaker constant of water interacting with water across vacuum.

Values of individual Hamaker constants (A_{ii}) can be obtained by fitting force-distance data, which is time-consuming and instrument-dependent. Instead, the approach recommended by Lifshitz can be used to predict A_{ii} based on values of dielectric constant and refractive index, both of which are commonly available.[39] The expression is given as:

$$A_{ii} = \frac{3}{4}k_bT\left(\frac{\varepsilon_i + 1}{\varepsilon_i - 1}\right)^2 + \frac{3h\nu_e}{16\sqrt{2}}\frac{(n_i^2-1)^2}{(n_i^2+1)^{3/2}} \quad (7.4)$$

where k_b is Boltzmann constant (1.38×10^{-23} J·K^{-1}); T is the temperature in Kelvin (K); ε_i represents the zero-frequency permittivity and n_i symbolizes the refractive index; ν_e is the main electronic absorption frequency in the ultraviolet region, typically around 3×10^{15} s^{-1}. This equation indicates that the interaction is always attractive for particles with identical permittivity and refractive index. For dissimilar particles, the interaction can be either attractive or repulsive, depending on the relative values of the index of refraction and dielectric constant. Appropriate

values for the index of refraction and dielectric constant are available in the literature for cellulose and model materials representative of major catalyst types (e.g., oxides, carbons, and polymers).

DLVO theory includes an important contribution from electrostatic repulsion (for similarly charged surfaces) or attraction. Cellulose and most catalyst materials, especially those bearing acid groups, will be charged when placed in aqueous solutions, either due to dissociation of ionizable functional groups or adsorption of ions.[40,41] To quantify the electrostatic repulsion, electrical potential distribution between the particles must be computed using the Poisson-Boltzmann (PB) distribution:[48]

$$\nabla^2\psi = \frac{8\pi cez}{\varepsilon}\sinh\left(\frac{ze\psi}{k_bT}\right) \tag{7.5}$$

where c is the ions concentration in unit of molecules L^{-1}; e is the electron charge; z is valence of the ionic species; ε is the dielectric constant of the aqueous solution; ψ is the electrical potential. For spherical particles, the PB equation can be reduced to:[49]

$$\frac{d^2\psi}{dx^2} = \kappa^2\psi \tag{7.6}$$

where κ is reciprocal of the Debye length, which characterizes the thickness of the diffusion layer and which varies from a few hundred nanometers in pure water to several nanometers in highly concentrated ions solution. The Debye length is defined as:

$$\kappa = \lambda_D^{-1} = \sqrt{\frac{\sum(z_ie)^2c}{\varepsilon_3\varepsilon_0k_bT}} \tag{7.7}$$

Solution of PB equation gives the potential as a function of radial distance (x) from the surface.

Many mathematical methods, both numerical and analytical, have been developed to solve the Poisson Boltzmann equation.[49-51] Among these mathematical methods, Hogg *at al*. provided

an analytical solution appropriate for spherical particles. The expression for U_{edl} given by the Hogg solution of the PB equation is shown as equation (8):[49]

$$U_{edl}(x) = \frac{\varepsilon_0 \varepsilon_3 R_1 R_2 (\psi_{01}^2 + \psi_{02}^2)}{4(R_1 + R_2)} \left[\frac{2\psi_{01}\psi_{02}}{(\psi_{01}^2 + \psi_{02}^2)} \ln\left(\frac{1 + \exp(-\kappa x)}{1 - \exp(-\kappa x)}\right) + \ln(1 - \exp(-2\kappa x)) \right] \quad (7.8)$$

where ε_0 is the vacuum permittivity and ε_3 represents the dielectric constant of water; R_1 and R_2 are radii of cellulose and solid-acid catalysts respectively; κ is the reciprocal of Debye length (λ_D), as defined in equation (7.7). ψ_{01} and ψ_{02} represent surface potential of cellulose and solid-acid catalysts respectively.

Figure 7.1 is a schematic showing the DLVO interaction resulting from the sum of equations (7.2) and (7.8). At large separation distances, the particles experience no net interaction. The vdw attraction increases drastically with decreasing particle separation for separation distances less than 5 nm; the magnitude of the vdw extraction depends on several factors, such as particle size, Hamaker constant, dielectric constant, and refractive index. The electrostatic interaction is a longer range force than vdw interaction; Figure 7.1 shows it as a repulsive interaction, as it is for similarly charged particles. The electrostatic interaction depends both on particle properties, chiefly the charge density, as well as solution properties such as ionic strength. Furthermore, for particles bearing acids or bases, solution pH will influence acid/base dissociation and hence charge density.

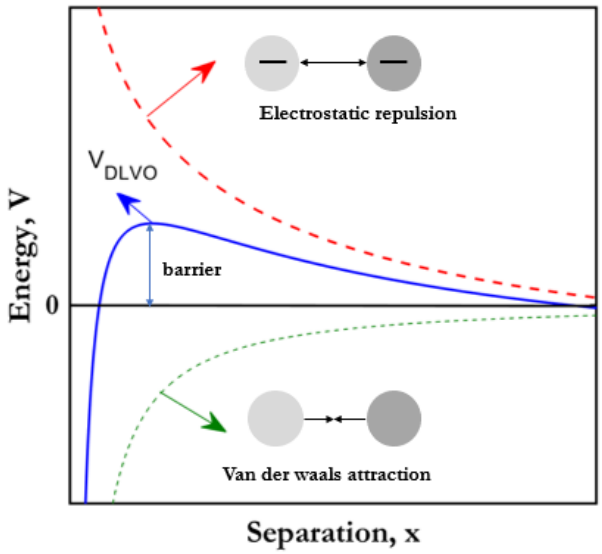

Figure 7. 1 Schematic of D.L.V.O. interaction energy as a function of particles separation. The red dash line represents electrostatic repulsion and the green dash line is the vdw attraction.

Combining vdw attraction and electrostatic repulsion results in an attractive well at short separation distances where vdw interactions dominate and a barrier which arises due to the mismatch in vdw and electrostatic spatial dependency. The repulsive barrier explains the stability of similarly charged particles, with colloidal stability typically observed for cases in which the magnitude of the barrier is greater than $25k_bT$.[52] Conversely, for catalyst-cellulose interaction, the barrier must be surmounted before catalysis can occur. In this case, barriers less than 10 k_bT would seem to be a reasonable requirement, bearing in mind that catalyst-cellulose interaction is just one part of a series of activated steps.

7.3.2 PKa-PH-Surface Potential Model

Solid catalyst surfaces will be charged upon immersion in aqueous media due to partial dissociation of their acid groups. The charge density depends on several factors, such as catalyst acidity, catalyst surface acid density and *pH* of the aqueous solution. To quantify this charge

density/surface potential in terms of measurable parameters, e.g. *pKa*, *pH* and acid surface coverage, a reliable mathematical model must be developed beforehand so that surface potential can be estimated for later D.L.V.O. analysis. This mathematical model could help propagate influences of the measurable factors to electrostatic forces on cellulose-catalyst adsorption. Accordingly, two predictive methods will be employed to estimate surface potential, depending on the types of catalysts. The first method applies to the cases where zeta potential (ζ) is known. In this case, equation (7.9) will be utilized to indirectly approximate surface potential:[53]

$$\psi_{02} = \frac{4k_bT}{ze}\tanh^{-1}(\tanh(\frac{ze\zeta}{4k_bT}) \times e^{\kappa d}) \quad (9)$$

where ζ is the zeta potential at given conditions, κ is reciprocal Debye length and *d* is the distance between particle surface and slipping plane, often taking the value of 5-6 Å.[54] Here, we will use equation (7.9) to approximate surface potential for cellulose, zirconia, ZSM5, Nafion, and activated carbon for different *pH* using literature zeta potential where available.

The second method applies to functionalized catalysts, including carboxylic/sulfonic acid functionalized catalysts, Nafion and Amberlyst-15 materials where surface acid coverage and acid dissociation equilibrium constant are approximately known. In this method, we generalize the surface potential dependence on acid surface coverage, *pKa* and aqueous solution *pH*.[55,56] We start from a catalyst (A) bearing acid head group (B) on the surface. This catalyst surface will obtain charges by the dissociation of both acid group and the substrate material through:

$$AH \rightleftarrows H^+ + A^- \quad (7.10)$$

$$BH \rightleftarrows H^+ + B^- \quad (7.11)$$

where *A* is the substrate materials, e.g. activated carbon, zeolite or metal oxides such as zirconia and silicon dioxide, as commonly reported in literatures B represents acid head group acid, e.g.

sulfonic acid (-SO_3H) or carboxylic acid (-COOH) group on catalysts. Both reactions represent the deprotonation of solid-acid. To simplify the model, we have made two assumptions. i). we assume that the catalyst surface consists of two types independent ionizable sites: the functionalized acids sites and the substrate materials, and both of them exist separately and do not affect the dissociation of each other; ii). further protonation of solid-acid can only happen under extremely acidic condition (typically under pH = 1.5, depending on the strength of the acid) and will not be considered here.[56] The extent of the dissociation for both catalyst and acid head group depend on the acidic strength, temperature and solution environment, and can be quantified by the equilibrium dissociation constant (Ka):

$$Ka_1 = \frac{[H^+]_0 \Gamma_{A^-}}{\Gamma_{AH}} \tag{7.12}$$

$$Ka_2 = \frac{[H^+]_0 \Gamma_{B^-}}{\Gamma_{BH}} \tag{7.13}$$

where $[H^+]_0$ is the protons activity around solid-acid catalyst surface, Γ_{AH} is surface acid density for undissociated acid and Γ_{A^-} is the surface density for dissociated acid or substrate catalyst. According to P.B. distribution equation, the proton activity around the solid surface and that in bulk phase can be correlated by:

$$[H^+]_0 = [H^+]_b \, exp\,(-\frac{e\psi_0}{k_b T}) \tag{7.14}$$

where $[H^+]_b$ is the proton activity in bulk phase, and it is normally determined by measuring solution pH. e is unit electron charge. ψ_0 is solid-acid surface potential and k_b is Boltzmann constant.

The resulting surface will become negatively charged and can be characterized by surface charge density (σ_0). By definition, surface charge density of catalyst upon added into water is the sum of net charge, described as:

$$\sigma_0 = eN_A \{\Gamma_{A^-} + \Gamma_{B^-}\} \quad (7.15)$$

where e is the unit electron charge, N_A is the Avogadro constant, $\Gamma_{A^-}$is the surface number density of dissociated group e.g. -OH^- and Γ_{B^-} is the number density for dissociated acid head group. Another correlation that relates measurable surface acid coverage to unmeasurable dissociated acid surface concentration is needed. Accordingly, the total acid concentration consists of dissociated and undissociated site density for both acid head group and substrate catalysts are:

$$\Gamma_{A_t} = \Gamma_{AH} + \Gamma_{A^-} \quad (7.16)$$

$$\Gamma_{B_t} = \Gamma_{BH} + \Gamma_{B^-} \quad (7.17)$$

Equation (10-17) can be utilized to solve for surface charge density as a function of measurable quantities, including *pH*, *pKa*, surface coverage (Γ_{tot}). However, upon solving the above equations, surface charge density and surface potential are inter-correlated. To obtain equations for surface potential and density individually, a separate equation is required. Here, Grahame equation relates surface charge density and surface potential for curved surface will be used:[57]

$$\sigma_0 = \frac{\varepsilon_0 \varepsilon_3 \kappa k_b T}{2\pi e} [\sinh\left(\frac{e\psi_0}{2k_b T}\right) + \frac{2}{\kappa a} \tanh\left(\frac{e\psi_0}{4k_b T}\right)] \quad (7.18)$$

where ε_0 is the vacuum permittivity and ε_3 represents the dielectric constant of water, κ is the reciprocal of Debye length, k_b is the Boltzmann constant and ψ_0 is the surface potential.

Solving equation (7.10-7.18) simultaneously, the surface potential (ψ_0) or surface charge density (σ_0) can be obtained implicitly. The determined surface potential is solely a function of parameters, including acid dissociation constant (Ka_1, Ka_2), surface acid coverage (Γ_{At}, Γ_{Bt}), *pH* of the reaction medium and radius of the catalyst particle (a). Further analysis will show that the predicted surface potential/surface charge density show congruence with literature reported values within the limit of experimental uncertainty.

7.4 Resultes and Discussions

Previous studies have claimed that short-ranged molecular interaction such as hydrogen bond and ions-induced dipole interaction between cellulose and catalyst may be reasons responsible for molecular-level binding and further C-O bond cleavage for converting cellulose to sugars. Shrotri et al. have synthesized carbon catalyst bearing carboxylic and hydroxyl acid and concluded that the polycyclic aromatic surface of the carbon catalyst adsorbs cellulose molecules *via* CH-π binding for further cellulose decomposition. Despite that those molecular interactions are directly related to the mechanism for cellulose depolymerization, those subset of vdw interactions are not the only interactions involved, instead, colloidal forces induced by electrostatic double-layer repulsion, hydration or steric interactions may be equally important to either promote or prevent cellulose-catalyst interaction given that the dimensions of cellulose and typical catalysts fall into colloidal domain. One of the key questions this manuscript attempts to answer is: whether current catalysts design and synthesis scheme is reasonable for promoting cellulose-catalysts adsorption? To answer this question, we examine the effect of D.L.V.O. and non-D.L.V.O. forces on cellulose-catalyst interaction. The first part examines the synergic effect of both electrostatic double-layer repulsive and vdw attractive forces, also termed D.L.V.O., on the interaction of three commonly used catalysts, including carboxylic acid functionalized activated carbon materials and zirconia, and Nafion polymer materials. The second part is to examine non-D.L.V.O. interactions, including hydration, hydrophobic and steric interaction.

7.4.1 Determination of Hamaker Constant and Surface Potential

Hamaker constant. To apply the D.L.V.O. theory to cellulose-catalyst adsorption, the focus of this work is then to obtain reliable parameters needed for D.L.V.O. calculations. The D.L.V.O. net interaction energy consists of two distinct contributions, vdw attraction and electrical double layer

repulsion. The vdw interaction always exists, and its magnitude is assessed by nonretarded Hamaker constant, a quantity that is typically determined by fitting force-distance curve for interacting particles. Accurate estimation of Hamaker constant would facilitate us evaluate the reported catalysts and also identify potential catalysts candidate for cellulose hydrolysis.

Fortunately, Lifshitz theory (eqn. 7.4) that use optical properties such as dielectric constant and refractive index has provided accurate estimation for a wide range of particles interaction in polar solvents such as water.[87] Accordingly, dielectric constant and refractive index for cellulose and some common catalysts substrate materials, including ZSM5, zirconia, activated carbon, magnetite, Nafion and polystyrene are extracted from literatures. Then Hamaker constant (A_{ii}) for individual materials interacting with itself across the vacuum is obtained using equation (7.4). Then equation (7.3) is being utilized to compute nonretarded Hamaker constant for cellulose-catalyst interaction in aqueous solution. The computed Hamaker constant (A_{132}) for cellulose and solid-acid catalysts are not generally available in literature. A_{ii} is compared with literature value where available. For example, the calculated Hamaker constant of cellulose interacting with itself in vacuum is approximately 6.4×10^{-20}J, which is close to 5.8×10^{-20} J reported by Bergström et al. using spectroscopic ellipsometry.[58] Hough and White use the exact solution of the Lifshitz theory to compute A_{132} for zirconia and obtain 20×10^{-20}J, which close to the value in **table 7.1**. Reported A_{ii} using "Quasi-Dynamic" method for polystyrene is about 7.9×10^{-20} J and close to 8.30×10^{-20}J.[88] Literature reported Hamaker constant for magnetite is about 40×10^{-20}J and is higher that calculated value (34.8×10^{-20}). Although the accuracy of Hamaker constant obtained from different physical instruments is still in debate, the Lifshitz theory still remains the most widely used theoretical approach to estimate Hamaker constant. The congruence of

calculated Hamaker constant with literature values suggests the promise of Lifshitz theory for determining A_{132} without involving experimental efforts.

Table 7. 1 Calculated Hamaker constant ($\times 10^{-20}$J) for different solid-acid catalysts interacting with cellulose in water using Lifshitz theory

Materials	n_i	ε_r	A_{ii}	A_{132}	Ref. as Cat.
Cellulose[59,60]	1.53	7.6	6.40	-	-
ZSM5[61,62]	1.49	3.5	6.88	0.64	71
ZrO_2[63,64]	2.15	18	26.20	2.88	30
C (A.C.)[65,66]	2.42	12	43.90	3.60	32
Fe_3O_4[67,68]	2.42	8.5	34.80	3.59	30
Nafion[69]	1.38	3.5	10.25	0.17	72
Polystyrene[70]	1.55	2.6	8.30	1.07	73

The results in **table 7.1** suggest that Hamaker constant (A_{132}) for cellulose-catalysts interaction across water (A_{132}) increases in the order of: activated carbon (A.C.) > Fe_3O_4 > ZrO_2 > polystyrene > ZSM5 >Nafion, spanning from 0.17×10^{-20}J to 3.60×10^{-20}J. Interestingly, activated carbon and metal oxides e.g. Fe_3O_4 and ZrO_2 are excellent candidates for adsorbing cellulose. This is in accord with the fact that carbon materials and metal oxides are protons donors because of its rich electron cloud density, resulting in strong vdw attraction. Not surprisingly, increasing the catalyst surface electron density has been a widely used approach to tailor catalyst catalytic performance. In contrast, polymer materials such as Nafion are chemically inert and have low tendency to adsorb cellulose. Polystyrene has an intermediate Hamaker constant (A_{132}) of 1.07×10^{-20} J, allowing it having greater attraction than ZSM5 and Nafion with cellulose. The catalysts showing in **table 7.1** cover three main categories, including polymer, zeolite and metal oxides solid materials. However, this does not necessarily represent all the catalysts within each category. In fact, even for the case

of metal oxides, the Hamaker constant (A_{ii}) can vary drastically. In evaluating individual catalyst vdw attraction, accurate optical properties such as dielectric constant refractive index should be obtained for the accurate prediction of Hamaker constant.

Surface Potential. As discussed in theory section, cellulose and catalyst surface are negatively charged, which will result a electrostatic repulsion between them. To quantify this electrostatic repulsion, equation (7.8) will be used to evaluate the repulsion energy. To use equation (7.8), surface potential values for both cellulose and catalysts have to be obtained beforehand. Two predictive methods are used here to indirectly determine surface potential for two different cases. The first method, as outlined in **Theory**, adopts equation (7.9) using literature reported zeta potential values if they are available. This method applies to cellulose and substrate of un-functionalized catalysts such as Nafion, zeolites and most metal oxides. Accordingly, literatures values of zeta potential at different *pH* or ionic strength for different catalysts are extracted and shown in **table 7.2**. Surface potential is predicted using equation (7.9) and the Debye length is taken based on the reported ionic strength if available. Unlike typical studies that approximate surface potential using zeta potential due to its well-established measuring technique, the equation (7.9) provides more accurate estimation for surface potential.

Table 7. 2 Zeta potential (ζ, mV) of cellulose and selected catalysts from literatures and predicted surface potential (ψ_{02}, mV)

Materials	***pH* = 2(3)** [d]		***pH* = 4**		***pH* = 6(5)** [d]		***pH* = 8**		**Ref. as Cat.**
	ζ	ψ_{02}	**ζ**	ψ_{02}	**ζ**	ψ_{02}	**ζ**	ψ_{02}	
[a] Cellulose [42]	-27	-33.2	-24	-25	-29	-30	-27.5	-28	-
[b] *ZrO_2* [74]	35	43.4	10	12	-10	-12	-22	-23	30
[c] *ZSM 5* [75]	-15	-18.3	-20	-22	-25	-27	-28	-29	71
[d] Nafion [76]	-45	-56.6	-65	-67	-68	-69	-	-	72

[e] Fe_3O_4 [77]	-	-	20	22	4	6	-30	-31	30
[f] *C (AC)* [78]	20	24.5	5	7	-10	-12	-15	-16	32

[a] Cellulose zeta potential was from Prathapan *et al*.[42] The ionic strength was determined based on *pH* and no electrolyte was added; [d] Nafion zeta potential at *pH* = 3 is used instead of *pH* = 2 and zeta potential for *pH* = 5 is used instead of *pH* = 6 due to data availability.

Table 7.2 shows that cellulose is consistently negatively charged with surface zeta potential around -27 mV in the *pH* range of 2 to 8 and shows as a weak function of *pH*. The zeta potential decreases dramatically at *pH* below 1, as measured by Prathapan et al.[42] This is because cellulose are extracted from wood materials by liquid acid hydrolysis during pulping process, such as sulfuric acid. The pretreated cellulose will have sulphate ester group on cellulose surfaces with *pKa* around 1.9, meaning that the protonation only occurs when the *pH* drops to around 1. As for zeta potential of representative catalysts without functionalization, they behave differently, depending on the surface acid strength. The isoelectric point (*pH* at which the surface has zero charge) for metal oxides such as zirconia and magnetite oxides are as large as 5-6, indicating that the surfaces get protonated and become positively charged at *pH* below 5-6 while becomes negatively charged at pH greater than 6. Nafion has a nearly constant negative zeta potential in *pH* range of 2-8 due to the complete dissociation of strong sulfonic acid. And the magnitude of predicted surface potential for Nafion is between -55 mV and -70 mV. Interestingly, predicted surface potential for activated carbon depends strongly on pH with positive charge at pH below approximately 5 and negative charge at pH larger than 5. This is likely due to that carbon materials can easily attract protons at lower pH through electrostatic attraction between electrons and protons. At higher pH above 5, hydroxyl ions are prone to adsorb on carbon materials. Zeolite such as ZSM-5 and Zeolite-Y are moderate in acid strength, and have isoelectric point below 2, meaning that ZSM5 becomes negatively charged in the pH range of 2-8. The magnitude of the surface potential

is around -19 mV to -30 mV, lowering than the expected. This is likely due to that zeolite has porous structure and only the acid sites on surfaces are available for deprotonation. Overall, the zeta potential reported in literatures can be reasonably explained using acid dissociation data. Therefore, the values in **Table 7.2** will be incorporated into equation (9) to extract the surface potential for subsequent D.L.V.O. calculations.

Currently, a general scheme for synthesizing catalysts for cellulose decomposition focuses on functionalizing catalytic domain and binding domain on existing catalyst substrates. Among the functional groups, carboxylic acid and sulfonic acid are two of the acids the have been successfully engineered on catalysts in literature. Unfortunately, surface potential or zeta potential for those catalysts are not generally reported in literature. Accordingly, as outlined in theory section, a generalized model that correlates surface potential and surface chemistry as well as pH must be developed. Therefore, equation (7.10-7.18) is being used to model the surface potential as a function of chemical properties such as *pKa* and *pH*. To demonstrate the robustness of the model, we have selected ZSM5 as substrate material. Three acid head groups with different pKa (-2, 1.0, 2.5) is assumed to be functionalized on ZSM5 with surface density as $0.075/nm^2$. In fact, these three pKa covers the typically reported acid strength. *p*-Toluic acid is being utilized to functionalize carbon materials and has the *pKa* around 2.86; methyl carboxylic acid such as formic acid and propanoic acid are weak in general, with *pKa* around 4.5. Sulfonic acid tends to be strong acid. For example, Methanesulfonic acid has the *pKa* around -1.9 while benzenesulfonic acid is much stronger with *pKa* around -2.8. The particle size is assumed as 1 um, which is reasonable for typical catalyst size.

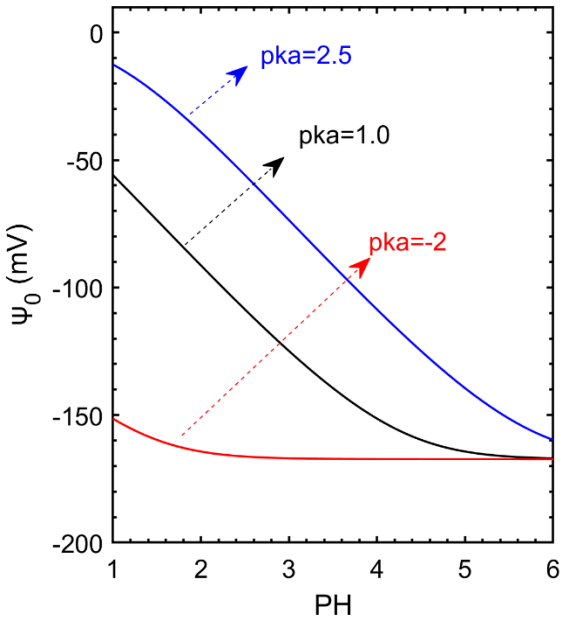

Figure 7. 2 The surface potential of ZSM5 and activated carbon bearing different acid head group as a function of media pH. The pKa of acid head group is taken as 2.5, 1.0 and -2 from weak acid to strong acid. The substrate (ZSM5 and activated carbon) surface density is assumed as 1.0/nm^2, functionalized acid surface density is taken as 0.05/nm^2. Equilibrium constant for ZSM5 is assumed as 5 and particle size is assumed as 1 um.

The predicted surface potential results as a function of pH are show in **figure 7.2**. Overall, predicted surface potential of ZSM5 bearing acid group increases as *pH* increases, in accord with the fact that the anions can attract counter-ions at high ionic strength aqueous solution and reduce the surface charge density or surface potential. In particular, this localized protonation becomes significant for weak acid. For strong acid such as sulfonic aid with pKa smaller than -2, the surface potential is somehow insensitive to *pH* change and stays relatively constant around -230 mV, as shown in **figure 7.2**. Predicted surface potential for weak acid (e.g. carboxylic acid with pKa around 2.5) varies from close to zero at low pH (around 1) to around -170V at *pH* close to 6. The

change of surface potential with respect to pH is steeper at pH between 2-3 and reaches to flat at pH about 5. For acid with intermediate strength (pKa = 1), the variation of the surface potential over pH between 1 and 6 follows the same trend as the cases for weaker acid (e.g. pKa = 2.5). Overall, the predicted surface potential captures.

7.4.2 Parametric Analysis

The counter-balance between dispersion attraction and electrostatic repulsion leads to a question that what are the potential strategies to overcome the repulsion barrier. In fact, some of the catalysts reported in literature are promising for overcoming the repulsion barrier and enhance cellulose-catalysts adsorption, based on their large Hamaker constant, but no systematic theoretical studies have been conducted for a wide range of catalysts bearing different acid strength. In principal, two main strategies that relies on either vdw attraction enhancement or electrostatic repulsion reduction might be useful for selecting or engineering catalysts. For vdw attraction, Hamaker constant is the crucial parameter that dictates the strength of colloid particle adsorption. According to **table 7.1**, metal oxides such as ZrO_2 and Fe_3O_4 are reported having excellent performance in decomposing cellulose while polymer-based material has weak vdw dispersion with cellulose. Despite the fact that those metal oxides can have strong Lewis acid sites that ionizes water and produce protons for later β-1,4 cleavage, the large Hamaker constant that resulting in large vdw attraction would (>$2 \times 10^{-20} J$) ensure the close contact for cellulose and catalyst. For electrostatic repulsion, surface potential and surface charge density are the two main parameters that determines the interaction strength. However, surface potential is dependent on other factors such as surface acid strength (*pKa*) and *pH* of the aqueous solution. Therefore, a generalized parametric studies that can map-out D.L.V.O. repulsion barrier in terms of Hamaker constant, pH and pKa is necessary from particle adsorption perspective. Unfortunately, the catalysts selection criteria in literature are not

based on the physical interactions, but mainly on the stability in hot-temperature conditions, feasibility for synthesis or cost.

Herein, we perform parametric studies to evaluate the sensitivity of cellulose/catalysts D.L.V.O. interactions under varied *pH* and catalyst Hamaker constant. In detail, we assume a catalyst bearing carboxylic acid with *pKa* assumed as 2.5 and acid loading is taken as 0.75/nm^2, as commonly reported in literature. Equation (7.10-7.18) are used to extract surface potentials for D.L.V.O. energy calculation. The *pH* of the reaction medium is varied from 2 to 5, which covers the typical cellulose hydrolysis *pH*. vdw dispersion is computed for catalyst with varying Hamaker constant from $1\times 10^{-20}J$ to $3.5\times 10^{-20}J$. Then the D.L.V.O. repulsion barrier is obtained as a function of *pH* for different catalysts, showing in **figure 7.3**. We then replace carboxylic acid with sulfonic acid with pKa around 2, which is also typical for commonly used sulfonic acid, as mentioned in previous section.

The results in **figure 7.3** indicates that the repulsion barrier of all selected catalysts reduces to below 5 k_bT at *pH* below 2.4 for acid strength with *pKa* above 2.5, suggesting potential adsorption between cellulose and all the selected catalysts, including ZSM5, polystyrene, ZrO_2, Fe_3O_4 and activated carbon. As the *pH* between 2.5 and 5, the repulsion barrier for Nafion and ZSM5 strongly depends on pH. For carboxylic acid functionalized ZSM5, the repulsion barrier reduces to below 5 k_bT when the pH is lower 4.0. The repulsion barrier for Nafion is significantly larger than other catalysts due to its small Hamaker constant ($0.17\times 10^{-20}J$). Surprisingly, polystyrene bearing carboxylic acid (*pKa* = 2) have zero repulsion barrier at *pH* range of 2-5. This is due to its larger Hamaker constant compared to Nafion. Catalysts substrates such as zirconia, iron oxides and activated carbon have excellent potential for adsorbing cellulose because their large Hamaker constant. Charmot[84] has shown that carboxylic acid functionalized mesoporous carbon

nanoparticle (MCN) catalysts can achieve glucans-to-glucose conversion about 80% at *pH* around 2 while the conversion drops to less than 20% at *pH* as high as 4.6. In fact, the cellulose and catalysts would be highly negatively charged at *pH* around 4.6. This large *pH* would most likely result in the cellulose and catalysts staying apart and form stable colloid dispersion phase. Another evidence is that enzymes that are typically weakly charged are capable of staying on cellulose and convert it into glucose. The implication is that lowering the *pH* would be a strategies for weakly charged catalysts to adsorb onto cellulose.

Catalysts substrate bearing sulfonic acid with pKa around -2 have strong repulsion to cellulose and its repulsion is somehow independent on pH. Figure 7.3(b) shows that Nafion, ZSM5 and polystyrene bearing sulfonic acid (pKa = -2) have repulsion barrier greater than 100 k_bT, suggesting the difficulties for them to stick on cellulose due to synergetic effect of large surface potential/surface charge density and small Hamaker constant. Because of the complete dissociation upon adding in water, the pH has limited effect on their surface potential, and hence the repulsion barrier. However, for zirconia, iron oxides and activated carbon, because of the strong attraction caused by large Hamaker constant (>$2.8\times 10^{-20}J$), the repulsion barrier reduces to below 5 k_bT for the whole range of pH.

We note that the analysis shown here is confined to acid *pKa* around -2 and 2.5 because it covers the typically reported acid strength. For acid *pKa* greater than 2.5 such as methane carboxylic acid or the form of formic acid end group, the adsorption between cellulose and catalysts is promising for typical *pH* range from 2-5. For acid with pKa smaller than -2, such as p-toluenesulfonic acid, the D.L.V.O. repulsion barrier is even larger in *pH* ranging from 2 to 5 for catalysts with Hamaker constant smaller than $1.510^{-20}J$. In fact, those catalysts will form stable “colloid” system with cellulose

and this colloidal stability can only be disrupted by external methods such as changing the ionic strength or pH.

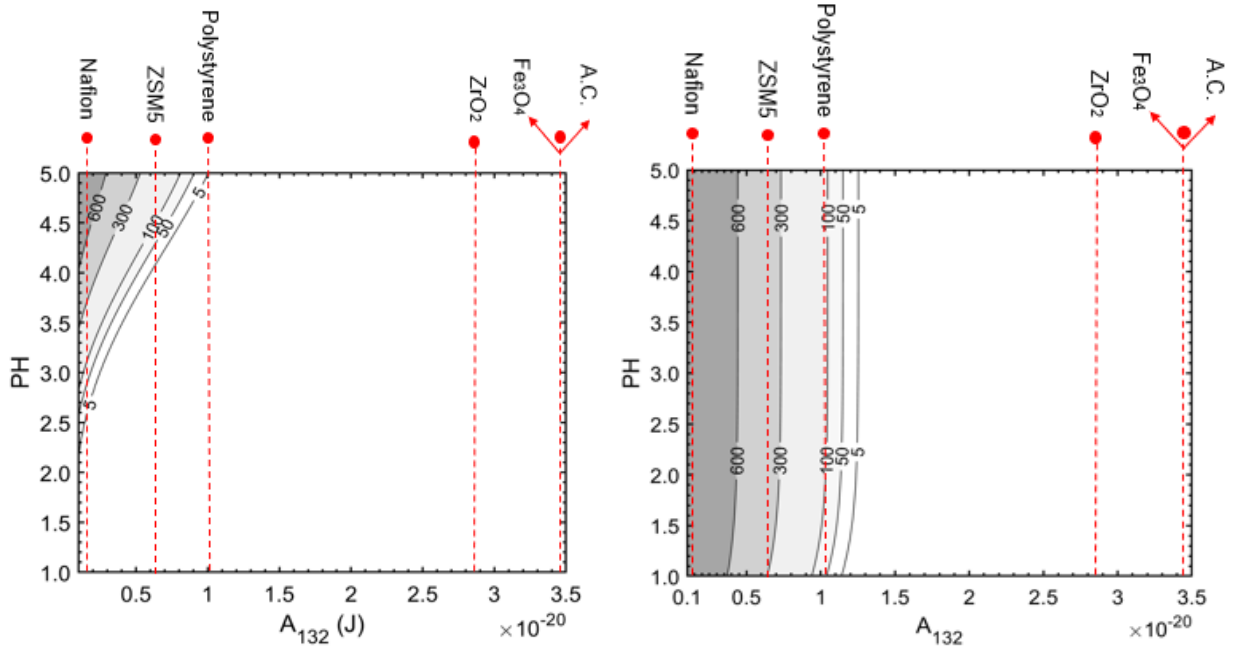

Figure 7. 3 D.L.V.O. interaction energy barrier as function of *pH* and Hamaker constant. The left is for pKa = 2.5 and the right is for pKa = -2. The pKa for substrate materials is assumed as 5 and has surface density of 1.5/nm^2. The surface acid density is assumed as 0.075/nm^2 and article size is taken as 1 um.

7.4.3 Particle Size Effect on Cellulose-Catalyst Adsorption

Previous studies have shown that particle size has a significant effect on the particle adsorption. Those studies have demonstrated that reducing either cellulose or catalysts to 100-500 nm can increase glucose yield significantly ball-mill, a mechanical breakdown of cellulose prior to hydrolysis, is a well-established routine not only because it recrystallize cellulose, but also it reduces cellulose particles size. They attribute the improved performance to its large specific surface area. However, limited theoretical studies on cellulose-catalysts adsorption studies with

respect to particle size are available. Despite that direct forces measurement by AFM between cellulose has been reported in literature to study cellulose colloid stability, those experimental data only reveals the physical interactions between cellulose, but not between cellulose and catalyst Moreover, those measurements are typically conducted in air instead of liquid. Therefore, a theoretical interaction potential prediction that takes account particle size is necessary to understand the physical interaction.

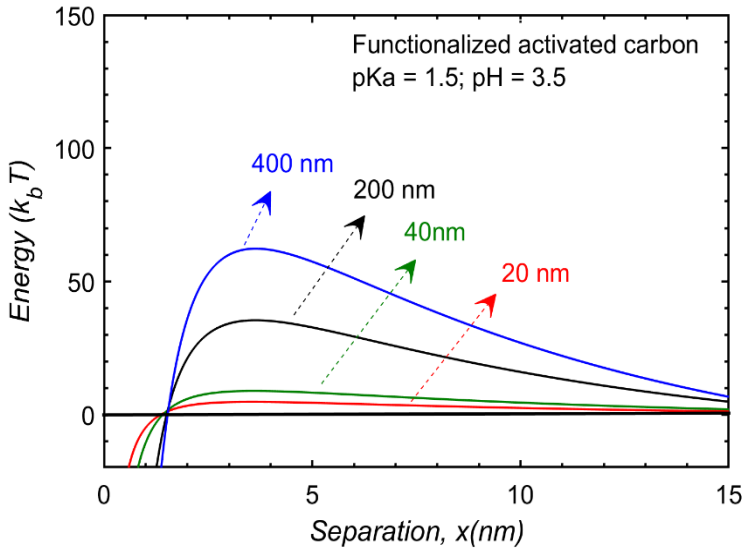

Figure 7. 4 D.L.V.O. interaction energy as a function of separation for different functionalized activated carbon particle size. The *pKa* is 1.5, acid head group coverage of activated carbon is assumed as 1.5/nm^2, *pH* is assumed as 3.5 and cellulose particle size is taken as 2 um.

In principal, the interaction energy, either vdw attraction or electrostatic repulsion are size-dependent because of additivity of energy, as shown in equation (2) and (8). Here, we use D.L.V.O. to take account catalyst size effect and **figure 7.4** is the resulting D.L.V.O. interaction energy between cellulose and catalyst (functionalized activated carbon) with respect to activated carbon particle size varying from 20 nm, 40 nm, 200 nm to 400 nm. The *pH* is fixed at 3.5, which is typical

for common reaction. We further assume that the catalysts have acid with pKa about 1.5 on the surface. We assume that Hamaker constant is independent on the particle size as shows by Pinchuk[27] that the damping factor that affecting Hamaker constant is negligible for our particle size. The results indicate that the D.L.V.O. repulsion barrier is as large as 62 k_bT for activated carbon with radius 400 nm. This huge repulsion barrier requires high kinetic energy provided by heater in order to overcome the barrier. Once the particle size reduces to around 100 nanometers, the repulsion energy barrier drops to below 20 *kbT*. This prediction is well explained by the fact that typical enzyme, which has the size around a few hundred nanometers or even smaller, can easily attach to cellulose surfaces at room temperature. However, the practical cellulose hydrolysis with particle size round 3 um requires much high temperature to accelerate the kinetic energy of particles.

7.4.4 D.L.V.O. interaction for cellulose and literature reported catalysts.

The parametric analysis has provided the quantitative tools that might be useful for analyzing the adsorption between cellulose and literature reported catalysts. Accordingly, we select four commonly reported catalysts in literature, namely, Nafion, ZSM5, functionalized activated carbon (pKa = 2.5) and sulfonated polystyrene (*pKa* = 1) as model catalysts. The *pH* varies from 2, 4 and 6 for Nafion and ZSM5 and from 2.5, 3.5, 4.5 and 5.5 for functionalized activated carbon and polystyrene. Those *pH* range is suitable for typical cellulose hydrolysis reaction in which *pH* is higher at beginning and lower towards the end of the reaction due to acid product generation. Under each *pH* condition, surface potentials for Nafion, ZSM5 and cellulose were computed using equation (9) and zeta potential from **table 7.2**; Surface potentials for functionalized activated carbon and polystyrene were determined using equation (10-18), as outlined in **theory** section. The calculated surface potentials were then incorporated into equation (8) for D.L.V.O. energy

calculation. The computed D.L.V.O. net interaction energy with respect to particle separation at different *pH* is shown in **figure 7.5**.

Overall, the results in **figure 7.5** demonstrate that electrostatic repulsion dominates over vdw attraction and results in a repulsion D.L.V.O. barrier at high *pH* because of the high negative surface potential for polymer-based catalysts and carboxylic/sulfonic acid functionalized catalysts. Specifically, D.L.V.O. interaction between cellulose and Nafion mainly repulsive from *pH* = 2 to 6. This could be explained by two reasons: firstly, the sulfonic acid on Nafion is strong acid with *pKa* below zero, and this much negative surface potential (around -60 mV) can hardly diminish even though the *pH* is as low as 2. Secondly, the vdw attraction is too weak (with Hamaker constant around 0.15 zJ) at separation above 1 nm and only becomes significant at shorter distance.

Cellulose and catalyst attract each other at separation greater than 15 nm due to the weak vdw attraction. At separation between 2 nm and 15 nm, electrostatic repulsion dominates the interaction and the repulsion barrier tends to be sensitively to *pH* variation. At high *pH* such as 3.5, the repulsion energy barrier is as high as 34 k_bT. Then it decreases to around zero k_bT when the *pH* increases to 2.8. This can be explained by the fact that the catalysts surface get protonated at lower *pH*, resulting in a less negatively charged surface and hence reducing the electrostatic repulsion. Additionally, the Debye length drops from 24 nm to 11 nm when the *pH* decreases from 3.5 to 2.8, allowing cellulose and activated carbon getting closer enough.

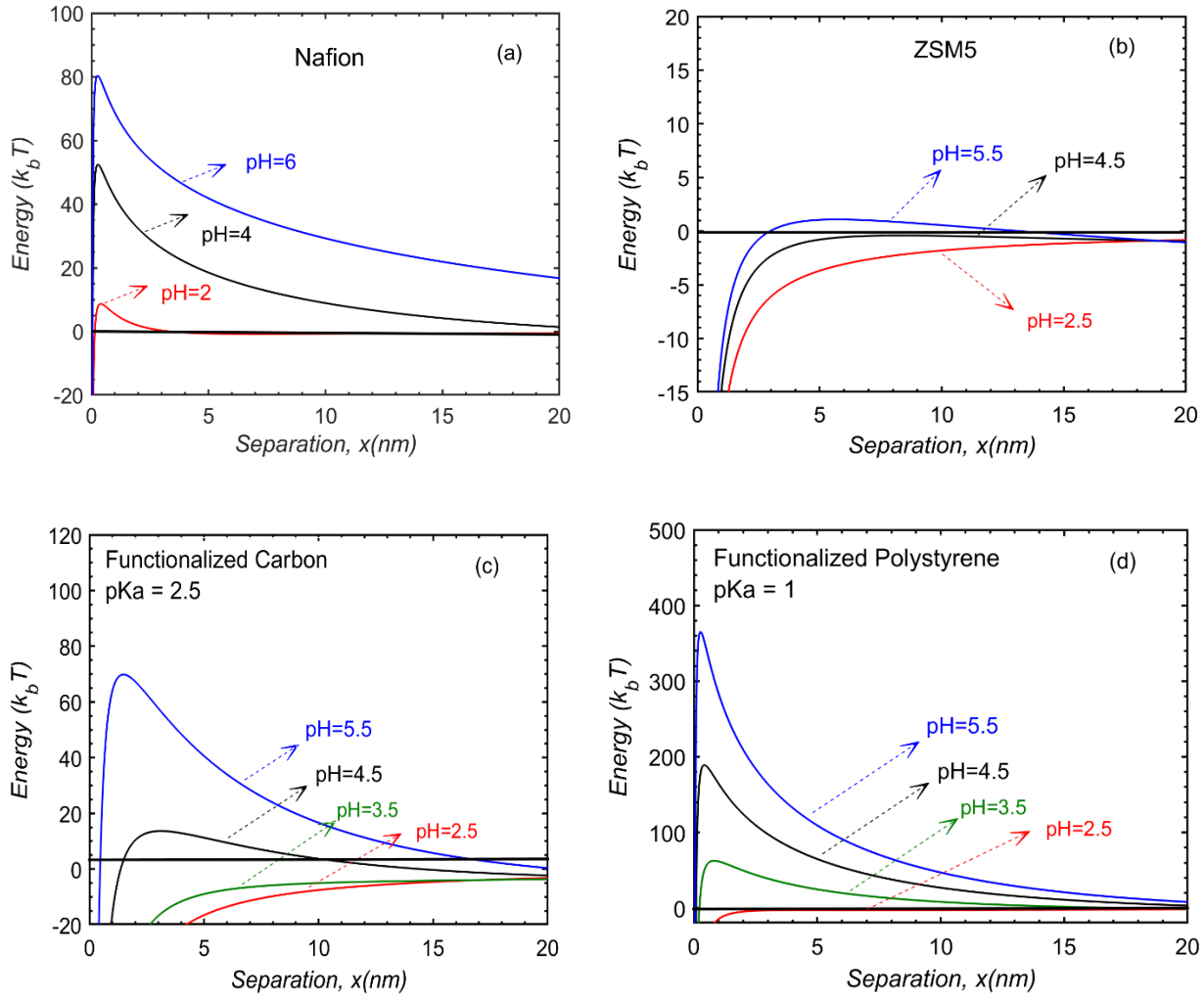

Figure 7. 5 D.L.V.O. interaction energy at different *pH* as a function of separation for (a) Nafion, (b) ZSM5, (c) carboxylic acid (*pKa* = 2.5) functionalized activated carbon and (d) sulfonated polystyrene (*pKa* = 1); cellulose particle radius is taken as 1 um while catalyst radius is assumed as 100 nm and ionic strength is taken as 0.1 mM.

The calculation here is limited to the case where absolute surface potential is typically low (<-60 mV) because of the limitation of Hogg's analytical solution. In fact, the surface potential of catalysts, especially for whose bearing sulfonic acid head group are much higher than -60 mV at *pH* ranging from 1.5 to 7, and sometimes even greater than -150 mV. This large amount of excess

charge on catalysts will repulse cellulose much strongly, leading to a much high energy barrier. We also notices that surface potential of cellulose is somehow independent on *pH*, as shown by Prathapan.

Although good adsorption not necessarily leads to high cellulose to glucose conversion because short-ranged forces such as hydration or hydrophobic interaction will play a role, there do have some literatures reported evidence. Geboers *et al*. shows that the conversion of glucose over Ru-loaded zeolites increases with addition of trace amount of mineral acids, including hydrochloride (HCl) or sulfuric acid (H_2SO_4). They attributes the improved performance to the enhanced cellulose-catalysts adsorption. we careful noted that although the D.L.V.O. calculation proves that lowering *pH* could increases the adsorption, lowering *pH* could also lead to high probability of protons attacking cellulose at high temperature. The analysis here confines only to adsorption, but not necessarily conversion.

high yield. Accordingly, studies have tested solid-acid catalysts with smaller particle size.

7.4.5 Non-D.L.V.O. interaction for cellulose and catalysts

Although D.L.V.O. theory can predict the interactions between particles to within 5% accuracy as some experiments confirmed, it often breaks down at small separation (below 2-5 nm) where the continuum theory fails to explain the dramatical change in either repulsion or attraction. At small separation about a few order of molecular scale, two of the main non-D.L.V.O., hydration (or solvation) and steric forces will come into play. Depending on the coordination between solvent and cellulose as well as solvent and catalysts, the non-D.L.V.O. forces could be strongly repulsive or attractive. In this section of discussion, we will qualitative describe the role of the non-D.L.V.O. interactions affecting cellulose-catalysts adsorption.

7.4.6 Hydration forces

The hydration force arises from the ordering of water molecules on liquid-solid interface and the ordering with itself at confined spaces, typically within 1-10 orders of solvent molecule size. Depending on the separations, surface roughness and chemical nature of the adjacent surfaces, the water molecules conform themselves in different configuration, leading to different water thin film density. In fact, the strength of the hydration forces is proportional to the water molecule density within the confinement, as an empirical correlation proposed by Tarazona and Vicente:

$$P(x) = -\rho_{\infty} k_b T cos\left(\frac{2\pi x}{\sigma}\right) e^{-\frac{D}{\sigma}} \qquad 7.19$$

where ρ_{∞} is the solvent number density. This force exponentially decays as the separation of particles increases, meaning that the force almost disappears at distances greater than 5 times of the solvent molecule size but increases dramatically as the separation falls within a few A. The hydration force behaves oscillatory fluctuating between attraction and repulsion, depending on whether the solvent molecules are been squeezed out or adsorbed in. This oscillatory forces can change to monotonically if the surface roughness are too large so that the solvent molecules are prevented being squeezed out.

The hydrophilicity of cellulose allows water molecules to adsorb on cellulose and form solid-liquid interfacial hydrogen bonds. Likewise, most of the solid acid catalysts, including zeolite, metal oxides and carbon materials are hydrophilic and have strong affinity to attract with water molecules. The strong affinity of water with cellulose and with catalysts will results in the localized immobility of water films. This thin layer of water films prevents further attachment between cellulose and catalyst, resulting a strong hydration repulsion. Polymer-based catalysts such as polystyrene and Nafion are typically hydrophobic in nature, allowing them to repel water and

somehow in direct contact with cellulose. As for the case of functionalized catalysts bearing hydrophilic groups such as -OH, -COOH and -SO_3H, those functional groups are hydrated prior contacting with cellulose, unless the molecular attraction between cellulose and those groups are stronger than those groups with water molecules. Since most of the theories that quantify the hydration are empirical, and the measurement technique for hydration forces is often interfered with D.L.V.O. forces, the magnitude or strength of hydration forces relative to D.L.V.O. forces is still in debates. However, modifying the catalysts and cellulose to somehow have hydrophobility could be a strategy to enhance cellulose-catalyst adsorption.

7.4.7 Steric forces

Cellulose is polymer materials in nature, and the surface roughness is too large to be ignored. In fact, cellulose used for hydrolysis reaction is normally ball-milled first to increase the accessibility and decease the crystal structure. This procedure may further make the cellulose rough with chains extending to the bulk solution. Under severely high temperature, those tangles of polymer-chains may start to overlap and interact with the chains from other particles. The scenario for catalysts is slightly different, depending on the catalysts type. Un-functionalized zeolite, metal oxides and carbon materials have a well-defined solid-liquid interface because the solid can resist high temperature and stay stable. As a result, the steric interaction, mostly is repulsion due to the unfavorable entropy reduction, between cellulose and bear catalysts are small in magnitude and instant in time scale. Catalysts that bears polymer functional groups tends to form strong steric repulsion with cellulose, and its magnitude depends on the surface coverage density as well as the nature of the catalyst-polymer adsorption, e.g. physical sorption or chemisorption. In fact, introducing polymer chains that could stick onto particles surfaces has been a strategy for

stabilizing colloid particles. In the case of cellulose hydrolysis, we would need the opposite, that is reducing the steric repulsion and “disrupt” the colloid “stability.

The thermo-stability of the polymer anchoring groups on catalysts may have an noneligible effect on the its steric interaction with cellulose. The weak binding for polymers chains on catalyst may cause the dissociation and of those groups and disperse into the liquid media. As a result of that,

7.4.8 Hydrophobic forces

The hydrophobic forces is less significant than both hydration forces and steric forces because cellulose and most catalysts are hydrophilic, as the cases for cellulose-zeolite, cellulose-metal oxides and cellulose-carbon materials. However, the hydrophobic interaction for polymer catalysts such as polystyrene is significant because of the their hydrophobility. As a result, the hydrophobic attraction for polystyrene is stronger than cellulose-polystyrene. Again, not only non-D.L.V.O. forces, the particle has to overcome electrostatic forces and vdw forces before reaching the short-ranged non-D.L.V.O. interaction. The statements are qualitive and more quantitatively theories have to develop to characterize or predict the synergetic effect of all types of interaction.

7.5 Conclusion

Hydrolyzing cellulose by solid-acid catalysts has attracted large amount of interests because of its benefits such as ease of separation, reusability and less-harm to environment. Current solid-acid catalysts design and synthesis have focused on molecular aspects such as hydrogen binding, covalent binding. As a result, the colloidal level of physical interactions between cellulose and catalysts in the presence of water remains largely unknown.

The present studies have filled the gap by using D.L.V.O. theory to quantify the interaction energy between cellulose and solid-acid catalysts. We select several commonly used catalysts, including

ZSM5, Nafion, polystyrene, ZrO_2, Fe_3O_4 and activated carbon materials to perform the D.L.V.O. analysis. Surface potential is predicted using a simple acid-base theory and Hamaker constant is determined using Lifshitz theory. We first perform the parametric analysis by determining repulsion energy barrier as function of Hamaker constant, *pH* and *pKa* of functionalized catalysts. The parametric analysis reveals that all selected catalysts including Nafion, polystyrene, activated carbon, zirconia and iron oxide bearing weak acid, e.g. carboxylic acid with pKa around or greater than 2.5, could potentially adsorb on cellulose because of the dominance of van der waals attraction over electrostatic repulsion. However, once the catalysts are functionalized with sulfonic acid with pKa about -2, polymer-based catalysts such as Nafion and polystyrene, and ZSM5 can repel cellulose because of large surface potential/surface charge density and small Hamaker constant. Metal oxides such as zirconia and iron oxides and activated carbon could adsorb cellulose within the pH range of 2-6 because of their large Hamaker constant, casting doubt on polymer-based substrate for designing catalysts for cellulose hydrolysis. We then analyze the particle size effect on cellulose-catalyst adsorption and find that the repulsion barrier will be reduced to less than 10 k_bT once the catalyst size is lowering to 50 nm. The analysis partially agreed with catalysts performance in literatures where weak acid is shown to have adsorption affinity with cellulose. The findings could help screen catalysts substrate materials and tune factors such as surface charge density and reaction media for enhancing cellulose-catalysts adsorption.

Lastly, we assessed the effect of non-D.L.V.O. forces involving hydration, steric and hydrophobic forces on cellulose-catalysts adsorption. Hydration forces is believed monotonically repulsive because cellulose and most catalysts (e.g. zeolite, metal oxides and carbon materials) are favorably hydrated, causing osmotic pressure. The surface roughness further prevents the water squeezing out from the confinement. Steric forces is likely repulsive because of the overlapping of the

polymer chins from cellulose and catalysts, and the entropy reduction. Hydrophobic attraction is relatively weak compared to other two due to the hydrophilicity of the interacting particles.

7.6 References

[1] Béguin, P., & Aubert, J.-P. (1994). The biological degradation of cellulose. FEMS Microbiology Reviews, 13(1), 25-58.

[2] Mascal, M., & Nikitin, E. B. (2008). Direct, High-Yield Conversion of Cellulose into Biofuel. Angewandte Chemie International Edition, 47(41), 7924-7926.

[3] Xiao, S., Liu, B., Wang, Y., Fang, Z., & Zhang, Z. (2014). Efficient conversion of cellulose into biofuel precursor 5-hydroxymethylfurfural in dimethyl sulfoxide–ionic liquid mixtures. Bioresource Technology, 151, 361-366.

[4] Dutta, S., De, S., Alam, M. I., Abu-Omar, M. M., & Saha, B. (2012). Direct conversion of cellulose and lignocellulosic biomass into chemicals and biofuel with metal chloride catalysts. Journal of Catalysis, 288, 8-15.

[5] Mielenz, J. R. (2001). Ethanol production from biomass: technology and commercialization status. Current Opinion in Microbiology, 4(3), 324-329.

[6] Rowell, R. M. (2007). Challenges in Biomass–Thermoplastic Composites. Journal of Polymers and the Environment, 15(4), 229-235.

[7] Melero, J. A., Iglesias, J., & Garcia, A. (2012). Biomass as renewable feedstock in standard refinery units. Feasibility, opportunities and challenges. Energy & Environmental Science, 5(6), 7393-7420.

[8] Nishiyama, Y., Langan, P., & Chanzy, H. (2002). Crystal Structure and Hydrogen-Bonding System in Cellulose Iβ from Synchrotron X-ray and Neutron Fiber Diffraction. J Am Chem Soc, 124(31), 9074-9082.

[9] Chundawat, S. P. S., Bellesia, G., Uppugundla, N., da Costa Sousa, L., Gao, D., Cheh, A. M., . . . Dale, B. E. (2011). Restructuring the Crystalline Cellulose Hydrogen Bond Network Enhances Its Depolymerization Rate. J Am Chem Soc, 133(29), 11163-11174.

[10] Das, K., Ray, D., Bandyopadhyay, N. R., Ghosh, T., Mohanty, A. K., & Misra, M. (2009). A study of the mechanical, thermal and morphological properties of microcrystalline cellulose particles prepared from cotton slivers using different acid concentrations. Cellulose, 16(5), 783-793.

[11] Hoeger, I. C., Nair, S. S., Ragauskas, A. J., Deng, Y., Rojas, O. J., & Zhu, J. Y. (2013). Mechanical deconstruction of lignocellulose cell walls and their enzymatic saccharification. Cellulose, 20(2), 807-818.

[12] Lindman, B., Karlström, G., & Stigsson, L. (2010). On the mechanism of dissolution of cellulose. Journal of Molecular Liquids, 156(1), 76-81.

[13] Medronho, B., & Lindman, B. (2014). Competing forces during cellulose dissolution: From solvents to mechanisms. Current Opinion in Colloid & Interface Science, 19(1), 32-40.

[14] Bochek, A. M. (2003). Effect of Hydrogen Bonding on Cellulose Solubility in Aqueous and Nonaqueous Solvents. Russian Journal of Applied Chemistry, 76(11), 1711-1719.

[15] Pinkert, A., Marsh, K. N., & Pang, S. (2010). Reflections on the Solubility of Cellulose. Industrial & Engineering Chemistry Research, 49(22), 11121-11130.

[16] Sun, Y., & Cheng, J. (2002). Hydrolysis of lignocellulosic materials for ethanol production: a review. Bioresource Technology, 83(1), 1-11.

[17] Yu, H., Qin, Z., Liang, B., Liu, N., Zhou, Z., & Chen, L. (2013). Facile extraction of thermally stable cellulose nanocrystals with a high yield of 93% through hydrochloric acid hydrolysis under hydrothermal conditions. Journal of Materials Chemistry A, 1(12), 3938-3944.

[18] Kim, J. S., Lee, Y. Y., & Torget, R. W. (2001). Cellulose Hydrolysis Under Extremely Low Sulfuric Acid and High-Temperature Conditions. In B. H. Davison, J. McMillan, & M. Finkelstein (Eds.), Twenty-Second Symposium on Biotechnology for Fuels and Chemicals (pp. 331-340). Totowa, NJ: Humana Press.

[19] Taherzadeh, M. J., & Karimi, K. (2007). Acid-based hydrolysis processes for ethanol from lignocellulosic materials : A review. BioResources, 2(3), 472–499.

[20] Horn, S. J., Vaaje-Kolstad, G., Westereng, B., & Eijsink, V. (2012). Novel enzymes for the degradation of cellulose. Biotechnology for Biofuels, 5(1), 45.

[21] Bhat, M. K., & Bhat, S. (1997). Cellulose degrading enzymes and their potential industrial applications. Biotechnology Advances, 15(3), 583-620.

[22] López-Mondéjar, R., Zühlke, D., Becher, D., Riedel, K., & Baldrian, P. (2016). Cellulose and hemicellulose decomposition by forest soil bacteria proceeds by the action of structurally variable enzymatic systems. *Scientific Reports, 6*, 25279.

[23] Klein-Marcuschamer, D., Oleskowicz-Popiel, P., Simmons, B. A., & Blanch, H. W. (2012). The challenge of enzyme cost in the production of lignocellulosic biofuels. Biotechnology and Bioengineering, 109(4), 1083-1087.

[24] Hägerdal, B., Ferchak, J. D., & Pye, E. K. (1980). Saccharification of cellolulose by the cellulolytic enzyme system of Thermonospora sp. I. Stability of cellulolytic activities with respect to time, temperature, and pH. Biotechnology and Bioengineering, 22(8), 1515-1526.

[25] Huang, Y.-B., & Fu, Y. (2013). Hydrolysis of cellulose to glucose by solid-acid catalysts. Green Chemistry, 15(5), 1095-1111.

[26] Onda, A., Ochi, T., & Yanagisawa, K. (2008). Selective hydrolysis of cellulose into glucose over solid-acid catalysts. Green Chemistry, 10(10), 1033-1037.

[27] Lai, D.-m., Deng, L., Li, J., Liao, B., Guo, Q.-x., & Fu, Y. (2011). Hydrolysis of Cellulose into Glucose by Magnetic Solid-acid. ChemSusChem, 4(1), 55-58.

[28] Yamaguchi, D., Kitano, M., Suganuma, S., Nakajima, K., Kato, H., & Hara, M. (2009). Hydrolysis of Cellulose by a Solid-acid Catalyst under Optimal Reaction Conditions. The Journal of Physical Chemistry C, 113(8), 3181-3188.

[29] Tyufekchiev, M., Duan, P., Schmidt-Rohr, K., Granados Focil, S., Timko, M. T., & Emmert, M. H. (2018). Cellulase-Inspired Solid-acids for Cellulose Hydrolysis: Structural Explanations for High Catalytic Activity. ACS Catalysis, 8(2), 1464-1468.

[30] Wattanapaphawong, P., Reubroycharoen, P., & Yamaguchi, A. (2017). Conversion of cellulose into lactic acid using zirconium oxide catalysts. RSC Advances, 7(30), 18561-18568.

Lee, L.-H. (1996). Correlation between Lewis Acid−Base Surface Interaction Components and Linear Solvation Energy Relationship Solvatochromic α and β Parameters. Langmuir, 12(6), 1681-1687.

[31] Rinaldi, R., Palkovits, R., & Schuth, F. (2008). Depolymerization of cellulose using solid catalysts in ionic liquids. Angew Chem Int Ed Engl, 47(42), 8047-8050.

[32] Suganuma, S., Nakajima, K., Kitano, M., Yamaguchi, D., Kato, H., Hayashi, S., & Hara, M. (2008). Hydrolysis of cellulose by amorphous carbon bearing SO3H, COOH, and OH groups. J Am Chem Soc, 130(38), 12787-12793.

[33] Tarabanko, N., Tarabanko, V. E., Kukhtetskiy, S. V., & Taran, O. P. (2019). Electrical Double Layer as a Model of Interaction between Cellulose and Solid-acid Catalysts of Hydrolysis. ChemPhysChem, 20(5), 706-718.

[34] Radtchenko, I. L., Papastavrou, G., & Borkovec, M. (2005). Direct Force Measurements between Cellulose Surfaces and Colloidal Silica Particles. Biomacromolecules, 6(6), 3057-3066.

[35] Carambassis, A., & Rutland, M. W. (1999). Interactions of Cellulose Surfaces: Effect of Electrolyte. Langmuir, 15(17), 5584-5590.

[36] Fall, A. B., Lindström, S. B., Sundman, O., Ödberg, L., & Wågberg, L. (2011). Colloidal Stability of Aqueous Nanofibrillated Cellulose Dispersions. Langmuir, 27(18), 11332-11338.

[37] Hamaker, H. C. (1937). The London—vdw attraction between spherical particles. Physica, 4(10), 1058-1072.

[38] Israelachvili, J. N. Intermolecular and Surfaces Forces, 3rd. ed.; Academic Press: London, 1991; p 307.

[39] Tokunaga, T. K. (2012). D.L.V.O.-Based Estimates of Adsorbed Water Film Thicknesses in Geologic CO2 Reservoirs. Langmuir, 28(21), 8001-8009.

[40] Budd, J., & Herrington, T. M. (1989). Surface charge and surface area of cellulose fibres. Colloids and Surfaces, 36(3), 273-288.

[41] Imaizumi, S., Matsumoto, H., Ashizawa, M., Minagawa, M., & Tanioka, A. (2012). Nanosize effects of sulfonated carbon nanofiber fabrics for high capacity ion-exchanger. RSC Advances, 2(7), 3109-3114.

[42] Prathapan, R., Thapa, R., Garnier, G., & Tabor, R. F. (2016). Modulating the zeta potential of cellulose nanocrystals using salts and surfactants. Colloids and Surfaces A: Physicochemical and Engineering Aspects, 509, 11-18.

[43] Myśliwiec, D., Chylińska, M., Szymańska-Chargot, M., Chibowski, S., & Zdunek, A. (2016). Revision of adsorption models of xyloglucan on microcrystalline cellulose. Cellulose, 23(5), 2819-2829.

[44] Hartmann, R., Kinnunen, P., & Illikainen, M. (2018). Cellulose-mineral interactions based on the D.L.V.O. theory and their correlation with flotability. Minerals Engineering, 122, 44-52.

[45] Abebe, D. G., & Farhat, T. R. (2010). Self-assembly of Nafion®/poly(vinyl alcohol) at pH = 1.2 and Nafion®/poly(allyl amine) at pH = 11. Soft Matter, 6(6), 1325-1335.

[46] Sidhpuria, K. B., Daniel-da-Silva, A. L., Trindade, T., & Coutinho, J. A. P. (2011). Supported ionic liquid silica nanoparticles (SILnPs) as an efficient and recyclable heterogeneous catalyst for the dehydration of fructose to 5-hydroxymethylfurfural. Green Chemistry, 13(2), 340-349.

[47] Nguyen, D., Such, C. H., & Hawkett, B. S. (2013). Polymer coating of carboxylic acid functionalized multiwalled carbon nanotubes via reversible addition-fragmentation chain transfer mediated emulsion polymerization. Journal of Polymer Science Part A: Polymer Chemistry, 51(2), 250-257.

[48] Connor, J. N., & Horn, R. G. (2001). Measurement of Aqueous Film Thickness between Charged Mercury and Mica Surfaces: A Direct Experimental Probe of the Poisson−Boltzmann Distribution. Langmuir, 17(23), 7194-7197.

[49] Hogg, R., Healy, T. W., & Fuerstenau, D. W. (1966). Mutual coagulation of colloidal dispersions. Transactions of the Faraday Society, 62(0), 1638-1651.

[50] Gregory, J. (1975). Interaction of unequal double layers at constant charge. Journal of Colloid and Interface Science, 51(1), 44-51.

[51] Hoek, E. M. V., & Agarwal, G. K. (2006). Extended D.L.V.O. interactions between spherical particles and rough surfaces. Journal of Colloid and Interface Science, 298(1), 50-58.

[52] Tadros, T. (2014). Chapter 2 - Colloid and interface aspects of pharmaceutical science. In H. Ohshima & K. Makino (Eds.), Colloid and Interface Science in Pharmaceutical Research and Development (pp. 29-54).

[53] Mikelonis, A. M., Youn, S., & Lawler, D. F. (2016). D.L.V.O. Approximation Methods for Predicting the Attachment of Silver Nanoparticles to Ceramic Membranes. Langmuir, 32(7), 1723-1731.

[54] van Oss, C. J., Giese, R. F., & Costanzo, P. M. (1990). D.L.V.O. and Non-D.L.V.O. Interactions in Hectorite. Clays and Clay Minerals, 38(2), 151-159.

[55] Nvari, R., Myers, M., Umana-Membreno, G. A., Baker, M., Spagnoli, D., Parish, G., & Nener, B. D. (2014). Charging mechanism of AlGaN/GaN open-gate pH sensor and electrolyte interface.

[56] Behrens, S. H., & Grier, D. G. (2001). The charge of glass and silica surfaces. The Journal of Chemical Physics, 115(14), 6716-6721.

[57] W. B. Russel, D. A. Saville, and W. R. Schowalter, Colloidal Dispersions, Cambridge Monographs on Mechanics and Applied Mathematics (Cambridge University Press, Cambridge, 1989).

[58] Bergström, L., Stemme, S., Dahlfors, T., Arwin, H., & Ödberg, L. (1999). Spectroscopic Ellipsometry Characterisation and Estimation of the Hamaker Constant of Cellulose. Cellulose, 6(1), 1-13.

[59] Shimazaki, Y., Miyazaki, Y., Takezawa, Y., Nogi, M., Abe, K., Ifuku, S., & Yano, H. (2007). Excellent Thermal Conductivity of Transparent Cellulose Nanofiber/Epoxy Resin Nanocomposites. Biomacromolecules, 8(9), 2976-2978.

[60] Stoops, W. N. (1934). The Dielectric Properties of Cellulose. J Am Chem Soc, 56(7), 1480-1483.

[61] Weidenthaler, C., Fischer, R. X., Shannon, R. D., & Medenbach, O. (1994). Optical Investigations of Intergrowth Effects in the Zeolite Catalysts ZSM-5 and ZSM-8. The Journal of Physical Chemistry, 98(48), 12687-12694.

[62] Dietrich, M., Rauch, D., Simon, U., Porch, A., & Moos, R. (2015). Ammonia storage studies on H-ZSM-5 zeolites by microwave cavity perturbation: Correlation of dielectric properties and ammonia storage. Journal of Sensors and Sensor Systems, 4, 263-269.

[63] Wood, D. L., & Nassau, K. (1982). Refractive index of cubic zirconia stabilized with yttria. Applied Optics, 21(16), 2978-2981.

[64] Harrop, P. J., & Wanklyn, J. N. (1967). The dielectric constant of zirconia. British Journal of Applied Physics, 18(6), 739-742.

[65] Dore, P., Nucara, A., Cannavò, D., De Marzi, G., Calvani, P., Marcelli, A., Peters, H. J. (1998). Infrared properties of chemical-vapor deposition polycrystalline diamond windows. Applied Optics, 37(24), 5731-5736.

[66] Shkal, F., Lopez, S., Slocombe, D., & Porch, A. (2018). Microwave Characterization of Activated Carbons. Journal of Computer and Communications, 06, 112-123.

[67] In E. D. Palik (Ed.), Handbook of Optical Constants of Solids (pp. xiii-xv). Burlington: Academic Press.

[68] Ansar, M., Atiq, S., Alamgir, M., & Nadeem, S. (2014). Available Online Publications Frequency and Temperature Dependent Dielectric Response of Fe 3 O 4 Nano-crytallites. Journal of Scientific Research, 6, 399-406.

[69] Majsztrik, P., Bocarsly, A., & Benziger, J. (2008). Viscoelastic Response of Nafion. Effects of Temperature and Hydration on Tensile Creep. Macromolecules, 41.

[70] Ghosh, G. (1999). Dispersion-equation coefficients for the refractive index and birefringence of calcite and quartz crystals. Optics Communications, 163(1), 95-102.

[71] Nandiwale, K. Y., Galande, N. D., Thakur, P., Sawant, S. D., Zambre, V. P., & Bokade, V. V. (2014). One-Pot Synthesis of 5-Hydroxymethylfurfural by Cellulose Hydrolysis over Highly

Active Bimodal Micro/Mesoporous H-ZSM-5 Catalyst. ACS Sustainable Chemistry & Engineering, 2(7), 1928-1932.

[72] Kim, S.-J., Dwiatmoko, A. A., Choi, J. W., Suh, Y.-W., Suh, D. J., & Oh, M. (2010). Cellulose pretreatment with 1-n-butyl-3-methylimidazolium chloride for solid-acid-catalyzed hydrolysis. Bioresource Technology, 101(21), 8273-8279. R.

[73] Chang, Y., Lee, C., & Bae, C. (2014). Polystyrene-based superacidic solid acid catalyst: synthesis and its application in biodiesel production. RSC Advances, 4(88), 47448-47454.

[74] Keramati, H., Saidi, M., & Zabetian, M. (2015). Stabilization of Suspension of Zirconia Microparticles Using Nanoparticle Halos Mechanism: Zeta Potential Effect. Journal of Dispersion Science and Technology, 37, 150415113054007.

[75] Sanz, O., Almeida, L. C., Zamaro, J. M., Ulla, M. A., Miró, E. E., & Montes, M. (2008). Washcoating of Pt-ZSM5 onto aluminium foams. Applied Catalysis B: Environmental, 78(1), 166-175.

[76] Barbati, A. C., & Kirby, B. J. (2014). Electrokinetic Measurements of Thin Nafion Films. Langmuir, 30(8), 1985-1993.

[77] Feng, J., Mao, J., Wen, X., & Tu, M. (2011). Ultrasonic-assisted in situ synthesis and characterization of superparamagnetic Fe3O4 nanoparticles. Journal of Alloys and Compounds, 509(37), 9093-9097.

[78] Zhang, G., Shi, L., Zhang, Y., Wei, D., Yan, T., Wei, Q., & Du, B. (2015). Aerobic granular sludge-derived activated carbon: mineral acid modification and superior dye adsorption capacity. RSC Advances, 5(32), 25279-25286.

[79] Geboers, J., Van de Vyver, S., Carpentier, K., Jacobs, P., & Sels, B. (2011). Efficient hydrolytic hydrogenation of cellulose in the presence of Ru-loaded zeolites and trace amounts of mineral acid. Chemical Communications, 47(19), 5590-5592.

[80] Phan-Xuan, T., Thuresson, A., Skepö, M., Labrador, A., Bordes, R., & Matic, A. (2016). Aggregation behavior of aqueous cellulose nanocrystals: the effect of inorganic salts. Cellulose, 23(6), 3653-3663.

[81] Missana, T., & Adell, A. (2000). On the Applicability of D.L.V.O. Theory to the Prediction of Clay Colloids Stability. Journal of Colloid and Interface Science, 230(1), 150-156.

[82] Smith, A. M., Maroni, P., & Borkovec, M. (2018). Attractive non-DLVO forces induced by adsorption of monovalent organic ions. Physical Chemistry Chemical Physics, 20(1), 158-164.

[83] Baccile, N., Laurent, G., Babonneau, F., Fayon, F., Titirici, M.-M., & Antonietti, M. (2009). Structural Characterization of Hydrothermal Carbon Spheres by Advanced Solid-State MAS 13C NMR Investigations. The Journal of Physical Chemistry C, 113(22), 9644-9654.

[84] Charmot, A., Chung, P.-W., & Katz, A. (2014). Catalytic Hydrolysis of Cellulose to Glucose Using Weak-Acid Surface Sites on Postsynthetically Modified Carbon. ACS Sustainable Chemistry & Engineering, 2(12), 2866-2872.

[85] Abitbol, T.; Kam, D.; Levi-Kalisman, Y.; Gray, D. G.; Shoseyov, O., Surface Charge Influence on the Phase Separation and Viscosity of Cellulose Nanocrystals. Langmuir 2018, 34 (13), 3925-3933.

[86] Bai, Y.; Huang, H.; Wang, C.; Long, R.; Xiong, Y., Engineering the surface charge states of nanostructures for enhanced catalytic performance. Materials Chemistry Frontiers 2017, 1 (10), 1951-1964.

[87] Faure, B.; Salazar-Alvarez, G.; Bergström, L., Hamaker Constants of Iron Oxide Nanoparticles. Langmuir 2011, 27 (14), 8659-8664.

[88] Fronczak, S. G.; Dong, J.; Browne, C. A.; Krenek, E. C.; Franses, E. I.; Beaudoin, S. P.; Corti, D. S., A New “Quasi-Dynamic” Method for Determining the Hamaker Constant of Solids Using an Atomic Force Microscope. Langmuir 2017, 33 (3), 714-725.

[89] Dong, X. M.; Gray, D. G., Effect of Counterions on Ordered Phase Formation in Suspensions of Charged Rodlike Cellulose Crystallites. Langmuir 1997, 13 (8), 2404-2409.

[90] Onda, A.; Ochi, T.; Yanagisawa, K., Selective hydrolysis of cellulose into glucose over solid acid catalysts. Green Chemistry 2008, 10 (10), 1033-1037.

Chapter 8

Revised Design Principals for Solid-acid Catalysts

8.1 Abstract

Solid-acid catalysts functionalized with catalytic groups have attracted intense interest for hydrolyzing cellulose into fermentable compounds. However, the solid-acid catalysts design has been guided by molecular level of interactions and the mechanism of cellulose-solid-acid catalyst particles adsorption remains unknown. Here, we applied colloidal stability theory, DLVO, to rationalize the solid-acid design for enhanced cellulose-solid-acid adsorption. The theoretical analysis shows that polymer-based solid-acid substrates such as polystyrene and Nafion are surprisingly ineffective for adsorbing cellulose due to the small Hamaker constant and repulsive electrostatic repulsion; both carbon and metallic oxide-based catalysts are effective for cellulose-solid-acid interaction because of the dominating van der Waals attraction. We have evaluated strategies for enhancing cellulose-catalyst interaction and concluded that raising reaction temperature or synthesizing acid/base bifunctional catalysts can effectively diminish electrostatic repulsion and promote cellulose-catalyst coagulation. The shear force is also analyzed and recommended that current shear rate must increase at least an order of magnitude in order to induce coagulation.

8.2 Revised Design Principals for Solid-acid Catalysts

The design of solid-acid for hydrolyzing cellulose has long been guided by molecular interaction. However, given that both cellulose and catalyst are present as solid before and after the reaction, DLVO theory must be used to rationalize catalyst design. Figure 8.1a and Figure 8.1b are schematic representations of the particle-particle interaction predicted by DLVO theory (top panel)

and the resulting colloidal suspensions (bottom panel), shown both for particles with similar (Figure 8.1a) and dissimilar charges (Figure 8.1b).

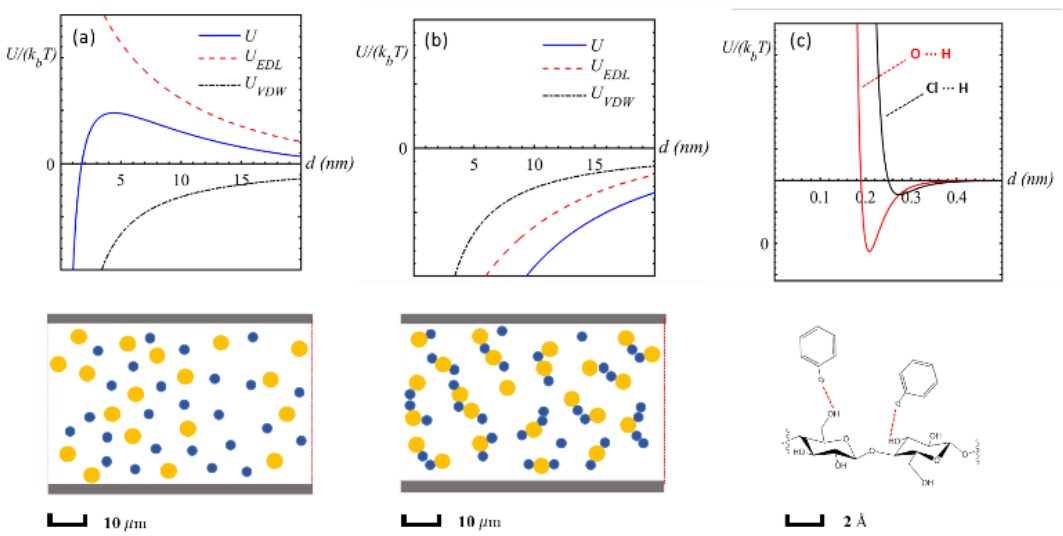

Figure 8. 1 Schematics of particle-particle interactional energy as functions of particle separation (yellow sphere represents cellulose and blue sphere represents solid-acid catalyst: (a) like-charge colloidal interactional energy as function of particle separation, (b) unlike-charge colloidal interaction as function of separation, (c) approximated single hydrogen bonding interaction energy between cellulose chain and chlorobenzene. Note that the *x*-axis scale is 20 nm in Figure 8.1a and Figure 8.1b and 0.5 nm in Figure 8.1c.

In the case of particles with similar charges, particles must surmount an energy barrier located several nanometers from the particle surface before they can interact. Crucially, the location of the barrier (>1-3 nm separation) is far beyond the range of molecular non-bond interaction such as hydrogen bonds (<2 Å), meaning that macro-particles should overcome the energy barrier caused by DLVO effect before hydrogen bonds or other forms of van der Waals interaction can be formed between particles. At best, catalyst particles might interact at a distance with cellulose, for example

by water mediated proton transfer;[1] however, decreasing the separation distance less than 10 nm incurs an increasing energy penalty that opposes such interaction.

The bottom panels of Figure 8.1 are particle-particle schematics. The net repulsive energy barrier predicted for similarly charged particles results in stable dispersions (Figure 8.1a, bottom panel). For dissimilarly charged particles, the net interaction is attractive, resulting in fast-coagulation (Figure 8.1b, bottom panel). For catalytic applications, coagulation is the desired outcome. That stated, catalyst particles bearing acid groups will invariably be negatively charged in solution. So, too, are cellulose particles. Accordingly, acid catalysts and cellulose are predicted to form stable colloids, rather than undergoing coagulation.

For comparison, Figure 8.1c is a molecular-level schematic representation of the interaction energy between a hydrogen bond donor (polysaccharide) and acceptor (chlorobenzene), the suggested interaction responsible for particle-particle catalysis. Unlike Figure 1a and 1b, Figure 1c shows that molecules or atoms experience no interaction barrier aside from the extremely short range (<1 Å) steric interaction. For similarly charged particles the situation is qualitatively different, and Figure 8.1 makes clear that applying molecular level explanations to colloidal phenomena, as has been done for solid-acid catalysis of cellulose, is insufficient.

The objective for catalysis is to design an "unstable dispersion" that encourages catalyst-cellulose interaction. Colloidal theory can be used for designing solid-acids for which the repulsive barrier for interacting with cellulose is <25 k_bT, an arbitrary value but one that is based on empirical observations of colloidal stability.[2] Ideally, this interaction could be tuned by changing *pH*, ionic strength, or temperature; accordingly, the solid catalyst could be used under one set of conditions for cellulose hydrolysis. Clearly, this level of manipulation is not possible without a firm scientific basis and theoretical analysis, which is what this work aims to develop.

For spherical particles, the DLVO equation can be reduced to a function of particle diameter, solution phase *pH*, ionic strength, Debye length, and a collection of parameters that are known or can be estimated for cellulose and many important solid-acid catalyst types, including inorganic materials, polymeric, and functionalized carbons.[3] The SI contains the details on how DLVO theory was applied to the catalyst-cellulose problem. The most important parameter affecting U_{VDW}, aside from particle diameter, is the Hamaker constant, A_{132}. The Hamaker constant depends on the catalyst material and values for several important catalyst materials interacting with cellulose across water are provided in Table 8.1. Similarly, for U_{EDL}, the most important parameter is the surface potential. As described in the SI, the surface potential is not typically known. However, the surface potential can be estimated from experimental measurements of the zeta potential or estimated from known values of surface acid density, ionic strength, and acid strength (pK_A). Table 8.1 provides some representative values of zeta potential representative catalyst materials at *pH* values of 1.0, 3.0, and 5.0, as reported in the literature.

Table 8. 1 Hamaker constants and reported zeta potential for representative solid-acid catalysts interacting with cellulose

Catalyst	Modifier acid	A_{132} ($\times 10^{-21}$ J)	□ (mV)			Ref.
			pH=1	*pH=3*	*pH=5*	
Cellulose	-	-	-16	-25	-27	[4]
[a] Carbon	Nitric acid	36.0	-30	-37	-40	[5]
[b] Fe_3O_4	Sulfonic acid	35.0	-	-40	-63	[6]
[c] ZrO_2	Citric acid	28.8	-	-18	-42	[7]
[d] Polystyrene	Acrylic acid	10.7	-	-28	-45	[8]
[e] Nafion	-	1.70	-	-45	-70	[9]

Note: [a,b,c,d,e] zeta potential at *pH* =1 is not reported; [e] zeta potential for bear Nafion without acid functionalization.

Table 8.1 defines ranges of the Hamaker constant and surface potential for cellulose and commonly used solid-acids. Cellulose is used as a representative biomass constituent, and the subject of many previous studies of solid-acid catalysis.[10] Figure 8.2 shows energy-distance curves for values of the Hamaker constant and surface potential that span the range expected from Table 8.1, with other factors held constant at representative values (pH = 5, fixed catalyst diameter of 1 μm and fixed cellulose particle diameter of 5 μm). Clearly, in most cases, a solid-acid particle will experience a barrier ranging from 10 k_bT to 200 k_bT as it approaches the cellulose surface. Carbon is an exception, due to its large Hamaker constant (Table 8.1). Inorganic oxides and especially polymers experience a prohibitively large repulsive barrier for interaction with cellulose.

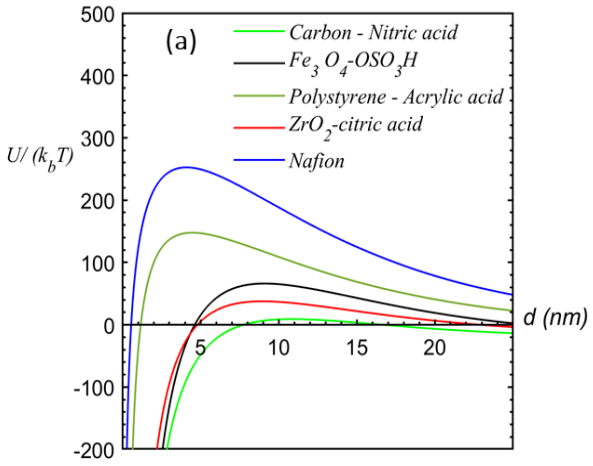

Figure 8. 2 DLVO interaction energy as a function of cellulose-catalyst separation for reported catalysts at pH = 5.

A problem with existing catalyst strategies is that partial de-protonation of the acid surface results in a negative surface potential (Table 8.1). Since cellulose possesses a negative surface potential at pH above 2 (Table 8.1), the resulting U_{EDL} often results in a repulsive barrier preventing catalyst-cellulose interaction, as shown in Figure 8.2. Keeping the catalyst protonated,

by lowering *pH* is one way to avoid the negative surface charge, as shown in a contour plot of energy barrier as a function of pK_A – *pH* (Figure 8.3) for representative values of the Hamaker constant (2×10^{-20} J) and acid density (5 nm^{-2}). Figure 8.3 shows that adjusting *pH* can effectively remove the catalyst-cellulose interaction barrier. However, the problem with acidifying the *pH* is that it requires addition of homogeneous acid, the very problem that was to be solved. For example, reducing the barrier to less than 200 k_bT for a catalyst with pK_A < 2 requires reducing the *pH* to less than 1.1.

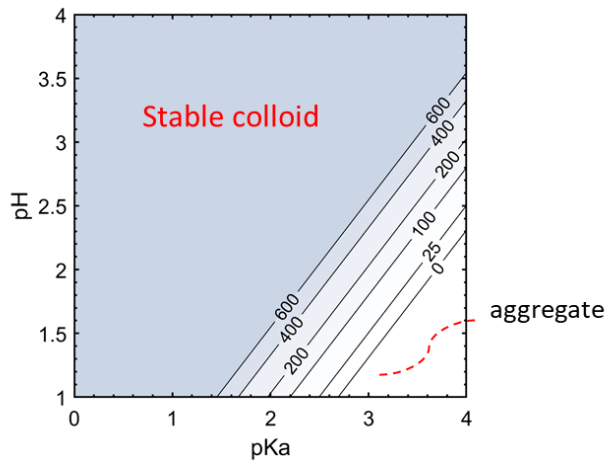

Figure 8. 3 DLVO maximum energy barrier as a function of acid group *pKa* and solution *pH*, assuming acid head group density of 5 nm^{-2}, Hamaker constant of 2×10^{-20} J.

An approach that does not depend on addition of liquid acids is selecting the catalyst material to maximize U_{VDW}. Figure 8.4 plots the energy barrier as a function of Hamaker constant for three representative values of the surface potential, and shows how this approach might work. Hamaker constants of representative materials are superimposed on the plot for reference. Maximizing the Hamaker constant, for example by using carbon-based or inorganic catalyst particles such as zirconia or iron oxide, has potential to reduce the particle-particle interaction barrier to <25 k_bT at

surface potential around – 35 mV. In contrast, polymer-based catalysts such as Nafion and polystyrene do not interact with cellulose without a substantial >25 k_bT barrier under any realistic conditions.

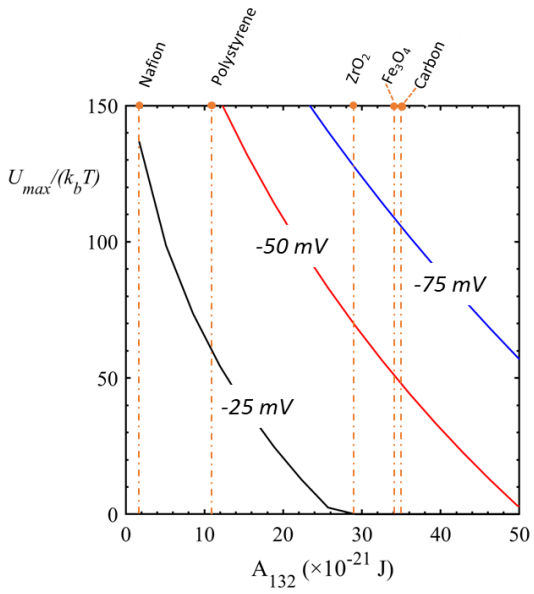

Figure 8. 4 The DLVO energy barrier height as function of Hamaker constant for different values of the surface potential.

Heating the reaction system to 140 – 170 ^oC is commonly described in the literature for decomposing cellulose under mild conditions.[11] The change of Hamaker constant is around 3% upon raising the temperature from 25 ^oC to 150 ^oC.[12] The change of temperature mainly affects dielectric constant and hence the Debye length of the reaction system. Figure 8.5 shows that increasing temperature to 150 ^oC may enhance carbon and zirconia-based catalysts ability to adsorb cellulose. Polymer based catalysts such as polyelectrolyte still lack the capacity to interact with cellulose under intermediate temperature.

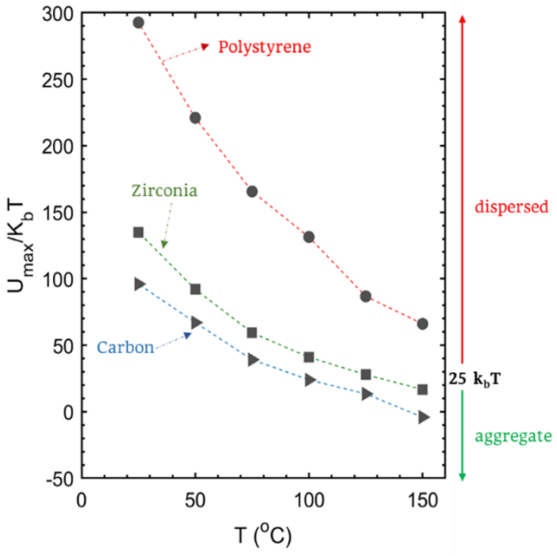

Figure 8. 5 DLVO energy barrier as a function of temperature for cellulose interacting with polystyrene, zirconia, and carbon catalysts. The cellulose diameter is assumed as 5 μm. The surface potential for the catalyst is assumed to be −30 mV and catalysts surface potential are assumed to be – 50 mV.

A final option is the use of a bifunctional catalyst consisting of acid and base groups, which has been successfully synthesized.[13-16] The need for the acid group is clear from the application. However, as shown previously in Figure 8.2, acid group dissociation leads to the catalyst acquiring a negative charge that then repels the negatively charged cellulose substrate. The role of the base therefore is to balance the negative charge of the partially dissociated acid. Naturally, a bifunctional catalyst must be designed carefully so that the acid and base groups do not simply react in solution to form the corresponding salt. Polyions are an example.[17, 18] Indeed, polyionic materials have been used previously to promote cellulose flocculation,[19] and several solid-acid catalysts proposed for cellulose hydrolysis have possessed cationic groups, including imidazolium,[20] previous work on acidic polymers bearing imidazolium groups have again

focused on molecular-level effects, for example using as inspiration the observation that some imidazolium-based ionic liquids are effective cellulose solvents.[20] Here, a colloidal perspective is advocated.

DLVO energy calculation can be used to model the effects of bifunctional catalysts on cellulose binding, using a procedure similar to that adopted to construct Figure 8.3; the Supporting Information provides details. Figure 8.6 provides particle-particle interaction curves for representative values of the density of acid to base sites at fixed Hamaker constants characteristic of inorganic solids (2×10^{-20} J), with cellulose particle diameter of 5 μm, catalyst diameter of 1 μm, a pH of 5. Figure 8.6 shows that a bifunctional catalyst can reduce the particle-particle interaction barrier to < 10 k_bT for values of the acid to base density ratio less than or equal to 1. In fact, for the case in which the base site density is twice that of the acid site density, the catalyst-cellulose interaction is attractive at all separations, meaning that a mixture of that bifunctional catalyst and cellulose may spontaneously coagulate.

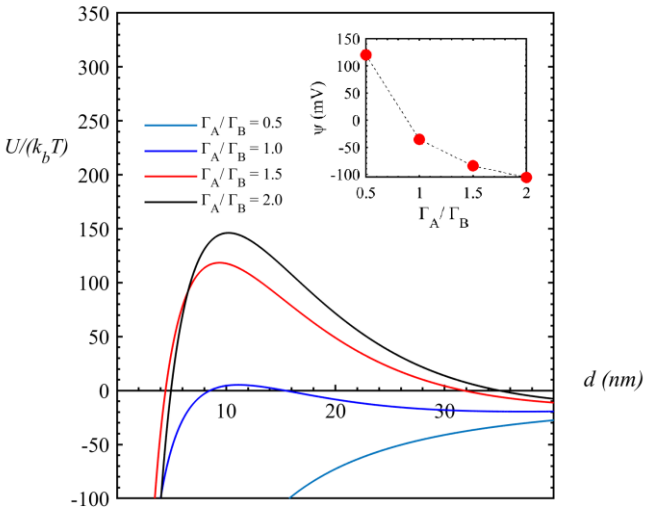

Figure 8. 6 Interaction energy of cellulose with bifunctional catalysts having different ratio of acid to base site density, assuming pK_a as 1 and pK_b as 5.75, total site density Γ_{tot} as 5 nm^{-2}.

For biomass hydrolysis using tightly bound bifunctional catalysts, recovering the catalyst after reaction may pose a challenge.[21] Colloidal-level analysis suggests several recovery strategies. Following with the theme of bifunctional catalysts, *pH* might be used to tune between attractive and repulsive interactions. Accordingly, the reaction might be performed at mildly acidic *pH*, at which conditions the base is protonated, and the catalyst recovered by adjusting the *pH* to de-protonate the base. As with performing the reaction at $pH < pK_A$, which is a viable strategy for promoting catalyst-cellulose aggregation (Figure 8.3), the *pH* adjustment approach must use small enough quantities of acids and bases not to offset the benefits of catalyst recovery. Similarly, adjusting the temperature might provide a method for catalyst recovery. The theoretical analysis presents calculations performed at room temperature, and the effect of temperature is provided in the SI. As a further option, non-aqueous solvents or solvent mixtures might be considered. The SI provides guidance on the effects of non-aqueous solvents on particle-particle interactions.

A final consideration is non-DLVO effects, generally categorized as steric, hydration, hydrophobic and shear forces.[3] Of these, cellulose and catalyst particles will both be hydrophilic, meaning that hydrophobic forces can be neglected.[3] Steric forces do not contribute to cellulose-solid-acid interaction aggregation but instead is typically repulsive and can cause stabilization,[22] which is not desirable. Magnitudes of hydration forces are difficult to predict [23] but tend to be important only at length scales much less than the repulsive barrier shown for many situations in cellulose-catalyst interaction in Figure 8.2.

Shear force-induced aggregation is an industrially implementable consideration. The SI provides theoretical details for the analysis. [24] At high shear rate above a critical shear rate ($\dot{\gamma}^*$), the shear force has ability to counterbalance electrostatic force caused barrier and diminish repulsive barrier. As shown in Figure 8.7, for a solid-catalyst with varying surface potential,

critical shear rate ($\dot{\gamma}^*$) increases drastically as catalyst becomes more negatively charged, suggesting that significantly strong mechanical stirring is required for overcoming energy barrier. Even for mildly negatively charged catalyst with surface potential around -50 mV, as indicated in Figure8.7, $\dot{\gamma}^*$ can range from 32 s^{-1} to 126 s^{-1}, depending on the catalyst size. This range is much greater than typical literature reported maximum stirring rate that spans from 200 rpm (2.5 s^{-1}) to 800 rpm (9 s^{-1})[25-27] The dependence of $\dot{\gamma}^*$ and coagulation rate constant on particle size are also discussed in literature, suggesting that large particles (a few micrometres) requires lower $\dot{\gamma}^*$ for coagulation while small particles (a few nanometers) requires larger $\dot{\gamma}^*$ for coagulation.[24, 28] However, in practice, using large size of catalyst may increase DLVO energy barrier,[29] which still requires high $\dot{\gamma}^*$; large size of catalyst also possesses low specific area, reducing specific catalytic site density and effectiveness of the solid catalyst. Therefore, reducing solid-catalyst size and increasing shear rate are recommended for enhancing cellulose-solid acid particle interaction.

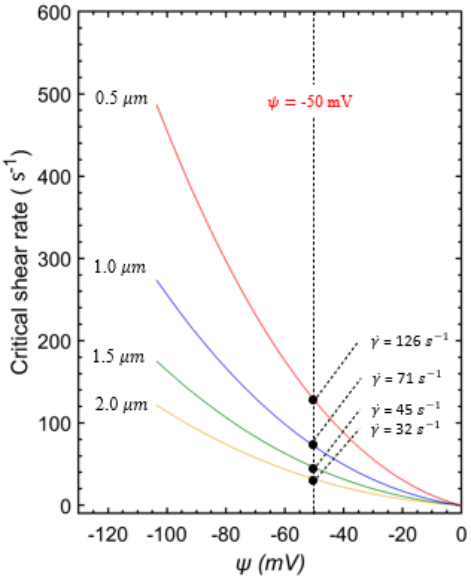

Figure 8. 7 Critical shear rate ($\dot{\gamma}^*$) as a function of catalyst surface potential, assuming catalyst Hamaker constant is 2×10^{-20} J; cellulose surface potential is -27 mV; cellulose diameter is 1 μm.

8.3 Conclusions

Solid-acids have potential to reduce the costs of producing simple sugars from cellulose-rich biomass. However, work in this field has been falsely guided by molecular-level explanations.[30-32] Colloidal-level considerations suggest point to new strategies for the design of cellulose-deconstruction solid-acid catalysts. The Hamaker constant must be maximized, particle size should be reduced as much as possible while permitting catalyst recovery, and repulsive forces originating from the electrical double layer must be minimized. Carbon-based or inorganic catalysts with bifunctional acid/base surface groups may be especially effective at meeting these requirements as carbon possesses a favorable Hamaker constant and base groups can neutralize the negative charge that acid groups confer to the catalyst surface. High shear rate is recommended for counterbalancing DLVO repulsive energy barriers and hence promote cellulose-solid acid catalyst coagulation.

8.4 Reference

1. Marx, D., *Proton transfer 200 years after von Grotthuss: Insights from ab initio simulations.* ChemPhysChem, 2006. **7**(9): p. 1848-1870.
2. Tadros, T., *Chapter 2 - Colloid and interface aspects of pharmaceutical science*, in *Colloid and Interface Science in Pharmaceutical Research and Development*, H. Ohshima and K. Makino, Editors. 2014, Elsevier: Amsterdam. p. 29-54.
3. Israelachvili, J.N., *Intermolecular and surface forces*. 2011: Academic press.
4. Prathapan, R., et al., *Modulating the zeta potential of cellulose nanocrystals using salts and surfactants.* Colloids and Surfaces A: Physicochemical and Engineering Aspects, 2016. **509**: p. 11-18.

5. Heister, E., et al., *Higher dispersion efficacy of functionalized carbon nanotubes in chemical and biological environments.* ACS nano, 2010. **4**(5): p. 2615-2626.
6. Chen, K., et al., *Removal of cadmium and lead ions from water by sulfonated magnetic nanoparticle adsorbents.* Journal of colloid and interface science, 2017. **494**: p. 307-316.
7. Hanaor, D., et al., *The effects of carboxylic acids on the aqueous dispersion and electrophoretic deposition of ZrO2.* Journal of the European Ceramic Society, 2012. **32**(1): p. 235-244.
8. Lu, Z., et al., *Monodisperse magnetizable silica composite particles from heteroaggregate of carboxylic polystyrene latex and Fe3O4 nanoparticles.* Nanotechnology, 2008. **19**(5): p. 055602.
9. Barbati, A.C. and B.J. Kirby, *Electrokinetic measurements of thin Nafion films.* Langmuir, 2014. **30**(8): p. 1985-1993.
10. Huang, Y.-B. and Y. Fu, *Hydrolysis of cellulose to glucose by solid acid catalysts.* Green Chemistry, 2013. **15**(5): p. 1095-1111.
11. Qiu, M., et al., *Efficient mechanochemical-assisted production of glucose from cellulose in aqueous solutions by carbonaceous solid acid catalysts.* ACS Sustainable Chemistry & Engineering, 2018. **6**(11): p. 13826-13833.
12. García-García, S., M. Jonsson, and S. Wold, *Temperature effect on the stability of bentonite colloids in water.* Journal of Colloid and Interface Science, 2006. **298**(2): p. 694-705.
13. Wang, D., et al., *A novel acid–base bifunctional catalyst (ZSM-5@ Mg 3 Si 4 O 9 (OH) 4) with core/shell hierarchical structure and superior activities in tandem reactions.* Chemical Communications, 2016. **52**(87): p. 12817-12820.

14. Wakchaure, V.N. and B. List, *A new structural motif for bifunctional Brønsted acid/base organocatalysis.* Angewandte Chemie International Edition, 2010. **49**(24): p. 4136-4139.

15. Robinson, A.M., J.E. Hensley, and J.W. Medlin, *Bifunctional catalysts for upgrading of biomass-derived oxygenates: a review.* ACS catalysis, 2016. **6**(8): p. 5026-5043.

16. Li, H., et al., *Efficient valorization of biomass to biofuels with bifunctional solid catalytic materials.* Progress in Energy and Combustion Science, 2016. **55**: p. 98-194.

17. Song, Y., et al., *Alkaline hydrolysis and flocculation properties of acrylamide-modified cellulose polyelectrolytes.* Carbohydrate polymers, 2011. **86**(1): p. 171-176.

18. Mei, Y., et al., *Catalytic activity of palladium nanoparticles encapsulated in spherical polyelectrolyte brushes and core− shell microgels.* Chemistry of Materials, 2007. **19**(5): p. 1062-1069.

19. Hubbe, M.A., *Flocculation and redispersion of cellulosic fiber suspensions: A review of effects of hydrodynamic shear and polyelectrolytes.* BioResources, 2007. **2**(2): p. 296-331.

20. Ishida, K., et al., *Hydrolysis of cellulose to produce glucose with solid acid catalysts in 1-butyl-3-methyl-imidazolium chloride ([bmIm][Cl]) with sequential water addition.* Biomass Conversion and Biorefinery, 2014. **4**(4): p. 323-331.

21. Li, J. and X. Liang, *Magnetic solid acid catalyst for biodiesel synthesis from waste oil.* Energy Conversion and Management, 2017. **141**: p. 126-132.

22. Zoppe, J.O., et al., *Surface interaction forces of cellulose nanocrystals grafted with thermoresponsive polymer brushes.* Biomacromolecules, 2011. **12**(7): p. 2788-2796.

23. Rehfeldt, F. and M. Tanaka, *Hydration forces in ultrathin films of cellulose.* Langmuir, 2003. **19**(5): p. 1467-1473.

24. Zaccone, A., et al., *Theory of activated-rate processes under shear with application to shear-induced aggregation of colloids.* Physical Review E, 2009. **80**(5): p. 051404.

25. Yamaguchi, D., et al., *Hydrolysis of cellulose by a solid acid catalyst under optimal reaction conditions.* The Journal of Physical Chemistry C, 2009. **113**(8): p. 3181-3188.

26. Tyufekchiev, M., et al., *Cellulase-inspired solid acids for cellulose hydrolysis: structural explanations for high catalytic activity.* Acs Catalysis, 2018. **8**(2): p. 1464-1468.

27. Liu, W.-J., et al., *Facile synthesis of highly efficient and recyclable magnetic solid acid from biomass waste.* Scientific reports, 2013. **3**(1): p. 1-7.

28. Mohammadi, M., et al., *Brownian dynamics simulations of coagulation of dilute uniform and anisotropic particles under shear flow spanning low to high peclet numbers.* The Journal of chemical physics, 2015. **142**(2): p. 024108.

29. He, Y.T., J. Wan, and T. Tokunaga, *Kinetic stability of hematite nanoparticles: the effect of particle sizes.* Journal of nanoparticle research, 2008. **10**(2): p. 321-332.

30. Onda, A., T. Ochi, and K. Yanagisawa, *Selective hydrolysis of cellulose into glucose over solid acid catalysts.* Green Chemistry, 2008. **10**(10): p. 1033-1037.

31. Shuai, L. and X. Pan, *Hydrolysis of cellulose by cellulase-mimetic solid catalyst.* Energy & Environmental Science, 2012. **5**(5): p. 6889-6894.

32. Yang, Q. and X. Pan, *Synthesis and application of bifunctional porous polymers bearing chloride and sulfonic acid as cellulase-mimetic solid acids for cellulose hydrolysis.* BioEnergy Research, 2016. **9**(2): p. 578-586.

Chapter 9

Polydiallyldimethylammonium chloride (PolyDDA) Enhanced Hydrolysis Reaction of Cellulose with Solid Acid

9.1 Abstract

Breaking down cellulose biopolymer into its monomers such as glucose is crucial for promoting sustainability. Liquid acid such as sulfuric acid has corrosive problems, restricting its economy feasibility. Enzymes are typically highly effective and selective, but enzymes are expensive, and the kinetics are slow. Functionalized solid-acid catalysts such as activated carbons bearing sulfonic acid, polystyrene bearing carboxylic acid are routinely reported resulting in as high as 90% glucose yield. However, two main issues exist: 1). Most solid acid leaches homogeneous liquid acid which is responsible for observed high glucose yield; 2). Solid acid and cellulose can repel each other in liquid medium due to electrostatic repulsion. To overcome electrostatic repulsion, we have tuned catalysts and cellulose surface charge by adding polyDDA, a polycations. Results show that introducing polyDDA into reaction significantly increases glucose yield by as much as 8-10%. To quantify and differentiate catalyzing contributions of homogeneous reaction (e.g. cellulose and liquid acid reaction) and heterogeneous reaction (e.g. cellulose and solid acid reaction), we prepared standard sulfuric acid at the same pH as hydrothermally treated Amberlyst-15-polyDDA resultant liquids, prepared sulfuric acid results in lower glucose yield compared to Amberlyst-15-polyDDA-cellulose reaction. Extra glucose yields may be due to other interactions such as cellulose-Amberlyst-15 interaction or leached species (other than liquid acid)-cellulose interaction. Further control tests and cellulose-catalysts coagulation test in the presence of polyDDA are recommended.

9.2 Introduction

Cellulose is the major component of biomass, accounting for around 40-60 wt% of all forms of biomass. This vast amount of cellulose market is projected to exceed $235 billion in next five years.[1] Producing valuable chemicals, including glucose, hydroxymethylfurfural from cellulose has bright future because its renewability and sustainability.[2-4] Depolymerization of cellulose into reduced sugars such as glucose and monosaccharide is important for biomass-based technology. However, cellulose consists of covalent bonds and hydrogen bonds, strengthening its stability.[5, 6] Cellulose is not soluble in most safe solvents such as water and ethanol,[7, 8] significantly reducing its reactivity during depolymerization reaction in liquid. Catalysts are needed to increase product yield. Mineral acid such as hydrochloride acid and sulfuric acid are corrosive and energy intensive in downstream separation; biologically decomposing cellulose using enzymes is not economically feasible because enzyme is expensive, and the production rate is slow.[9-11]

Solid acid catalysts, a class of organic/organic particles that possess unique binding and catalyzing sites, have attracted many interests in the past few years. Various materials have been used to develop solid catalysts, including zeolite, metal oxide, carbon materials and polymer-based.[12, 13] Functionalizing those particles with sulfonic acid or carboxylic acid groups have reportedly claimed resulting in near 90% glucose yield.[14, 15] However, as pointed out by Tyufekchiev,[16] observed high reactivity and glucose yield attributes to leached and degraded acid groups (e.g. HCl) from catalysts surfaces.

Another major problem with current solid acid catalyst design is that most of reported studies have not revealed cellulose-solid acid interaction in colloidal level. Instead, molecular interaction like dispersion, π-π interaction is claimed responsible for particles-particles adsorption

in liquid environment. Unarguably, colloidal theory is more applicable for rational solid acid design than intuitive molecular binding approach. As we previously show, cellulose and most solid acid catalysts are negatively charged, forming an electrical repulsion barrier that prevents particle-particle interaction. Indeed, reaction medium remains a colloidal suspension before and after reaction as observed in many studies.[17]

To enhance solid-acid-cellulose adsorption in liquid media, electrical repulsion barrier has to be overcome. Strategies that can improve colloidal aggregation is analyzed in our previous studies, including increase of ionic strength by adding salt solution, decrease pH to less than pKa or reduce particles size. Those method typically requires addition of other ions and protons, which will make interaction much complicated. Another widely used approach is use of coagulant.[18-20] Commonly used coagulant includes Aluminum sulfate (Alum), polyaluminium chloride (PAC) and ferric sulfate.[21-24] when selecting a coagulant for cellulose hydrolysis, it is important to choose one with thermal stability and high water solubility. This is because hydrolysis reaction is normally conducted at 140-200 ^{o}C.[25] Low solubility of coagulant may be ineffective for regulate particles surface charge sue to separated phases.

Polydiallyldimethylammonium chloride (polyDADMAC or polyDDA), an important industrial polycations employed for precipitate containment or food residue. Benefits of polyDDA includes low toxicity, high water solubility and dense charge.[26-30] Indeed, polyDDA can dissolve in aqueous solutions and disperse as polymer chains. Free chains can attach to anionic surfaces, neutralizing negative charge and promote aggregation.[31] PolyDDA can also tolerate temperature as high as 250 ^{o}C.[32] Despite its wide use in colloidal field where coagulant is utilized for aggregation enhancement, polyDDA has not been employed in solid-acid hydrolyzed cellulose degradation reaction.

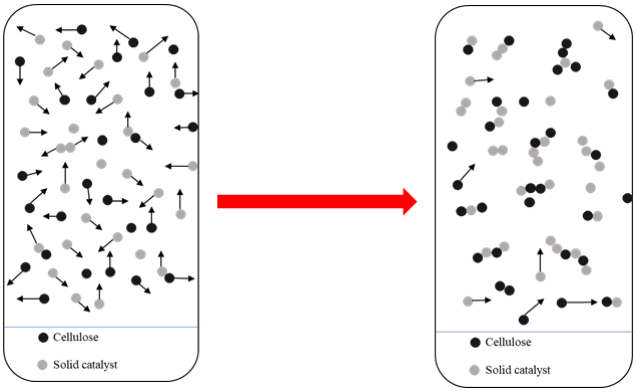

Figure 9. 1 Schematic of polyelectrolyte enhanced cellulose-solid acid coagulation.

In this chapter, we investigate polyDDA effect on cellulose hydrolysis reaction with solid acid particles. Specifically, we have selected four solid acid catalysts, Amberlyst-15, ZSM-22, ZSM-5 and vinyl sulfonic acid char. We first mixed cellulose with solid acid and polyDDA to examine which catalysts give the most noticeable glucose yield. We then selected best catalysts, to do a more detailed analysis. We first measured zeta potential of solid catalyst at fixed reaction pH. To eliminate homogeneous reaction contribution, we tested supernatant of solid catalysts and heterogeneous contribution is analyzed. Lastly, we recommended a method for evaluating solid acid catalysts.

9.3 Experimental

9.3.1 Materials

All chemicals are used as received, unless otherwise indicated. ZSM-22 was purchased from ACS advanced materials supplierADDRESS. Amberlyst-15, microcrystalline cellulose (>99%), polydiallyl-dimethylammonium chloride (PolyDDA) (MW 200,000-300,000) and nano-ZSM-5 were purchased from Sigma Aldrich. Acetone, sulfuric acid and ethanol are purchased from

different sources. Glucose, hydroxymethylfurfural and levulinic acid were purchased from Sigma Aldrich.YOU GAVE CITY AND STATE EARLIER

9.3.2 Ball-milling

Microcrystalline cellulose was ball-milled using a vibratory shaker Retsch MM2000 to decrystallize cellulose. 1 gram of raw microcrystalline cellulose was placed in two steel chambers (18 mm in. diameter and 55.5 in. length). Three stainless balls with different radii were mixed with cellulose. Ball-milling procedure lasted for 50 minutes at room temperature (22 ^{o}C).DID YOU CHARACTERISE THE PARTICLE SIZE AT THE END?

9.3.3 Zeta potential measurement

Zeta potential was measured for both cellulose and Amberlyst-15. Prior to the measurement, cellulose and Amberlyst-15 were ball-milled for 30 minutes to reduce the particle size TO WHAT so as to fit into the system size capacity. Then an array of cellulose-water-polyDDA and Amberlyst-15-water-polyDDA suspensions were prepared with increased polyDDA concentrations. ZetaSizer ZEN 3600 from Malvern Panalytical was used for measuring zeta potential and particle size distribution. Disposable folded capillary cells were used to prepare the samples. Specifically, methanol was first injected into the cells by syringe to pre-wet the cell chamber, followed by injecting the prepared particle suspension into the cell. Prior to measurement, the sample cell was degassed to remove air bubbles.

9.3.4 Cellulose Hydrolysis

1). Ball-milled microcrystalline cellulose was hydrolyzed into water-soluble products in the presence of both solid catalysts and polyDDA. To investigate effect of polyDDA dosage on cellulose-catalysts catalyzing performance, 0.2 g cellulose was mixed with 0.1 g of catalysts (ZSM-22, ZSM-5, Amberlyst-15 and vinyl sulfonic acid char) and 3 mL deionized water. Then

the mixtures were magnetically stirred at room temperature for 10 minutes in a 15 mL heavy-wall vial. Meanwhile, the coagulant solution was prepared by blending 0, 0.1 mL and 0.5 mL polyDDA solution (equivalent to 0, 0.02g and 0.1g) with 2 mL deionized water. Then 0.5 mL of the coagulant solution was added into cellulose-catalysts mixtures every 5 minutes.

2). The prepared suspensions were submerged into an oil bath that was preheated to 150 ^{o}C. The stirring speed was adjusted to 200 rpm. After the reaction reached the desired time, the resulting liquid mixture was transferred to a 50 mL centrifuge tube and was centrifuged at 2500 rpm for 20 minutes. After the centrifugation, 0.5 mL of the liquid supernatant was diluted to 10 times for later HPLC analysis. Other remaining liquids was transferred to vials and the pH was measured. For comparison, the previous experiment was repeated in the absence of polyDDA or catalysts to evaluate the catalytic performance of polyDDA and catalysts.

3). The homogeneous acid hydrolysis was conducted by preparing an array of different sulfuric acid aqueous solution that has the same concentration as solid-acid catalyzed mixtures.

4). To evaluate the effect on Amberlyst-15 leaching on cellulose hydrolysis, 0.1 g of Amberlyst-15 was mixed with 0, 0.25, 0.5, 0.75 and 0.9 mL of the polyDDA solution and 5 mL of water for each sample. The prepared liquid suspensions were sealed in a 15 mL heavy wall pressure tube and was treated at 150 ^{o}C for 1 hour. Then the resultant suspensions were centrifuged, and the top supernatant were transferred to glass vials. Then 0.25 mL of the liquids were mixed with 0.1 g cellulose and let it react at 150 ^{o}C for 1 hour. Afterwards, the suspension was centrifuged, and the liquids samples were analyzed using HPLC.

9.3.5 Product Quantification:

The liquid product composition was analyzed with High Performance Liquid Chromatography (HPLC, Agilent 1200 series) coupled with a Bio-Rad Aminex HPX-87H column. SOLVENT SYSTEM?The calibration curve was obtained by measuring the composition of known concentration of standards at 0.25, 0.5, 0.75, 1, 1.25, 2 and 2.25 g/L. The mobile phase was 5 mM sulfuric acid.

9.4 Results and Discussions

9.4.1 Effects of polyDDA on Glucose Yield

The first objective is to compare performance of selected solid acid catalysts and identify the most effective solid acid catalysts, in the presence of polyDDA. Figure 9.2 shows all solid acid catalysts can break down cellulose into glucose and glucose yield increases as time increases. The reaction rate is significantly different. Amberlyst-15 has the highest glucose yield at all tested times and its reaction rate is the highest. In contrast, ZSM-5 and vinyl sulfonic acid have the lowest glucose yield and its reaction rates are identical and small. ZSM-22 has the second largest glucose yield. Amberlyst-15 and ZSM-22 are the best catalysts BASED ON GLUCOSE YIELDS

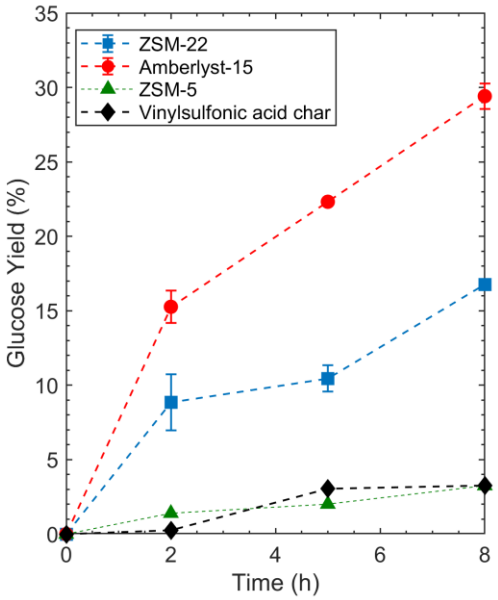

Figure 9. 2 Glucose yield as functions of time for different solid acid catalysts: ZSM-22, ZSM-5, Amberlyst-15 and vinyl sulfonic acid. Reaction conditions: 0.2g ball milled cellulose (50 minutes), 0.1 g catalyst, 0.1mL polyDDA, 150 ^{o}C.

We then decided to choose two best-performed catalysts, Amberlyst-15 and ZSM-22 to do a more detailed analysis. We first extract polyDDA effect by comparing cellulose-solid acid catalysts reaction with polyDDA to the situation where polyDDA is absent. Figure 9.3a and 9.3b show glucose yield difference for ZSM-22 and Amberlyst-15, respectively. Figure 9.3a shows adding polyDDA increases glucose yield from 2% to around 9% at 1 hour. Similarly, polyDDA boosts glucose yield from 9% to around 16% at 1 hour reaction. Not only polyDDA increases maximum glucose yield, it also speeds reaction rate, and it is particularly true for ZSM-22, in which polyDDA increases glucose production rate 4 folds.

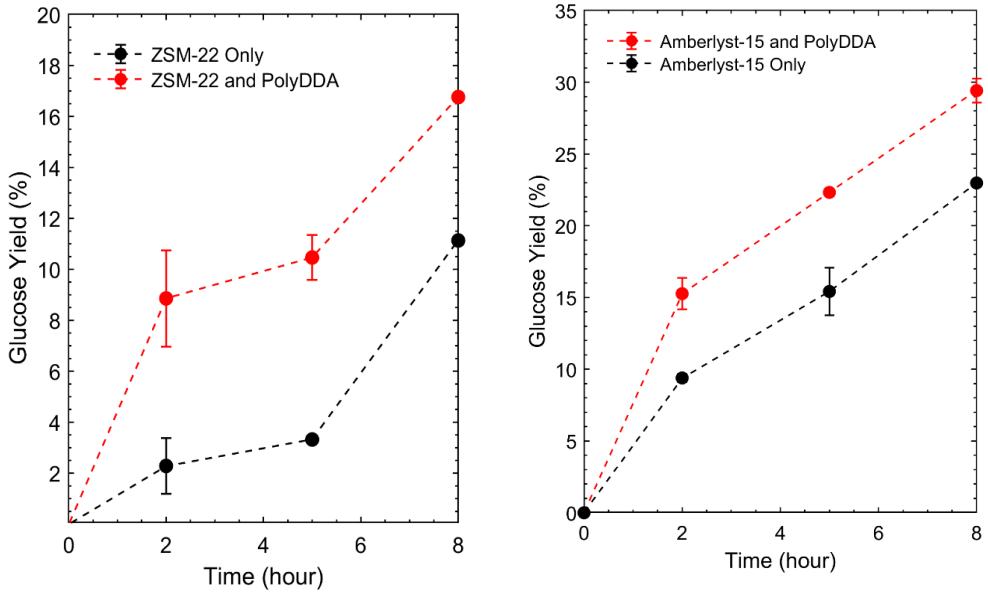

Figure 9. 3 Glucose yield as functions of time for celluloas reacting with Amberlyst-15 and ZSM-22. Reaction conditions: 0.2g ball-milled cellulose (50 minutes), 0.1g solid catalyst, 0.1mL polyDDA, 150 ^{o}C

9.4.2 Differentiating Homogeneous and Hetergeeneous Contributions

Despite an apparent improvement for glucose yeild is observed for both Amberlyst-15 and ZSM-22, this improvement may be a mixed effect resulting from complicated interaction between cellulose and solid catalysts, cellulose and liquid, and solid catalysts-polyDDA interaction. Of those potential undesired interactions, polyDDA-solid cataolysts interaction is worth particular attention. Because polyDDA is positively charge polymer chains, those chains tend to find negative counterions to balance its positive charge. Solid catalyst, Amberlyst-15 and ZSM-22 may have negative charge sites, attracting polymer chains and relases protons. Therefore, we decided to measure pH after reaction. Figure 9.4 shows measured pH after reaction for all selected catalysts.

Overall, Amberlyst-15 has the lowest pH while ZSM-5 has the highest pH, sugggesting polyDDA performs ions exchange with Amberlyst-15 the most and ZSM-5 is the most stable

catalyst. It is interesting to see that vinyl sulfonic acid and ZSM-5 has relartively similar glucose yield but vinyl sulfonic acid is more acidic than ZSM-5 liquid, suggetsing that pH is not the only factors affecting glucose yield. Possible cellulose-solid acid interaction may also contribute to glucosE yield. Overall, figure 9.4 indicates an exponential trend relating glucose yield with measured pH: as pH decreases, glucose yield increases significantly between 1.5-2.5. When pH is larger than 3, glucose yeild stays relatively CONSTANT and independent on pH.

Figure 9.4 can qualitively show stability of solid catalysts by observing horizontal pH variance. For example, Amberlyst-15 spans pH from 1.5 to 2, suggesting proton coentrations changes from around 0.01 M to 0.03 M. ZSM-22 is more stable than Amberlyst-15 because its pH ranges from 0.001 to 0.01 M. ZSM-5 and vinyl sulfonic acid are most stable catalysts with proton concentration stays around 0.001 M.[33-36]

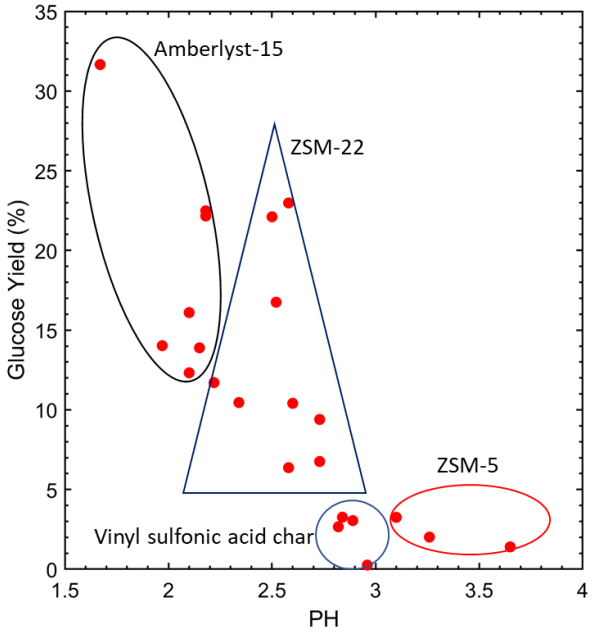

Figure 9. 4 Measured glucose yield as function of pH after reaction for all tested solid acid catalysts: Amberlyst-15, ZSM-22, ZSM-5 and vinyl sulfonic acid. Circles represent catalysts categories. Data points include 2, 5 and 8 hours reaction.

Figure 9.4 shows homogeneous acid clearly contributes to glucose yield. The main source of homogeneous acid is solid catalysts surfaces. Question now becomes how much homogeneous acid contributes to overall yield and how much contributions come from particle-particle interaction? As figure 9.5 shows, polycations may have two pathways that can later on affect glucose production. The first pathway involves an ions exchange reaction between polyDDA and solid catalysts and relases protons. Those protons are highlyb reatcive, contributing to part of glucose yield. The second pathway, however, involves complicated mechanism. First of all, polyDDA chains may bridge cellulose with solid catalysts and enhance their interaction. Observing brridging effect is challenging as reaction is not observable. Another possible explaination is that

polyDDA can form patches on partcicles, those patches significantly decreases surface potential, reducing electrostatic repulsion and promoting adsorption.

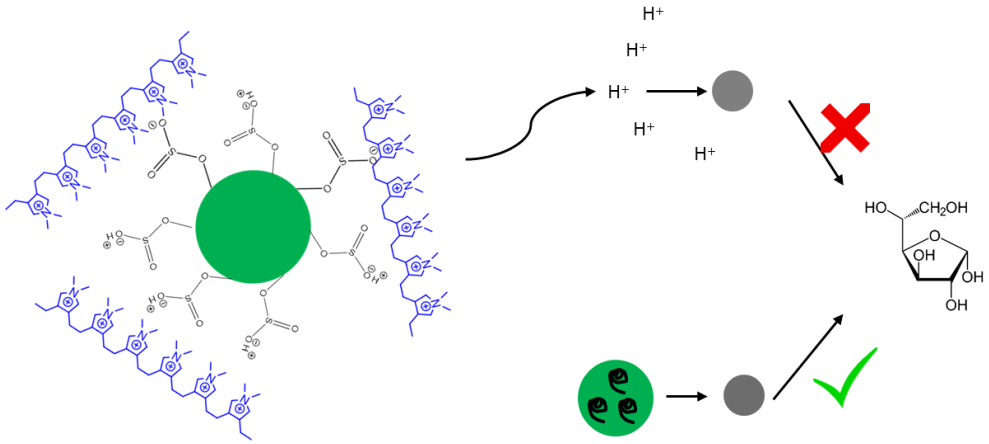

Figure 9. 5 Schematic showing tow possible explination for improved glucose yield promoted by polyDDA. Green circle represents solid-acid catalysts and gray circle represents cellulose. First pathway is proton attacking cellulose and second pathway is cellulose-solid-acid interaction. The red cross is undesired pathway while green check is desired pathway.

In either events, e.g. ions exchange or patches, solid catalysts will leach homogeneous acid into reaction medium. Those homogeneous remains in liquid and catalyze cellulose. To elucidate homogeneous acid conntribution, we tested supernatant's activity. In details, we first hydrothermally treated Amberlyst-15 in the presence of polyDDA, mimicing cellulose hydrolysis reaction without adding cellulose. After treatment, top clear liquid is separated from liquid particles. pH of recycled liquid is measured and a standard sulfuric acid with the same pH is prepared to hydrolyzing cellulose.

From Figure 9.6, Amberlyst-15 has the lowest glucose yield (9%) while polyDDA-promoted run has the highest glucose yield (15%). Interestingly, sulfuric acid-only has intermediate glucose yield at around 11%. Comparing sulfuric acid's glucose yield with Amberlyst-15's glucoe yield, it seems that ion exchange effect only contributes to roughly 1-2% glucose yield. Hwever, when comparing sulfuric acid's glucose yeild to Amberlyst-15 and polyDDA mixtures' glucose yield, around 4% glucos yield increases once introducing polyDDA. Therefore, ion exchange or acid leaching effect is significantly smaller compared to solid-solid interaction's contribution.

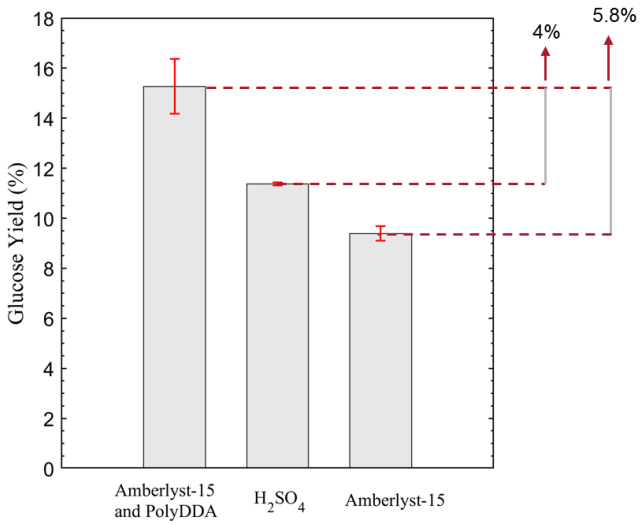

Figure 9. 6 Glucose yield for three conditions: Cellulose and Amberlyst-15, cellulose, Amberlyst-15 and polyDDA, cellulose and sulfuric acid (sulfuric acid has the same pH as supernatant). Reaction conditions: 1 hour at 150 ^{o}C.

To further emilnate other factors that might contribute to observed high glucose yield, we systematically varied polyDDA dosages and evalute its effect on glucose yield. First, we mixed ball-milled cellulose with varied wt% of polyDDA, including 1%, 2%, 3% and 4%. Figure 9.7

shows that glucose yield of cellulose-polyDDA is very low and less than 2%, suggesting that polyDDA itself can not degrade cellulose. We then hydrothermally treated Amberlyst-15 with varied amount od polyDDA for one hour. After treatment, supernatant is extracted and pH is measured. We then prepare a standard sulfuric acid solution based on measured pH, and use those prepared sulfuric acid to hydrolyze cellulose. As polyDDA concentration increases, pH of supernatants decreases as well, in the sequence of 2.04, 1.85, 1.71 and 1.51. Figure 9.7 shows that sulfuric acid hydrolyzed cellulose has significantly low glucose yeild compared to cellulose-Amberlyst-15-polyDDA mixtures, indicating leached sulfuric acid is not the only reason for high glucose yield. For example, when polyDDA mass fraction is 3%, glucose yield difference is as large as 8%. This extra 8% glucose yield can noy be explained by leached species, including leached sulfuric acid. more detailed control tests are recommended to understand or differentiate homogeneous and hetergeneous contributions.

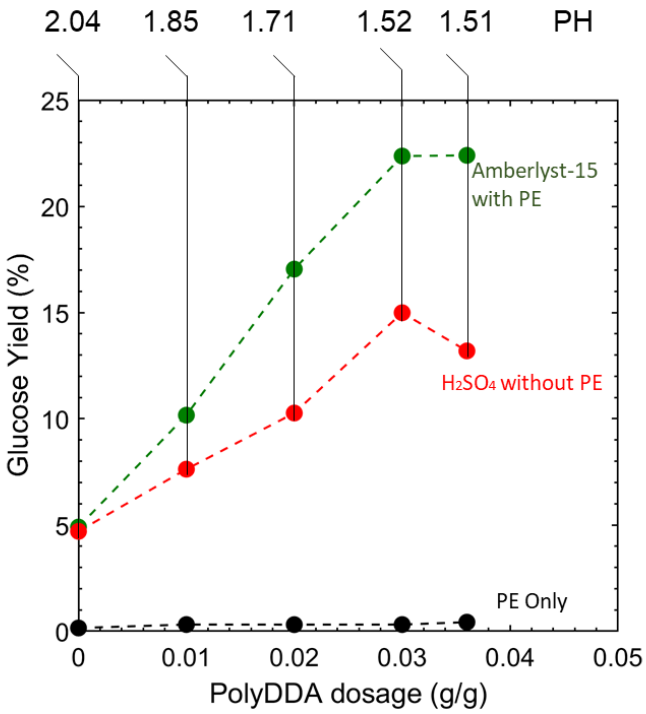

Figure 9. 7 Ball-milled cellulose reacting with Amberlyst-15 and PolyDDA. PolyDDA concentration is varied as 1 wt%, 2wt%, 3 wt% and 4 wt%. Black line represents cellulose interacting with polyDDA, green data points repreesents cellulose reacting with Amberlyst-15 in the presence of polyDDA, and red data points represents cellulose reacting

9.5 Conclusion

In the study, we present a polyDDA promoted cellulose hydrolysis reaction with solid acid catalysts. we have tested four different solid acid catalysts, including ZSM-22, ZSM-5, Amberlyst-15 and vinyl sulfonic acid. Among those catalysts, ZSM-5 and vinyl sulfonic acid have the lowest glucose yield while ZSM-22 and Amberlyst-15 have the highest glucose yield. Further pH measurements confirm that high reactivity of ZSM-22 and Amberlyst-15 is due to its low pH and high protons concentrations released by polyDDA-catalyst ions exchange effect. To further differentiate homogeneous and heterogeneous effect on glucose yield, we hydrothermally treated

Amberlyst-15 with polyDDA, and supernatants' *pH* is measured. A standard sulfuric acid solution based on measured pH is prepared and is used to decomposing cellulose. Surprisingly, prepared sulfuric acid has much lower glucose yield than cellulose-polyDDA-Amberlyst-15 combination. The extra glucose yield is believed coming from cellulose-Amberlyst-15 interaction.

9.6 References

1. Wüstenberg, T., *Cellulose and cellulose derivatives in the food industry: fundamentals and applications*. 2014: John Wiley & Sons.
2. Mascal, M. and E.B. Nikitin, *Direct, High-yield conversion of cellulose into biofuel.* Angewandte Chemie, 2008. **120**(41): p. 8042-8044.
3. Sorokina, K.N., et al., *Cellulose biorefinery based on a combined catalytic and biotechnological approach for production of 5-HMF and ethanol.* ChemSusChem, 2017. **10**(3): p. 562-574.
4. Kuo, I.-J., et al., *Cellulose-to-HMF conversion using crystalline mesoporous titania and zirconia nanocatalysts in ionic liquid systems.* Rsc Advances, 2013. **3**(6): p. 2028-2034.
5. Heng, J., et al., *Cellobiose as a Model Carbohydrate for Predicting Solubilities in Nonaqueous Solvents.* Industrial & Engineering Chemistry Research, 2021. **60**(4): p. 1859-1871.
6. Pinkert, A., K.N. Marsh, and S. Pang, *Reflections on the solubility of cellulose.* Industrial & Engineering Chemistry Research, 2010. **49**(22): p. 11121-11130.
7. Archer, W.L., *Determination of Hansen solubility parameters for selected cellulose ether derivatives.* Industrial & engineering chemistry research, 1991. **30**(10): p. 2292-2298.

8. Hudson, S.M. and J.A. Cuculo, *The solubility of unmodified cellulose: A critique of the literature.* Journal of Macromolecular Science—Reviews in Macromolecular Chemistry, 1980. **18**(1): p. 1-82.

9. Kobayashi, H., et al., *High-yielding one-pot synthesis of glucose from cellulose using simple activated carbons and trace hydrochloric acid.* Acs Catalysis, 2013. **3**(4): p. 581-587.

10. Mansfield, S.D., C. Mooney, and J.N. Saddler, *Substrate and enzyme characteristics that limit cellulose hydrolysis.* Biotechnology progress, 1999. **15**(5): p. 804-816.

11. Philippidis, G.P., T.K. Smith, and C.E. Wyman, *Study of the enzymatic hydrolysis of cellulose for production of fuel ethanol by the simultaneous saccharification and fermentation process.* Biotechnology and bioengineering, 1993. **41**(9): p. 846-853.

12. Onda, A., T. Ochi, and K. Yanagisawa, *Selective hydrolysis of cellulose into glucose over solid acid catalysts.* Green Chemistry, 2008. **10**(10): p. 1033-1037.

13. Zuo, Y., Y. Zhang, and Y. Fu, *Catalytic conversion of cellulose into levulinic acid by a sulfonated chloromethyl polystyrene solid acid catalyst.* ChemCatChem, 2014. **6**(3): p. 753-757.

14. Shuai, L. and X. Pan, *Hydrolysis of cellulose by cellulase-mimetic solid catalyst.* Energy & Environmental Science, 2012. **5**(5): p. 6889-6894.

15. Zeng, M. and X. Pan, *Insights into solid acid catalysts for efficient cellulose hydrolysis to glucose: progress, challenges, and future opportunities.* Catalysis Reviews, 2020: p. 1-46.

16. Tyufekchiev, M., et al., *Reaction engineering implications of cellulose crystallinity and water-promoted recrystallization.* Green Chemistry, 2019. **21**(20): p. 5541-5555.

17. Dong, X.M., J.-F. Revol, and D.G. Gray, *Effect of microcrystallite preparation conditions on the formation of colloid crystals of cellulose.* Cellulose, 1998. **5**(1): p. 19-32.

18. Miller, S.M., et al., *Toward understanding the efficacy and mechanism of Opuntia spp. as a natural coagulant for potential application in water treatment.* Environmental science & technology, 2008. **42**(12): p. 4274-4279.

19. Jarvis, P., B. Jefferson, and S.A. Parsons, *How the natural organic matter to coagulant ratio impacts on floc structural properties.* Environmental science & technology, 2005. **39**(22): p. 8919-8924.

20. Toivonen, M.S., et al., *Interfacial polyelectrolyte complex spinning of cellulose nanofibrils for advanced bicomponent fibers.* Biomacromolecules, 2017. **18**(4): p. 1293-1301.

21. Tetteh, E.K. and S. Rathilal, *Application of organic coagulants in water and wastewater treatment.* Org. Polym, 2019.

22. Antov, M.G., M.B. Šćiban, and N.J. Petrović, *Proteins from common bean (Phaseolus vulgaris) seed as a natural coagulant for potential application in water turbidity removal.* Bioresource technology, 2010. **101**(7): p. 2167-2172.

23. Zouboulis, A. and N. Tzoupanos, *Alternative cost-effective preparation method of polyaluminium chloride (PAC) coagulant agent: Characterization and comparative application for water/wastewater treatment.* Desalination, 2010. **250**(1): p. 339-344.

24. Dorea, C., *Coagulant-based emergency water treatment.* Desalination, 2009. **248**(1-3): p. 83-90.

25. Guo, H., et al., *Cellulose-derived superparamagnetic carbonaceous solid acid catalyst for cellulose hydrolysis in an ionic liquid or aqueous reaction system.* Green Chemistry, 2013. **15**(8): p. 2167-2174.

26. Yang, M., et al., *Polycation-induced benzoperylene probe excimer formation and the ratiometric detection of heparin and heparinase.* Biosensors and Bioelectronics, 2016. **75**: p. 404-410.

27. Wang, S., et al., *Colorimetric determination of carbendazim based on the specific recognition of aptamer and the poly-diallyldimethylammonium chloride aggregation of gold nanoparticles.* Spectrochimica Acta Part A: Molecular and Biomolecular Spectroscopy, 2020. **228**: p. 117809.

28. Trisaranakul, W., et al., *A simple and rapid method based on anti-aggregation of silver nanoparticles for detection of poly (diallyldimethylammonium chloride) in tap water.* Analytical Sciences, 2016. **32**(7): p. 769-773.

29. Noskov, B., et al., *Dynamic surface properties of polyelectrolyte/surfactant adsorption films at the air/water interface: Poly (diallyldimethylammonium chloride) and sodium dodecylsulfate.* Langmuir, 2007. **23**(19): p. 9641-9651.

30. McLean, D., et al., *Synthesis of guar gum-graft-poly (acrylamide-co-diallyldimethylammonium chloride) and its application in the pulp and paper industry.* BioResources, 2011. **6**(4): p. 4168-4180.

31. Samanta, R. and V. Ganesan, *Influence of protein charge patches on the structure of protein–polyelectrolyte complexes.* Soft Matter, 2018. **14**(46): p. 9475-9488.

32. Jia, X., et al., *Thermal stability of poly (diallyldimethylammonium chloride) with different molecular weight.* Journal of Macromolecular Science, Part A, 2020. **57**(1): p. 83-90.

33. Hoff, T.C., et al., *Thermal stability of aluminum-rich ZSM-5 zeolites and consequences on aromatization reactions.* The Journal of Physical Chemistry C, 2016. **120**(36): p. 20103-20113.

34. Kunin, R., et al., *Characterization of amberlyst 15. macroreticular sulfonic acid cation exchange resin.* Industrial & Engineering Chemistry Product Research and Development, 1962. **1**(2): p. 140-144.

35. Jamil, A.K., et al., *Hydrothermally stable acid-modified ZSM-22 zeolite for selective propylene production via steam-assisted catalytic cracking of n-hexane.* Microporous and Mesoporous Materials, 2018. **260**: p. 30-39.

36. Yuan, L., et al., *Effect of char sulfonic acid and ammonium polyphosphate on flame retardancy and thermal properties of epoxy resin and polyamide composites.* Journal of Fire Sciences, 2017. **35**(6): p. 521-534

Chapter 10

Salt-Promoted Cellulose Hydrolysis: A Hofmeister Series Study

10.1 Abstract

Depolymerizing cellulose into reduced sugars is an important step for promoting lignocellulosic based renewable energy economy. Hydrolysis reaction of cellulose in the presence of diluted homogeneous acid catalyst such as hydrochloride acid (*HCl*) remains the most economically feasible technology. Cellulose is typically mechanically pretreated to remove crystallites prior acid hydrolysis. However, cellulose recrystallization in hydrothermal condition prevents continuous breakdown of cellulose into glucose. Here, we examined inorganic and organic salts effect on cellulose crystallization during hydrolysis reaction. Cellulose is hydrothermally reacted with HCl in assists of a series of salts based on Hofmeister series. X-Ray diffraction and Raman show that some salts such as guanidinium chloride can reduce crystallites size; ssNMR indicates formation of cellulose II is suppressed, possibly due to salts-chains interaction. Subsequent hydrolysis reactions show salting-in salt yields higher glucose while salting-out salts result in lower glucose yield. Molecular dynamic simulation was performed in Gromacs and it shows guanidinium chloride relaxes glycosidic bonds while ammonium chloride remains cellulose structures. Interaction of salts-cellulose may have implications for the community to select proper salts that promotes high glucose yield.

10.2 Introduction

Cellulose is the most abundant biopolymers produced by photosynthesis reaction. The annual production is estimated around 75 to 100 billion tonnes.[1] Decomposing this vast amount of cellulose into reduced sugars has attracted intense interests in the past few decades. Various technologies have been designed and developed to degrade lignocellulose into monosaccharides.

Those technologies specifically incorporate enzymes or solid acid catalysts.[2-4] However, enzymes are expensive, making the technologies not economically feasible. Instead, diluted acid hydrolysis remains dominant approach for hydrolyzing cellulose.[5] The benefits of using diluted acid as catalysts include cost effectiveness, low recovery cost and environmentally feasible.

Before hydrolyzing cellulose, mechanically pretreatment is necessary because it will partially convert crystalline cellulose into amorphous phase, and amorphous cellulose is known more reactive than crystalline cellulose. This process is typically conducted in a vibrational shaker. [6-8] Despite that mechanical pretreatment such as ball-milling removes three-dimensional lattice structures, recrystallization of amorphous cellulose into crystalline structure is observed for decades upon wetting in hydrothermal conditions.[9-11] The newly formed crystalline structure, cellulose II, prevents successive breakdown and reduces glucose yield.

Mechanism of water-induced cellulose recrystallization attributes to hydrophobic effect of non-polar part of cellulose. To suppress cellulose recrystallization and improve subsequent glucose yield, solvents with reduced hydrophobic effect is tested in literatures.[10] For example, X-ray diffraction shows amorphous cellulose treated in ethanol retains its amorphous structures and hence significantly increases product yield. γ-Valerolactone is also observed suppressed cellulose recrystallization.[12] However, reaction between cellulose and organic solvent-i.e., ethanol, may produce undesired or low value chemicals, e.g. ethyl-glucopyranoside. Therefore, water seems still the optimum choice due to its high selectivity as over 90% products are glucose.

To use water as reacting media, reducing its hydrophobic effect is the logical step. Various approaches have been studied to reduce water hydrophobicity.[13] Of those, electrification, raising temperature or introducing inorganic/organic salts are the most widely used approaches. Indeed, inorganic salt have been widely used for promoting cellulose hydrolysis.[15-18] In selecting salt

for cellulose hydrolysis, many factors can be considered, but the role of salt in preventing cellulose re-crystallization remains unknown and unexplored in most literatures. Furthermore, molecular level of understanding is unknown in terms how the salt decomposing cellulose.

Hofmeister series has been an empirical series that provides qualitive guide for selecting salt for protein denaturation.[19-22] The original idea of Hofmeister series is to classified anions or cations based on their ability to dissolve proteins. Some salts, termed "salting out", reduces proteins solubility and precipitates proteins. Conversely, "salting-in" salt, which can enhance protein solubility, are widely used for improved protein dissolution. Not surprisingly, proteins and cellulose have similarities, e.g., both of them are amphiphile, containing both hydrophobic and hydrophilic groups. Applying Hofmeister series criteria to select salts for decomposing cellulose is reasonable. Despite that inorganic salts such as sodium chloride, salts effect on cellulose crystallinity has not been studied in literature.[23]

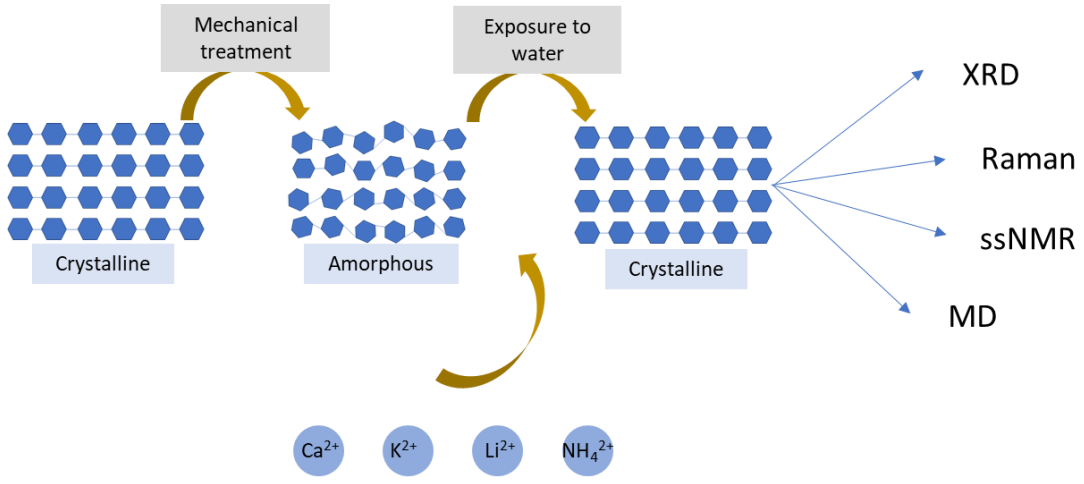

Figure 10. 1 Schematics of approach for studying salts effect on cellulose recrystallization and hydrolysis reaction.

In this study, we investigate salts effect on cellulose recrystallization and how it influences glucose yield in the presence of diluted hydrochloride acids. Specifically, we selected a series of

inorganic salts, including NH_4Cl, $CaCl_2$, KCl, LiCl, C $(NH_2)_3$ Cl, based on published Hofmeister series. Then we treated ball-milled cellulose with those inorganic salts with the same ionic strength. Crystalinity of salt-treated cellulose was thoroughly characterized by X-ray diffraction, Roman and solid-state NMR for structure evaluation. To elucidate the molecular level of interaction and structure changes of cellulose chain in inorganic salt solutions, molecular dynamics simulation was conducted in Gromacs and radical distribution for water-cellulose and salt-cellulose interaction were studied. Lately, after cellulose structure characterization, we hydrolyzed cellulose in the presence of selected inorganic salt and hydrochloride acid. A new Hofmeister series based on selected salts' ability to suppress recrystallization and their ability for hydrolyzing cellulose is constructed for rational salts selection.

10.3 Experimental

10.3.1 Materials and Chemicals

Microcrystalline cellulose, Avicel PH-101 and hydrochloride acid solution (0.1N) were purchased from Sigma Aldrich. Guanidinium chloride was obtained from Sigma Aldrich. Calcium chloride was purchased from Sigma Aldrich. Lithium chloride was obtained from company y. Potassium chloride and ammonium chloride were obtained from Sigma Aldrich. Zinc chloride was purchased from Merk KGaA. Lithium chloride was obtained from Millipore Sigma. Sodium hydroxide, sodium chloride, sodium bicarbonate and sodium phosphate were obtained from Sigma Aldrich. Glucose, formic acid and levulinic acid were purchased from company Sigma Aldrich for HPLC calibration preparation. All chemicals are used as received.

10.3.2 Ball-Milling Pretreatment

Microcrystalline cellulose (MCC) was ball-milled for different durations to generate a series of samples with varying degrees of crystallinity. Briefly, 1.0 gram of MCC was placed in a stainless-

steel cylinder (18 mm diameter×55.5 mm length, 10 mL). Three stainless steel balls 6 (2×9.5 mm diameter and 1×15.85 mm diameter) were placed in the cylinder. The cylinder was clamped within the holder of a vibratory shaker Retsch MM2000 and samples were ball milled for 10, 20, 30, 40, and 50 minutes.

10.3.3 Cellulose Hydrolysis

Cellulose was hydrolyzed with different aqueous salt solutions. Specifically, cellulose was first ball-milled for 50 minutes to remove crystallinity. Then 0.1 g of ball-milled cellulose was mixed with 2 mL aqueous salt solution which consists of 0.05 M HCl and 0.5M salt (NH_4Cl, $CaCl_2$, KCl, LiCl, C $(NH_2)_3$ Cl). The reaction was carried out in a 15 mL heavy wall pressure glass tube (ChemGlass) sealed by a screw cap with a Viton O-ring seal. The stirring bar was set as 200 rpm and reaction temperature was set as 150^oC heated in an oil bath. The reaction time was set as 0.5h, 1h, 2h, 3h and 4h. After the desired reaction time, the pressure tube was removed from oil bath and cooled down in ice bath. After the cooling, resultant liquid suspension was transferred to 50 mL centrifuge glass tube. Further liquid-solid separation was conducted in a centrifuge for 20 minutes at 2500 rpm. After centrifuge, top clear liquid was transferred to glass vials for further HPLC analysis. The residue solid was washed by acetone twice and dried at 65 ^oC overnight.

Several control tests were conducted to analyze the inorganic salt effects. Cellulose hydrolysis with 0.05 M hydrochloride acid was conducted in similar fashion except removing the salt; the effect of salts on cellulose hydrolysis was carried out by mixing 0.1 g cellulose with 0.5 M guanidinium chloride and reacting for 4 hours under 150 ^oC; avicel-101 was used as crystalline cellulose, and it was reacted with 0.05 M hydrochloride acid and 0.5M guanidinium chloride for 4 hours at 150 ^oC. All other analysis remained the same as inorganic salt-hydrochloride acid-cellulose reaction.

10.3.4 HPLC Analysis

Liquid products were analyzed High Performance Liquid Chromatography (HPLC, Shimadzu LC-40 model). A diode array detector (DAD) was used for organic acids and furanic compounds and a refractive index detector (RID) for carbohydrate detection. Bio-Rad Aminex HPX-87H (Phenomenex) was used for product separation. The mobile phase was 5 mM sulfuric acid. The mobile phase flow rate was 0.6 mL/min and analyzing temperature was 35 ^{o}C and UV-vis detection wavelength was set to 284 nm. A series of standard glucose solutions was prepared for obtaining calibration curve, which are 0.25, 0.5, 1, 2 and 5 g/L.

10.3.5 X-Ray Diffraction (XRD)

X-Ray diffraction (XRD) analysis was carried out with Rigaku Geigerflex diffractometer using CuKα radiation at 37.5 kV and 25 mA. A step size of 0.05° was used with 1 second accumulation time. Diffractograms of different samples were compared after area normalization and baseline subtraction. Crystallinity index was calculated by the widely used method first developed by Segal. In this method, the crystalline contribution is determined by the intensity of the 002 peak at 22.5° and the amorphous by the intensity at 18.3°.

10.3.6 Raman Microscopy

Raman spectral analysis of cellulose samples was carried out with a Horiba Xplora Raman Microscope using 785 nm excitation laser and 10× Olympus magnification lens. The acquisition range was set from 300 cm^{-1} to 1600 cm^{-1}.

10.3.7 Solid State Nuclear Magnetic Resonance (ssNMR)

NMR experiments were performed using a Bruker DSX400 spectrometer operating at a 13C resonance frequency of 100 MHz, using a 4-mm magic-angle spinning probe in double-resonance mode at a spinning frequency of 9 kHz and at room temperature. The 13C chemical shifts were

externally referenced on the neat TMS scale using the carboxyl peak of α-glycine at 176.49 ppm. Typical 90° pulse lengths were 3.6 μs for 1H and 4 μs for 13C. MultiCP64 with composite-pulse excitation and storage65 was used to obtain nearly quantitative 13C spectra. Five blocks of CP were implemented with 90–100% amplitude ramps on the 1H channel. The contact time for each CP period was 1.1 ms, resulting in a total combined CP contact time of 5.5 ms. The delays for 1H9 repolarization were 4 s for all samples, while the recycle delay was 8 s. A rotation-synchronized Hahn spin echo66 was used to achieve dead-time-free detection, generated by a 180° pulse with EXORCYCLE67 phase cycling after the last multiCP block. During the 18.7-ms detection, proton decoupling with the SPINAL64 scheme68 was applied, at a 1H strength of $\nu 1 \approx 85$ kHz. The number of scans averaged was 512 for MCC, 1280 for MCC-BM50, 768 for MCC-BM50-SP, and 832 for MCC-BM50-AC (see nomenclature defined below in 2.11).

A 5-s T1C filter69 was used to remove signals from segments with short 13C spin-lattice relaxation times T1C due to fast segmental motions, such as non-crystalline cellulose C6 side groups, retaining the sharp crystalline-C6 peaks of cellulose I and II, which are well resolved. The same numbers of scans as for the multiCP spectra were averaged. Direct polarization with 2-s recycle delay was used to select signals of mobile segments with fast T1C relaxation, yielding the band of non-crystalline cellulose C6 complementary to the T1C-filtered crystalline peaks. For all four samples 4096 scans were averaged. Zirconia rotors (Bruker Biospin) were used as received for magic-angle spinning of all samples.

10.3.8 Molecular Dynamics (MD) Simulations

All atoms-molecular dynamics simulation (MD) was conducted using GROMACS (version-5.0). The initial cellulose chain structure is a 8-glucose-chain 1-β cellulose fibril and 4 cellulose fibril chains was randomly solvated in the simulation box pre-defined as 6 nm cubic box. Packmol was

used to assemble the solute molecules that consists of the 1M guanidine hydrochloride or ammonium chloride and 4 cellulose fibril chains. The cutoff radius of nonbonded interactions was set to 1.2 A and the particle mesh Ewald (PME) summation method was used to calculate the electrostatic potential with periodic boundary conditions. Charmm36 force field is used to extract parameters.[24, 25]

The simulation was performed in the following steps: 1). Packmol package was used to prepare solvent box that consists of 1 M salt (guanidine hydrochloride or ammonium chloride). 2). The solvent box was solvated by TIP3P water molecules. Then four cellulose fibril chains were inserted into the box randomly. 3). The system was equilibrated to minimize the energy. 4). The system was equilibrated under NVT ensemble for 200 ps.[26-28]

$$V = \sum_{\text{bonds}} k_r\left(r - r_{eq}\right)^2 + \sum_{\text{angles}} k_\theta\left(\theta - \theta_{eq}\right)^2 + \sum_{\text{dihedrals}} \frac{V_n}{2}[1 + \cos(n\phi - \gamma)] + \sum_{\text{impropers}} K^x\left(x - x_{eq}\right)^2 + \sum_{i<j} \frac{q_i q_j}{4\pi\varepsilon_o R_{ij}} + \sum_{\text{bonds}} 4\varepsilon_{ij}\left[\left(\frac{\sigma_{ij}}{R_{ij}}\right)^{12} - \left(\frac{\sigma_{ij}}{R_{ij}}\right)^{6}\right]$$

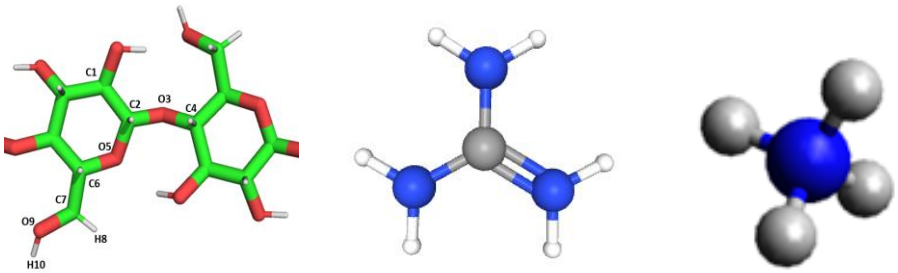

Figure 10. 2 Structures of cellulose chains and guanidinium chloride and ammonium chloride (Left to Right).

10.4 Results and Discussions

Cellulose hydrolysis or pretreatment in the presence of inorganic salts are studied over years.[15, 29-32]. However, their studies on salt selection are either not well-rationalized or salts effect on cellulose structure change is not well-characterized.[33-35] The discussion section is divided into three sections. The first section is to characterize hydrothermally treated amorphous cellulose using three different characterization techniques, including X-ray diffraction, Raman and Solid-state NMR. Characterization will provide information on salts performance on crystallization suppression. The second part of discussion is to test salts' performance in hydrolyzing cellulose. Lastly, based on salts' performance on glucose yield, we selected two representative salts, including the best-performed and worst-performed salts, and gain molecular information how these two representative salts interacting with cellulose. To summarize the study, a new Hofmeister series is constructed for future salt selecting.

10.4.1 X-Ray Diffraction and Raman Analysis of Amorphous Cellulose Treated in Salts Solutions

To investigate how salt cations affect the cellulose structures along the reaction, we first ball-milled cellulose for 50 minutes to remove crystalline structures at the interfaces. Then we

hydrothermally treated the cellulose with inorganic salt solutions at 150 ^{o}C for 2 hours. Then treated cellulose was removed and washed with acetone for x-ray analysis.

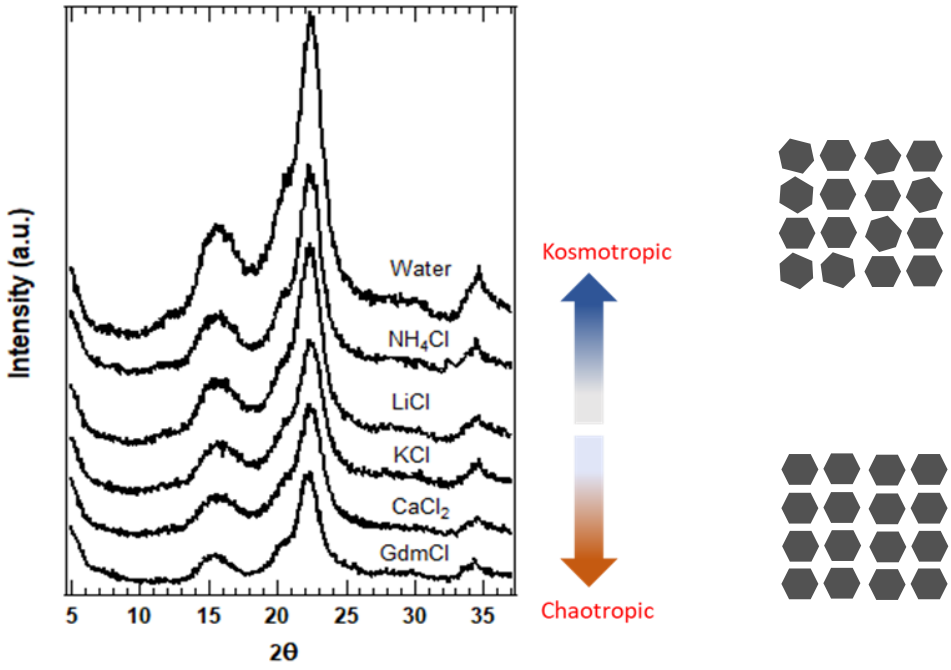

Figure 10. 3 X-ray diffraction showing effect of cations on cellulose re-crystallization in hydrothermal conditions. The raw cellulose was ball-milled for 50 minutes. The treatment conditions are: 150 ^{o}C, 2 hours.

Figure 10.3 shows the x-ray patterns after hydrothermal treatments. Apparently, cellulose without salt re-crystallizes because the peak intensity at 16^{o} and 22^{o} are the highest among the treated samples, which is consistent with previous reported study.[10] For cellulose treated with different inorganic salts, they behave differently. For instance, cellulose treated with ammonium chloride recrystallizes most comparted to other aqueous salts, suggesting its ineffectiveness on suppressing cellulose re-crystallization. In contrast, guanidinium chloride prevents the cellulose re-crystallization most effectively. Sequentially, the effectiveness of selected salts in suppressing

cellulose crystallization is in the order of GdmCl > $CaCl_2$ > LiCl > KCl > NH_4Cl. Interestingly, the sequence is consistent with hydrolysis performance except for LiCl. However, considering the error bar in hydrolysis data, the performance of LiCl and KCl are deemed as identical.

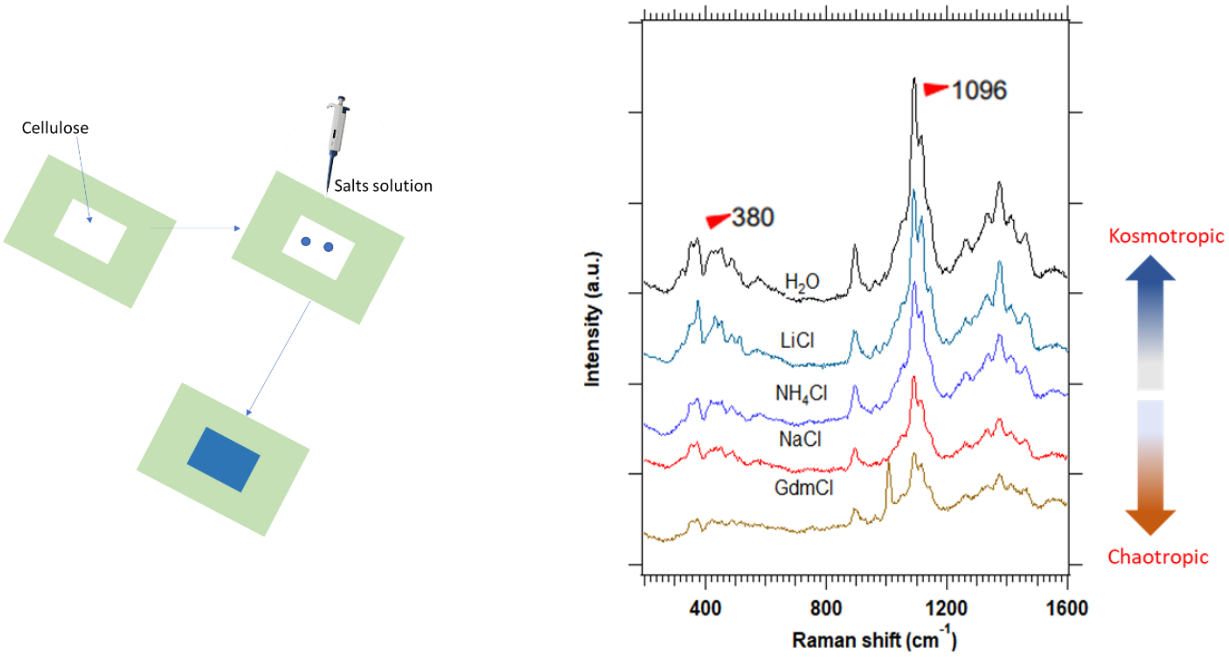

Figure 10. 4 Raman spectroscopy showing effect of cations on cellulose re-crystallization in hydrothermal conditions. The raw cellulose was ball-milled for 50 minutes. Two droplets of aqueous salt solutions are introduced to wet cellulose powder.

Since X-ray diffraction only provides information on atoms arrangements on Miller planes, e.g. 110 and 200, it does not capture chemical bonds dynamics. Cellulose is a complicated structure containing covalent bonds and non-covalent bonds such as hydrogen bonds, Raman spectroscopy characterizes vibration bonds, which is applicable here. To illustrate the dynamics of vibrational bonds changes, we developed a simple wetting technique in which a small quantity of droplets (e.g. two) are spread onto cellulose powder and the powder samples is immediately exposed to Raman laser. Figure 10.4 shows the simple technique and results. In figure 10.4, bands at 380 cm^{-}

^{1} and 1100 cm^{-1} are highlighted since they are related to cellulose crystalinity. Figure 10.4 clearly indicates that 50 minutes ball-milled cellulose wetted by pure D.I. water restores its crystalinity the most comparing to other samples treated with salt solutions. 50 minutes ball-milled microsatellite treated with guanidinium chloride has the lowest peak intensity, suggesting its low crystalinity and it is consistent with XRD observation. Salts in between, NH_4Cl , NaCl and LiCl have intermediate peak intensity. Considering all samples are treated with salts within 2 minutes, it suggests recrystallization is a fast process in all cases, even in guanidinium chloride.

10.4.2 Solid State NMR Analysis of Amorphous Cellulose Treated with Salt Solutions

To gain greater insight, selected samples were further analyzed using quantitative 13C ssNMR and result is shown in figure 10.5. Specific focus was placed on the C4 and C6 regions of the NMR spectrum, as these regions contain distinguishable contributions from carbons in crystalline interior chains and nanocrystalline surface or truly amorphous chains. Five samples are analyzed: water-treated Avicel101 (2h), 500mM guanidinium chloride treated microcrystalline cellulose (50 minutes ball-milled) for 0.5 and 2 hours, 500 mM guanidinium chloride and 50mM HCl treated microcrystalline cellulose (50 minutes ball-milled) and 500 mM ammonium chloride treated microcrystalline cellulose (50 minutes ball-milled). Bands between 60-65 ppm corresponds to formation of cellulose II. As we expected, the presence of HCl removes part of cellulose I and suppress growth of cellulose II. Samples treated with ammonium chloride and guanidinium chloride have identical cellulose II and cellulose I, suggesting that crystallinity might not be the factors effecting glucose yield.

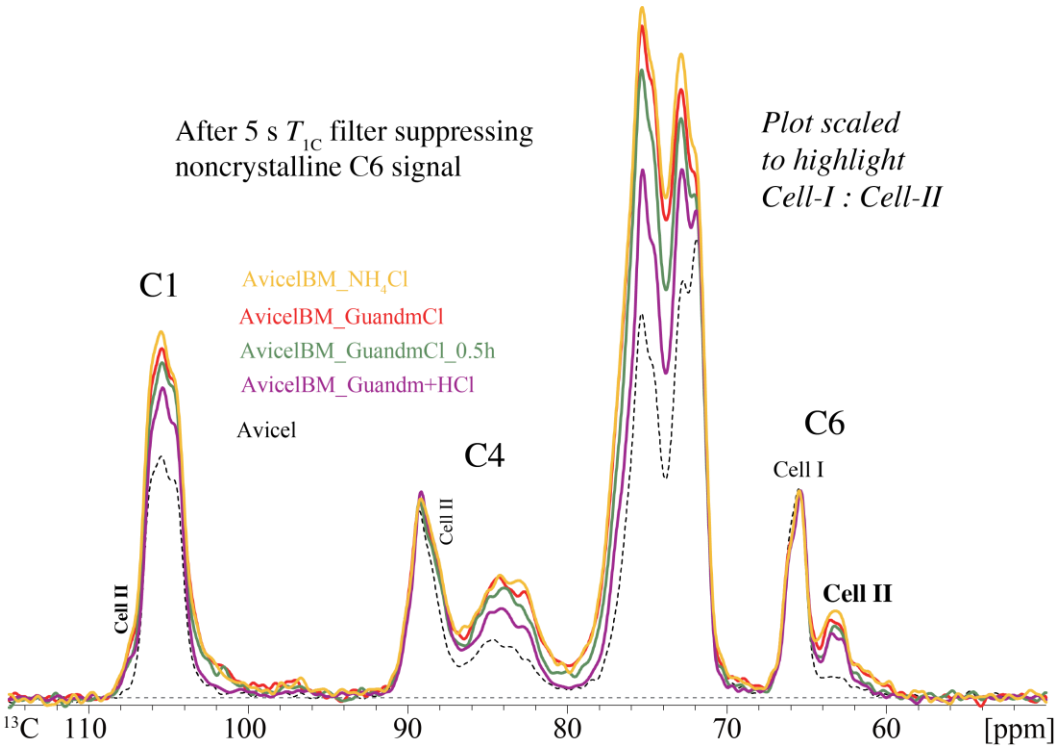

Figure 10. 5 The C4 and C6 13C NMR spectra of selected cellulose samples. The black curve represents the overall spectra; the red curve is signal from domains with long T1C relaxation times, and the green curve is signal from regions with short T1C relaxation times.

10.4.3 Inorganic salts Promoted Cellulose Hydrolysis

The first objective is to investigate the effect on different cations on decomposing cellulose into glucose in the presence of liquid acid. Accordingly, microcrystalline cellulose was ball-milled for 50 minutes to convert crystalline structure into amorphous structures. Ball-milled cellulose was hydrolyzed in the presence of the inorganic salts, which are NH_4, LiCl, KCl, $CaCl_2$ and GdmCl and hydrochloride acid. Figure 10.6 shows the glucose yield for all selected inorganic aqueous alt solutions. Apparently, glucose yields for all the selected inorganic salts increase except for ammonium chloride which has the same glucose yield as the control test. In general, the glucose yield is in the sequence of GdmCl > $CaCl_2$ > KCl > LiCl > NH_4Cl. Interestingly, this sequence

agrees with Hofmeister's empirical series.[20] Since ammonium chloride is known as salting-out salt, meaning that adding ammonium chloride will cause its preferential interactions with water, resulting in less interaction with solute e.g. cellulose., and stabilize the cellulose structure. In contrast, guanidinium cation, which is on the opposite side of the Hofmeister series, is known as "chaotropic agent" which can strengthen interaction of cellulose with guanidinium cations.

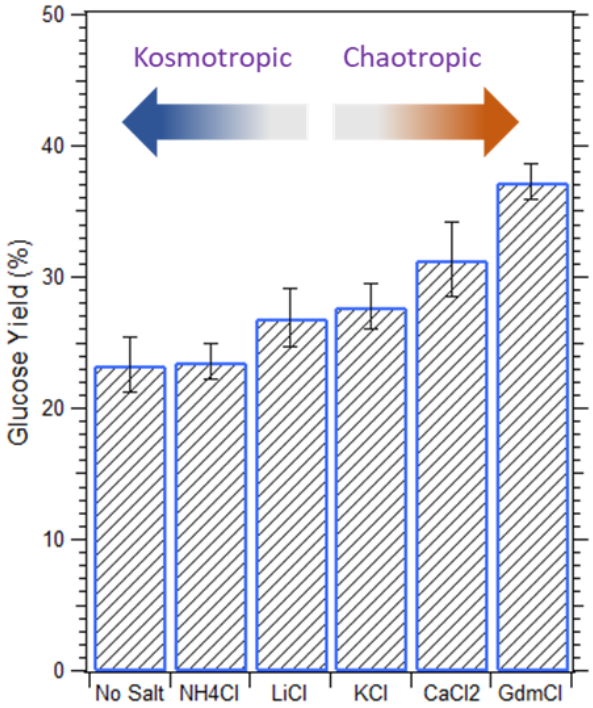

Figure 10. 6 Glucose yield of ball-milled microcrystalline cellulose hydrolyzed in different aqueous-salt solutions. The reaction conditions are: 150 ^{o}C, 4 hours, 0.05M HCl.

10.4.4 Guanidinium Chloride Promoted Cellulose Hydrolysis

To shine light into why guanidinium chloride performs better than other selected inorganic salts, we have decided to isolate guanidinium chloride from the list. We first tested the time-effect of cellulose hydrolysis reaction in the presence of guanidinium chloride with varied HCl concentration. Figure 10.7 shows glucose yield as a function of time for three conditions: red data

points represent glucose yield of ball-milled cellulose reacting with 50mM in the absence of guanidinium chloride while black data points represent the same conditions with added guanidinium chloride (500 mM). Two significant changes can be observed: 1). Maximum glucose yield difference is as large as 12% comparing red and black data points. This attributes to guanidinium chloride preventing amorphous cellulose to recrystallize, as shown in Figure 10.8A and 9.8B. Interestingly, the rate of glucose production is roughly decreasing as time becomes larger. This is because recrystallization is a dynamic process as well. Figure 10.8A and 10.8B show that cellulose slowly recovers its crystalinity when time increases from 30 minutes to 240 minutes, suggesting guanidinium chloride can slow down recrystallization, but cannot eliminate it.

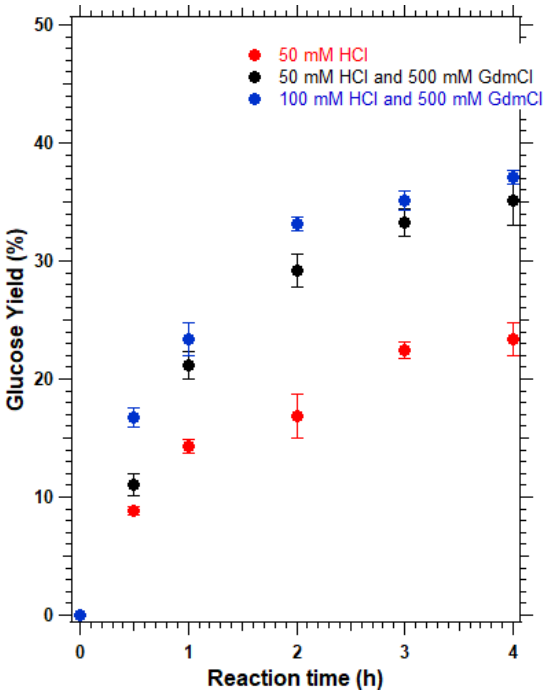

Figure 10. 7 Cellulose hydrolysis in the presence of guanidinium chloride and hydrochloride acid. Cellulose was ball-milled for 50 minutes before reaction. The reaction conditions are: 150 ^{o}C, 0.05 M HCl and 0.5 M guanidinium chloride.

To increase glucose yield in the presence of guanidinium chloride, we increase HCl concentration from 50 mM to 100 mM. Surprisingly, glucose yield is only slightly improved, suggesting that added HCl may also trigger and speed up recrystallization. Indeed, Figure 10.8C and 8D show that cellulose restore 80% of its intensity (and crystalinity) even within 30 minutes. As we increase reaction time to 240 minutes, cellulose completely recovers its crystalinity. With that being said, even though we start with 100 mM HCl, it removes amorphous phase faster and forms cellulose crystals faster as well comparing with 50mM HCl reaction.

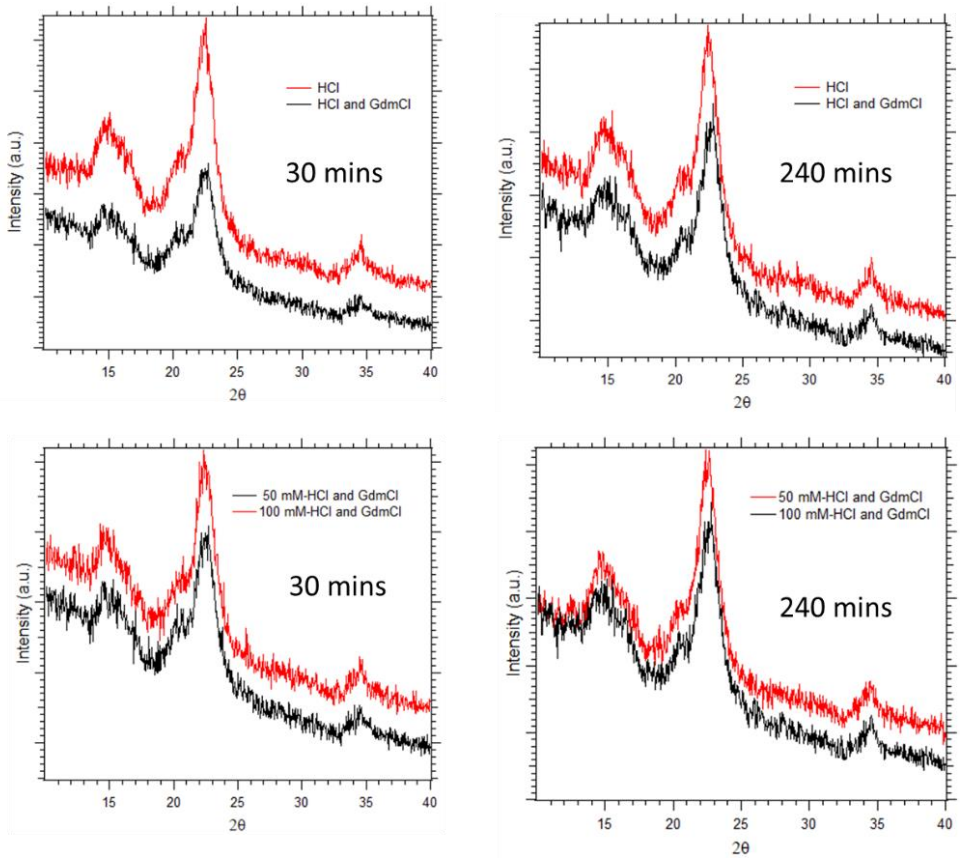

Figure 10. 8 X-ray diffraction of recovered cellulose for 30 minutes and 240 minutes after the reaction.

10.4.5 Maximizing glucose yield in the presence of guanidinium chloride

The presence of guanidinium chloride suppresses transition of amorphous cellulose into crystalline structure, cellulose II. This suppression effect takes place only for cellulose with amorphous phase. For highly crystalline cellulose, guanidinium chloride has negligible influence on glucose yield, as shown in Figure 10.9. In figure 10.9, we evaluated two extreme cases that Avicel101 is the most crystalline structures and 50-minutes ball-milled cellulose is the most amorphous sample. Both samples are hydrolyzed with and without guanidinium chloride (500 mM). Avicel101 has no visible differences as the glucose yield is close to 8-10% at 150^{o}C for 4 hours. However, for 50 minutes ball-milled cellulose, not only glucose yield has jumped to 34% in the presence of guanidinium chloride, but also glucose yield difference is about 10%, suggesting that guanidinium chloride's effect is maximized for amorphous cellulose.

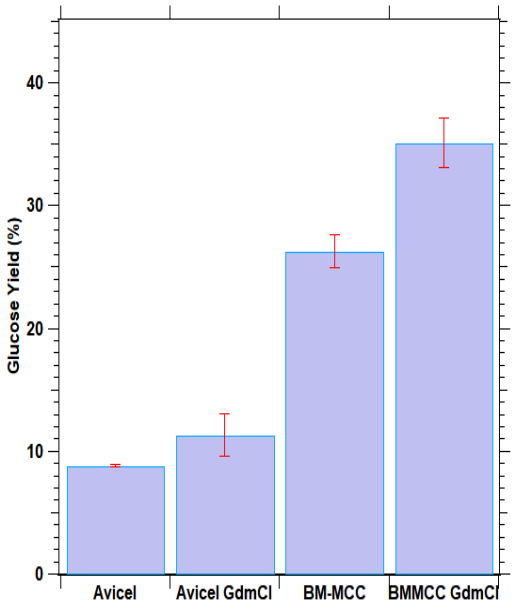

Figure 10. 9 Glucose yield of Avicel101 and 50 minutes ball-milled microcrystalline cellulose with and without guanidinium chloride. Reaction conditions: 50mM HCl, 4 hours at 150 ^{o}C.

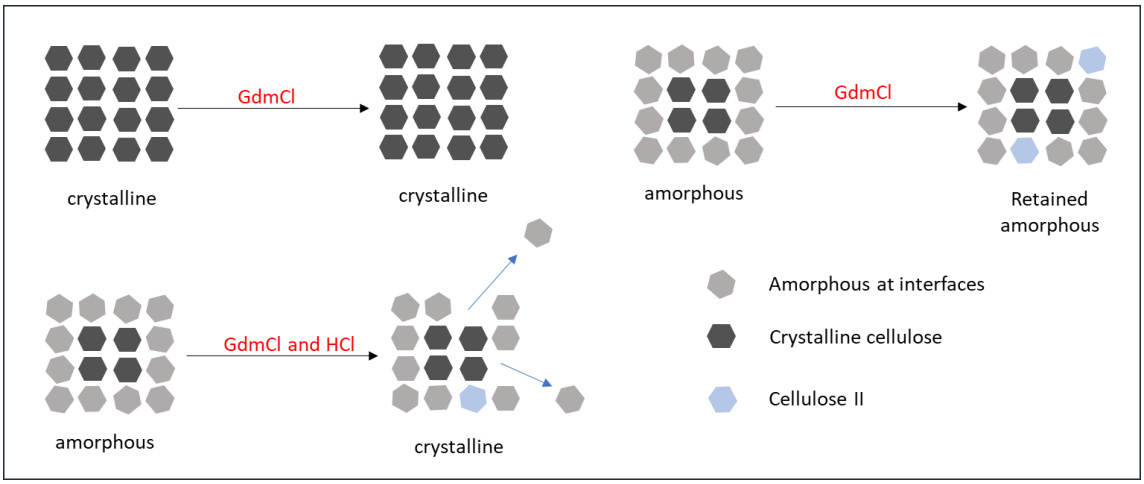

Figure 10. 10 Schematics of how guanidinium chloride and HCl affect cellulose crystalinity: 1). Crystalline cellulose remains crystalline structure after guanidinium chloride treatment; 2). Guanidinium chloride retains amorphous phase and forms cellulose II; 3).HCl re-crystallize cellulose by forming mostly cellulose I and removing amorphous phase.

Figure 10.10 summarizes some of main points from analysis. Results show that guanidinium chloride does not convert crystalline cellulose into amorphous phase. Instead, guanidinium chloride does not affect Avicel crystalinity at all. After ball-milling cellulose and treated with HCl and guanidinium, part of cellulose I are removed by HCl. Small amount cellulose II are formed, suggesting that guanidinium chloride forms cellulose II but not cellulose I. When treating amorphous cellulose without HCl, a portion of cellulose I are converted cellulose II, possibility explaining why guanidinium chloride improves glucose yield because cellulose II is much reactive than cellulose I.

10.4.6 Molecular Dynamic Simulations

So far, all characterization method used can only provide macroscopic properties such as crystal size and crystalinity. Fundamentally, crystals rely on arrangement and conformation of individual atoms or molecules. Knowing how salts, especially those representative salts such as ammonium

chloride and guanidinium chloride, affect conformation of cellulose is important. Accordingly, we performed a simple molecular dynamic simulation using Gromacs and the method is specified in experimental section.

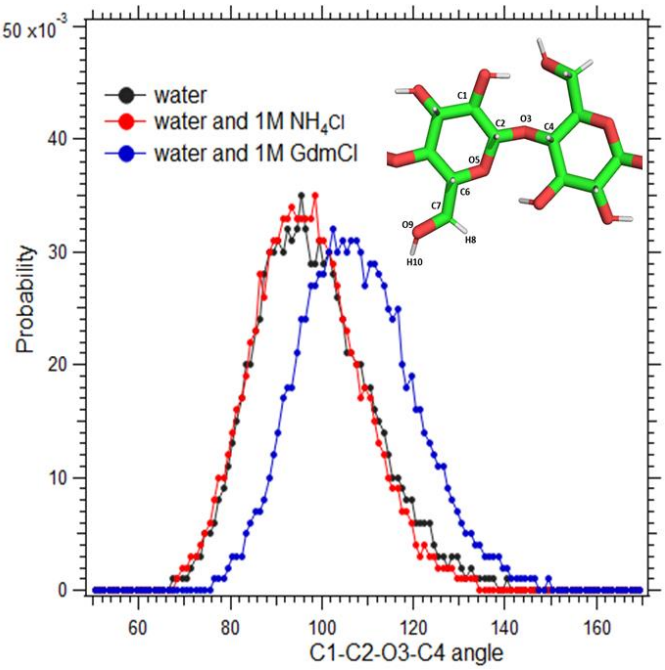

Figure 10. 11 Dihedral angle distribution of labelled C1-C2-O3-C4.

Specifically, we are interested in angles distribution around glycosidic bond as its direct relation with glucose production. Accordingly, we simulate three systems: 1M guanidinium chloride with 4 cellulose chains, 1M ammonium chloride with 4 cellulose chains and pure cellulose chains interacting with water. Dihedral angles for labeled C1-C2-O3-C4 is computed for all three samples. Interestingly, angle distribution for cellulose-water system is centered around 94^{o}, which is almost identical to water-ammonium chloride-cellulose mixture whose angle is around 96^{o}, suggesting that ammonium chloride effect on cellulose might be like water's effect on cellulose. However, when we simulate water-guanidinium chloride-cellulose mixture, we noticed the angles

become slightly spreading, suggesting that the bonds are influenced and relaxed to some extent once mixing with guanidinium chloride.[36, 37]

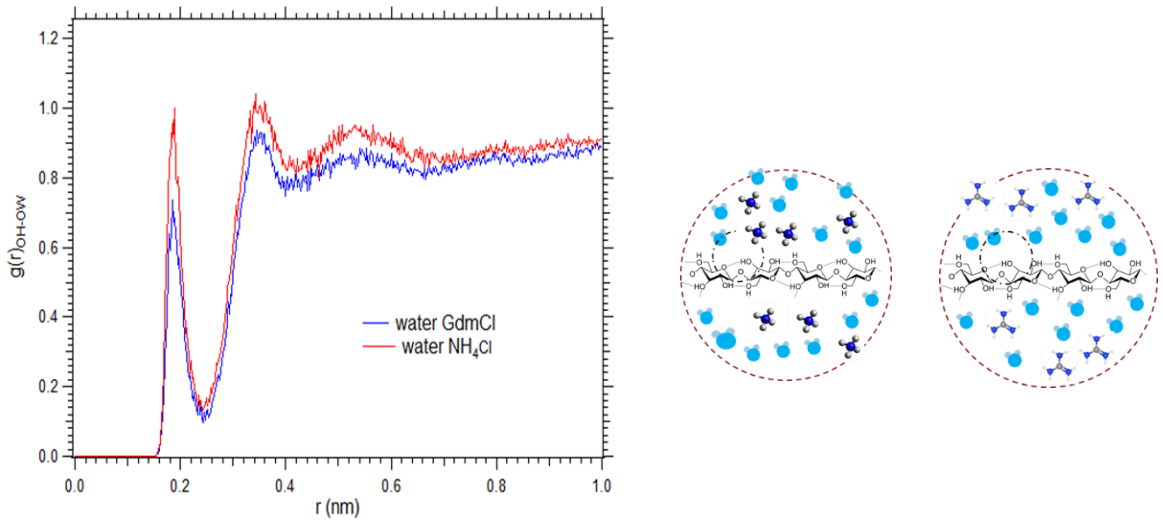

Figure 10. 12 radical distribution function of -OH (cellulose) with water molecules in the presence of ammonium chloride and guanidinium chloride respectively.

The interaction between -OH group of cellulose with water is believed an important type of interaction contributing to cellulose crystallization. Hydrogen bonding between -OH and water may help cellulose keep amorphous phase as it prevents cellulose self-binding by hydrogen bonds, a phenomenon called hydrophobic effect. Therefore, we performed radical distribution for cellulose's -OH with water's oxygen for both ammonium chloride and guanidinium chloride. The first hydration peak is at around 0.2 nm, which is hydrogen bonding. As separation increases, number density around -OH varies for these two salts. Number density of guanidinium chloride is slightly greater than ammonium chloride, suggesting that water molecules are pushed away by guanidinium cations. But the differentiation is small, indicating that both ammonium cations and

guanidinium cations may have the accessibility to interact with interior part of cellulose, which may interfere its crystalline structures.

10.4.7 Hofmeister Series for Salts Effect on Cellulose Hydrolysis and Crystallization suppression

Lastly, to summarize salts effect on both crystalinity and glucose production, we construct our own qualitive Hofmeister series. In figure 10.13, the blue data points are the series for cations with fixed anions, chloride anions. The yellow dots represent anions with fixed sodium cations. The black line is glucose yield while the red line represents crystalinity. For various cations with fixed anions, the correlation between glucose yield and crystalinity is clearly positive. While for anions with fixed cations, the correlation is weak. This is mainly due to protons activity. For example, CO_3^{2-} is a weak acid, it thus constrains protons and reduce proton's ability to attack cellulose. We recommend choosing salts with care when varying anions as some anions may form weak acid with protons.

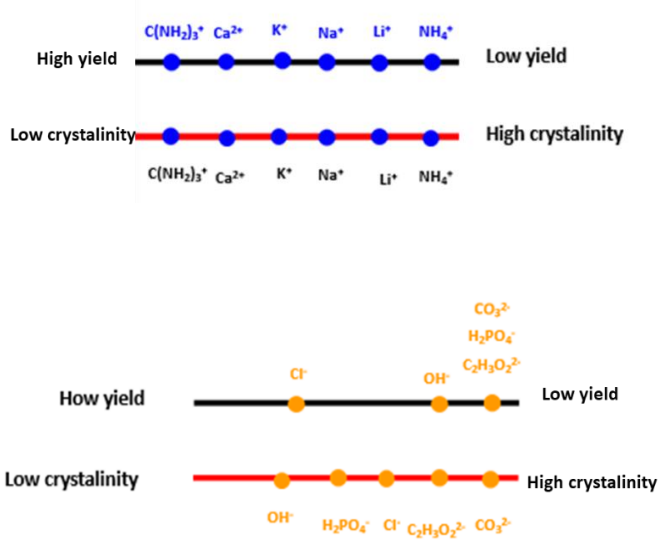

Figure 10. 13 Hofmeister series of selected inorganic salts for depressing cellulose recrystallization and promoting cellulose hydrolysis in presence diluted hydrochloride acid.

10.5 Conclusions

In this study, we evaluate salts' ability to suppress cellulose crystalinity and its implication for cellulose hydrolysis. Specifically, we found that "salting-in" salt such as guanidinium chloride, can double glucose yield. X-ray diffraction, Raman suggest guanidinium chloride can suppress cellulose recrystallization and increases cellulose reactivity. "salting-out" salt such as lithium chloride and ammonium chloride, are unable to keep amorphous cellulose. ssNMR indicates that guanidinium chloride treated Avicel has relatively larger amorphous cellulose compared to ammonium chloride treated sample. Meanwhile, guanidinium chloride can form more active cellulose II compared to samples with HCl.

Molecular dynamics simulation was performed to gain conformation changes of cellulose. The results indicate that guanidinium chloride relaxes glycosidic bonds and the bonds around it. Radical distribution functions between water and -OH of cellulose suggests that guanidinium cations have more accessibility and possibility to interact with cellulose -OH than ammonium cations. Lastly, a new version of Hofmeister series was constructed to help the community identify proper salts for improved cellulose depolymerization.

10.6 Reference

1. Xie, H., et al., *Recent strategies in preparation of cellulose nanocrystals and cellulose nanofibrils derived from raw cellulose materials.* International Journal of Polymer Science, 2018. **2018**.
2. Horn, S.J., et al., *Novel enzymes for the degradation of cellulose.* Biotechnology for biofuels, 2012. **5**(1): p. 1-13.
3. Onda, A., T. Ochi, and K. Yanagisawa, *Selective hydrolysis of cellulose into glucose over solid acid catalysts.* Green Chemistry, 2008. **10**(10): p. 1033-1037.

4. Huang, Y.-B. and Y. Fu, *Hydrolysis of cellulose to glucose by solid acid catalysts.* Green chemistry, 2013. **15**(5): p. 1095-1111.
5. Kong-Win Chang, J., et al., *Two-step thermochemical cellulose hydrolysis with partial neutralization for glucose production.* Frontiers in chemistry, 2018. **6**: p. 117.
6. Piras, C., S. Fernández-Prieto, and W. De Borggraeve, *Ball milling: a green technology for the preparation and functionalisation of nanocellulose derivatives. Nanoscale Adv 1: 937–947*. 2019.
7. Ferreira, R.R., et al., *Use of ball mill to prepare nanocellulose from eucalyptus biomass: Challenges and process optimization by combined method.* Materials Today Communications, 2020. **22**: p. 100755.
8. Ling, Z., et al., *Effects of ball milling on the structure of cotton cellulose.* Cellulose, 2019. **26**(1): p. 305-328.
9. Hermans, P. and u.A. Weidinger, *On the recrystallization of amorphous cellulose.* Journal of the American Chemical Society, 1946. **68**(12): p. 2547-2552.
10. Tyufekchiev, M., et al., *Reaction engineering implications of cellulose crystallinity and water-promoted recrystallization.* Green Chemistry, 2019. **21**(20): p. 5541-5555.
11. Caulfield, D.F. and R.A. Steffes, *Water-induced recrystallization of cellulose.* Review Process: Non-Refereed (Other), 1969.
12. Trevorah, R.M., et al., *Structural and Morphological Analysis of Cellulose Pulp Produced from the Fractionation of Eucalyptus obliqua Sawdust Using γ-Valerolactone.* ACS omega, 2021. **6**(6): p. 4126-4136.
13. Nauruzbayeva, J., et al., *Electrification at water–hydrophobe interfaces.* Nature communications, 2020. **11**(1): p. 1-10.

14. Owen, B.B., et al., *The dielectric constant of water as a function of temperature and pressure1, 2.* The Journal of Physical Chemistry, 1961. **65**(11): p. 2065-2070.
15. Lara-Serrano, M., et al., *High enhancement of the hydrolysis rate of cellulose after pretreatment with inorganic salt hydrates.* Green Chemistry, 2020. **22**(12): p. 3860-3866.
16. Deng, W., et al., *Cellulose hydrolysis in acidified LiBr molten salt hydrate media.* Industrial & Engineering Chemistry Research, 2015. **54**(19): p. 5226-5236.
17. vom Stein, T., et al., *Salt-assisted organic-acid-catalyzed depolymerization of cellulose.* Green Chemistry, 2010. **12**(10): p. 1844-1849.
18. de Almeida, R.M., et al., *Cellulose conversion to isosorbide in molten salt hydrate media.* ChemSusChem: Chemistry & Sustainability Energy & Materials, 2010. **3**(3): p. 325-328.
19. Xie, W.J. and Y.Q. Gao, *A simple theory for the Hofmeister series.* The journal of physical chemistry letters, 2013. **4**(24): p. 4247-4252.
20. Okur, H.I., et al., *Beyond the Hofmeister series: Ion-specific effects on proteins and their biological functions.* The Journal of Physical Chemistry B, 2017. **121**(9): p. 1997-2014.
21. Moghaddam, S.Z. and E. Thormann, *The Hofmeister series: Specific ion effects in aqueous polymer solutions.* Journal of colloid and interface science, 2019. **555**: p. 615-635.
22. Ferreira, L., V. Uversky, and B. Zaslavsky, *Effects of the Hofmeister series of sodium salts on the solvent properties of water.* Physical Chemistry Chemical Physics, 2017. **19**(7): p. 5254-5261.
23. Liu, Z., et al., *Dissolution of cellobiose in the aqueous solutions of chloride salts: Hofmeister series consideration.* Cellulose, 2016. **23**(1): p. 295-305.

24. Vanommeslaeghe, K., et al., *CHARMM general force field: A force field for drug‐like molecules compatible with the CHARMM all‐atom additive biological force fields.* Journal of computational chemistry, 2010. **31**(4): p. 671-690.

25. Huang, J. and A.D. MacKerell Jr, *CHARMM36 all‐atom additive protein force field: Validation based on comparison to NMR data.* Journal of computational chemistry, 2013. **34**(25): p. 2135-2145.

26. Pronk, S., et al., *GROMACS 4.5: a high-throughput and highly parallel open source molecular simulation toolkit.* Bioinformatics, 2013. **29**(7): p. 845-854.

27. Liu, H., et al., *Understanding the interactions of cellulose with ionic liquids: a molecular dynamics study.* The Journal of Physical Chemistry B, 2010. **114**(12): p. 4293-4301.

28. Manna, B. and A. Ghosh, *Dissolution of cellulose in ionic liquid and water mixtures as revealed by molecular dynamics simulations.* Journal of Biomolecular Structure and Dynamics, 2019. **37**(15): p. 3987-4005.

29. Dupont, A.-L., *Cellulose in lithium chloride/N, N-dimethylacetamide, optimisation of a dissolution method using paper substrates and stability of the solutions.* Polymer, 2003. **44**(15): p. 4117-4126.

30. Chundawat, S.P., et al., *Ammonia-salt solvent promotes cellulosic biomass deconstruction under ambient pretreatment conditions to enable rapid soluble sugar production at ultra-low enzyme loadings.* Green Chemistry, 2020. **22**(1): p. 204-218.

31. Liebert, T., *Cellulose solvents–remarkable history, bright future*, in *Cellulose solvents: for analysis, shaping and chemical modification*. 2010, ACS Publications. p. 3-54.

32. Yang, G., et al., *Comparison of Effects of Sodium Chloride and Potassium Chloride on Spray Drying and Redispersion of Cellulose Nanofibrils Suspension.* Nanomaterials, 2021. **11**(2): p. 439.

33. Park, S., et al., *Cellulose crystallinity index: measurement techniques and their impact on interpreting cellulase performance.* Biotechnology for biofuels, 2010. **3**(1): p. 1-10.

34. Walker, T.W., et al., *Solid-state NMR studies of solvent-mediated, acid-catalyzed woody biomass pretreatment for enzymatic conversion of residual cellulose.* ACS Sustainable Chemistry & Engineering, 2020. **8**(16): p. 6551-6563.

35. Li, H. and J. Xu, *Optimization of microwave-assisted calcium chloride pretreatment of corn stover.* Bioresource technology, 2013. **127**: p. 112-118.

36. Chami Khazraji, A. and S. Robert, *Self-assembly and intermolecular forces when cellulose and water interact using molecular modeling.* Journal of Nanomaterials, 2013. **2013**.

37. Einfeldt, J., D. Meißner, and A. Kwasniewski, *Polymerdynamics of cellulose and other polysaccharides in solid state-secondary dielectric relaxation processes.* Progress in Polymer Science, 2001. **26**(9): p. 1419-1472.

1. Wüstenberg, T., *Cellulose and cellulose derivatives in the food industry: fundamentals and applications*. 2014: John Wiley & Sons.

2. Mascal, M. and E.B. Nikitin, *Direct, High‐yield conversion of cellulose into biofuel.* Angewandte Chemie, 2008. **120**(41): p. 8042-8044.

3. Sorokina, K.N., et al., *Cellulose biorefinery based on a combined catalytic and biotechnological approach for production of 5-HMF and ethanol.* ChemSusChem, 2017. **10**(3): p. 562-574.
4. Kuo, I.-J., et al., *Cellulose-to-HMF conversion using crystalline mesoporous titania and zirconia nanocatalysts in ionic liquid systems.* Rsc Advances, 2013. **3**(6): p. 2028-2034.
5. Heng, J., et al., *Cellobiose as a Model Carbohydrate for Predicting Solubilities in Nonaqueous Solvents.* Industrial & Engineering Chemistry Research, 2021. **60**(4): p. 1859-1871.
6. Pinkert, A., K.N. Marsh, and S. Pang, *Reflections on the solubility of cellulose.* Industrial & Engineering Chemistry Research, 2010. **49**(22): p. 11121-11130.
7. Archer, W.L., *Determination of Hansen solubility parameters for selected cellulose ether derivatives.* Industrial & engineering chemistry research, 1991. **30**(10): p. 2292-2298.
8. Hudson, S.M. and J.A. Cuculo, *The solubility of unmodified cellulose: A critique of the literature.* Journal of Macromolecular Science—Reviews in Macromolecular Chemistry, 1980. **18**(1): p. 1-82.
9. Kobayashi, H., et al., *High-yielding one-pot synthesis of glucose from cellulose using simple activated carbons and trace hydrochloric acid.* Acs Catalysis, 2013. **3**(4): p. 581-587.
10. Mansfield, S.D., C. Mooney, and J.N. Saddler, *Substrate and enzyme characteristics that limit cellulose hydrolysis.* Biotechnology progress, 1999. **15**(5): p. 804-816.
11. Philippidis, G.P., T.K. Smith, and C.E. Wyman, *Study of the enzymatic hydrolysis of cellulose for production of fuel ethanol by the simultaneous saccharification and fermentation process.* Biotechnology and bioengineering, 1993. **41**(9): p. 846-853.

12. Onda, A., T. Ochi, and K. Yanagisawa, *Selective hydrolysis of cellulose into glucose over solid acid catalysts.* Green Chemistry, 2008. **10**(10): p. 1033-1037.

13. Zuo, Y., Y. Zhang, and Y. Fu, *Catalytic conversion of cellulose into levulinic acid by a sulfonated chloromethyl polystyrene solid acid catalyst.* ChemCatChem, 2014. **6**(3): p. 753-757.

Chapter 11

Conclusions and Recommendation

In this dissertation we focus on solving some fundamental questions regarding cellulose depolymerization in hydrolysis reaction. Instead of attempting various catalysts/solvents or other hydrolysis promoters, we emphasize on molecular or colloidal interactions understanding before we do any catalysts or process design for converting cellulose into reduced monomers.

The very first question we want to address is how exactly solid-acid catalysts work to break down cellulose. Since cellulose and solid-acid catalysts are solid particles before and even after reaction in hydrothermal conditions, those particles disperse, suspend and collide with each other during reaction. In this process, surface properties such as hydrophobicity, dispersity, surface charge density and even particles size can be important and dictate the colloid interaction. We first want to understand surface energy of our cellulose and solid-acid particles as surface energy is related to Hamaker constant and subsequently van der Waals attraction of colloidal particles. However, when we decide to measure surface energy of our powders and materials using contact angle measurements, we have a problem that most of contact angle testing liquids are not compatible with cellulose particles, either due to their reactivity with cellulose or their toxicity.

Chapters 3-6 is seeking to develop a brand-new technique for precisely measuring surface free energy. instead of using several pure liquids whose chemistry are completely different, we simply use two liquids, one is water and another one is a benign solvent such as dimethyl sulfoxide, formamide or ethylene glycol. We mix water with one of selected organic solvent in various composition so that we systematically change their surface tensions as well. Measuring contact angles of liquid mixtures on various surfaces such as PVC, PDMS and PMMA allows us to precisely determine surface free energy. we also developed a mixing rule for extracting liquid

mixture surface tension data that contains rich chemical information, such as dispersive forces, polar forces, acid and base interactions. This new technique relies on two important factors: liquid surface tensions parameters and statistical analysis. We have used existing mixing rule, including cubic mixing rule, for extracting abundant surface tension parameters. However, this method might be even more powerful than we thought. The mixing principles can easily be extended to more complicated liquid system, such as ternary or quaternary system. For cellulose hydrolysis reaction in liquid mixtures, understanding the nature of liquid mixtures by analyzing its forces type and its interfacial interaction with cellulose or solid-particles is crucially important for developing technologies decomposing cellulose. Therefore, we recommend using generalized mixing theory to thoroughly characterize any organic solvents/solvents mixtures. Measuring contact angles of corresponding liquid mixtures on biomass would be beneficial to understand interactions at solvent-cellulose interfaces.

This method also relies on statistical analysis. In principal, getting more liquid mixtures and their contact angles would be helping get good statistical confidence. The question here is that some liquids may be not compatible with solid material. For example, we use water-dimethyl sulfoxide mixtures to measure PVC surface energy and the results are significantly high. It turns out dimethyl sulfoxide can swell/dissolve PVC, introducing extra energy so it overestimates PVC surface energy. Greedy sometimes is good, but sometimes it is bad. Therefore, we recommend using compatible liquids and the notion “the more the better” is not necessarily true since it will bring systematic errors.

In reality, “flat surface” is an relative concept that comes with a “reference surface”. With that being said, most surfaces are rough surface. For rough surface, such as cellulose, Wenzel model has to be considered since roughness would make hydrophilic more hydrophilic and hydrophobic

more hydrophobic. We attempted to unify wetting theory by combining liquid surface tension parameters, solid surface energy parameters, surface roughness and wetting parameters all together. Results are very impressive for three types of surfaces: smooth PDMS, regularly patterned PDMS and irregularly patterned surfaces. Unified model can predict contact angles on all those surfaces very well. We recommended testing more surfaces with different surface chemistry.

Getting back to cellulose. In chapter 6, we extended our liquid mixture technique to cellulose and chitin particles. we specifically used water-formamide and water-dimethyl sulfoxide and Washburn method to extract contact angles. The obtained contact angles is slightly larger than literature values. Using those contact angles to determine surface energy of cellulose underestimates surface energy a bit. We recommend preparing packed column carefully and consistently. By saying carefully, we have seen that packing density, porosity and uniformity can all affect penetration of liquid mixtures.

Using obtained cellulose surface energy parameters, we use classic DLVO theory to study colloidal interaction of cellulose with solid acid catalysts. specifically, Hamaker constant of cellulose was obtained from surface energy. However, electrostatic repulsion between cellulose and most functionalized catalysts is so large that it prevents most of solid acid catalysts interacting with cellulose. Here, we rationalize solid acid catalysts design by examining approaches to overcome electrostatic repulsion barrier. Increasing proton concentration or ionic strength may be helpful for cellulose-solid acid aggregation. However, adding salts or protons may trigger much complicated reaction and homogeneous reaction will dominate. Another approach is to use materials with high Hamaker constant. Carbon materials and metal oxide such as zirconia or iron oxide might be effective for adsorption cellulose. Non-DLVO forces are also discussed in detail in Chapter 7. Increasing shear rate can overcome electrostatic repulsion barrier. To summarize the

findings, we recommend the following strategies for developing solid acid catalysts: a). carbon-based substrate is the optimum option while polymer-based catalysts are ineffective for adsorbing cellulose; b). Weak acid such as carboxylic are ideal groups to be installed on catalysts surface. However, strong acid could also work since dissociated protons will hydrolyzing cellulose, resulting in high product yield. The challenges need to be considered here is how to functionalize carbon materials with high density of acid sites, at the same time, making those acid sites hydrothermally stable; 3). The last consideration is the shear rate. Our calculations shows that there is an critical shear rate at which particles have high probability to collide with each other and completely overcome repulsion barrier. This critical shear rate is dependent on a number of factors such as particle size, particle diffusivity and repulsion energy barrier. We recommended using highest allowable shear rate to induce fast coagulation.

Manipulating particle surface charge is a well-established approach for enhancing particles coagulation especially in water treatment industry. One way to tune surface charge is adding coagulant or polyelectrolyte. **In Chapter 8**, we introduced small amount of poly-diallyldimethyl-ammonium chloride (polyDDA), a water soluble and hydrothermally stable polycations, into cellulose-solid acid mixtures. Glucose yield is significantly improved. However, polyDDA does ions exchange with acid sites on solid acid particles (e.g. Amberlyst-15), releasing liquid acid into reacting medium and increases glucose yield. We quantify how much glucose yield those released acid can contribute, and we find that glucose yield from liquid acid is around 8% lower than mixture of solid-acid and polyDDA. We recommend supernatant test (described in Chapter 8) to further verifying “real-heterogeneous-catalysis” effect. Besides glucose yield, measuring zeta potential of both solid acid and cellulose at various polyDDA dosage will help identify a suitable polyDDA dosage that completely or mostly neutralizes surface charges. Visualization method such

as light scattering, SEM or simply microscope are also necessary for observing particles-particles interaction dynamics and coagulation.

Not only cellulose-catalyst interaction is important, but the solvent also-cellulose interaction is crucial too. We typically ball-milled cellulose prior to reaction. However, both water-induced and catalyst (e.g. HCl) induced cellulose recrystallization is a fast and spontaneous process that significantly suppresses cellulose's continuous breakdown. The recrystallization is solvent-dependent. Choosing a solvent or modifying water mixtures may be helpful for suppressing its recrystallization. Previous studies have attempted various organic solvent such as ethanol and dimethyl sulfoxide, and ethanol is found suppressing cellulose recrystallization, but organic solvents tend to form other derivatives. In Chapter 9, we evaluated salts effect on cellulose recrystallization suppression performances. Benefits of inorganic salts include high glucose selectivity, ease of separation and wide range of selection. Indeed, salts sometimes are integral part of biomass, utilizing incorporated salts is inevitable. Although we have identified guanidinium chloride is the best tested slats, our salts selection is not thorough and systematic. In fact, Hofmeister series is an empirical series, and it behaves differently for different proteins. We recommended conducted a wide search and make a reasonable comparison.

Specifically, molecular dynamics simulation can be used to screen salts who are able to interact strongly with either cellulose or water molecules. During simulations, care should be taken on "apple to apple" comparison. For example, monoanion should be compared to monoanions while dianions should be comparted to dianions to eliminate ionic strength effect. Ions may also differentiate based on their solvation free energy, size and ionic strength. Gaining insight into how those parameters affect its interaction with cellulose might be a good starting point. Another drawback of current work on MD simulation is that we used single cellulose chains. Those chains

actually only represent chemical features such as atoms and bonds of cellulose. However, it has no way represents structure feature of cellulose such as crystalline or amorphous phases. To improve current simulation outcome, it would be beneficial to create (or use existing) rigid 3-dimensional cellulose structures.

We then ball-milled cellulose to remove crystallites. Ball-milled cellulose was treated in various inorganic salts solutions. X-ray diffraction and Raman show guanidinium chloride suppress formation of new crystallite while ammonium chloride has almost no visible effect compared to cellulose treated with just water. We attribute guanidinium chloride's crystallite suppression effect to its ability to disrupt water hydrogen bonds. Water with disturbed hydrogen bonds can no longer have the same level of hydrophobic effect on cellulose. Reduced hydrophobic effect forces cellulose to have more access interacting with water rather itself. However, guanidinium chloride and ammonium chloride have similar effect on cellulose crystalinity based on analysis with ss NMR, which might suggest that salt effect is much more complicated than we thought. We recommend running NMR for both cellulose (ball-milled) treated with guanidinium and ammonium in the presence of HCl. If crystalinity is not the main reason for glucose yield, the presence of salts might affect proton activity and thus glucose yield.

Chapter 12

Appendix A

Accurate Measurement of Acid and Base Surface Energy of Polymer Materials Using Aqueous Mixtures and van Oss-Chaudhury-Good (vOCG) Model

Matlab Code

```
clear all
hold on
xw = 0:0.2:1;
xd = 1 - xw;
xf = 1 - xw;
xe = 1 - xw;
% xet = 1 - xw;
lw_w = 21.8;
la_w = 25.5;
lb_w = (51/2)^2/la_w;
% lb_w = 25.5;
lp_w = 51;
l_w = 72.8;

ld_d = 36;
la_d = 0.5;
lb_d = 44;
lp_d = 7;
l_d = 43;
% delta_d = 0.15;
ad = 0.869;
bd = 0.603;
theta_wd_pdms = [89.62222222
92.67777778
94.24444444
97.23333333
98.66666667
108.0666667
]';
theta_wf_pdms = [98.96666667
100.0555556
101.9444444
103.4333333
106.4555556
109.1888889
]';
theta_we_pdms = [95.44444444
97.38888889
98.14444444
101.1333333
102.5555556
110.1333333
```

```
]';
l_wdmix_exp = [44 45 47 53.5 58 72];
%scatter(xw,l_wdmix_exp)
%hold on

                        modelfundd = @(delta_d,xw) xw.^2*lw_w+2*xw.*(1-xw)*(1-
delta_d(1))*sqrt(lw_w*ld_d)+(1-xw).^2*ld_d...
                            + xw.*(1-xw)*sqrt(lw_w*ld_d)*delta_d(2).*(xw.^2 -
(1-xw).^2)...
                            + 2*sqrt((xw.^2*la_w+2*xw.*(1-xw)*(1-
delta_d(1))*sqrt(la_w*la_d)+(1-xw).^2*la_d...
                            + xw.*(1-xw)*sqrt(la_w*la_d)*delta_d(2).*(xw.^2 -
(1-xw).^2)).*(xw.^2*lb_w+2*xw.*(1-xw)*(1-delta_d(1))*sqrt(lb_w*lb_d)+(1-
xw).^2*lb_d...
                            + xw.*(1-xw)*sqrt(lb_w*lb_d)*delta_d(2).*(xw.^2 -
(1-xw).^2)));

delta_d0 = [0.5 0.02];

mdld = fitnlm(xw,l_wdmix_exp,modelfundd,delta_d0)
delta_d = mdld.Coefficients.Estimate;

%xw = 0:0.01:1;
lw_wdmix = xw.^2*lw_w+2*xw.*(1-xw)*(1-delta_d(1)).*sqrt(lw_w*ld_d(1))+(1-
xw).^2*ld_d + xw.*(1-xw)*sqrt(lw_w*ld_d)*delta_d(2).*(xw.^2 - (1-xw).^2);
la_wdmix = xw.^2*la_w+2*xw.*(1-xw)*(1-delta_d(1)).*sqrt(la_w*la_d(1))+(1-
xw).^2*la_d + xw.*(1-xw)*sqrt(lw_w*la_d)*delta_d(2).*(xw.^2 - (1-xw).^2);
lb_wdmix = xw.^2*lb_w+2*xw.*(1-xw)*(1-delta_d(1)).*sqrt(lb_w*lb_d(1))+(1-
xw).^2*lb_d + xw.*(1-xw)*sqrt(lw_w*lb_d)*delta_d(2).*(xw.^2 - (1-xw).^2);
l_wdmix = lw_wdmix + 2*sqrt(la_wdmix.*lb_wdmix);
%plot(xw,l_wdmix)
%hold on

ld_f = 39;
la_f = 2.28;
lb_f = 39.6;
lp_f = 19;
l_f = 58;

af = 0.698;
bf = 0.78;
xw=0:0.2:1;
l_wfmix_exp = l_w-(1+bf*xw./(1-af*xw)).*xf*(l_w-l_f);
%scatter(xw,l_wfmix_exp)
%hold on

                        modelfunf = @(delta_f,xw) xw.^2*lw_w+2*xw.*(1-xw)*(1-
delta_f(1))*sqrt(lw_w*ld_f)+(1-xw).^2*ld_f...
                            + xw.*(1-xw).*sqrt(lw_w*ld_f)*delta_f(2).*(xw.^2 -
(1-xw).^2)...
                            + 2*sqrt((xw.^2*la_w+2*xw.*(1-xw)*(1-
delta_f(1))*sqrt(la_w*la_f)+(1-xw).^2*la_f...
                            + xw.*(1-xw).*sqrt(la_w*la_f)*delta_f(2).*(xw.^2 -
(1-xw).^2)).*(xw.^2*lb_w+2*xw.*(1-xw)*(1-delta_f(1))*sqrt(lb_w*lb_f)+(1-
xw).^2*lb_f...
```

```
                            + xw.*(1-xw).*sqrt(lb_w*lb_f)*delta_d(2).*(xw.^2 -
(1-xw).^2)));

delta_f0 = [0.5 0.5];

mdlf = fitnlm(xw,l_wfmix_exp,modelfunf,delta_f0)
delta_f = mdlf.Coefficients.Estimate;
%xw = 0:0.01:1;
lw_wfmix = xw.^2*lw_w+2*xw.*(1-xw)*(1-delta_f(1)).*sqrt(lw_w*ld_f(1))+(1-
xw).^2*ld_f + xw.*(1-xw)*sqrt(lw_w*ld_f)*delta_f(2).*(xw.^2 - (1-xw).^2);
la_wfmix = xw.^2*la_w+2*xw.*(1-xw)*(1-delta_f(1)).*sqrt(la_w*la_f(1))+(1-
xw).^2*la_f + xw.*(1-xw)*sqrt(la_w*la_f)*delta_f(2).*(xw.^2 - (1-xw).^2);
lb_wfmix = xw.^2*lb_w+2*xw.*(1-xw)*(1-delta_f(1)).*sqrt(lb_w*lb_f(1))+(1-
xw).^2*lb_f + xw.*(1-xw)*sqrt(lb_w*lb_f)*delta_f(2).*(xw.^2 - (1-xw).^2);
l_wfmix = lw_wfmix + 2*sqrt(la_wfmix.*lb_wfmix);
%plot(xw,l_wfmix)
%hold on

ld_e = 29;
la_e = 3;
lb_e = 30.1;
lp_e = 19;
l_e = 48;
l_wemix_exp = [47 50 52.5 55 58.5 72];
xw=0:0.2:1;
%scatter(xw,l_wemix_exp)
%hold on

                      modelfune = @(delta_e,xw) xw.^2*lw_w+2*xw.*(1-xw)*(1-
delta_e(1))*sqrt(lw_w*ld_e)+(1-xw).^2*ld_e...
                            + xw.*(1-xw).*sqrt(lw_w*ld_e)*delta_e(2).*(xw.^2 -
(1-xw).^2)...
                            + 2*sqrt((xw.^2*la_w+2*xw.*(1-xw)*(1-
delta_e(1))*sqrt(la_w*la_e)+(1-xw).^2*la_e...
                            + xw.*(1-xw).*sqrt(la_w*la_e)*delta_e(2).*(xw.^2 -
(1-xw).^2)).*(xw.^2*lb_w+2*xw.*(1-xw)*(1-delta_e(1))*sqrt(lb_w*lb_e)+(1-
xw).^2*lb_e...
                            + xw.*(1-xw).*sqrt(lb_w*lb_e)*delta_e(2).*(xw.^2 -
(1-xw).^2)));

delta_e0 = [0.1 0.1];

mdle = fitnlm(xw,l_wemix_exp,modelfune,delta_e0)
delta_e = mdle .Coefficients.Estimate;

%xw = 0:0.01:1;
lw_wemix = xw.^2*lw_w+2*xw.*(1-xw)*(1-delta_e(1)).*sqrt(lw_w*ld_e(1))+(1-
xw).^2*ld_e + xw.*(1-xw)*sqrt(lw_w*ld_e)*delta_e(2).*(xw.^2 - (1-xw).^2);
la_wemix = xw.^2*la_w+2*xw.*(1-xw)*(1-delta_e(1)).*sqrt(la_w*la_e(1))+(1-
xw).^2*la_e + xw.*(1-xw)*sqrt(la_w*la_e)*delta_e(2).*(xw.^2 - (1-xw).^2);
lb_wemix = xw.^2*lb_w+2*xw.*(1-xw)*(1-delta_e(1)).*sqrt(lb_w*lb_e(1))+(1-
xw).^2*lb_e + xw.*(1-xw)*sqrt(lb_w*lb_e)*delta_e(2).*(xw.^2 - (1-xw).^2);
l_wemix = lw_wemix + 2*sqrt(la_wemix.*lb_wemix);
%plot(xw,l_wemix)
%hold on
```

```
%figure
scatter(l_wdmix_exp,l_wdmix)
hold on
scatter(l_wfmix_exp,l_wfmix)
hold on
scatter(l_wemix_exp,l_wemix)
hold on
xx = 0:0.01:100;
yy = xx;
plot(xx,yy);
xlim([30 80]);
ylim([30 80]);

xwd = sqrt(lw_wdmix./lb_wdmix);
ywd = sqrt(la_wdmix./lb_wdmix);
zwd_pdms = l_wdmix.*(1+cos(theta_wd_pdms/180*pi))./sqrt(lb_wdmix)/2;

xwf = sqrt(lw_wfmix./lb_wfmix);
ywf = sqrt(la_wfmix./lb_wfmix);
zwf_pdms = l_wfmix.*(1+cos(theta_wf_pdms/180*pi))./sqrt(lb_wfmix)/2;

xwe = sqrt(lw_wemix./lb_wemix);
ywe = sqrt(la_wemix./lb_wemix);
zwe_pdms = l_wemix.*(1+cos(theta_we_pdms/180*pi))./sqrt(lb_wemix)/2;

% scatter3(xwd,ywd,zwd)
% hold on
% scatter3(xwf,ywf,zwf)
% hold on
% scatter3(xwe,ywe,zwe)
lball = [lb_wdmix lb_wfmix lb_wemix];
laall = [la_wdmix la_wfmix la_wemix];
lall = [l_wdmix l_wfmix l_wemix];

xall = [xwd xwf xwe];
yall = [ywd ywf ywe];
zall_pdms = [zwd_pdms zwf_pdms zwe_pdms];

x = [xall', yall'];
y = [zall_pdms'];
modelfun = @(b,x) x(:,1)*sqrt(b(1))+x(:,2)*sqrt(b(2))+sqrt(b(3));
b0 = [10 0 20];
mdl = fitnlm(x,y,modelfun,b0)
b_pdms = mdl.Coefficients.Estimate;
x2 = 0:0.01:1.2;
y2 = 0:0.01:1.2;
hold on

z2 = zeros(121,121);
%for i = 1:121;
%    for j = 1:121;
%z2(i,j) = x2(i)*sqrt(a)+y2(j)*sqrt(b)+sqrt(c);
%    end
```

```
%end
%surf(x2,y2,z2)
%[X,Y] = meshgrid(0:0.01:1.2,0:0.01:1.2);
%Z = X*sqrt(b_pdms(1))+Y*sqrt(b_pdms(2))+sqrt(b_pdms(3));
%surf(X,Y,Z)
%view(3)
%hold on
%scatter3(xall,yall,zall)
angpred_wd_pdms =
(acos((xwd*sqrt(b_pdms(1))+ywd*sqrt(b_pdms(2))+sqrt(b_pdms(3)))*2.*sqrt(lb_wd
mix)./l_wdmix-1))/pi*180;
angpred_wf_pdms =
(acos((xwf*sqrt(b_pdms(1))+ywf*sqrt(b_pdms(2))+sqrt(b_pdms(3)))*2.*sqrt(lb_wf
mix)./l_wfmix-1))/pi*180;
angpred_we_pdms =
(acos((xwe*sqrt(b_pdms(1))+ywe*sqrt(b_pdms(2))+sqrt(b_pdms(3)))*2.*sqrt(lb_we
mix)./l_wemix-1))/pi*180;
angall_pdms = [theta_wd_pdms theta_wf_pdms theta_we_pdms];
thetaall_pdms = [theta_wd_pdms,theta_wf_pdms,theta_we_pdms];
% DLVO theory cellulose - solid acid interactions
hold on

for i = 1:1;
PH(i) = 4.5 + 2*(i-1);
x = 0 : 0.01 : 100; % Unit nm jiang shi duo
%>>>>>>>>>>>>>>>>>>>particle size <<<<<<<<<<<<<<<<<<
ratio = 50;

R1 = 1000; % nm cellulose size
R2 = R1/ratio;
% nm solid acid size

% solid acid catalyst list: TBD

% >>>>>>>>>>>>>>>> dielectric constant <<<<<<<<<<<<<<
e0 = 8.85e-12; % e0--vacuum
e1 = 7.6; % e1--cellulose
e2 = 12; % e2--solid acid
e3 = 78; %  e3--water

% >>>>>>>>>>>>>>>>>Refractive index<<<<<<<<<<<<<<<<<<
n1 = 1.53; % cellulose
n2 = 2.42; % solid acid
n3 = 1.33; % water

% >>>>>>>>>>>>>>>>>>Other parameters<<<<<<<<<<<<<<<<<<
ve = 3e15; % rotational frequency
h = 6.626e-34; % Plack constant
kb = 1.38e-23; % Boltzman constant
avo = 6.022e23; % avogadro constant
```

```
T = 298; % Temperature

z = 1; % Valance
q = 1.602e-19; % electron charge
```

Appendix B

D.L.V.O. Analysis of Cellulose and Solid-Acid Catalyst Interaction for Hydrolysis Reaction

List of Symbols

U	DLVO total interaction energy (J)
U_{vdw}	van der Waals attraction energy (J)
U_{edl}	Electrical double layer interaction energy (J)
A_{132}	Hamaker constant of cellulose (1) interacting with catalyst (2) across water (3) (J)
A_{11}	Hamaker constant of cellulose-cellulose interaction in vacuum (J)
A_{22}	Hamaker constant of catalyst-catalyst interaction in vacuum (J)
A_{33}	Hamaker constant of water-water interaction in vacuum (J)
R_1	Radius of cellulose particle (m)
R_2	Radius of catalyst particle (m)
x	Cellulose-catalyst separation (m)
k_b	Boltzmann constant, 1.38×10^{-23} (J K^{-1})
T	Temperature (K)
ε_i	Relative permittivity of cellulose (ε_1), catalyst (ε_2), water (ε_3) and free space (ε_0)

n_i	Refractive index of cellulose (ε_1), catalyst (ε_2), water (ε_3)
h	Planck constant (J s)
v_e	Rotational frequency (s^{-1})
ψ	Electrical potential (V)
ψ_0	Surface electrical potential (V)
c	Ions number concentration (L^{-1})
z	Valence number
e	Charge of an electron, 1.60×10^{-19} (C)
κ	Reciprocal of Debye length (m^{-1})
λ_D	Debye length (m)
ζ	Zeta potential of catalyst and cellulose particle surface (V)
k_{a_1}	Acid dissociation constant
k_{a_2}	Acid dissociation constant
Γ_{AH}	Surface coverage of undissociated AH acid (mol m^{-2})
Γ_{BH}	Surface coverage of undissociated BH acid (mol m^{-2})
Γ_{A^-}	Surface coverage of dissociated acid A^- (mol m^{-2})
Γ_{B^-}	Surface coverage of dissociated acid B^- (mol m^{-2})

Γ_{At}	Total AH acid surface coverage (mol m^{-2})
Γ_{Bt}	Total BH acid surface coverage (mol m^{-2})
σ_0	Surface charge density (C m^{-2}).

Number of articles published on cellulose hydrolysis using solid acid in 14 years

Figure 12.1 indicates that the field grew rapidly between 2007-2014, reaching a steady value between 50 and 80 publications per year from 2014-2019. The result is that the field has expanded from a handful of publications in 2007 to a cumulative total of more than 500 over a 13-year time period.

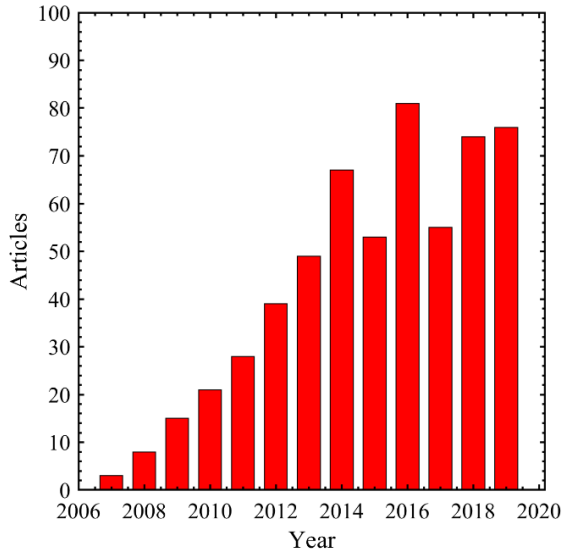

Figure 12. 1 shows the number of annually published articles since 2006. The data was obtained from Web of Science with the search keywords “solid acid catalyst cellulose hydrolysis”.

Shear Force Effect on Cellulose-Catalyst Aggregation

Shear-induced aggregation is discussed and derived by Zaccone et al.[1] where is a shear rate-dependent Arrhenius form equation is obtained for aggregation rate constant of two-body particle interaction:

$$k_{ij} = \sqrt{\frac{3\pi\alpha u\gamma\left(R_i + R_j\right)R_iR_j - U_m''|_{x_m}}{k_BT}}\, e^{\left[-U_m + 6\pi u\gamma\left(R_i+R_j\right)R_iR_j\right]/k_BT} \tag{19}$$

where k_{ij} is coagulation rate constant, u is viscosity, γ is shear rate, U_m is DLVO energy barrier and $U_m''|_{x_m}$ is the second derivate of *Um* with respect to separation (*x*) evaluated at DLVO energy barrier.

The activation energy for shear-induced aggregation takes the form of:

$$E_a = \frac{\left[-U_m + 6\pi u\gamma\left(R_i + R_j\right)R_iR_j\right]}{k_BT} \tag{20}$$

In the case where shear force counterbalances DLVO energy barrier and diminish the barrier, this critical shear rate is an important condition defining the transition from slow aggregation to fast aggregation[1]. Thus, the critical shear rate becomes:

$$\dot{\gamma}^* = \frac{U_m}{6\pi u\left(R_i + R_j\right)R_iR_j} \tag{21}$$

Since for a specific solid catalyst with fixed Hamaker constant, energy barrier (Um) is strongly dependent on surface potential and particle size. Therefore, surface potential of solid catalyst is systematically varied from 0 mV to -120 mV for catalyst radius of 0.5, 1, 1.5 and 2 μm. Then equation (1) is used to determining the maximum energy barrier for specific surface potential and catalyst radius. Finally, equation (21) is employed for calculating critical shear rate.

In our typical hydrolysis setup, a magnetic stirring bar is inserted into a 15-mL heavy wall glass tube (ChemGlass LLC.). The stirring speed, which affects the shear flow of the reaction medium, is often set in the rage of 200-600 rpm. Figure 12.2 shows the schematic. For simplification, we assume that the stirring bar forms a rotating cylinder with diameter of the length of the stirring bar. This assumption will make the schematic similar to Taylor–Couette flow.[2]

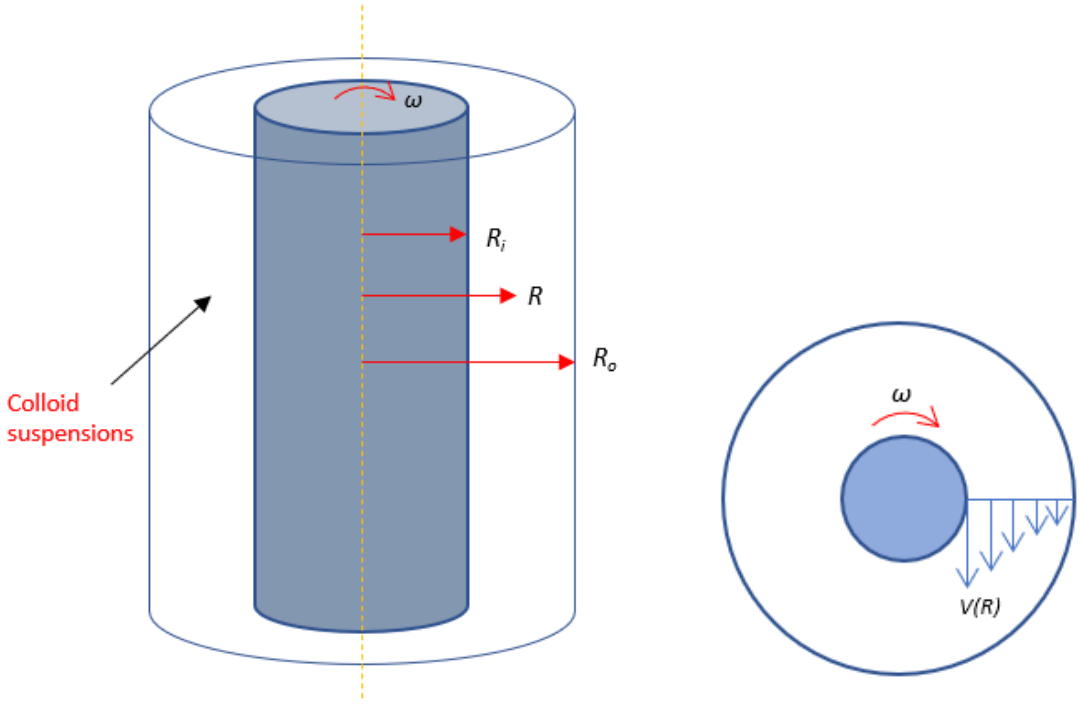

Figure 12. 2 Schematic of reaction system of lab-scale batch reactor for cellulose hydrolysis. Left is the side view of the glass tube reactor and right is top view for velocity profile. where ω is angular velocity of the inner cylinder (or the rotating speed of stirring bar), R_i and R_o are radius of inner and outer cylinders respectively, R is an arbitrary radius.

The velocity profile is given by:

$$v(R) = \frac{\omega R_i^2}{R_o^2 - R_i^2}\left(\frac{R_o^2}{R} - R\right) \tag{22}$$

Therefore, the corresponding shear rate between the moving fluid and stationary cylinder is:

$$\gamma(R) = \frac{\omega R_i^2}{(R_o^2 - R_i^2)(R_o - R)}\left(\frac{R_o^2}{R} - R\right) \quad R_i < R < R_o \tag{23}$$

Equation (23) will be used to extract shear rate profile along the radial direction. Notice that equation (23) can apply to the shear rate at glass tube (e.g. R = R_o) because of the denominator term (R_o-R). Figure 12.3 shows some representative shear rate when the inner cylinder (or the stirring bar) rotates at the speed of 200, 400, 600 and 800 rpm. In general, shear rate maximizes in the center of the reactor and then it decreases nonlinearly along outward radial direction.

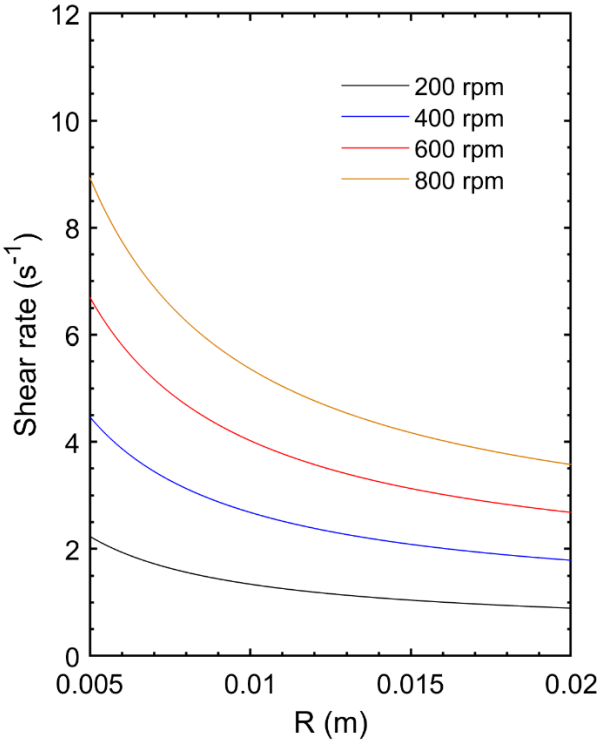

Figure 12. 3 Shear rate distribution within glass tube reactor. R_o is assumed as 2 cm and inner cylinder radius R_i is 0.5 cm.

Temperature Effect on Cellulose-Solid-Acid Interactions

Most reported hydrolysis reaction are performed within the temperature range of 350-450K. Under mildly high temperature, the first order effect of changing temperature is from thermal fluctuations, which is easily accounted for using k_bT in the DLVO analysis. And the particle-particle collisions changes caused by raising temperature is negligible considering the hydrodynamics friction is large enough to reduce thermal fluctuation.

A secondary direct effect is the dependence of the Hamaker constant and surface potential on changing temperature. The van der Waals attraction is caused by electronic fluctuation, and it is weakly dependent or independent on external temperature fluctuations. Therefore, van der Waals attraction between cellulose and solid acid is relatively constant under given reaction condition. The effect of temperature on catalyst surface potential/charge density is much more complicated to consider. First, temperature affect water dielectric and ionization constants (ε and K_w). In fact, the dielectric constant varies from 78 at 25 °C to approximately 35 at 200 °C, the upper range of temperatures used for catalytic cellulose hydrolysis.[3] As a result, Debye length will increase and water will be much less effective at screening charges than room temperature water, enhancing electrostatic repulsion and resulting in net colloidal stabilization for similarly charged particles. Second, water ionization constant (K_w) increase from 1×10^{-14} to 1×10^{-11} when water is heated from 25 to around 200 °C, with the net effect being to adjust protonation/deprotonation equilibria, especially for weak acids and bases. Comparatively, the dissociation constants[4] of carboxylic acids – and probably sulfonic acids – are much weaker functions of temperature than water over the same temperature range. Accordingly, the main effect of temperature on acid-base interactions should be due to the temperature dependence of water dissociation. Lastly, despite that increasing temperature may enhance the acid dissociation,

resulting in higher ionic strength than at room temperature. This increased ionic strength may contribute to the aggregation; however, this would largely depend on how sensitive the acid dissociation to temperature and whether it is endothermal or exothermal reaction. Therefore, the effect of temperature on electrostatic interaction is complicated to consider.

To simplify the temperature effect, we have taken dielectric constant of water, cellulose and solid-acid catalyst (e.g. carbon, zirconia and polystyrene) under different temperature and substitute those into equations(1-8). The results and analysis are provided in the manuscript.

Solvent Effect on Cellulose-Solid-Acid Interaction

Heating water to temperatures greater than 100 °C has been compared with the effect of changing solvents;[5] Accordingly, an alternative strategy for manipulating catalyst-cellulose binding is to change the solvent entirely. Various alcohol water mixtures,[6] tetrahydrofuran-water mixtures,[7] and mixtures of g-Valero lactone and water [8] have been suggested for biomass deconstruction solvents, and combining non-aqueous solvents with solid acid catalysts may provide substantial technological benefits. Unfortunately, colloidal stability in non-aqueous solvents has been the subject of limited studies, meaning that more work is required to arrive at definitive conclusions.

From the considerations presented here, a first order effect of changing solvent will (generally) be to decrease the dielectric constant, accentuating both attractive and repulsive electrical double layer interactions and with only a handful of exceptions for unusual solvents, such as formamide (e = 109.5) or methylformamide (e = 182.4).[9] Accordingly, negatively charged solid acids will more strongly repel negatively charged cellulose in non-aqueous solvents than in water, assuming that the values of the surface potentials themselves are not changed when the solvent is switched. That stated, non-aqueous solvents will shift acid-base dissociation equilibrium

to favor the neutral forms of acids and bases compared with water, meaning that the assumption of constant surface potential is likely erroneous and instead absolute values of the surface potential will be less in non-aqueous solvents than in water. Similarly, the activity of the proton itself is greater in non-aqueous solvents than in water,[10] meaning that combining the other strategies presented here – manipulating particle size, maximizing Hamaker constant, and using bifunctional catalysts to control surface potential – with use of non-aqueous solvents has potential to open entirely new avenues.

Reference

DLVO Matlab Code

```
%% Hamaker constant
%>>>>>>>>>>>>>>>>>>>>>>>>> 1-cellulose; 2-solid acid; 3-water
<<<<<<<<<<<<<
A_11 = 3/4*kb*T*((e1-1)/(e1+1))^2+3*h*ve/16/(2^0.5)*(n1^2-
1)^2/(n1^2+1)^1.5;
A_33 = 3/4*kb*T*((e3-1)/(e3+1))^2+3*h*ve/16/(2^0.5)*(n3^2-
1)^2/(n3^2+1)^1.5;
A_22 = 3/4*kb*T*((e2-1)/(e2+1))^2+3*h*ve/16/(2^0.5)*(n2^2-
1)^2/(n2^2+1)^1.5;
A_132 = (A_11^0.5-A_33^0.5)*(A_22^0.5-A_33^0.5);
%% van der Waals interaction
%%
w_vdw = -A_132./6*(2*R1*R2./(x.*(2*R1+2*R2+x))+...
    (2*R1*R2./(2*R1+x)./(2*R2+x))+log((x.*(2*R1+2*R2+...
    x)./(2*R1+x)./(2*R2+x)))./(kb*T);

%% Electrical double layer repulsion
%%
% >>>>>>>>>>>>>>>>>>> ions concentration <<<<<<<<<<<<<<<<<<
% c_H = 10^(-1*PH)*1000; % proton concentration mol/m^3

% electrolyte concentration
z = 1;
% >>>>>>>>>>>>>>>>>>>>>>>> debye length <<<<<<<<<<<<<<<<<<
F = 1.5/(avo*1e-18); % 1/nm^2


Ka1 = 10^(-2.5); % pka = -log(c)
Ka2 = 0;
```

```
%% >>>>>>>>>>>>>>>>>>>>> surface potential of cellulose and
solid acid <<<<<<<<<<<<<<<<<<<
% >>>>>>>>>>>>>> Zeta potential <<<<<<<<<<<<<<<<<<
zeta_1 = -0.020; % zeta potential of cellulose
zeta_2 = [-0.015 -0.020 -0.025];
% solid acid zeta potential

n = 5;
phi_22 = zeros (1,n);
PH = zeros(1,n);
dey = zeros(1,n);
c_a = zeros(1,n);
inv = zeros(1,n);
sigma = zeros(1,n);
for i = 1:1:n;
    c_a(i) = 10^(-PH(i))*1e3; % anion
    c_c = 0e-3*1e3;
    c_e = 0.000e-3*1e3;
    dey(i) = sqrt(e3*e0*kb*T/(q^2*z^2*(2*c_c  + 1*c_a(i))*avo));
    inv(i) = 1/dey(i); % inverse debye length
    fcn = (@( phi_22) -
e3*e0*inv(i)*kb*T/2/pi/q*(sinh(q*phi_22/2/kb/T)+2/inv(i)/...
          (R2*1e-9)*tanh(q*phi_22/4/kb/T))-q*avo*F*(Ka1-
Ka2*((10^(-PH(i))*1000)...
          *exp(-q*phi_22/kb/T)).^2)/(Ka1+((10^(-
PH(i))*1000)*exp(-q*phi_22/kb/T))...
          +Ka2*((10^(-PH(i))*1000)*exp(-q*phi_22/kb/T)).^2));
   % fimplicit(fcn)
      phi_22(i) = fzero(fcn,1)
    sigma = q*avo*F*(Ka1-Ka2*c_a(i)*exp(-
q*phi_22(i)))/(Ka1+c_a(i)*exp(-q*phi_22(i))+Ka2*(c_a(i)*exp(-
q*phi_22(i)))^2)*1000;
% end
phi_1 = 4*kb*T/(z*q)*atanh(tanh(z*q*zeta_1/(4*kb*T))/exp(-
d0/dey(i)));
 % phi_21(1,i) =
4*kb*T/(z*q)*atanh(tanh(z*q*zeta_2(i)/(4*kb*T))/exp(-
d0/dey(i)));
w_net2 = zeros (6,10001);

Hogg analytical solution for electrical double layer repulsion
for j = 1:1:n;
   for k = 1:10001;
        w_dl = -(e3*e0*R1*10^(-9)*R2*10^(-9)*(phi_1^2 +
phi_22(i)^2)/4/(R1 * ...
```

```
              10^(-9) + R2*10^(-
9))*(2*phi_1*phi_21(i)/(phi_1^2+phi_22(i)^2)*...
              log((1+exp(-inv(i)*(1e-9)*x))/(1-exp(-inv(i)*(1e-
9)*x)))+...
              log(1 - exp(-2*inv(i)*(1e-9)*x))))/(kb*T);
          w_net2 = w_dl + w_vdw;
%    end
% end
for m = 1:1:n
     plot(x,w_net2)
     m(1,i) = max(w_net2);
     p(1,i) = (find(w_net2 == m(1,i))-1)*0.01;

     xlim([0 10]);
     ylim([-20 100]);
end
yyaxis left
plot(PH,m);
yyaxis right
plot(PH,phi_22);

hold on
end
```


1. Zaccone, A., et al., *Theory of activated-rate processes under shear with application to shear-induced aggregation of colloids.* Physical Review E, 2009. **80**(5): p. 051404.
2. Wang, H., *Experimental and numerical study of Taylor-Couette flow*. 2015.
3. Akerlof, G., *Dielectric constants of some organic solvent-water mixtures at various temperatures.* Journal of the American Chemical Society, 1932. **54**(11): p. 4125-4139.
4. Lown, D. and H. Thirsk, *Effect of the solution vapour pressure on the temperature dependence of the dissociation constant of acetic acid in water.* Journal of the Chemical

Society, Faraday Transactions 1: Physical Chemistry in Condensed Phases, 1972. **68**: p. 1982-1986.

5. Peterson, A.A., et al., *Thermochemical biofuel production in hydrothermal media: a review of sub-and supercritical water technologies.* Energy & environmental science, 2008. **1**(1): p. 32-65.
6. Tyufekchiev, M., et al., *Rapid Depolymerization of Decrystallized Cellulose to Soluble Products via Ethanolysis under Mild Conditions.* ChemSusChem, 2020.
7. Smith, M.D., et al., *Cosolvent pretreatment in cellulosic biofuel production: effect of tetrahydrofuran-water on lignin structure and dynamics.* Green Chemistry, 2016. **18**(5): p. 1268-1277.
8. Mellmer, M.A., et al., *Effects of γ-valerolactone in hydrolysis of lignocellulosic biomass to monosaccharides.* Green Chemistry, 2014. **16**(11): p. 4659-4662.
9. Wohlfarth, C., *Static dielectric constants of pure liquids and binary liquid mixtures: supplement to IV/6*. Vol. 17. 2008: Springer Science & Business Media.
10. Mellmer, M.A., et al., *Solvent effects in acid-catalyzed biomass conversion reactions.* Angewandte chemie international edition, 2014. **53**(44): p. 11872-11875.

Appendix C

Salt-Promoted Cellulose Hydrolysis: A Hofmeister Series Study

ss-NMR

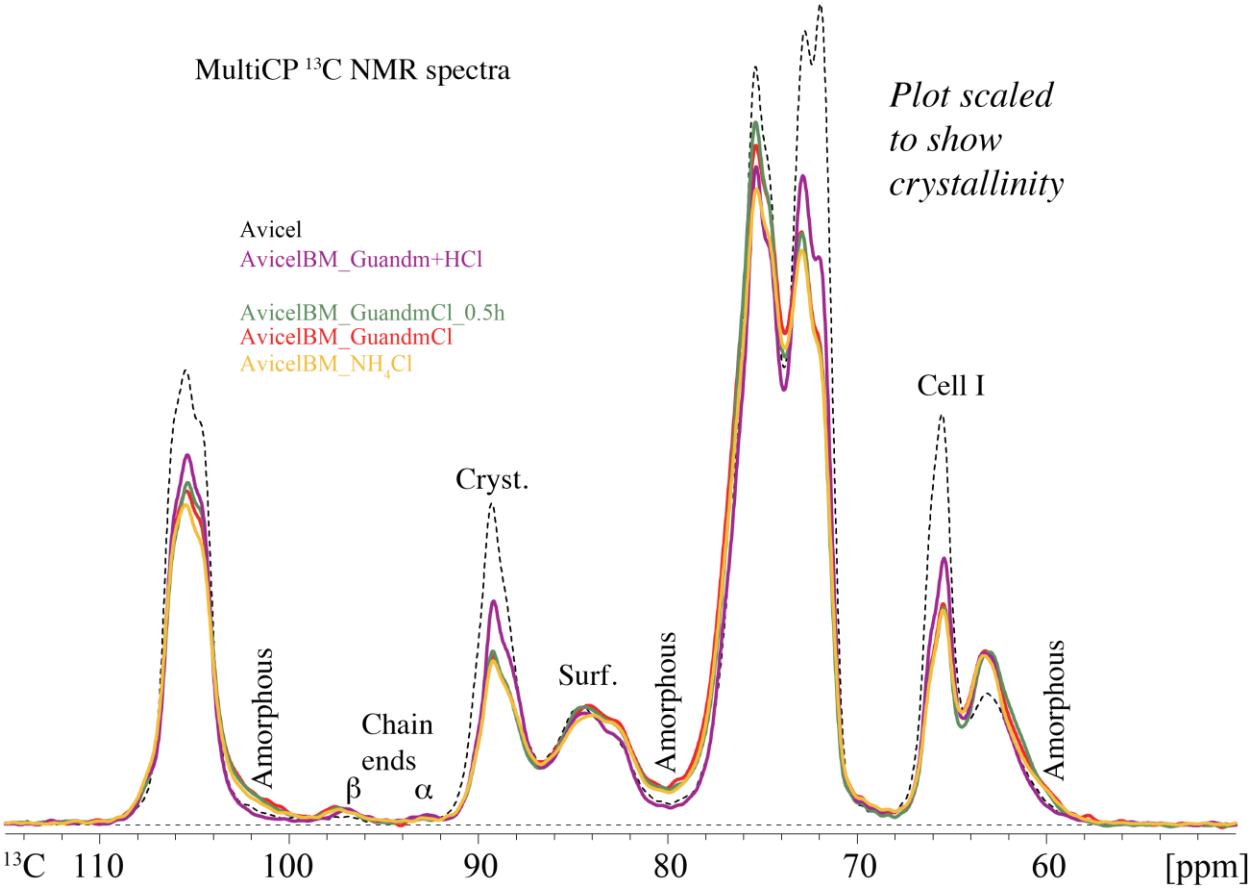

Figure 12. 4 ssNMR of Avicel and microcrystalline cellulose treated with guanidinium chloride and ammonium chloride